On the role of terrestrial ecosystems in a changing Arctic

Gustafson, Adrian

2022

Document Version:
Publisher's PDF, also known as Version of record

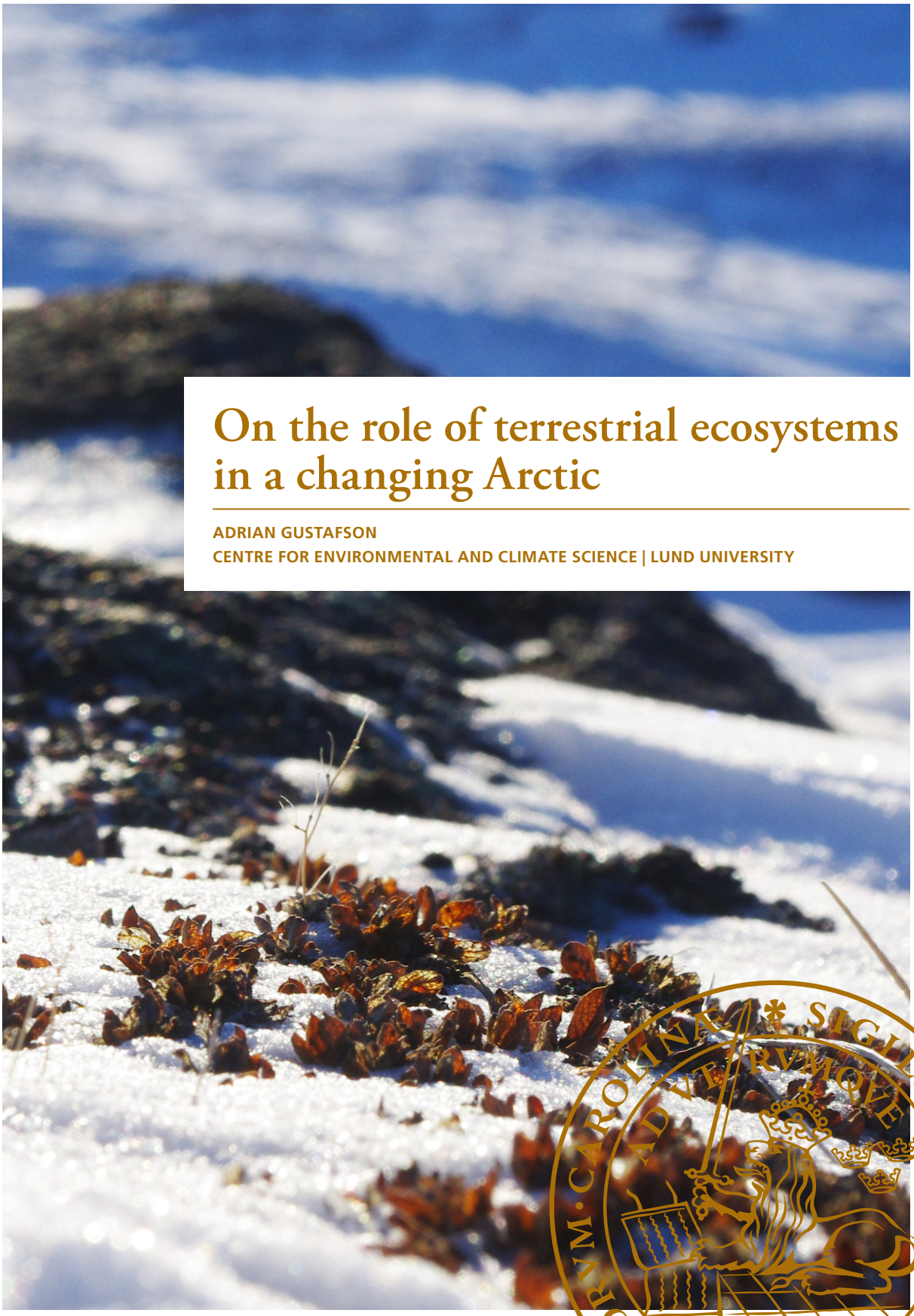

On the role of terrestrial ecosystems in a changing Arctic

ADRIAN GUSTAFSON
CENTRE FOR ENVIRONMENTAL AND CLIMATE SCIENCE | LUND UNIVERSITY

On the role of terrestrial ecosystems in a changing Arctic

I. Gustafson, A., Miller, P. A., Björk, R. G., Olin, S., Smith, B 2021. *Nitrogen restricts future sub-arctic treeline advance in an individual-based dynamic vegetation model*. Biogeosciences, 18, 6329-6347. doi: 10.5194/bg-18-6329-2021:

II. Gustafson, A., Miller P. A., Zhang, W., Tang, J., Björk, R. G., Smith, B. *The contribution of shrubs to Arctic land surface feedbacks*. Manuscript.

III. Gustafson, A., Olin, S., Ahlström, A., Pongracz, A., Niederazik, L., Tang, J., Smith, B., Miller P. A. *High latitude terrestrial ecosystems' contribution to global warming – will the Arctic be a sink or source of greenhouse gases in the 21st century?* Manuscript.

IV. Tang, J., Zhou, P., Miller, P. A., Schurgers, G., Gustafson, A., Makkonen, R., Fu, Y., Rinnan, R. *High latitude vegetation changes will determine future plant volatile impacts on atmospheric organic aerosols*. Under review at Nature Portfolio. Doi: 10.21203/rs.3.rs-1143422/v1

Printed by Media-Tryck, Lund 2022 NORDIC SWAN ECOLABEL 3041 0903

LUND UNIVERSITY

Faculty of Science
Centre for Environmental and Climate Science

ISBN 978-91-8039-328-7

On the role of terrestrial ecosystems in a changing Arctic

Adrian Gustafson

LUNDS
UNIVERSITET

DOCTORAL DISSERTATION

Doctoral dissertation for the degree of Doctor of Philosophy (PhD) at the Faculty of Science at Lund University to be publicly defended on 16th of September at 10.00 in Blå Hallen, Sölvegatan 37, Lund

Faculty opponent
Anders Bryn

Organization LUND UNIVERSITY Faculty of Science Center for Environmental and Climate Science Author: Adrian Gustafson	**Document name** DOCTORAL DISSERTATION **Date of issue** Sponsoring organization

Title and subtitle
On the role of terrestrial ecosystems in a changing Arctic

Abstract

The global temperature rise is proportional to the cumulative amount of CO_2 emissions to the atmosphere. This observation is consistent between climate models and historical observations. It has also given rise to the concept of a carbon budget, which sets a threshold for the amount of CO_2 that can be emitted into the atmosphere while still fulfilling political goals such as the Paris Agreement.

Terrestrial ecosystems are major regulators of greenhouse gases, not least CO_2. Since ecosystems may either buffer or add to the anthropogenic emissions depending on if the ecosystem act as a source or a sink of carbon, their functioning is vital to estimating the 'budget space' of allowable CO_2 emissions for humanity to stay away from dangerous climate change.

The Arctic not only contains vast amounts of carbon, but it also warms at a double rate compared to the globe as a whole. The warming will both mobilise carbon that is currently stored in frozen soils, but also induce vegetation shifts such as treeline advance and increased abundance of shrubs. These changes will both affect the biogeochemical cycling of Arctic ecosystems, but also interact with regional climate through changed albedo and partitioning of net radiation. The magnitude and scale of these changes are however uncertain. In this thesis, I use the dynamic vegetation model LPJ-GUESS and a version that has been coupled to a regional climate model – RCA-GUESS – to quantify these complex and interacting processes.

The thesis finds that the boreal forests will continue to be of large importance for future regulation of both carbon sequestration, nitrous oxide emissions and land-surface feedbacks. The forests acted as a large and persistent sink of CO_2 under a range of climate change scenarios. The forests will expand northward, however, simulations of local treelines revealed that the advance of treelines may be modulated by the soil nitrogen availability. The forest advance also resulted in the greatest climate warming through decreased albedo, although this effect was mostly local.

Furthermore, the northward migration of needle-leaved forests and increased abundance of shrubs contributed to indirect climate cooling through increased emissions of biogenic volatile organic compounds (BVOCs).

Tundra regions also acted as a sink of CO_2 throughout the 21st century, albeit weaker than boreal forests. Furthermore, the model generally performed worse in these areas, making reliable estimates difficult.

This thesis investigates a broad range of interactions between vegetation and climate and quantifies the feedbacks from biogeochemical cycling, land-surface change and atmospheric chemistry.

Key words Northern high latitudes, Arctic climate change, climate-vegetation feedbacks, shrubs, shrubification, treeline migration, LPJ-GUESS, RCA-GUESS, nitrogen, carbon

Classification system and/or index terms (if any)

Supplementary bibliographical information		**Language** English
ISSN and key title		**ISBN** 978-91-8039-328-7 (print) 978-91-8039-329-4 (electronic)
Recipient's notes	**Number of pages** 236	Price
	Security classification	

Signature 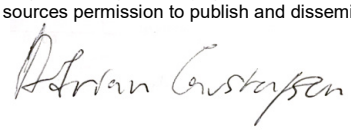 Date 2022-07-19

On the role of terrestrial ecosystems in a changing Arctic

Adrian Gustafson

LUNDS
UNIVERSITET

Cover photo by Adrian Gustafson

Faculty of Science
Center for Environmental and Climate Science

ISBN 978-91-8039-328-7 (print)
ISBN 978-91-8039-329-4 (electronic)

Printed in Sweden by Media-Tryck, Lund University
Lund 2022

Table of Contents

List of papers

I. **Gustafson, A.**, Miller, P. A., Björk, R. G., Olin, S., Smith, B 2021. *Nitrogen restricts future sub-arctic treeline advance in an individual-based dynamic vegetation model*. Biogeosciences, 18, 6329-6347. doi: 10.5194/bg-18-6329-2021:

II. **Gustafson, A.**, Miller P. A., Zhang, W., Tang, J., Björk, R. G., Smith, B. *The contribution of shrubs to Arctic land surface feedbacks*. Manuscript.

III. **Gustafson, A.**, Olin, S., Ahlström, A., Pongracz, A., Niederazik, L., Tang, J., Smith, B., Miller P. A. *High latitude terrestrial ecosystems' contribution to global warming – will the Arctic be a sink or source of greenhouse gases in the 21st century?* Manuscript.

IV. Tang, J**.**, Zhou, P., Miller, P. A., Schurgers, G., **Gustafson, A.**, Makkonen, R., Fu, Y., Rinnan, R. *High latitude vegetation changes will determine future plant volatile impacts on atmospheric organic aerosols*. Under review at Nature Portfolio. Doi: 10.21203/rs.3.rs-1143422/v1

Author contributions

I. **AG** designed the study with contributions from PAM and SO. **AG** also performed necessary model code developments and carried out model simulations and data analysis. RGB and BS contributed scientific advice and input throughout the study and contributed to the writing. **AG** prepared the manuscript with contributions from all co-authors.

II. **AG** designed the study with contributions from PAM and BS. **AG** also performed necessary code development and carried out the model simulations and data analysis. WZ and JT contributed with data and advice for the evaluation. **AG** prepared the manuscript with contributions from all co-authors.

III. **AG** designed the study with contributions from SO, AA and PAM. **AG** also performed pre-processing of forcing data for the model, and performed the simulations and large parts of the data analysis. AP performed the analysis of methane impacts on high latitude GWP in coordination with **AG**. **AG** prepared the manuscript with contributions from all co-authors. PAM contributed with a detailed model description and AP contributed to the writing of the methane section of the manuscript.

IV. JT designed the study with contributions from GS, RR, PAM and **AG**. JT perfomed model simulations with LPJ-GUESS and data analysis. **AG** also performed necessary model code developments. PZ performed model simulations with TM5 and contributed with some of the figures in the manuscript. JT prepared the manuscript with contributions from all co-authors.

Populärvetenskaplig sammanfattning

Den globala temperaturökningen är proportionell mot den totala mängden utsläpp av koldioxid till atmosfären. Detta fenomen har observerats i uppmätta historiska tidsserier och återfinns i våra klimatmodeller. Denna observation har i sin tur gett upphov till koncept så som utsläppsbudgetar, vilka anger hur mycket koldioxid som maximalt får släppas ut för att kunna hålla politiskt uppsatta mål – till exempel Parisavtalet.

Våra ekosystem reglerar till stor del flöden av koldioxid på Jorden och hur dessa fungerar nu och hur de kommer att fungera i framtiden påverkar därmed den mängd koldioxid som kan släppas ut. Ekosystemen kan antingen buffra våra utsläpp genom att ta upp mer koldioxid via fotosyntesen än de släpper ut via nedbrytning av organiskt material. Det motsatta gäller också, ekosystemen kan i stället för att ta upp koldioxid börja släppa ut mer koldioxid än de tar upp. I sådana fall minskas ’budgetutrymmet’ och den tid vi har på oss för att ställa om till ett samhälle som håller oss under 2 graders uppvärmning.

Arktiska jordar lagrar enorma mängder kol, mer än dubbelt så mycket som finns i all jordens växtlighet eller den mängd som finns i atmosfären. Stora delar av dessa jordar är frusna, men när temperaturen ökar finns en osäkerhet kring ifall en del av detta kol kommer att brytas ned och hamna i atmosfären. Små förändringar i dessa ekosystem kan få stora konsekvenser för vårt samhälle. Till saken hör dessutom att medeltemperaturen i Arktis ökar mer än dubbelt så snabbt som den globala medeltemperaturen.

När Arktis blir varmare blir också ekosystemen mer produktiva och kan ta upp mer koldioxid. Dessutom förändras vegetationen så att buskar blir vanligare och träd kan börja etablera sig längre norrut. Vegetationsförändringen medför även förändringar i markytans egenskaper såsom den andel inkommande solstrålning som reflekteras (albedo) samt hur mycket luften nära marken värms. Här finns en potentiell så kallad återkopplingseffekt – en temperaturökning sker vilket leder till ökad växtlighet, vilket i sin tur leder till lägre albedo, som till sist bidrar till ytterligare temperaturökning.

I den här avhandlingen använder jag ekosystemmodellen LPJ-GUESS för att försöka uppskatta hur snabbt växtligheten kommer att förändras samt vad det kommer medföra i form av växthusgasflöden så som koldioxid, metan och lustgas. Jag använder även en version av modellen som kopplas till en regional

klimatmodell, RCA-GUESS, för att uppskatta hur stora återkopplingseffekterna på klimatet är.

Modellen visar att Arktis kommer att bli en nettosänka av kol i framtiden eftersom skogen kommer att förflytta sig norrut, samt att växtligheten tilltar i de boreala skogar som redan finns. Detta gäller trots att stora ökningar av utsläpp av andra växthusgaser såsom metan och lustgas kan förväntas. De platser där skogen avancerar norrut riskerar dock att drabbas av en stark lokal uppvärmning till följd av lägre albedo. Denna uppvärmning verkar dock vara just lokal och inte ha så stor påverkan på hela Arktis. Dessa resultat är ganska tillförlitliga och i viss mån även förväntade.

Den ökade mängden träd, framför allt barrträd, och buskar kan också ha en annan, indirekt, effekt på klimatet. Detta eftersom de släpper ut så kallade BVOCer (detta står för 'Biogenic Volatile Organic Compounds' på engelska), alltså växtskapade flyktiga organiska ämnen. Dessa reagerar med andra ämnen i atmosfären för att till sist bilda aerosoler, alltså luftpartiklar, som både kan hjälpa till att bilda fler moln, vilka sänker temperaturen under sommaren, samt reflektera den inkommande strålningen från solen. Nettoeffekten från ökad mäng barrträd är alltså en något reducerad regional uppvärmning. Denna effekt uteblev dock i områden där lövträd avancerade eftersom dessa inte släpper ut samma BVOCer.

Till sist analyserade vi även tundra-ekosystem, där en större mängd buskar växte mot slutet av århundradet jämfört med dagens tundra-ekosystem. Dessa regioner fungerade också som kolsänkor i olika framtida klimat. Den ökade mängden buskar kan också leda till en snabbare temperaturökning nära markytan, framför allt på våren. I jämförelse med mer utbredda skogar så täcker den ökade mängden buskar en större yta, men har i gengäld mindre effekt på albedo och därmed uppvärmningen av markytan i våra simuleringar.

Att tundra-ekosystemen skulle vara sänkor av kol även i framtiden är ett mer osäkert resultat med tanke på de många studier som tyder på att tundraekosystem troligtvis kommer att släppa ut koldioxid i ett varmare klimat. Det skulle kunna vara så att modellen saknar processer som kommer att bli viktiga i framtiden, till exempel hur jordlevande bakterier och svampar hjälper till att antingen bilda ett kollager i marken, eller snabbt kunna bryta ner det ifall mer näringsrik förna tillförs, så kallad 'priming'. Dessa processer kommer att förmodligen bli framtida utmaningar att förstå bättre och implementera i våra modeller.

Popular summary

The rise in global temperatures is proportional to the total amount of carbon dioxide emissions to the atmosphere. This phenomenon has been observed in historical time-series of temperature and carbon dioxide and is consistent with climate model simulations. This observation has in turn given rise to concepts such as a carbon budget, which dictated the allowable amount of carbon dioxide that can be emitted to the atmosphere while still fulfilling political goals such as the Paris agreement.

Terrestrial ecosystems regulate large fluxes of carbon dioxide and other greenhouse gases on Earth, and how these ecosystems function in the future could thus affect the amount of carbon dioxide that can be emitted in the future. Ecosystems may either buffer anthropogenic emissions by taking up more carbon through photosynthesis than what is emitted by decomposition of organic material or add the emissions by releasing larger amounts of carbon dioxide than what is taken up. In the latter case, the 'budget space' and the time frame we have to transition into a sustainable society in order to stay below 2 degrees global warming will shrink.

Arctic soils contain vast amounts of carbon, more than double the amount that is stored in the vegetation on Earth or the atmosphere. Large parts of these soils are perennially frozen, however, when temperatures increase there is a large uncertainty as to how much of this carbon that might end up in the atmosphere as carbon dioxide. Small changes in these vast stores may thus lead to large implications for our human societies. Furthermore, temperature rise in the Arctic is more than twice as fast compared to the average global temperature rise.

As the Arctic becomes warmer, the ecosystems may also be more productive and thus sequester a larger amount of carbon dioxide. Moreover, a more productive vegetation will lead to increases in the abundance of shrubs and northward migration of trees. Changes in the vegetation will also change the properties of the land surface, such as the amount of incoming solar radiation that is reflected back to space (albedo), or the partitioning of absorbed solar radiation into surface temperature warming and evapotranspiration. Here a potential feedback may arise – temperature warming will lead to increased stature of the vegetation, which will lower the albedo with additional surface warming as a result.

In this thesis, I will use the vegetation model LPJ-GUESS to estimate how fast the vegetation change will occur in a different climate, and the implications of this for greenhouse gas fluxes such as carbon dioxide, methane and nitrous oxide. I will also

use a version of the model which is coupled to a regional climate model – RCA-GUESS – to estimate the magnitude of the feedback effects on the climate.

The model shows that the Arctic will be a net sink of carbon in the future because the forests will migrate northwards and the southern boreal forests will increase their growth. This effect will occur, despite large increases in other greenhouse gases such as methane or nitrous oxide. In the areas where forests will migrate northward, strong climate warming can be expected as a result of a lowered albedo. This temperature increase however seems to be local and does not have a large effect on the pan-Arctic climate. These results are robust, and to some degree can be expected.

The increased amount of trees, most of all coniferous trees, and shrubs may also have an indirect effect on the climate. This is because they release so called 'Biogenic Volatile Organic Compounds' (BVOCs). These compounds react with other gases in the atmosphere and form aerosols, or air particles. These may increase cloud formation and also reflect some of the incoming solar radiation, which may lower the surface temperatures in summer. The increased amount of coniferous trees may thus have a small regional cooling effect. This effect was however not seen in areas with increased broadleaved trees as these do not release the same kinds of BVOCs.

Finally, we analysed tundra ecosystems, where a shrubs became more abundant in the future compared to present day. Like forests, these ecosystems acted as carbon sinks in different future climates. The increased abundance of shrubs contributed to a faster rate of near-surface air temperature increase, especially in spring. Compared to forests, the effect on albedo – and thus warming – was smaller in our simulations, however, they cover a larger area than the expanding forest.

The result that tundra ecosystems will act as a carbon sink in the future is more uncertain given the many studies suggesting that the tundra will likely be a source of carbon dioxide in the future. The model may lack processes that will be of greater importance in the future, for instance how soil microbes will aid in soil carbon sequestration, or rapidly decompose carbon stores if more nutrient rich litter is added – so called 'priming'. These processes will comprise future challenges to understand and incorporate in our models.

List of abbreviations

AOD	Aerosol Optical Depth
BVOC	Biogenic Volatile Organic Compound
CMIP	Coupled Model Intercomparison Project
CORDEX	Coordinated Regional Downscaling Experiment
DVM	Dynamic Vegetation Model
ECS	Equilibrium Climate Sensitivity
ESM	Earth System Model
GCM	General Circulation Model/Global Climate Model
GHG	Greenhouse gas
GPP	Gross Primary Production
GWP	Global Warming Potential
IPCC	Intergovernmenal Panel on Climate Change
LAI	Leaf Area Index
LSM	Land Surface Model
LSS	Land Surface Scheme
NEE	Net Ecosystem Exchange
NPP	Net Primary Production
NPI	Normalised Phenology Index
NPMI	Normalised Physiognomy Index
PFT	Plant Functional Type
PNV	Potential Natural Vegetation
RCM	Regional Climate Model
RCP	Representative Concentration Pathway
R_a	Autotrophic vegetation
R_{eco}	Ecosystem Respiration
R_h	Heterotrophic respiration
SSP	Shared Socio-economic Pathway
SOA	Secondary Organic Aerosol
SOM	Soil Organic Matter
TBM	Terrestrial Biosphere Model
TCR	Transient Climate Response

Introduction

The global temperature increase is proportional to the cumulative emissions of CO_2 to the atmosphere (Canadell et al., 2021; Matthews et al., 2009). This carbon-climate feedback is consistent between climate models and historic trends of CO_2 emissions and warming (Matthews et al., 2009). Thus, every ton of CO_2 added to or removed from the atmosphere through anthropogenic or natural sources will affect global climate change. Terrestrial ecosystems are major regulators of greenhouse gases (GHGs) such as CO_2, and the global terrestrial ecosystems have historically buffered approximately 25% of the anthropogenic greenhouse gas emissions (Friedlingstein et al., 2019), how future ecosystems will respond to the warming is however still uncertain.

The rise in global temperatures is not evenly distributed around the globe but is almost twice (IPCC, 2021), or even three times (AMAP, 2021), as fast towards the high latitudes. During the period 1971-2019, the average Arctic surface temperature increased by 3.1°C (AMAP, 2021). This phenomenon of stronger warming towards the high latitudes is termed polar amplification. For the northern high latitudes, the phenomenon is called Arctic amplification. Unlike global warming, the relatively stronger warming towards the poles is not due to a stronger sensitivity to atmospheric CO_2 concentration in these regions but due to internal feedbacks that are stronger at the high latitudes (Serreze & Barry, 2011). An example of such a feedback that amplifies the northern high latitudes' response to warming is the loss of Arctic sea ice and associated albedo and latent heat changes (Serreze & Barry, 2011). As the climate warms a larger proportion of the sea ice is melted during summer. This exposes the comparatively much darker sea surface to the sun's radiation, which warms the surface water as the albedo is decreased. Moreover, the retreat of the insulating sea ice cover also allows for a greater latent heat flux from the ocean to the atmosphere. In autumn, the warmer ocean slows down refreeze of sea ice, which may further amplify the sea ice retreat next spring. Feedbacks also occur on land (Chapin et al., 2005; Zhang et al., 2014), and from terrestrial ecosystems, which will be discussed in this thesis.

Climate warming affects both the cryosphere, such as sea ice, glaciers and permafrost soils (soils which are frozen for two or more consecutive years), and the natural ecosystems (AMAP, 2021; Hofgaard et al., 2012). Arctic soils store an estimated 1100-1500 PgC (Hugelius et al., 2014; Schuur et al., 2015), which is double the amount stored in the atmosphere (~829 PgC) currently or what is stored

in global terrestrial vegetation (450-650 PgC)(Ciais et al., 2013). Thus, even small changes in these carbon stocks may feed back to the global climate.

The net balance between carbon uptake and release of CO_2 to the atmosphere from the terrestrial ecosystems will determine whether the Arctic will be a source or sink of carbon in the future. Warmer temperatures, longer growing seasons, and increased atmospheric CO_2 are all expected to increase photosynthetic carbon assimilation by plants (Dusenge et al., 2019; Fernández-Martínez et al., 2018), and thus the gross primary productivity (GPP). On the other hand, warming permafrost soils may mobilise carbon that is currently frozen (Schuur et al., 2015) and increase rates of soil organic matter (SOM) mineralisation (Crowther et al., 2016). Warmer temperatures and changing precipitation regimes may increase fire frequencies which may also increase the flux of greenhouse gases to the atmosphere as well as reduce the ecosystem carbon store (Bruhwiler et al., 2021; Stuart Chapin Iii et al., 2009). Although uncertain, the Arctic has been estimated to be a small sink of CO_2 in the past (Bruhwiler et al., 2021; McGuire et al., 2012). How the Arctic will respond to climate warming and other environmental perturbations is however uncertain and the quantification of the responses is an aim of this thesis.

The Arctic terrestrial land area is comprised of ~8.6% peatlands, which is a disproportionally large fraction compared to 2.6% for the globe as a whole (Xu et al., 2018). Methane (CH_4) is formed in the water-logged soils of peatlands (Bridgham et al., 2013). This makes the high latitudes an important source of natural CH_4 emissions (Saunois et al., 2020; Stavert et al., 2022). Estimates of Arctic CH_4 emissions differ somewhat with the method used to estimate them, with 9 [2-18] $TgCH_4\ yr^{-1}$ for bottom-up (process models) approaches and 13 [7-16] $TgCH_4\ yr^{-1}$ for top-down (inversion-models) approaches (Saunois et al., 2020). Estimates from process models indicate that peatlands in a strong mitigation scenario might remain a sink of CO_2 while turning into a source in the future (Qiu et al., 2022). How peatlands and their associated greenhouse gas fluxes might behave in the future is still uncertain.

Temperature estimates for the 21st century are highly uncertain, ranging from 0.34°C $decade^{-1}$ to 0.99°C $decade^{-1}$ (Cai et al., 2021). Most of this uncertainty stems mainly from uncertainties in the sensitivity of the climate system to perturbations in greenhouse gas concentrations (i.e., model uncertainty), but also from the uncertain future itself (i.e., scenario uncertainty). These large uncertainties in climate warming further make estimates of changes in the natural ecosystems and the Arctic carbon cycle uncertain.

Arctic environmental change

During the last decades, satellite observations have noted an increase in spectral vegetation greenness (Myers-Smith et al., 2020). This greenness is likely due to longer growing seasons (Bhatt et al., 2017) as well as productivity and increased biomass of Arctic vegetation (Epstein et al., 2012). Decreasing sea ice has likely contributed to warmer springs and an earlier onset of the growing season (Bhatt et al., 2017; Bhatt et al., 2010), which favours plant productivity. Site-level monitoring has revealed increases in vegetation height and other size-related traits (Bjorkman et al., 2018; Elmendorf et al., 2012), especially in regions which are not limited by moisture. Furthermore, spectral greening has often been associated with an increased abundance of shrubs (Forbes et al., 2010; Mekonnen et al., 2021).

Shrub cover

Increases in shrub cover, or 'shrubification', occur through either infilling of shrub-free patches, increased stature of shrubs, or through range expansion of shrubs into herbaceous tundra (Myers-Smith et al., 2011). Many studies report an increase in deciduous shrubs such as alder (*Alnus spp.*), willows (*Salix spp.*) and dwarf birch (*Betula nana*) (Myers-Smith et al., 2011; Ropars & Boudreau, 2012), but some studies also report increases in evergreen shrub cover (e.g., Elmendorf et al., 2012). The relative abundance of evergreen to deciduous shrubs may be driven by soil moisture, with deciduous shrubs abundant in moister conditions (Scharn et al., 2021).

The advance of shrubs is mainly linked to temperature increase but is also sensitive to soil moisture (Elmendorf et al., 2012; García Criado et al., 2020; Myers-Smith et al., 2015; Myers-Smith et al., 2011; Myers-Smith et al., 2018), but are still heterogenous and site-dependent. Shrub growth may however be modulated by soil nitrogen (Martin et al., 2022; Mekonnen et al., 2021). Shrub advance as well as the relative abundance between deciduous and evergreen types may be controlled by strong herbivory pressure (Vowles & Björk, 2018; Vowles et al., 2017).

Forest and Treeline advance

The transition from forests to tundra, the forest-tundra ecotone, is interesting to study as this is one of the world's largest ecological boundaries and represents a rather abrupt shift in ecosystem structure and functioning (Hofgaard et al., 2012). Treelines form at either high altitudes or at high latitudes, and at surprisingly similar temperature conditions, something first described by Alexander von Humboldt (Körner & Spehn, 2019). Indeed, historical treeline positions have been observed to correlate well with an air temperature isotherm of 6-7°C average growing season

ground temperature (Körner & Paulsen, 2004). However, as temperatures have warmed, treelines have not always followed. A study of global treelines found that approximately half of the reported treelines had advanced while only 1% retreated, the rest were stationary (Harsch et al., 2009). A similar large-scale pattern was found for latitudinal treelines from satellite-derived observations (Berner & Goetz, 2022). Treeline advance is however expected to continue in the future as temperatures warm (Mamet et al., 2019; Rees et al., 2020), although at what rate is uncertain.

Despite the strong historical correlations between temperature isolines and treelines that have been observed, the causes of treeline formation are still a matter of scientific discussion. Obviously, for treeline migration to occur tree species need to disperse and establish beyond their current range (Holtmeier & Broll, 2007; Lett & Dorrepaal, 2018). While latitudinal treelines may be limited by their dispersal (Brown et al., 2018; Rees et al., 2020), altitudinal treelines are often not limited by dispersal (Kollas et al., 2012; Körner, 1998). Seedlings of the treeline-forming species do however establish beyond the treeline (Hofgaard et al., 2009; Sundqvist et al., 2008), but remain stunted in their growth rather than grow into full trees. A simple explanation could include increased growth as the forests become more productive in a warmer climate with longer growing seasons, yielding increases in the carbon available for growth. Thus, this productivity, or 'source' limitation, could potentially explain the low-temperature ranges of trees. The source limitation hypothesis is however contradicted by observations of ample stores of non-structural carbohydrates in trees close to or at the treeline (Hoch & Körner, 2012; Körner, 2003). These observations in combination with indications that meristematic activity may be more sensitive to cold temperatures than photosynthesis (Körner, 2003) have yielded an opposing hypothesis that the plant-level carbon sink, i.e., biomass production, could be more limiting for growth than the source (Körner, 2015; Körner et al., 2016). Despite whether trees are limited by either their photosynthetic capacity or growth capacity, the advance of trees and forests is still expected in a warmer climate.

In Arctic regions, heterogeneity of treeline advance may be driven by differences in the snowpack. The snowpack may insulate low trees and shrubs from frost damage during the cold period, while also shortening the growing season. The thickness of the snowpack may thus either promote or inhibit the establishment of tree seedlings (Lett & Dorrepaal, 2018). Furthermore, in regions with high densities of grazers, e.g., reindeers, or browsers, i.e., moose, treelines have been hypothesised to be held back by herbivory (Cairns & Moen, 2004; Van Bogaert et al., 2011).

Feedbacks from ecosystem change

The changing landcover with an increasing abundance of shrubs and advancing treelines have both direct and indirect implications for the climate system and biogeochemical cycling.

As mentioned above, longer growing seasons and higher temperatures are expected to increase ecosystem productivity (Dusenge et al., 2019). A larger net uptake of CO_2 would constitute a cooling feedback to the global climate as CO_2 is removed from the atmosphere and stored in vegetation and soils (Bonan, 2008). Vegetation biomass has likely increased during the recent decades, storing a larger amount of carbon, although it is ambiguous whether the Arctic is a greater carbon sink due to this (Mekonnen et al., 2021, and references therein).

Warming temperatures may induce higher rates of SOM mineralisation and consequently, nitrogen mineralisation (Chapin, 1983; Nadelhoffer et al., 1991), which favours shrubs whose growth are often nitrogen-limited (Martin et al., 2022; Mekonnen et al., 2021). Nitrogen cycling in summer may be enhanced by the advancement of deciduous shrubs with higher quality litter (Buckeridge et al., 2009), measured as a lower litter C:N ratio. Tall woody shrubs, as opposed to herbaceous vegetation or low-stature shrubs, may furthermore trap snow in winter (Sturm et al., 2001). The insulating snow cover could subsequently raise winter soil temperatures and increase SOM mineralisation. Mineralisation of organic material and recycling of nutrients is often the largest source of nitrogen in tundra environments (Chapin, 1983), as such the added winter mineralisation could provide a positive feedback to shrub growth and expansion (Sturm et al., 2001). Encroachment of low evergreen shrubs, would on the other hand not necessarily cause this snow-trapping, and could through their relatively more recalcitrant litter contribute to increased soil carbon sequestration (Vowles & Björk, 2018). There are also indications that taller shrubs with larger canopies could lower surface soil temperatures in summer as they absorb incoming solar radiation (Blok et al., 2010), which could reduce permafrost degradation.

Tall woody vegetation that protrudes through the snow could however contribute to biogeophysical feedbacks through a decreased albedo of up to 30% in winter and spring (Sturm, 2005). Similarly, conversion from tundra to forested ecosystems is associated with reduced albedo with warming consequences (de Wit et al., 2014; Zhang et al., 2013). Due to the low albedo during the snow season, the biogeophysical effects of boreal forests are vital to land surface feedbacks to local and regional surface temperature (Bonan, 2008). Forest canopies on the other hand provide a relatively stronger latent heat flux from the land surface compared to tundra ecosystems, which may cool the climate in summer (Zhang et al., 2014). Coniferous forests differ from deciduous forests in their partitioning of sensible and latent heat flux – the so-called Bowen ratio (Bonan, 2008). Deciduous forests

produce a relatively larger sensible heat flux in summers compared to coniferous forests, which have a larger fraction of sensible heat flux (Bonan, 2008).

An indirect feedback to the regional climate may arise from plant emissions of Biogenic Volatile Organic Compounds (BVOCs). Plant-emitted BVOCs are mainly comprised of different terpenoids, including isoprene and different species of monoterpenes (Penuelas & Staudt, 2010). The generation of BVOCs is linked to photosynthesis and is thus subject to factors such as nutrients, water availability and CO_2 concentration. BVOC emissions are also positively linked with temperatures (Yli-Juuti et al., 2021). However, high concentrations of CO_2 could inhibit BVOC production (Almut Arneth et al., 2007). The BVOC species emitted is highly dependent on plant species, and so the vegetation composition is of high relevance when predicting BVOC emissions (Penuelas & Staudt, 2010).

The emitted BVOCs are part in a series of atmospheric chemical reactions which result in increased concentrations of secondary organic aerosols (SOA) and cloud condensation nuclei (CCN)(Roldin et al., 2019). Aerosols scatter incoming solar radiation and act as CCNs. Anthropogenic aerosol concentrations are lower in the Arctic, which may result in a relatively larger impact on the regional climate from plant-emitted aerosols. This would provide a negative feedback to the climate (Yli-Juuti et al., 2021). The strength of this feedback and the sensitivity of BVOC emissions to increasing plant productivity, CO_2 concentration and vegetation composition under future conditions are however not very well quantified.

Investigating Arctic environmental change

In this thesis, modelling will be the main tool for investigating Arctic environmental change. It is thus worth writing a few sentences on different kinds of models and the context in which they are used.

A model is an abstraction of reality. Analogous to a map of a landscape, the model cannot be said to include all features and details of the landscape. However, by studying the map we might understand something about the landscape, like how long the distance from A to B is, if the terrain will be easy or difficult and how long it would take us to get there. Like map-reading, modelling and the studying of models is a skill that needs to be learnt.

Kinds of models

Models come in different kinds, shapes and forms. They differ in what system they represent, and their temporal and spatial resolution. Furthermore, while the

overarching system that is represented is similar, the models differ in what processes they include and how these are represented, i.e., their structure.

General circulation models (GCMs), also called global climate models, simulate variations in global climate over space and time in response to atmospheric greenhouse gases. Most of today's GCMs incorporate a coupling between the ocean, sea ice, and the atmosphere but may also account for a dynamically changing landcover. The land surface part of a GCM is often referred to as a land surface scheme (LSS) or land surface model (LSM). These vary greatly in complexity and but generally need to include processes to solve the fluxes of energy and water between the land-surface and the atmosphere. LSMs generally also simulate runoff from land to lakes and oceans, thus incorporating the terrestrial hydrologic cycle. GCMs that also incorporate the full carbon cycle, of which the land component is a vital part, are referred to as Earth System Models (ESMs).

GCMs generally operate on a coarse grid, ranging from approximately 100x100km up to 250x250 km in size., although the resolution has increased as computing power has increased. To overcome this gap, especially for purposes of climate impact studies, Regional Climate Models (RCMs) have been developed. These models can be viewed as a 'box' over a geographic domain and operates on a grid with finer resolution, from approximately 50 km down to 1 km. They require large scale climate at the domain boundaries as input as well as atmospheric greenhouse gas concentrations. Furthermore, RCMs may be designed to be generic and applicable to most regions of the Earth or be specialised to one specific region of the Earth, e.g., the Arctic.

Parallel to the development of climate models, Terrestrial Biosphere Models (TBMs) have been developed. Their mission is to simulate the distribution and functioning of terrestrial ecosystems in response to climate and other forcing variables such as atmospheric CO_2 concentration, land-use and nitrogen deposition. Thus, their use is somewhat overlapping to that of LSMs. A special case of TBMs is Dynamic Vegetation Models (DVMs) in which the vegetation is evolving over time in response to external forcing. DVMs often include the carbon cycle and detailed ecological processes such as succession, competition for resources, disturbance and fire.

CMIP programmes

The earth system's response to perturbations such as increased greenhouse gas concentrations in the atmosphere and land-use change is uncertain. Furthermore, the models intended to quantify these responses have different conceptualisations, which add another uncertainty to the future projections of the earth system. The coupled model intercomparison project (CMIP) is an organised effort to compare and evaluate GCMs with a coupled atmosphere and ocean. Phase 5 of CMIP (CMIP5; Taylor et al., 2012) also included a few GCMs with dynamic vegetation

and the coupled climate-carbon cycle. The CMIP phases are also major inputs to the Intergovernmental Panel on Climate Change (IPCC) assessment reports.

Two emergent model properties are given particular importance in the evaluation. The Equilibrium Climate Sensitivity (ECS) is the amount of global surface temperature warming between two climate equilibriums associated with an abrupt doubling or quadrupling of atmospheric CO_2 concentration. The ECS was constrained to a likely range of 1.5-4.5 K in the fifth assessment report (IPCC, 2013). A notable difference between CMIP5 and CMIP6 is that the ECS is beyond this range for several GCMs in the latter (Nijsse et al., 2020; Tokarska et al., 2020), something that has been attributed to a stronger cloud feedback (Zelinka et al., 2020). The second property which is important for model evaluation is the transient climate response (TCR). This is the response of a yearly 1% increase in atmospheric CO_2 concentration over 140 years.

CORDEX

The coarse spatial resolution used by the GCMs is often judged as irrelevant for climate impact studies. The COordinated Regional Downscaling EXperiment (CORDEX) was organised as an effort to dynamically downscale the large spatial resolution simulated by the CMIP5 GCMs (Giorgi et al., 2009; Jones et al., 2011). The project has set up standardised domains for RCMs globally which participating models can utilise. The CORDEX project evaluates RCMs and is a standard part of CMIP6 (Gutowski Jr et al., 2016).

Scenarios

The socio-economic development of the world is another uncertainty in projections of the future. Thus, common drivers have been developed under the different CMIP programmes. For the CMIP5 experiments, different greenhouse gas concentration scenarios were created, termed Representative Concentration Pathways (RCPs) (Moss et al., 2010; Taylor et al., 2012). These build on a range of projections of population growth, policy interventions and technological developments. The labelling of the scenarios corresponds approximately to the amount of resulting radiative forcing in the year 2100 compared to pre-industrial conditions. Consequently, RCP 8.5 corresponds to an increased radiative forcing of 8.5 W m^{-2}.

During CMIP6 the scenarios were designed from narratives of the future development of the world (Meinshausen et al., 2020; O'Neill et al., 2016). Five narratives, or Shared Socio-economic Pathways (SSPs), were designed from different combinations of challenges for climate change mitigation and adaptation efforts (O'Neill et al., 2017). Qualitative descriptions of factors such as population growth, economic and technological development, use of fossil fuels, etc were combined to produce the five pathways. The five SSPs are sustainability (SSP1),

Middle of the road (SSP2), regional rivalry (SSP3), Inequality (SSP4), and Fossil-fueled development (SSP5). The SSPs were later integrated with the RCPs to create scenarios of the future, for instance SSP1-2.6 for the sustainability-pathway where radiative forcing is approximately 2.6 W m^{-2} at the end of the century.

Aims and objectives

This thesis aims to broadly investigate the role of high latitude vegetation shifts on climate and biogeochemical cycling. Furthermore, a large part of the work is aimed at evaluating the models used in each study. The overall aims and objectives of the thesis are:

- To estimate future Arctic vegetation shifts
- To identify drivers and modulating factors of high latitude vegetation change
- To quantify the direct and indirect climate effects of vegetation change
- To quantify the high latitude greenhouse gas fluxes in order to determine the contribution of 21st-century climate change.

This will be done through four separate studies presented in four separate papers.

Paper I

In this paper, we aimed at evaluating the processes in the model at a local level where plenty of comparison data is available. We also wanted to estimate the rate of future treeline advances and changes in shrub cover and disentangle their drivers.

Paper II

This paper will aim at investigating the direct, i.e., albedo and latent heat, climate feedback from vegetation change. Furthermore, the paper will evaluate the regional ESM RCA-GUESS against historic climate data.

Paper III

This paper will investigate the effects of changed vegetation on biogeochemical cycling and greenhouse gas generation from natural ecosystems. The paper aims at quantifying net emissions of CO_2, CH_4 and N_20 under four different future scenarios.

Paper IV

This paper aims at quantifying the indirect climate feedback from BVOC emissions under five different future scenarios.

Methods

Model description

LPJ-GUESS

The Lund-Potsdam-Jena General Ecosystem Simulator (LPJ-GUESS) is an individual-based dynamic vegetation model optimised for regional and global applications (Smith et al., 2001; Smith et al., 2014), although it is not restricted to this scale.

The basic simulation unit in the model is a gridcell of arbitrary size. The gridcell is then further divided into separate stands of which the fraction of the gridcell is specified in the model instructions. The stands represent different landcover classes and enable the simulation of land-use and land-use change. The standard landcover class is the potential natural vegetation (PNV), i.e., the assumed vegetation that would be naturally present based solely on climatic, soil and nitrogen deposition conditions of each site. Additional landcover classes that the model is capable of simulating are peatlands, managed forests, pastures and agricultural crops. Each stand further includes a number of patches, intended to represent heterogeneity within each stand. The number of patches in each stand may vary, where anthropogenically managed stands generally only have one patch and naturally varying stands have more patches. The model output is the average of all the patches in each stand. Stochastic processes in the model, such as fire, disturbance, mortality, and establishment, are simulated on the patch level.

Vegetation and Plant functional types

Vegetation is represented by plant cohorts belonging to a set of Plant Functional Types (PFTs). These are generalisations of plant species with similar life forms (tree, shrub, grass or moss), life history strategies (shade tolerance, longevity, etc) and phenology class (deciduous or evergreen). A cohort is a group of equally aged individuals. In a patch, differently aged cohorts are competing for light, water and nutrients. The vegetation structure in the model is the emergent outcome of the competition between cohorts of the same and different PFT in each patch. Competition for light and nitrogen is asymmetric, i.e., the individual with the largest canopy or root biomass will have an advantage in the competition under scarcity.

Water uptake is symmetrically distributed among individuals based on root fractions and water availability in each soil layer. The PFTs also have a pre-determined bioclimatic envelope within which they are allowed to establish. The bioclimatic envelope sets a hard limit on vegetation distribution while competition can potentially limit the geographical distribution of a PFT.

LPJ-GUESS traditionally include a set of global PFTs, ranging from the tropics to the boreal and tundra regions. In this thesis, only boreal and tundra species will be in focus. In addition, six additional shrub PFTs have been parameterised and calibrated in this thesis. These shrub PFTs include evergreen and deciduous PFTs of each physiognomic class tall, low and prostrate shrub.

Carbon and nitrogen cycling

Fluxes of carbon and water in the canopy are modelled in a coupled photosynthesis and stomatal conductance scheme adopted from the BIOME3 model (Haxeltine & Prentice, 1996). Plant respiration is comprised of three parts: leaf, maintenance and growth respiration. Leaf respiration is set as a fixed fraction of plant assimilated carbon. Growth- and maintenance respiration on the other hand is dependent on temperature, biomass, and stoichiometric constraints. The remaining assimilated carbon after respiration is allocated to new plant biomass, following a set of predefined allometric rules. The leaf:root ratio is however set dynamically, where an individual will allocate a larger part of the carbon to the roots if stressed by nitrogen limitation or drought.

The decomposition of plant litter in the model is modelled through a CENTURY-based soil scheme (Parton et al., 2010; Parton et al., 1993; Smith et al., 2014). This is a type of box-transfer scheme, where decomposing litter is transferred between pools of SOM of differing recalcitrance. The rate of the transfer is based on first order Michaelis-Menten kinetics. For each time step, a fraction of the carbon mass is lost as CO_2 to the atmosphere.

Nitrogen is added to the system either through deposition, biological fixation or (in managed stands) as fertilisation. The biological fixation of nitrogen is based on an empirical relationship to evapotranspiration (Cleveland et al., 1999). Nitrogen is also mineralised from SOM decomposition and a fraction of the mineralised nitrogen is immobilised by the soil microbes. The amount of immobilised nitrogen is dependent on stoichiometric requirements for each SOM-pool. If microbial demand for nitrogen exceeds the supply, the decomposition rate is reduced. Nitrogen is also lost from the system, either through leaching or through volatilisation from wildfires.

Spinup and initialisation

To initialise LPJ-GUESS, a 500-year spinup is conducted. During this spinup, a 30-year detrended reference climate is used, usually extracted from the first 30 years of

the forcing climate dataset. LPJ-GUESS starts with bare ground, which is subsequently built up during the spinup towards an equilibrium between climate, vegetation distribution and the carbon cycle.

Methane module

The methane module of LPJ-GUESS was adopted from the implementation in the LPJ DGVM (Wania et al., 2009a, 2009b, 2010). Methane dynamics are simulated on a separate peatland stand. In this stand the soil column is divided into a catothelm, which is permanently flooded, and an acrothelm, which has a fluctuating water table. The depth of the acrothelm is fixed to 30 cm. The peatland stand furthermore has additional associated PFTs, which have specific peatland properties, for instance, aerenchyma and tolerance to inundation stress. The peatland PFTs include two peatland shrubs, flood tolerant C_3 grasses and graminoids as well as a *Sphagnum spp.* moss PFT.

The CENTURY-based SOM decomposition scheme provides the substrate input for CH_4 generation. Furthermore, the production of CH_4 in each soil layer is dependent on the O_2 availability in that layer. CH_4 is reduced through oxidation to CO_2 in each layer after production. This rate is dependent on the layer O_2 concentration in such a way that the stoichiometric constraints can be satisfied.

$$CH_4 + 2O_2 => CO_2 + H_2O$$

CH_4 can escape to the atmosphere through three pathways: diffusion, plant-mediated transport and ebullition. The gas diffusion equation for both O_2 and CH_4 is numerically solved by the Crank-Nicholson method. The diffusivity of each gas is dependent on the temperature in each layer and the layer porosity. Plant-mediated transport of CH_4 only occurs in aerenchymatous PFTs and is dependent on the fraction of roots in each soil layer as well as on the cross-sectional area of the plant tillers. Finally, plant ebullition is determined by a threshold set by the maximum CH_4 solubility at a given soil temperature. If the produced CH_4 concentration exceeds this threshold after oxidation, diffusion or plant transport, the excess gas is released into the atmosphere.

BVOC module

LPJ-GUESS includes a BVOC module capable of simulating emissions of both isoprene and monoterpenes (A. Arneth et al., 2007; Schurgers et al., 2009). The rate of BVOC production is derived from the photosynthetic electron transport part (J). A PFT-specific standardised parameter, ε_s, for each BVOC type is used to determine the fraction of the electron transport rate that is attributed to the production of a specific BVOC. This value of this parameter is determined from measured emissions under standard conditions. Furthermore, this standardised parameter is modified by the leaf temperature and a CO_2 factor. The CO_2 factor acts inhibiting to

BVOC production under concentrations larger than pre-industrial (370 ppm) and enhancing for concentrations below this concentration. Isoprene generation is further modified by a seasonality factor which is determined by the growing degree day (GDD_5) requirement for production in spring and by temperature and day length in autumn. Monoterpenes may also have an optional storage pool, which size is set by a PFT-specific parameter, *m*. Emission from this pool is then calculated by dividing the storage pool size by a temperature-dependent turnover.

RCA-GUESS

RCA4 – a regional atmospheric model

The Rossby Center Atmospheric model is a generic RCM intended for dynamic downscaling of global climate at any location of the Earth (Samuelsson et al., 2015; Samuelsson et al., 2011). In this thesis, the dynamic coupling to the LSS of RCA4 was updated, originally described by Smith et al. (2011). Arctic applications of the model have previously not included any nitrogen dependencies, permafrost or soil freezing. Furthermore, only the global set of PFTs has been used in previous studies, i.e., no explicit representation of shrubs.

The LSS of RCA4 is a tiled LSS, meaning that each gridcell is divided into smaller fractions with different landcover classes, not unlike the division of LPJ-GUESS. Three landcover tiles are represented in the model. These include a forest fraction, an open land fraction and a fraction for snow on open land. Additionally, the forest has a snow-covered sub-tile. In its stand-alone implementation, RCA4 receives information about the size of each tile from the ECOCLIMAP (Masson et al., 2003) map over landcover parameters along with other landcover information. The parameters are provided on a monthly basis but are not evolving during the simulation.

Model coupling

In the coupled model, which is used in this thesis, LPJ-GUESS is fed daily temperature, precipitation and net shortwave radiation calculated by RCA4. LPJ-GUESS then simulates the daily LAI and updates the landcover fractions on an annual basis. The forest is further divided into fractions of deciduous and evergreen forests. LPJ-GUESS also simulates biogeochemical cycling of the land surface; however, this output is not used by RCA4.

The spinup of RCA-GUESS is performed in two steps. In the first step, each model is first spun up separately. LPJ-GUESS, which requires a longer time to spin up, runs its standard 500-year spinup forced with CRU-NCEP (Viovy, 2018) while RCA4 is forced by the selected boundary conditions. The two models are then run in the coupled mode for 30 years to be able to equilibrate. Data from this part of the spinup is saved and detrended for the second stage in the spinup. During the second

spinup stage, LPJ-GUESS is forced with the climate generated by RCA4 during the first spinup stage, while RCA4 is forced with land surface parameters generated with LPJ-GUESS. Finally, the models are run in coupled mode with transient climate and greenhouse gas forcings.

Paper I

In this paper, we employed LPJ-GUESS over the Torneträsk region in northern Sweden. The model was forced with a spatially highly resolved (50m x 50m) local climate dataset, generated by Yang et al. (2011). The temperature data was generated using local loggers, placed in the terrain to capture meso- and microclimatic features such as lapse rates, aspect and local lake effects. The microclimatic features were then extended back in time by Yang et al. (2011) using the long climate record measured at the Abisko Scientific Research Station (ANS). The historic data was created at a monthly resolution between the years 1913 to 2000.

To simulate future vegetation change we similarly extended the climate dataset into the future between the years 2001 to 2100. Using three CMIP5 GCMs as sources for macroclimatic changes under one low (RCP 2.6) and one high (RCP 8.5) emissions scenario, the projection climate was created. An additional 'no trend' climate scenario was created by randomly sampling from the historical dataset. The GCM climate for the gridcell containing the Abisko area was extracted. This climate was then bias-adjusted against each gridcell in the microclimatic dataset generated by Yang et al. (2012). Bias adjustment was done through the delta-change approach. In this method an average monthly bias is generated by comparing a 30-year reference period in two datasets. The difference is subsequently added or multiplied to the climate variable to adjust the bias in that dataset. Nitrogen deposition from both historic and scenario periods were extracted from the dataset by Lamarque et al. (2013).

We then performed model runs of future treeline advance and shrub increase for all GCMs and scenarios where all forcing variables were transient. To disentangle the driving factors, we subsequently performed a factorial model experiment where each factor, climate, nitrogen deposition and CO_2 were varied one at a time. To make the CO_2 and nitrogen deposition scenarios more robust, we added two CO_2 scenarios (RCP 4.5 and RCP 6.0) and four nitrogen deposition scenarios. Since nitrogen deposition is projected to decrease in this area, we added scenarios where deposition increased by 2.5x, 5x, 7.5x and 10x compared to the year 2000 value.

The model was evaluated against data from local observations. We collected data for treeline position (Callaghan et al., 2013), treeline advance (Van Bogaert et al., 2011), biomass change (Hedenås et al., 2011), shrub densification (Rundqvist et al., 2011), LAI (Ovhed & Holmgren, 1996), and GPP (Olsson et al., 2017).

Paper II

In this paper, we employed the regional Earth system model RCA-GUESS over the Arctic CORDEX domain (https://cordex.org/domains/region-11-arctic/, last accessed 2022-03-21). The simulations were purely historic and driven with ERA-Interim reanalysis data at the domain boundaries. As described above, LPJ-GUESS was coupled to the regional atmospheric model RCA4 to simulate the biogeophysical effects of dynamic vegetation change.

We performed two simulations with RCA4. In the first simulation the standard set of PFTs, which are usually included in GCMs. In the second simulation, the six shrub PFTs developed for this thesis were added to the standard set of PFTs. The effects of including shrubs in an ESM were estimated by differencing the dynamic vegetation run in each simulation pair, as well as comparing absolute values against each other and evaluation data.

The Arctic is a vast and data-sparse area. Large-scale evaluation data for models are thus often satellite inferred or upscaled from a few measurement stations. For climate variables, reanalysis datasets such as ERA-Interim (Dee et al., 2011) are commonly used for model evaluation as these are often considered the most reliable. In our study, we compare the model vegetation output to GLASS-GLC (Liu et al., 2020) for landcover changes, GIMMS (Mao & Yan, 2019) for LAI climatology. The climate generated is compared against ERA-Interim to discover any biases in the simulated climate. Furthermore, we evaluate albedo against both ERA-Interim and the GlobAlbedo product (Muller et al., 2012). Latent heat flux was furthermore evaluated against the upscaled eddy-covariance data by Jung et al. (2011). Annual carbon fluxes were also evaluated against upscaled flux data by Virkkala et al. (2021).

Paper III

In this study, we used LPJ-GUESS forced with daily weather data generated from three CMIP6 GCMs under four future scenarios (SSP1-2.6, SSP2-4.5, SSP3-7.0 and SSP5-8.5). In addition, a purely historic simulation with CRU-NCEP (Viovy, 2018) was conducted for evaluation purposes. All weather data, including CRU-NCEP, were re-gridded and bias-adjusted against the Watch Forcing Data Era-Interim (WFDEI) dataset (Weedon et al., 2014) as a pre-processing step. Re-gridding was done bilinearly using the Climate Data Operator tool. Bias-adjustment of the climate data was done using the ISI-MIP approach (Lange, 2019). This approach uses quantile mapping rather than simple differencing approaches, such as the one used in **Paper I**. Quantile mapping preserves both trends and extreme values better than the delta-change approach. For this paper, we used a domain comprised of all terrestrial land north of 60°N.

The study makes use of newly implemented features in LPJ-GUESS, allowing simulations of permafrost, peatlands, CH4-fluxes (described above), and N_2O emissions. The N_2O emissions are enabled by a new nitrogen scheme, adapted from Pilegaard (2013). Furthermore, the new model implements a new fire model, SimFIRE-BLAZE (Knorr et al., 2014; Pellegrini et al., 2018; Rabin et al., 2017). These new features enable an analysis of climate feedback from non-CO_2 greenhouse gases as well as CO_2 from high-latitude ecosystems.

To compare the climate effect of the simulated greenhouse gas emissions we calculate the Global Warming Potential over a 100-year time window (GWP_{100}). The conversion from emissions to CO_2eq was done by first summing the fluxes of each gas over the domain and then multiplying them with each gas's respective global potential factor. Conversion to CO_2eq was done by multiplying CH_4 with a factor of 27 while N_2O was multiplied by 273 following the updated values from the IPCC Sixth Assessment report (Forster et al., 2021). CO_2 by definition has a factor of 1 for conversion to CO_2eq.

The model was evaluated against several datasets. Simulated biomass carbon densities were evaluated against satellite inferred estimates of aboveground biomass (Liu et al., 2020). The GPP, R_{eco} and NEE were evaluated against Virkkala et al. (2021) as in **Paper II**. An upscaled eddy-covariance CH_4 dataset by Peltola et al. (2019) for seasonality patterns and total emissions. We also compare our simulations to other estimates of CH_4 (Saunois et al., 2020) and N_2O (Voigt et al., 2020).

Paper IV

In this study, LPJ-GUESS was employed together with the atmospheric chemistry transport model version 5 (TM5; Bergman et al., 2022). First, LPJ-GUESS was forced with monthly climate data from 3 different GCMs under five of the CMIP6 SSPs (SSP1-1.9, SSP1-2.6, SSP2-4.5, SSP3-7.0, SSP5-8.5). The GCMs were selected to represent a broad range of climate sensitivities, one high (CanESM5), one medium (MRI-ESM2-0) and one low (GFDL-ESM4) sensitivity GCM were selected. The 15 (3 GCMs x 5 SSPs) scenarios covered a broad range of climate warming by the end of the century, ranging from 1°C to 12°C for the region. LPJ-GUESS were run for each scenario, simulating vegetation composition and emissions of isoprene and monoterpenes.

In addition to the 15 scenarios, factorial experiments using only one GCM (CanESM5) under two (SSP1-1.9 and SSP5-8.5) scenarios were conducted. These factorial experiments were done to test the modelled BVOC emission's sensitivity to CO_2, nitrogen deposition, climate, and vegetation change. This was done by either keeping the CO_2 concentration experienced by vegetation constant (noCO_2) or keeping the CO_2 concentration experienced by isoprene synthesis constant

(noCO2Iinhibition), and in another run, vegetation distribution was not allowed to change (noVegDym). Lastly, nitrogen deposition was increased in one final run so that nitrogen could be assumed to not be limiting for vegetation productivity (noNlim).

Secondly, vegetation LAI and composition as well as BVOC fluxes were fed into TM5 for atmospheric calculations of secondary organic aerosols (SOA) generation and aerosol optical depth (AOD). Due to the expensive computational requirements of TM5, the simulations were only run for the year 2009. Furthermore, TM5 was forced with ERA-Interim (Dee et al., 2011) and thus the climate change impacts were not analysed in this part of the paper.

Finally, radiative forcing due to atmospheric SOA changes was calculated from the TM5 results for the factorial experiments.

Results and discussion

Vegetation change and its drivers (Paper I, III and IV)

On the local scale, in Abisko (**Paper I**), LPJ-GUESS simulated a historic treeline advance of 0.84 m yr^{-1}. This can be considered to be within the range of available estimates for the area of approximately 0.6 m yr^{-1} (Van Bogaert et al., 2011). The observed average is influenced by a severe moth out-brake that is not accounted for in the model, which induced treeline retreat in some parts of the region.

The rate of this elevational shift continued into the projection period with a rate of between 0.45 to 1.95 m yr^{-1} depending on the GCM scenario. During the historic period, the treeline tracked the theoretically limiting 6-7°C isotherm closely, however, in the projection this relationship was broken as the temperature isoline advanced faster than the treeline. Furthermore, the deviation between the treeline and the isotherm was greater in the warmer GCM scenarios. This suggests that future treeline advances may be limited by things other than temperature. This result may be regarded as contrasting from the observations of the historic global correlation between temperature and the treeline (Körner & Paulsen, 2004). Observations of current treeline positions may be robust but are by necessity a snapshot in time. It is thus difficult to infer future migration rates from the treeline-isotherm correlation alone, as have been done by some models (Paulsen & Körner, 2014).

In our results the limiting factor was nitrogen. In the projection simulations, nitrogen deposition decreased, and nitrogen mineralisation could not sustain an increased tree growth, thus limiting rates of treeline advance. This was further strengthened by the factorial experiments, where we forced LPJ-GUESS with a climate without trend but added nitrogen. Tree PFTs above the treeline that had only displayed stunted growth increased their biomass which advanced the treeline.

Factorially increasing atmospheric CO_2 increased GPP in the trees, but it did not drive treelines (Fig 1). Furthermore, the treeline trees had a positive NPP of approximately 60 gC m^{-2} yr^{-1}, indicating no carbon limitation on simulated growth at the treelines. The extent of the simulated forest is in other words not completely dependent on productivity, which is also evident from the CO_2 fertilisation experiment. Measurements of mobile carbon stores in treeline trees globally have similarly found no shortage of carbon in treeline trees (Hoch & Körner, 2012), in

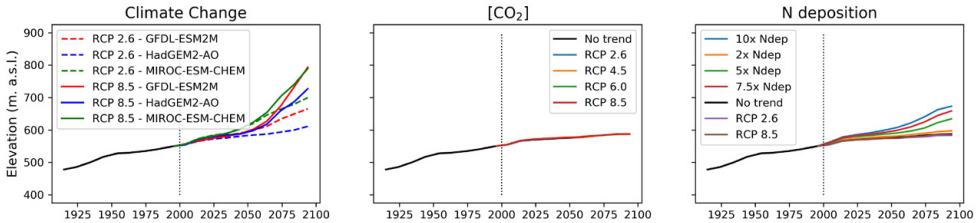

Fig 1 Simulated treeline advance and its drivers in Paper I. The data is from a model experiment with factorially changing either climate (a), CO_2 concentration (b) or nitrogen deposition (c). As nitrogen deposition decreased in the projection simulations, we added simulations where nitrogen deposition was either 2x, 5x, 7.5x or 10x the year 2000 value.

line with the results of **Paper I**. Increasing CO_2 concentration did however induce strong shifts in shrub growth, which increased their biomass with 150% above the treeline (**Paper I**). The model thus suggests that shrub growth is largely inhibited by productivity rather than nutrients.

Much of the knowledge about plant and ecosystem response to elevated CO_2 comes from Free Air CO_2 enrichment (FACE) experiments. These experiments generally show increases in leaf-level productivity (Ainsworth & Long, 2005; Walker et al., 2021), which can also be expected from what we know about plant physiology (Dusenge et al., 2019). There is however substantial uncertainty whether this increased productivity is translated into biomass (De Kauwe et al., 2014; Walker et al., 2021). The increased shrub biomass is difficult to verify since very few CO_2 enhancement experiments have been conducted above the treeline or included shrubs in the analysis. One FACE experiment in the Swiss alps did analyse shrub growth but saw mixed effects of increasing CO_2 concentration on shrub growth (Dawes et al., 2013).

On the pan-Arctic scale, tundra vegetation in our future simulations shifted towards a woodier and evergreen vegetation while the southern boreal forests were shifting from evergreen to deciduous in both **Paper III** and **Paper IV**. Both shifts could be expected as more shrubs are expected to colonise the tundra in the warmer future (Myers-Smith et al., 2015) and temperate trees could be expected to shift northwards. In **Paper I** there was a relationship between soil moisture and the abundance of deciduous in relation to evergreen shrubs, where higher soil moisture favoured deciduous vegetation. Similar relationships have also been observed from long-term monitoring (Scharn et al., 2021). The type of shrub (i.e., evergreen or deciduous) could have implications for biogeochemical cycling (Buckeridge et al., 2009; Vowles & Björk, 2018). How biogeochemical cycling in LPJ-GUESS responds to the advance of either evergreen or deciduous shrubs remains to be analysed in future studies.

Climate feedbacks (Paper II and IV)

In this section, I will analyse feedbacks to the pan-Arctic climate. I will separate between direct and indirect feedback, where the direct feedbacks stem from albedo changes or changes in the partitioning of latent to sensible heat flux (analysed in **Paper II**). The indirect feedbacks stem from the emissions of BVOCs which feed back to the climate through the formation of SOA and CCN with subsequent effects on cloud formation and light scattering (analysed in **Paper IV**).

In our coupled simulations with interactive climate-vegetation feedbacks, the inclusion of shrubs increased the rate of climate warming over mid-Siberia and the Canadian Archipelago by approximately 2°C over the time-period 1981-2013 (Fig 2), corresponding to a rate of approximately 0.66°C decade^{-1} of additional warming in these areas in spring due to the inclusion of shrubs. Summer warming was however much more moderate with slightly additional warming over the Siberian tundra and cooling over Northern Canada.

The largest differences in warming were however due to differences in tree cover in a few gridcells in Siberia. The much-lowered albedo in these gridcells contributed to differential warming of over 8°C in spring and up to 1.5°C in summer. Additional warming due to this effect was however only localised to those few gridcells. The differences in forest extent could be attributed to a competitive effect between shrubs and trees in the model which reduced the extent of the tree cover. These results highlight the potential importance of treeline advances for climate feedbacks.

The inclusion of shrubs amplified warming in some areas but reduced it in others. The net effect of including shrubs in our simulation on the pan-Arctic climate was however not statistically significant.

Finally, the RCA-GUESS simulations displayed a large cold-bias over the tundra region in our comparison against the ERA-Interim reanalysis data (Dee et al., 2011). This cold bias was amplified in our simulations with dynamic vegetation compared to stand-alone RCA4 (Berg et al., 2013) which has prescribed land-surface parameters. The colder temperatures simulated by RCA4 created a reinforcing negative feedback loop where the original cold-bias reduced vegetation productivity and nitrogen mineralisation while simultaneously lowering soil temperatures and the plant available water. The reduced vegetation in turn drove an over-estimation of albedo and subsequently amplified the cold bias. This response has likely not been present in previous RCA-GUESS simulations

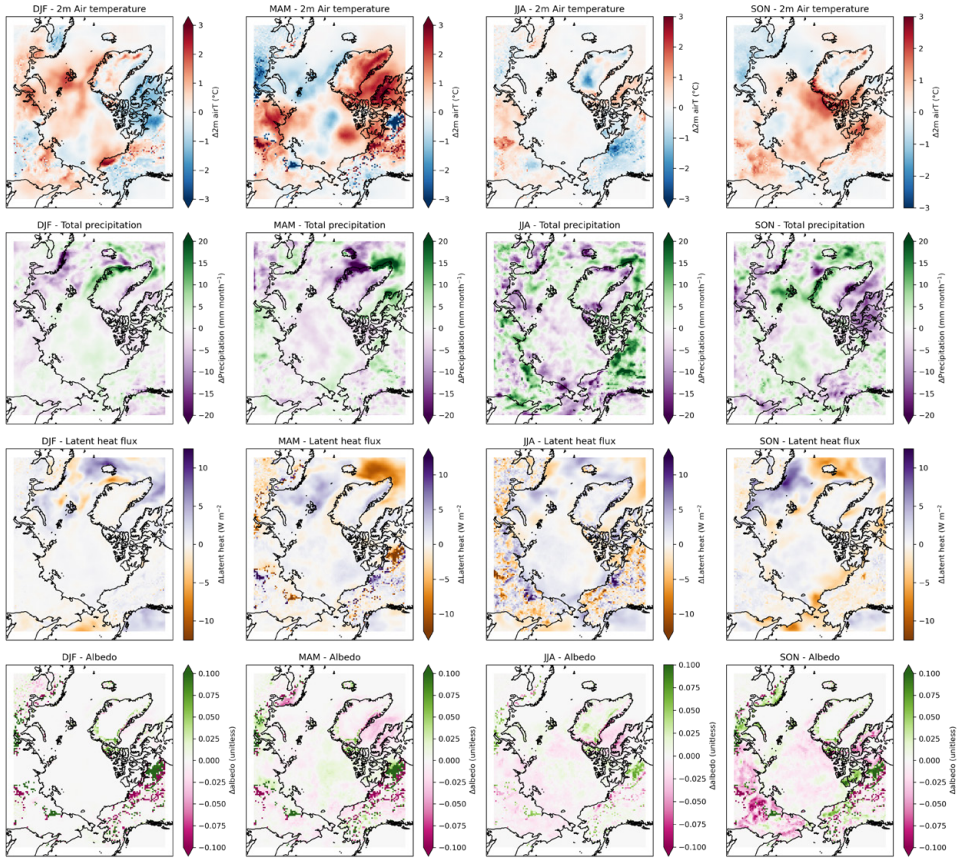

Fig 2 Difference in seasonal 2m air temperature (top row), latent heat flux (middle row) and albedo (lower row) change from inclusion of shrubs in the simulations. Values are the difference in each variable between the end (2008-2013) and start (1980-1985) and between simulations (Shrub – NoShrub). Figure is from Paper II.

(e.g., Zhang et al., 2020; Zhang et al., 2014; Zhang et al., 2018) as these have not included frozen ground or carbon-nitrogen interactions. Such a bias should probably be resolved before any simulations of future climate change feedbacks are attempted with this version of the model.

The simulated BVOC emissions in **Paper IV** were highly dependent on the type of vegetation climate scenario, where isoprene emissions increased with up to 120% in the GCM with the highest climate sensitivity (CanESM5), while monoterpenes increased by 36%. In the GCMs with lower climate sensitivity, the isoprene emissions did not increase significantly, and monoterpene emissions decreased. Vegetation distribution and composition were found to be a strong driver of BVOC emissions, while CO_2 inhibition strongly modulated the emitted BVOCs in the high

emission scenarios, which was evident from the factorial runs when the CO_2 inhibition was removed. In the southern parts of our simulation domain, broad-leaved trees expanded at the expense of needle-leaved trees resulting in reductions in monoterpene emissions. Contrary to this, isoprene emissions increased in the high Arctic as shrubs and needle-leaved trees expanded northwards.

The decreased monoterpene emissions led to a decrease in SOA formation in the lower latitudes of our domain, and thus a decrease in the SOA formation with a resulting regional warming of 0.79 Wm^{-2}. Contrary, in the high latitudes, the increased BVOC emissions had a strong effect on SOA formation and thus the SOA attributable optical depth by up to 45%. This in turn led to regional radiative cooling of -2.25 Wm^{-2} and -2.09 Wm^{-2} for the coolest (CanESM5-SSP1-1.9) and strongest (CanESM5-SSP5-8.5) warming scenario, respectively. The optical depth is a measure of the distance that the light must travel to reach the surface, and thus a proxy for the light scattering effect. Furthermore, effects on this scale are only made possible as the Arctic has a relatively low background concentration of aerosols, and thus the BVOC-induced particle formation can have a strong effect in the high latitudes.

The model results from **Paper II** and **Paper IV** display the complexity of the feedbacks from vegetation change. This thesis makes no effort in comparing or ranking the importance of the respective feedback, i.e., albedo-induced surface warming versus indirect radiative cooling from BVOC emissions, as the feedbacks are likely to interact. This will with no doubt be a topic for future studies. The results nonetheless point to the importance of including shrubs in detailed high-latitude simulations as they are involved in both feedbacks.

Feedbacks on biogeochemical cycling (Paper III)

As global climate change is dependent on CO_2 emissions to the atmosphere, the Arctic ecosystems may either modulate or amplify global warming. In **Paper III** we investigate this for the terrestrial land 60°N and for both CO_2 and non-CO_2 greenhouse gases, i.e., CH_4 and N_2O, under different scenarios of climate change.

LPJ-GUESS simulated a net cooling effect on global climate, despite large increases in both CH_4 and N_2O flux (Fig 3). Furthermore, the intermediately warmed scenarios had the strongest cooling effect, while both SSP1-2.6 and the two warmest scenarios (EC-Earth3-Veg SSP3-7.0 and EC-Earth3-Veg SSP5-8.5) more often displayed years when the region had a warming effect on global climate. The largest contributor to the net GWP_{100} was CO_2 for all scenarios, as such the net exchange of CO_2 drove the magnitude of the cooling effect.

The net CO_2 exchange was mainly determined by the boreal forests, which acted as large and persistent carbon sinks in our simulations. Tundra also acted as a net

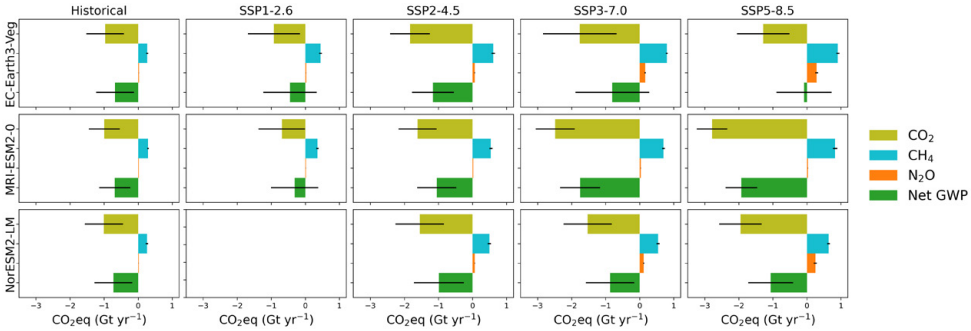

Fig 3 Contribution of each flux CO2, CH4 and N2O to net GWP100 summed over the simulation domain at the end of the historical (2001-2010) and scenario (2091-2100) periods. Black bars represent ± 1 standard deviation of interannual variability. The figure is taken from Paper III.

carbon sink, although a weaker sink than the forests, and with an increasing trend over the 21st century. On the other hand, GPP on the tundra was underestimated compared to both upscaled eddy-covariance fluxes (Virkkala et al., 2021) and satellite-derived GPP (Li & Xiao, 2019), and so the sink strength could also have been underestimated.

The boreal forests also became large sources of N_2O at the end of the century for two of the GCMs, but not for MRI-ESM2-0, which was selected as our mid-range climate sensitivity GCM. This source stemmed from excess nitrogen in the soil as nitrogen uptake by the vegetation was outpaced by the net mineralisation. Although some emerging evidence for this pathway of N_2O formation exists (Burnett et al., 2022), models of N_2O emissions in the high latitudes are still poorly constrained (Pilegaard, 2013; Voigt et al., 2020) and our results should be regarded as uncertain.

Peatland CH_4 fluxes were the second largest contributor to the net GWP_{100}. These fluxes also depended on both the hydroclimate, but also on the vegetation growing on the peatlands with peatlands that had a greater abundance of flood-tolerant graminoids being more sensitive to increasing soil temperatures.

The finding that the northern high latitudes would have a net cooling effect contrasts with expectations of the Arctic turning into a net source of CO_2 in the future (Belshe et al., 2013; Crowther et al., 2016; Schuur et al., 2015). As very few – if any – other estimates of GWP_{100} for this region under future climate change exists, it is difficult to verify or compare our results to other estimates. The results are robust within LPJ-GUESS and the results were also more dependent on scenario than previous studies suggest (Ahlström et al., 2012). The uncertainty thus seems to be smaller between GCMs than between scenarios. There is however always an uncertainty associated with the model and the model's conceptualisations of ecosystem processes. This will be briefly discussed in the outlook section.

Key findings

In this thesis I find the following key take-away messages:

- The correlation between the treeline position and the theoretically limiting 6-7°C isotherm may be broken in the future as a result of nitrogen limitations
- Treeline advance is likely important for local climate feedbacks, which is less discussed than effects on shrub increase.
- The Arctic will have a cooling effect on the global climate through increased uptake of CO_2, despite many-fold increases in the other potent greenhouse gases CH_4 and N_2O.
- Vegetation shifts may induce a slight indirect cooling from the emissions of BVOCs. This cooling is however dependent on the vegetation distribution where needle-leaved forests induced a cooling response, while broad-leaved forests had a slight positive climate warming due to the BVOC effect.

Outlook and environmental science perspective

This thesis discusses a broad range of climate-vegetation interactions which are both complex and interacting. Such a broad analysis of a large region is only made possible with a tool such as LPJ-GUESS and other DVMs. Models do offer a tractable way to estimate climate impacts and biogeochemical and biogeophysical fluxes in areas where observations are scarce or difficult to obtain or – as in the case of remotely sensed data – to verify. Without a doubt, these analyses come with a large degree of uncertainty, stemming not only from difficulties of evaluating models at the pan-Arctic or even global scale but also from the conceptualisations of the processes within the models themselves.

As a modeller it is always tempting to or even necessary to improve the realism of the model. For models to stay relevant for both policy and science, they need to evolve – it is a part of their life-cycle. This is however not unproblematic. Models are initially developed with the purpose to solve a specific set of tasks, for instance we could want to obtain an estimate of Arctic carbon fluxes and develop a model to solve this problem. As all models are flawed, there will be biases in some regions which we in the next iteration of the model would like to remidy with an added process. The added complexity may yield a more realistic result, but may also conceal a bias in the original model.

Over the course of time, the model may be given a large number of new processes and sets of purposes, some of which may remedy biases and others that may conceal them. A larger model is also more difficult to 'falsify' as it is difficult to track down biases from one part of the model that may yield biases in another part of the model. As an example from **Paper III**, it is difficult to know whether the low-bias in ecosystem respiration from the tundra is due to a bias stemming from the bias in GPP or if there is a bias or missing process in the decomposition module. The next generation of land-surface models has already been called upon to not only improve the realism, but also the robustness and reliability of the simulations (Prentice et al., 2015). I also believe that models will need to be more transparent, i.e., we need to be able to easier probe the models for process biases. In order to do this, modules may need to be broken out from the larger framework, and models would thus be 'split-up' into smaller models that can then be coupled to each other. In **Paper II** there was a large cold-bias over the tundra which was amplified by our dynamic

vegetation and improved realism of nitrogen cycling. I firmly believe that such a bias would have been harder to spot had the model not been coupled as other sub-modules could have been calibrated to compensate for such a bias. As models are common tools for assessments of future climate change, with global implications for policymaking, it is vital that these models represent the best available data and knowledge.

Science develops very quickly and new knowledge is rapidly gained in many fields. For a large-scale model, this can be difficult to keep up with to stay relevant as some of the core assumptions may become outdated. An example of a rapidly moving field where the paradigm is shifting is the cycling of soil organic matter.

Here the older humification theory is replaced with new evidence of formation of soil organic matter through microbial processes and stabilisation by the soil matrix (Cotrufo et al., 2013; Lehmann & Kleber, 2015). This may render older conceptualisations such as the CENTURY-model (Parton et al., 1993) obsolete in favour of new conceptualisations. Smaller models could be more quickly developed and tested, and also easier abandoned if deemed unrealistic. As a new paradigm forms, there may be larger uncertainties in how to represent or conceptualise processes in a model, as old explanations are no longer viable.

Bradford et al. (2016) advocate a broad range of conceptualisations in such a case. As knowledge is gained, some conceptualisations will inevitably need to be abandoned and models may converge around one or a few conceptualisations. Ideally, this should be done in cooperation between modellers and empiricists.

Models for policy

As stated in the introduction, the global average temperature increase is proportional to the emissions of CO_2 to the atmosphere. To avoid dangerous climate change and fulfil the Paris Agreement of keeping global warming below 2°C within this century and pursuing the limit of 1.5°C (UNFCCC, 2015), a threshold of maximally allowed cumulative emissions can thus be set. The concept of a carbon budget has evolved from this reasoning and transformed the problem from a flux problem (i.e., at what rate can we emit greenhouse gases?) to a stock problem (i.e., what amount of greenhouse gases can we emit?). The budget space will shrink with continued CO_2 emissions but may be expanded if carbon sinks are enhanced. The functioning of our natural ecosystems, i.e., if they turn from sources to sinks or vice versa, is in that regard vital for human societies in estimating the carbon budget space.

Models like LPJ-GUESS and other DVMs can help in determining how natural and anthropogenic ecosystems will respond to environmental perturbations. As such the models will need to be reliable and robust, and also maintain the scope for which they were developed. Furthermore, policymaking should not – and does likely not – rely on the output of a single model, but should look at ensembles of models.

Examples of such ensembles are obviously the CMIP and CORDEX programmes, but for LSMs there is also the TRENDY ensemble (Sitch et al., 2015), which compares and evaluates DVMs. Differences between models in ensembles could be regarded as a strength, as that means that a larger range of conceptualisations is covered. It is however important to find ways to constrain results from models that lie outside the plausible range of the system that is studied. Such efforts are emerging for GCMs under CMIP6 (See for instance, Nijsse et al., 2020; Tokarska et al., 2020) where future predictions are constrained by historical data. Similar efforts are still lacking for DVMs, but will likely be developed in the future.

References

Ahlström, A., Schurgers, G., Arneth, A., & Smith, B. (2012). Robustness and uncertainty in terrestrial ecosystem carbon response to CMIP5 climate change projections. *Environmental Research Letters*, *7*(4). https://doi.org/10.1088/1748-9326/7/4/044008

Ainsworth, E. A., & Long, S. P. (2005). What have we learned from 15 years of free-air CO2 enrichment (FACE)? A meta-analytic review of the responses of photosynthesis, canopy properties and plant production to rising CO2. *New Phytol*, *165*(2), 351-371. https://doi.org/10.1111/j.1469-8137.2004.01224.x

AMAP. (2021). *Arctic Climate Change Update 2021: Key Trends and Impacts. Summary for Policy-makers*.

Arneth, A., Miller, P. A., Scholze, M., Hickler, T., Schurgers, G., Smith, B., & Prentice, I. C. (2007). CO2inhibition of global terrestrial isoprene emissions: Potential implications for atmospheric chemistry. *Geophysical research letters*, *34*(18). https://doi.org/10.1029/2007gl030615

Arneth, A., Niinemets, Ü., Pressley, S., Bäck, J., Hari, P., Karl, T., Noe, S., Prentice, I. C., Serça, D., Hickler, T., Wolf, A., & Smith, B. (2007). Process-based estimates of terrestrial ecosystem isoprene emissions: incorporating the effects of a direct CO2-isoprene interaction. *Atmospheric Chemistry and Physics*, *7*(1), 31-53. https://doi.org/10.5194/acp-7-31-2007

Belshe, E. F., Schuur, E. A., & Bolker, B. M. (2013). Tundra ecosystems observed to be CO2 sources due to differential amplification of the carbon cycle. *Ecol Lett*, *16*(10), 1307-1315. https://doi.org/10.1111/ele.12164

Berg, P., Döscher, R., & Koenigk, T. (2013). Impacts of using spectral nudging on regional climate model RCA4 simulations of the Arctic. *Geoscientific Model Development*, *6*(3), 849-859. https://doi.org/10.5194/gmd-6-849-2013

Bergman, T., Makkonen, R., Schrödner, R., Swietlicki, E., Phillips, V. T. J., Le Sager, P., & van Noije, T. (2022). Description and evaluation of a secondary organic aerosol and new particle formation scheme within TM5-MP v1.2. *Geoscientific Model Development*, *15*(2), 683-713. https://doi.org/10.5194/gmd-15-683-2022

Berner, L. T., & Goetz, S. J. (2022). Satellite observations document trends consistent with a boreal forest biome shift. *Glob Chang Biol*, *28*(10), 3275-3292. https://doi.org/10.1111/gcb.16121

Bhatt, U. S., Walker, D. A., Raynolds, M. K., Bieniek, P. A., Epstein, H. E., Comiso, J. C., Pinzon, J. E., Tucker, C. J., Steele, M., Ermold, W., & Zhang, J. (2017). Changing seasonality of panarctic tundra vegetation in relationship to climatic variables. *Environmental Research Letters*, *12*(5). https://doi.org/10.1088/1748-9326/aa6b0b

Bhatt, U. S., Walker, D. A., Raynolds, M. K., Comiso, J. C., Epstein, H. E., Jia, G., Gens, R., Pinzon, J. E., Tucker, C. J., Tweedie, C. E., & Webber, P. J. (2010). Circumpolar Arctic Tundra Vegetation Change Is Linked to Sea Ice Decline. *Earth Interactions*, *14*(8), 1-20. https://doi.org/10.1175/2010ei315.1

Bjorkman, A. D., Myers-Smith, I. H., Elmendorf, S. C., Normand, S., Ruger, N., Beck, P. S. A., Blach-Overgaard, A., Blok, D., Cornelissen, J. H. C., Forbes, B. C., Georges, D., Goetz, S. J., Guay, K. C., Henry, G. H. R., HilleRisLambers, J., Hollister, R. D., Karger, D. N., Kattge, J., Manning, P., Prevey, J. S., Rixen, C., Schaepman-Strub, G., Thomas, H. J. D., Vellend, M., Wilmking, M., Wipf, S., Carbognani, M., Hermanutz, L., Levesque, E., Molau, U., Petraglia, A., Soudzilovskaia, N. A., Spasojevic, M. J., Tomaselli, M., Vowles, T., Alatalo, J. M., Alexander, H. D., Anadon-Rosell, A., Angers-Blondin, S., Beest, M. T., Berner, L., Bjork, R. G., Buchwal, A., Buras, A., Christie, K., Cooper, E. J., Dullinger, S., Elberling, B., Eskelinen, A., Frei, E. R., Grau, O., Grogan, P., Hallinger, M., Harper, K. A., Heijmans, M., Hudson, J., Hulber, K., Iturrate-Garcia, M., Iversen, C. M., Jaroszynska, F., Johnstone, J. F., Jorgensen, R. H., Kaarlejarvi, E., Klady, R., Kuleza, S., Kulonen, A., Lamarque, L. J., Lantz, T., Little, C. J., Speed, J. D. M., Michelsen, A., Milbau, A., Nabe-Nielsen, J., Nielsen, S. S., Ninot, J. M., Oberbauer, S. F., Olofsson, J., Onipchenko, V. G., Rumpf, S. B., Semenchuk, P., Shetti, R., Collier, L. S., Street, L. E., Suding, K. N., Tape, K. D., Trant, A., Treier, U. A., Tremblay, J. P., Tremblay, M., Venn, S., Weijers, S., Zamin, T., Boulanger-Lapointe, N., Gould, W. A., Hik, D. S., Hofgaard, A., Jonsdottir, I. S., Jorgenson, J., Klein, J., Magnusson, B., Tweedie, C., Wookey, P. A., Bahn, M., Blonder, B., van Bodegom, P. M., Bond-Lamberty, B., Campetella, G., Cerabolini, B. E. L., Chapin, F. S., 3rd, Cornwell, W. K., Craine, J., Dainese, M., de Vries, F. T., Diaz, S., Enquist, B. J., Green, W., Milla, R., Niinemets, U., Onoda, Y., Ordonez, J. C., Ozinga, W. A., Penuelas, J., Poorter, H., Poschlod, P., Reich, P. B., Sandel, B., Schamp, B., Sheremetev, S., & Weiher, E. (2018). Plant functional trait change across a warming tundra biome. *Nature*, *562*(7725), 57-62. https://doi.org/10.1038/s41586-018-0563-7

Blok, D., Heijmans, M. M. P. D., Schaepman-Strub, G., Kononov, A. V., Maximov, T. C., & Berendse, F. (2010). Shrub expansion may reduce summer permafrost thaw in Siberian tundra. *Global Change Biology*, *16*(4), 1296-1305. https://doi.org/10.1111/j.1365-2486.2009.02110.x

Bonan, G. B. (2008). Forests and Climate Change: Forcings, Feedbacks, and the Climate Benefits of Forests. *Science*, *320*, 1444-1449. https://doi.org/10.1126/science.1155121

Bradford, M. A., Wieder, W. R., Bonan, G. B., Fierer, N., Raymond, P. A., & Crowther, T. W. (2016). Managing uncertainty in soil carbon feedbacks to climate change. *Nature Climate Change*, *6*(8), 751-758. https://doi.org/10.1038/nclimate3071

Bridgham, S. D., Cadillo-Quiroz, H., Keller, J. K., & Zhuang, Q. (2013). Methane emissions from wetlands: biogeochemical, microbial, and modeling perspectives from local to global scales. *Glob Chang Biol*, *19*(5), 1325-1346. https://doi.org/10.1111/gcb.12131

Brown, C. D., Dufour-Tremblay, G., Jameson, R. G., Mamet, S. D., Trant, A. J., Walker, X. J., Boudreau, S., Harper, K. A., Henry, G. H. R., Hermanutz, L., Hofgaard, A., Isaeva, L., Kershaw, G. P., & Johnstone, J. F. (2018). Reproduction as a bottleneck to treeline advance across the circumarctic forest tundra ecotone. *Ecography*, *42*(1), 137-147. https://doi.org/10.1111/ecog.03733

Bruhwiler, L., Parmentier, F.-J. W., Crill, P., Leonard, M., & Palmer, P. I. (2021). The Arctic Carbon Cycle and Its Response to Changing Climate. *Current Climate Change Reports*, *7*(1), 14-34. https://doi.org/10.1007/s40641-020-00169-5

Buckeridge, K. M., Zufelt, E., Chu, H., & Grogan, P. (2009). Soil nitrogen cycling rates in low arctic shrub tundra are enhanced by litter feedbacks. *Plant and Soil*, *330*(1-2), 407-421. https://doi.org/10.1007/s11104-009-0214-8

Burnett, M. S., Schütte, U. M. E., & Harms, T. K. (2022). Widespread capacity for denitrification across a boreal forest landscape. *Biogeochemistry*, *158*(2), 215-232. https://doi.org/10.1007/s10533-022-00895-y

Cai, Z., You, Q., Wu, F., Chen, H. W., Chen, D., & Cohen, J. (2021). Arctic warming revealed by multiple CMIP6 models: evaluation of historical simulations and quantification of future projection uncertainties. *Journal of Climate*, 1-52. https://doi.org/10.1175/jcli-d-20-0791.1

Cairns, D., & Moen, J. (2004). Herbivory Influences Tree Lines. *Journal of Ecology*, *92*(6), 1019-1024.

Callaghan, T. V., Jonasson, C., Thierfelder, T., Yang, Z., Hedenas, H., Johansson, M., Molau, U., Van Bogaert, R., Michelsen, A., Olofsson, J., Gwynn-Jones, D., Bokhorst, S., Phoenix, G., Bjerke, J. W., Tommervik, H., Christensen, T. R., Hanna, E., Koller, E. K., & Sloan, V. L. (2013). Ecosystem change and stability over multiple decades in the Swedish subarctic: complex processes and multiple drivers. *Philos Trans R Soc Lond B Biol Sci*, *368*(1624), 20120488. https://doi.org/10.1098/rstb.2012.0488

Canadell, J. G., Monteiro, P. M. S., Costa, M. H., Cotrim da Cunha, L., Cox, P. M., Eliseev, A. V., Henson, S., Ishii, M., Jaccard, S., Koven, C., Lohila, A., Patra, P. K., Piao, S., Rogelj, J., Syampungani, S., Zaehle, S., & Zickfeld, K. (2021). Global Carbon and other Biogeochemical Cycles and Feedbacks. In V. Masson-Delmotte, P. Zhai, A. Pirani, S. L. Connors, C. Péan, S. Berger, N. Caud, Y. Chen, L. Goldfarb, M. I. Gomis, M. Huang, K. Leitzell, E. Lonnoy, J. B. R. Matthews, T. K. Maycock, T. Waterfield, O. Yelekçi, R. Yu, & B. Zhou (Eds.), *Climate Change 2021: The Physical Science Basis. Contribution of Working Group I to the Sixth Assessment Report of the Intergovernmental Panel on Climate Change*. Cambridge University Press.

Chapin, F. S., 3rd, Sturm, M., Serreze, M. C., McFadden, J. P., Key, J. R., Lloyd, A. H., McGuire, A. D., Rupp, T. S., Lynch, A. H., Schimel, J. P., Beringer, J., Chapman, W. L., Epstein, H. E., Euskirchen, E. S., Hinzman, L. D., Jia, G., Ping, C. L., Tape, K. D., Thompson, C. D., Walker, D. A., & Welker, J. M. (2005). Role of land-surface changes in arctic summer warming. *Science*, *310*(5748), 657-660. https://doi.org/10.1126/science.1117368

Chapin, F. S. I. (1983). Direct and Indirect Effects of Temperature on Arctic Plants. *Polar Biology*, *2*(1), 47-52.

Ciais, P., Sabine, C., Bala, G., Bopp, L., Brovking, V., Canadell, J., Chhabra, A., DeFries, R., Galloway, J., Heimann, M., Jones, C. D., Le Quéré, C., Myneni, R. B., Piao, S., & Thornton, P. (2013). Carbon and Other Biogeochemical Cycles. In T. F. Stocker, D. Qin, G.-K. Plattner, M. Tignor, S. K. Allen, J. Boschung, A. Nauels, Y. Xia, V. Bex, & P. M. Midgley (Eds.), *The Physical Science Basis. Contribution of Working Group I to the Fifth Assessment Report of the Intergovernmental Panel on Climate Change*. Cambridge University Press.

Cleveland, C. C., Townsend, A. R., Schimel, D. S., Fisher, H., Howarth, R. W., Hedin, L. O., Perakis, S. S., Latty, E. F., Von Fischer, J. C., Elseroad, A., & Wasson, M. F. (1999). Global patterns of terrestrial biological nitrogen (N2) fixation in natural ecosystems. *Global Biogeochemical Cycles*, *13*(2), 623-645. https://doi.org/10.1029/1999gb900014

Cotrufo, M. F., Wallenstein, M. D., Boot, C. M., Denef, K., & Paul, E. (2013). The Microbial Efficiency-Matrix Stabilization (MEMS) framework integrates plant litter decomposition with soil organic matter stabilization: do labile plant inputs form stable soil organic matter? *Glob Chang Biol*, *19*(4), 988-995. https://doi.org/10.1111/gcb.12113

Crowther, T. W., Todd-Brown, K. E., Rowe, C. W., Wieder, W. R., Carey, J. C., Machmuller, M. B., Snoek, B. L., Fang, S., Zhou, G., Allison, S. D., Blair, J. M., Bridgham, S. D., Burton, A. J., Carrillo, Y., Reich, P. B., Clark, J. S., Classen, A. T., Dijkstra, F. A., Elberling, B., Emmett, B. A., Estiarte, M., Frey, S. D., Guo, J., Harte, J., Jiang, L., Johnson, B. R., Kroel-Dulay, G., Larsen, K. S., Laudon, H., Lavallee, J. M., Luo, Y., Lupascu, M., Ma, L. N., Marhan, S., Michelsen, A., Mohan, J., Niu, S., Pendall, E., Penuelas, J., Pfeifer-Meister, L., Poll, C., Reinsch, S., Reynolds, L. L., Schmidt, I. K., Sistla, S., Sokol, N. W., Templer, P. H., Treseder, K. K., Welker, J. M., & Bradford, M. A. (2016). Quantifying global soil carbon losses in response to warming. *Nature*, *540*(7631), 104-108. https://doi.org/10.1038/nature20150

Dawes, M. A., Hagedorn, F., Handa, I. T., Streit, K., Ekblad, A., Rixen, C., Körner, C., & Hättenschwiler, S. (2013). An alpine treeline in a carbon dioxide-rich world: synthesis of a nine-year free-air carbon dioxide enrichment study. *Oecologia*, *171*(3), 623-637. https://doi.org/10.1007/s00442-012-2576-5

De Kauwe, M. G., Medlyn, B. E., Zaehle, S., Walker, A. P., Dietze, M. C., Wang, Y. P., Luo, Y., Jain, A. K., El-Masri, B., Hickler, T., Warlind, D., Weng, E., Parton, W. J., Thornton, P. E., Wang, S., Prentice, I. C., Asao, S., Smith, B., McCarthy, H. R., Iversen, C. M., Hanson, P. J., Warren, J. M., Oren, R., & Norby, R. J. (2014). Where does the carbon go? A model-data intercomparison of vegetation carbon allocation and turnover processes at two temperate forest free-air CO2 enrichment sites. *New Phytol*, *203*(3), 883-899. https://doi.org/10.1111/nph.12847

de Wit, H. A., Bryn, A., Hofgaard, A., Karstensen, J., Kvalevag, M. M., & Peters, G. P. (2014). Climate warming feedback from mountain birch forest expansion: reduced albedo dominates carbon uptake. *Glob Chang Biol*, *20*(7), 2344-2355. https://doi.org/10.1111/gcb.12483

Dee, D. P., Uppala, S. M., Simmons, A. J., Berrisford, P., Poli, P., Kobayashi, S., Andrae, U., Balmaseda, M. A., Balsamo, G., Bauer, P., Bechtold, P., Beljaars, A. C. M., van de Berg, L., Bidlot, J., Bormann, N., Delsol, C., Dragani, R., Fuentes, M., Geer, A. J., Haimberger, L., Healy, S. B., Hersbach, H., Hólm, E. V., Isaksen, L., Kållberg, P., Köhler, M., Matricardi, M., McNally, A. P., Monge-Sanz, B. M., Morcrette, J. J., Park, B. K., Peubey, C., de Rosnay, P., Tavolato, C., Thépaut, J. N., & Vitart, F. (2011). The ERA-Interim reanalysis: configuration and performance of the data assimilation system. *Quarterly Journal of the Royal Meteorological Society*, *137*(656), 553-597. https://doi.org/10.1002/qj.828

Dusenge, M. E., Duarte, A. G., & Way, D. A. (2019). Plant carbon metabolism and climate change: elevated CO2 and temperature impacts on photosynthesis, photorespiration and respiration. *New Phytol*, *221*(1), 32-49. https://doi.org/10.1111/nph.15283

Elmendorf, S. C., Henry, G. H. R., Hollister, R. D., Björk, R. G., Boulanger-Lapointe, N., Cooper, E. J., Cornelissen, J. H. C., Day, T. A., Dorrepaal, E., Elumeeva, T. G., Gill, M., Gould, W. A., Harte, J., Hik, D. S., Hofgaard, A., Johnson, D. R., Johnstone, J. F., Jónsdóttir, I. S., Jorgenson, J. C., Klanderud, K., Klein, J. A., Koh, S., Kudo, G., Lara, M., Lévesque, E., Magnússon, B., May, J. L., Mercado-Dı´az, J. A., Michelsen, A., Molau, U., Myers-Smith, I. H., Oberbauer, S. F., Onipchenko, V. G., Rixen, C., Martin Schmidt, N., Shaver, G. R., Spasojevic, M. J., Þórhallsdóttir, Þ. E., Tolvanen, A., Troxler, T., Tweedie, C. E., Villareal, S., Wahren, C.-H., Walker, X., Webber, P. J., Welker, J. M., & Wipf, S. (2012). Plot-scale evidence of tundra vegetation change and links to recent summer warming. *Nature Climate Change*, *2*(6), 453-457. https://doi.org/10.1038/nclimate1465

Epstein, H. E., Raynolds, M. K., Walker, D. A., Bhatt, U. S., Tucker, C. J., & Pinzon, J. E. (2012). Dynamics of aboveground phytomass of the circumpolar Arctic tundra during the past three decades. *Environmental Research Letters*, *7*(1). https://doi.org/10.1088/1748-9326/7/1/015506

Fernández-Martínez, M., Sardans, J., Chevallier, F., Ciais, P., Obersteiner, M., Vicca, S., Canadell, J. G., Bastos, A., Friedlingstein, P., Sitch, S., Piao, S. L., Janssens, I. A., & Peñuelas, J. (2018). Global trends in carbon sinks and their relationships with CO2 and temperature. *Nature Climate Change*, *9*(1), 73-79. https://doi.org/10.1038/s41558-018-0367-7

Forbes, B. C., Fauria, M. M., & Zetterberg, P. (2010). Russian Arctic warming and 'greening' are closely tracked by tundra shrub willows. *Global Change Biology*, *16*(5), 1542-1554. https://doi.org/10.1111/j.1365-2486.2009.02047.x

Forster, P., Storelvmo, T., Armour, K., Collins, W., Dufresne, J.-L., Frame, D., Lunt, D. J., Mauritsen, T., Palmer, M. D., Watanabe, M., Wild, M., & Zhang, H. (2021). The Earth's Energy Budget, Climate Feedbacks, and Climate Sensitivity. In V. Masson-Delmotte, P. Zhai, A. Pirani, S. L. Connors, C. Péan, S. Berger, N. Caud, Y. Chen, L. Goldfarb, M. I. Gomis, M. Huang, K. Leitzell, E. Lonnoy, J. B. R. Matthews, T. K. Maycock, T. Waterfield, O. Yelekçi, R. Yu, & B. Zhou (Eds.), *Climate Change 2021: The Physical Science Basis. Contribution of Working Group I to the Sixth Assessment Report of the Intergovernmental Panel on Climate Change* (pp. 923-1054). Cambridge University Press. https://doi.org/10.1017/9781009157896.009

Friedlingstein, P., Jones, M. W., O'Sullivan, M., Andrew, R. M., Hauck, J., Peters, G. P., Peters, W., Pongratz, J., Sitch, S., Le Quéré, C., Bakker, D. C. E., Canadell, J. G., Ciais, P., Jackson, R. B., Anthoni, P., Barbero, L., Bastos, A., Bastrikov, V., Becker, M., Bopp, L., Buitenhuis, E., Chandra, N., Chevallier, F., Chini, L. P., Currie, K. I., Feely, R. A., Gehlen, M., Gilfillan, D., Gkritzalis, T., Goll, D. S., Gruber, N., Gutekunst, S., Harris, I., Haverd, V., Houghton, R. A., Hurtt, G., Ilyina, T., Jain, A. K., Joetzjer, E., Kaplan, J. O., Kato, E., Klein Goldewijk, K., Korsbakken, J. I., Landschützer, P., Lauvset, S. K., Lefèvre, N., Lenton, A., Lienert, S., Lombardozzi, D., Marland, G., McGuire, P. C., Melton, J. R., Metzl, N., Munro, D. R., Nabel, J. E. M. S., Nakaoka, S.-I., Neill, C., Omar, A. M., Ono, T., Peregon, A., Pierrot, D., Poulter, B., Rehder, G., Resplandy, L., Robertson, E., Rödenbeck, C., Séférian, R., Schwinger, J., Smith, N., Tans, P. P., Tian, H., Tilbrook, B., Tubiello, F. N., van der Werf, G. R., Wiltshire, A. J., & Zaehle, S. (2019). Global Carbon Budget 2019. *Earth System Science Data*, *11*(4), 1783-1838. https://doi.org/10.5194/essd-11-1783-2019

García Criado, M., Myers-Smith, I. H., Bjorkman, A. D., Lehmann, C. E. R., Stevens, N., & Josée Fortin, M. (2020). Woody plant encroachment intensifies under climate change across tundra and savanna biomes. *Global Ecology and Biogeography*, *29*(5), 925-943. https://doi.org/10.1111/geb.13072

Giorgi, F., Jones, C., & Asrar, G. R. (2009). Addressing climate information needs at the regional level: the CORDEX framework. *WMO bulletin*, *58*(3), 175-183.

Gutowski Jr, W. J., Giorgi, F., Timbal, B., Frigon, A., Jacob, D., Kang, H.-S., Raghavan, K., Lee, B., Lennard, C., Nikulin, G., O'Rourke, E., Rixen, M., Solman, S., Stephenson, T., & Tangang, F. (2016). WCRP COordinated Regional Downscaling EXperiment (CORDEX): a diagnostic MIP for CMIP6. *Geoscientific Model Development*, *9*(11), 4087-4095. https://doi.org/10.5194/gmd-9-4087-2016

Harsch, M. A., Hulme, P. E., McGlone, M. S., & Duncan, R. P. (2009). Are treelines advancing? A global meta-analysis of treeline response to climate warming. *Ecol Lett*, *12*(10), 1040-1049. https://doi.org/10.1111/j.1461-0248.2009.01355.x

Haxeltine, A., & Prentice, I. C. (1996). A General Model for the Light-Use Efficiency of Primary Production. *Functional Ecology*, *10*(5). https://doi.org/**10.2307/2390165**

Hedenås, H., Olsson, H., Jonasson, C., Bergstedt, J., Dahlberg, U., & Callaghan, T. V. (2011). Changes in Tree Growth, Biomass and Vegetation Over a 13-Year Period in the Swedish Sub-Arctic. *AMBIO*, *40*, 672-682, Article 672. https://doi.org/0.1007/s13280-011-0173-1

Hoch, G., & Körner, C. (2012). Global patterns of mobile carbon stores in trees at the high-elevation tree line. *Global Ecology and Biogeography*, *21*(8), 861-871. https://doi.org/10.1111/j.1466-8238.2011.00731.x

Hofgaard, A., Dalen, L., & Hytteborn, H. (2009). Tree reqruitment above the treeline and potential for climate-driven treeline change. *Journal of Vegetation Science*, *20*, 1133-1144.

Hofgaard, A., Harper, K. A., & Golubeva, E. (2012). The role of the circumarctic forest–tundra ecotone for Arctic biodiversity. *Biodiversity*, *13*(3-4), 174-181. https://doi.org/10.1080/14888386.2012.700560

Holtmeier, F. K., & Broll, G. E. (2007). Treeline advance - driving processes and adverse factors. *Landscape Online*, *1*, 1-33. https://doi.org/10.3097/lo.200701

Hugelius, G., Strauss, J., Zubrzycki, S., Harden, J. W., Schuur, E. A. G., Ping, C. L., Schirrmeister, L., Grosse, G., Michaelson, G. J., Koven, C. D., amp, apos, Donnell, J. A., Elberling, B., Mishra, U., Camill, P., Yu, Z., Palmtag, J., & Kuhry, P. (2014). Estimated stocks of circumpolar permafrost carbon with quantified uncertainty ranges and identified data gaps. *Biogeosciences*, *11*(23), 6573-6593. https://doi.org/10.5194/bg-11-6573-2014

IPCC. (2013). *5th assessment report: The physical scince basis; Summary for policymakers*.

IPCC. (2021). *Climate Change 2021: The Physical Science Basis. Contribution of Working Group I to the Sixth Assessment Report of the Intergovernmental Panel on Climate Change*. C. U. Press.

Jones, C., Giorgi, F., & Asrar, G. R. (2011). The Coordinated Regional Downscaling EXperiment: CORDEX, an International Downscaling Link to CMIP5. *Clivar Exchanges*, *16*, 34-39.

Jung, M., Reichstein, M., Margolis, H. A., Cescatti, A., Richardson, A. D., Arain, M. A., Arneth, A., Bernhofer, C., Bonal, D., Chen, J., Gianelle, D., Gobron, N., Kiely, G., Kutsch, W., Lasslop, G., Law, B. E., Lindroth, A., Merbold, L., Montagnani, L., Moors, E. J., Papale, D., Sottocornola, M., Vaccari, F., & Williams, C. (2011). Global patterns of land-atmosphere fluxes of carbon dioxide, latent heat, and sensible heat derived from eddy covariance, satellite, and meteorological observations. *Journal of Geophysical Research*, *116*. https://doi.org/10.1029/2010jg001566

Knorr, W., Kaminski, T., Arneth, A., & Weber, U. (2014). Impact of human population density on fire frequency at the global scale. *Biogeosciences*, *11*(4), 1085-1102. https://doi.org/10.5194/bg-11-1085-2014

Kollas, C., Vitasse, Y., Randin, C. F., Hoch, G., & Korner, C. (2012). Unrestricted quality of seeds in European broad-leaved tree species growing at the cold boundary of their distribution. *Ann Bot*, *109*(2), 473-480. https://doi.org/10.1093/aob/mcr299

Körner, C. (1998). A re-assessment of high elevation treeline positions and their explanation. *Oecologia*, *115*(4), 445-459.

Körner, C. (2003). Carbon limitation in trees. *Journal of Ecology*, *91*(1), 4-17.

Körner, C. (2015). Paradigm shift in plant growth control. *Curr Opin Plant Biol*, *25*, 107-114. https://doi.org/10.1016/j.pbi.2015.05.003

Körner, C., Basler, D., Hoch, G., Kollas, C., Lenz, A., Randin, C. F., Vitasse, Y., Zimmermann, N. E., & Turnbull, M. (2016). Where, why and how? Explaining the low-temperature range limits of temperate tree species. *Journal of Ecology*, *104*(4), 1076-1088. https://doi.org/10.1111/1365-2745.12574

Körner, C., & Paulsen, J. (2004). A World-Wide Study of High Altitude Treeline Temperatures. *Journal of Biogeography*, *31*(5), 713-732. https://www.jstor.org/stable/3554841

Körner, C., & Spehn, E. (2019). A Humboldtian view of mountains. *Science*, *365*(6458), 1061. https://doi.org/10.1126/science.aaz4161

Lamarque, J. F., Dentener, F., McConnell, J., Ro, C. U., Shaw, M., Vet, R., Bergmann, D., Cameron-Smith, P., Dalsoren, S., Doherty, R., Faluvegi, G., Ghan, S. J., Josse, B., Lee, Y. H., MacKenzie, I. A., Plummer, D., Shindell, D. T., Skeie, R. B., Stevenson, D. S., Strode, S., Zeng, G., Curran, M., Dahl-Jensen, D., Das, S., Fritzsche, D., & Nolan, M. (2013). Multi-model mean nitrogen and sulfur deposition from the Atmospheric Chemistry and Climate Model Intercomparison Project (ACCMIP): evaluation of historical and projected future changes. *Atmospheric Chemistry and Physics*, *13*(16), 7997-8018. https://doi.org/10.5194/acp-13-7997-2013

Lange, S. (2019). Trend-preserving bias adjustment and statistical downscaling with ISIMIP3BASD (v1.0). *Geoscientific Model Development*, *12*(7), 3055-3070. https://doi.org/10.5194/gmd-12-3055-2019

Lehmann, J., & Kleber, M. (2015). The contentious nature of soil organic matter. *Nature*, *528*(7580), 60-68. https://doi.org/10.1038/nature16069

Lett, S., & Dorrepaal, E. (2018). Global drivers of tree seedling establishment at alpine treelines in a changing climate. *Functional Ecology*, *32*(7), 1666-1680. https://doi.org/10.1111/1365-2435.13137

Li, & Xiao. (2019). Mapping Photosynthesis Solely from Solar-Induced Chlorophyll Fluorescence: A Global, Fine-Resolution Dataset of Gross Primary Production Derived from OCO-2. *Remote Sensing*, *11*(21). https://doi.org/10.3390/rs11212563

Liu, H., Gong, P., Wang, J., Clinton, N., Bai, Y., & Liang, S. (2020). Annual dynamics of global land cover and its long-term changes from 1982 to 2015. *Earth System Science Data*, *12*(2), 1217-1243. https://doi.org/10.5194/essd-12-1217-2020

Mamet, S. D., Brown, C. D., Trant, A. J., & Laroque, C. P. (2019). Shifting globalLarixdistributions: Northern expansion and southern retraction as species respond to changing climate. *Journal of Biogeography*, *46*(1), 30-44. https://doi.org/10.1111/jbi.13465

Mao, J., & Yan, B. (2019). Global Monthly Mean Leaf Area Index Climatology, 1981-2015. In: ORNL Distributed Active Archive Center.

Martin, A. C., Macias-Fauria, M., Bonsall, M. B., Forbes, B. C., Zetterberg, P., & Jeffers, E. S. (2022). Common mechanisms explain nitrogen-dependent growth of Arctic shrubs over three decades despite heterogeneous trends and declines in soil nitrogen availability. *New Phytol*, *233*(2), 670-686. https://doi.org/10.1111/nph.17529

Masson, V., Champeaux, J.-L., Chauvin, F., Meriguet, C., & Lacaze, R. (2003). A Global Database of Land Surface Parameters at 1-km Resolution in Meteorological and Climate Models. *Journal of Climate*, *16*(9), 1261-1282. https://doi.org/10.1175/1520-0442(2003)16<1261:Agdols>2.0.Co;2

Matthews, H. D., Gillett, N. P., Stott, P. A., & Zickfeld, K. (2009). The proportionality of global warming to cumulative carbon emissions. *Nature*, *459*(7248), 829-832. https://doi.org/10.1038/nature08047

McGuire, A. D., Christensen, T. R., Hayes, D., Heroult, A., Euskirchen, E., Kimball, J. S., Koven, C., Lafleur, P., Miller, P. A., Oechel, W., Peylin, P., Williams, M., & Yi, Y. (2012). An assessment of the carbon balance of Arctic tundra: comparisons among observations, process models, and atmospheric inversions. *Biogeosciences*, *9*(8), 3185-3204. https://doi.org/10.5194/bg-9-3185-2012

Meinshausen, M., Nicholls, Z. R. J., Lewis, J., Gidden, M. J., Vogel, E., Freund, M., Beyerle, U., Gessner, C., Nauels, A., Bauer, N., Canadell, J. G., Daniel, J. S., John, A., Krummel, P. B., Luderer, G., Meinshausen, N., Montzka, S. A., Rayner, P. J., Reimann, S., Smith, S. J., van den Berg, M., Velders, G. J. M., Vollmer, M. K., & Wang, R. H. J. (2020). The shared socio-economic pathway (SSP) greenhouse gas concentrations and their extensions to 2500. *Geoscientific Model Development*, *13*(8), 3571-3605. https://doi.org/10.5194/gmd-13-3571-2020

Mekonnen, Z. A., Riley, W. J., Berner, L. T., Bouskill, N. J., Torn, M. S., Iwahana, G., Breen, A. L., Myers-Smith, I. H., Criado, M. G., Liu, Y., Euskirchen, E. S., Goetz, S. J., Mack, M. C., & Grant, R. F. (2021). Arctic tundra shrubification: a review of mechanisms and impacts on ecosystem carbon balance. *Environmental Research Letters*, *16*(5). https://doi.org/10.1088/1748-9326/abf28b

Moss, R. H., Edmonds, J. A., Hibbard, K. A., Manning, M. R., Rose, S. K., van Vuuren, D. P., Carter, T. R., Emori, S., Kainuma, M., Kram, T., Meehl, G. A., Mitchell, J. F., Nakicenovic, N., Riahi, K., Smith, S. J., Stouffer, R. J., Thomson, A. M., Weyant, J. P., & Wilbanks, T. J. (2010). The next generation of scenarios for climate change research and assessment. *Nature*, *463*(7282), 747-756. https://doi.org/10.1038/nature08823

Muller, J.-P., Lopéz, G., Watson, G., Shane, N., Kennedy, T., Yuen, P., Lewis, P., Fischer, J., Guanter, L., Domench, C., Preusker, R., North, P., Heckel, A., Danne, O., Krämer, U., Zühlke, M., Brockmann, C., & Pinnok, S. (2012). The ESA GlobAlbedo Project for mapping the Earth's land surface albedo for 15 years from European sensors. IEEE Geoscience and Remote Sensing Symposium (IGARSS) 2012, IEEE, Munich, Germany.

Myers-Smith, I. H., Elmendorf, S. C., Beck, P. S. A., Wilmking, M., Hallinger, M., Blok, D., Tape, K. D., Rayback, S. A., Macias-Fauria, M., Forbes, B. C., Speed, J. D. M., Boulanger-Lapointe, N., Rixen, C., Lévesque, E., Schmidt, N. M., Baittinger, C., Trant, A. J., Hermanutz, L., Collier, L. S., Dawes, M. A., Lantz, T. C., Weijers, S., Jørgensen, R. H., Buchwal, A., Buras, A., Naito, A. T., Ravolainen, V., Schaepman-Strub, G., Wheeler, J. A., Wipf, S., Guay, K. C., Hik, D. S., & Vellend, M. (2015). Climate sensitivity of shrub growth across the tundra biome. *Nature Climate Change*, *5*(9), 887-891. https://doi.org/10.1038/nclimate2697

Myers-Smith, I. H., Forbes, B. C., Wilmking, M., Hallinger, M., Lantz, T., Blok, D., Tape, K. D., Macias-Fauria, M., Sass-Klaassen, U., Lévesque, E., Boudreau, S., Ropars, P., Hermanutz, L., Trant, A., Collier, L. S., Weijers, S., Rozema, J., Rayback, S. A., Schmidt, N. M., Schaepman-Strub, G., Wipf, S., Rixen, C., Ménard, C. B., Venn, S., Goetz, S., Andreu-Hayles, L., Elmendorf, S., Ravolainen, V., Welker, J., Grogan, P., Epstein, H. E., & Hik, D. S. (2011). Shrub expansion in tundra ecosystems: dynamics, impacts and research priorities. *Environmental Research Letters*, *6*(4). https://doi.org/10.1088/1748-9326/6/4/045509

Myers-Smith, I. H., Hik, D. S., & Aerts, R. (2018). Climate warming as a driver of tundra shrubline advance. *Journal of Ecology*, *106*(2), 547-560. https://doi.org/10.1111/1365-2745.12817

Myers-Smith, I. H., Kerby, J. T., Phoenix, G. K., Bjerke, J. W., Epstein, H. E., Assmann, J. J., John, C., Andreu-Hayles, L., Angers-Blondin, S., Beck, P. S. A., Berner, L. T., Bhatt, U. S., Bjorkman, A. D., Blok, D., Bryn, A., Christiansen, C. T., Cornelissen, J. H. C., Cunliffe, A. M., Elmendorf, S. C., Forbes, B. C., Goetz, S. J., Hollister, R. D., de Jong, R., Loranty, M. M., Macias-Fauria, M., Maseyk, K., Normand, S., Olofsson, J., Parker, T. C., Parmentier, F.-J. W., Post, E., Schaepman-Strub, G., Stordal, F., Sullivan, P. F., Thomas, H. J. D., Tømmervik, H., Treharne, R., Tweedie, C. E., Walker, D. A., Wilmking, M., & Wipf, S. (2020). Complexity revealed in the greening of the Arctic. *Nature Climate Change*, *10*(2), 106-117. https://doi.org/10.1038/s41558-019-0688-1

Nadelhoffer, K. J., Giblin, A. E., Shaver, G. R., & Laundre, J. A. (1991). Effects of Temperature and Substrate Quality on Element Mineralization in Six Arctic Soils. *Ecology*, *72*(1), 242-253.

Nijsse, F. J. M. M., Cox, P. M., & Williamson, M. S. (2020). Emergent constraints on transient climate response (TCR) and equilibrium climate sensitivity (ECS) from historical warming in CMIP5 and CMIP6 models. *Earth System Dynamics*, *11*(3), 737-750. https://doi.org/10.5194/esd-11-737-2020

O'Neill, B. C., Tebaldi, C., van Vuuren, D. P., Eyring, V., Friedlingstein, P., Hurtt, G., Knutti, R., Kriegler, E., Lamarque, J.-F., Lowe, J., Meehl, G. A., Moss, R., Riahi, K., & Sanderson, B. M. (2016). The Scenario Model Intercomparison Project (ScenarioMIP) for CMIP6. *Geoscientific Model Development*, *9*(9), 3461-3482. https://doi.org/10.5194/gmd-9-3461-2016

O'Neill, B. C., Kriegler, E., Ebi, K. L., Kemp-Benedict, E., Riahi, K., Rothman, D. S., van Ruijven, B. J., van Vuuren, D. P., Birkmann, J., Kok, K., Levy, M., & Solecki, W. (2017). The roads ahead: Narratives for shared socioeconomic pathways describing world futures in the 21st century. *Global Environmental Change*, *42*, 169-180. https://doi.org/10.1016/j.gloenvcha.2015.01.004

Olsson, P.-O., Heliasz, M., Jin, H., & Eklundh, L. (2017). Mapping the reduction in gross primary productivity in subarctic birch forests due to insect outbreaks. *Biogeosciences*, *14*(6), 1703-1719. https://doi.org/10.5194/bg-14-1703-2017

Ovhed, M., & Holmgren, B. (1996). Modelling and measuring evapotrasnpiration in a mountain birch forest. *Ecological Bulletins*, *45*, 31-44. http://www.jstor.org/stable/20113181

Parton, W. J., Hanson, P. J., Swanston, C., Torn, M., Trumbore, S. E., Riley, W., & Kelly, R. (2010). ForCent model development and testing using the Enriched Background Isotope Study experiment. *Journal of Geophysical Research*, *115*(G4). https://doi.org/10.1029/2009jg001193

Parton, W. J., Scurlock, J. M. O., Ojima, D. S., Gilmanov, T. G., Scholes, R. J., Schimel, D. S., Kirschner, T., Menaut, J.-C., Seastedt, T., Garcia Moya, E., Kamnalrut, A., & Kinyamario, J. I. (1993). Observations and modeling of biomass and soil organic matter dynamics for the grassland biome worldwide. *Global Biogeochemical Cycles*, *7*(4), 785-809.

Paulsen, J., & Körner, C. (2014). A climate-based model to predict potential treeline position around the globe. *Alpine Botany*, *124*(1), 1-12. https://doi.org/10.1007/s00035-014-0124-0

Pellegrini, A. F. A., Ahlstrom, A., Hobbie, S. E., Reich, P. B., Nieradzik, L. P., Staver, A. C., Scharenbroch, B. C., Jumpponen, A., Anderegg, W. R. L., Randerson, J. T., & Jackson, R. B. (2018). Fire frequency drives decadal changes in soil carbon and nitrogen and ecosystem productivity. *Nature*, *553*(7687), 194-198. https://doi.org/10.1038/nature24668

Peltola, O., Vesala, T., Gao, Y., Räty, O., Alekseychik, P., Aurela, M., Chojnicki, B., Desai, A. R., Dolman, A. J., Euskirchen, E. S., Friborg, T., Göckede, M., Helbig, M., Humphreys, E., Jackson, R. B., Jocher, G., Joos, F., Klatt, J., Knox, S. H., Kowalska, N., Kutzbach, L., Lienert, S., Lohila, A., Mammarella, I., Nadeau, D. F., Nilsson, M. B., Oechel, W. C., Peichl, M., Pypker, T., Quinton, W., Rinne, J., Sachs, T., Samson, M., Schmid, H. P., Sonnentag, O., Wille, C., Zona, D., & Aalto, T. (2019). Monthly gridded data product of northern wetland methane emissions based on upscaling eddy covariance observations. *Earth System Science Data*, *11*(3), 1263-1289. https://doi.org/10.5194/essd-11-1263-2019

Penuelas, J., & Staudt, M. (2010). BVOCs and global change. *Trends Plant Sci*, *15*(3), 133-144. https://doi.org/10.1016/j.tplants.2009.12.005

Pilegaard, K. (2013). Processes regulating nitric oxide emissions from soils. *Philos Trans R Soc Lond B Biol Sci*, *368*(1621), 20130126. https://doi.org/10.1098/rstb.2013.0126

Prentice, I. C., Liang, X., Medlyn, B. E., & Wang, Y. P. (2015). Reliable, robust and realistic: the three R's of next-generation land-surface modelling. *Atmospheric Chemistry and Physics*, *15*(10), 5987-6005. https://doi.org/10.5194/acp-15-5987-2015

Qiu, C., Ciais, P., Zhu, D., Guenet, B., Chang, J., Chaudhary, N., Kleinen, T., Li, X., Müller, J., Xi, Y., Zhang, W., Ballantyne, A., Brewer, S. C., Brovkin, V., Charman, D. J., Gustafson, A., Gallego-Sala, A. V., Gasser, T., Holden, J., Joos, F., Kwon, M. J., Lauerwald, R., Miller, P. A., Peng, S., Page, S., Smith, B., Stocker, B. D., Sannel, A. B. K., Salmon, E., Schurgers, G., Shurpali, N. J., Wårlind, D., & Westermann, S. (2022). A strong mitigation scenario maintains climate neutrality of northern peatlands. *One Earth*, *5*(1), 86-97. https://doi.org/10.1016/j.oneear.2021.12.008

Rabin, S. S., Melton, J. R., Lasslop, G., Bachelet, D., Forrest, M., Hantson, S., Kaplan, J. O., Li, F., Mangeon, S., Ward, D. S., Yue, C., Arora, V. K., Hickler, T., Kloster, S., Knorr, W., Nieradzik, L., Spessa, A., Folberth, G. A., Sheehan, T., Voulgarakis, A., Kelley, D. I., Prentice, I. C., Sitch, S., Harrison, S., & Arneth, A. (2017). The Fire Modeling Intercomparison Project (FireMIP), phase 1: experimental and analytical protocols with detailed model descriptions. *Geoscientific Model Development*, *10*(3), 1175-1197. https://doi.org/10.5194/gmd-10-1175-2017

Rees, W. G., Hofgaard, A., Boudreau, S., Cairns, D. M., Harper, K., Mamet, S., Mathisen, I., Swirad, Z., & Tutubalina, O. (2020). Is subarctic forest advance able to keep pace with climate change? *Glob Chang Biol*, *26*(7), 3965-3977. https://doi.org/10.1111/gcb.15113

Roldin, P., Ehn, M., Kurten, T., Olenius, T., Rissanen, M. P., Sarnela, N., Elm, J., Rantala, P., Hao, L., Hyttinen, N., Heikkinen, L., Worsnop, D. R., Pichelstorfer, L., Xavier, C., Clusius, P., Ostrom, E., Petaja, T., Kulmala, M., Vehkamaki, H., Virtanen, A., Riipinen, I., & Boy, M. (2019). The role of highly oxygenated organic molecules in the Boreal aerosol-cloud-climate system. *Nat Commun*, *10*(1), 4370. https://doi.org/10.1038/s41467-019-12338-8

Ropars, P., & Boudreau, S. (2012). Shrub expansion at the forest–tundra ecotone: spatial heterogeneity linked to local topography. *Environmental Research Letters*, *7*(1). https://doi.org/10.1088/1748-9326/7/1/015501

Rundqvist, S., Hedenas, H., Sandstrom, A., Emanuelsson, U., Eriksson, H., Jonasson, C., & Callaghan, T. V. (2011). Tree and shrub expansion over the past 34 years at the tree-line near Abisko, Sweden. *AMBIO*, *40*(6), 683-692. https://doi.org/10.1007/s13280-011-0174-0

Samuelsson, P., Gollvik, S., Kupiainen, M., Kourzeneva, E., & van de Berg, W. J. (2015). *The surface processes of the Rossby Centre regional atmospheric climate model (RCA4)* (0283-7730 ; 157). (Meteorologi, Issue. SMHI. http://urn.kb.se/resolve?urn=urn:nbn:se:smhi:diva-2840

Samuelsson, P., Jones, C. G., Will´En, U., Ullerstig, A., Gollvik, S., Hansson, U., Jansson, E., Kjellstro¨M, C., Nikulin, G., & Wyser, K. (2011). The Rossby Centre Regional Climate model RCA3: model description and performance. *Tellus A: Dynamic Meteorology and Oceanography*, *63*(1), 4-23. https://doi.org/10.1111/j.1600-0870.2010.00478.x

Saunois, M., Stavert, A. R., Poulter, B., Bousquet, P., Canadell, J. G., Jackson, R. B., Raymond, P. A., Dlugokencky, E. J., Houweling, S., Patra, P. K., Ciais, P., Arora, V. K., Bastviken, D., Bergamaschi, P., Blake, D. R., Brailsford, G., Bruhwiler, L., Carlson, K. M., Carrol, M., Castaldi, S., Chandra, N., Crevoisier, C., Crill, P. M., Covey, K., Curry, C. L., Etiope, G., Frankenberg, C., Gedney, N., Hegglin, M. I., Höglund-Isaksson, L., Hugelius, G., Ishizawa, M., Ito, A., Janssens-Maenhout, G., Jensen, K. M., Joos, F., Kleinen, T., Krummel, P. B., Langenfelds, R. L., Laruelle, G. G., Liu, L., Machida, T., Maksyutov, S., McDonald, K. C., McNorton, J., Miller, P. A., Melton, J. R., Morino, I., Müller, J., Murguia-Flores, F., Naik, V., Niwa, Y., Noce, S., O'Doherty, S., Parker, R. J., Peng, C., Peng, S., Peters, G. P., Prigent, C., Prinn, R., Ramonet, M., Regnier, P., Riley, W. J., Rosentreter, J. A., Segers, A., Simpson, I. J., Shi, H., Smith, S. J., Steele, L. P., Thornton, B. F., Tian, H., Tohjima, Y., Tubiello, F. N., Tsuruta, A., Viovy, N., Voulgarakis, A., Weber, T. S., van Weele, M., van der Werf, G. R., Weiss, R. F., Worthy, D., Wunch, D., Yin, Y., Yoshida, Y., Zhang, W., Zhang, Z., Zhao, Y., Zheng, B., Zhu, Q., Zhu, Q., & Zhuang, Q. (2020). The Global Methane Budget 2000–2017. *Earth System Science Data*, *12*(3), 1561-1623. https://doi.org/10.5194/essd-12-1561-2020

Scharn, R., Brachmann, C. G., Patchett, A., Reese, H., Bjorkman, A., Alatalo, J., Björk, R. G., Jägerbrand, A. K., Molau, U., & Björkman, M. P. (2021). Vegetation responses to 26 years of warming at Latnjajaure Field Station, northern Sweden. *Arctic Science*. https://doi.org/10.1139/as-2020-0042

Schurgers, G., Arneth, A., Holzinger, R., & Goldstein, A. H. (2009). Process-based modelling of biogenic monoterpene emissions combining production and release from storage. *Atmospheric Chemistry and Physics*, *9*(10), 3409-3423. https://doi.org/10.5194/acp-9-3409-2009

Schuur, E. A., McGuire, A. D., Schadel, C., Grosse, G., Harden, J. W., Hayes, D. J., Hugelius, G., Koven, C. D., Kuhry, P., Lawrence, D. M., Natali, S. M., Olefeldt, D., Romanovsky, V. E., Schaefer, K., Turetsky, M. R., Treat, C. C., & Vonk, J. E. (2015). Climate change and the permafrost carbon feedback. *Nature*, *520*(7546), 171-179. https://doi.org/10.1038/nature14338

Serreze, M. C., & Barry, R. G. (2011). Processes and impacts of Arctic amplification: A research synthesis. *Global and Planetary Change*, *77*(1-2), 85-96. https://doi.org/10.1016/j.gloplacha.2011.03.004

Sitch, S., Friedlingstein, P., Gruber, N., Jones, S. D., Murray-Tortarolo, G., Ahlström, A., Doney, S. C., Graven, H., Heinze, C., Huntingford, C., Levis, S., Levy, P. E., Lomas, M., Poulter, B., Viovy, N., Zaehle, S., Zeng, N., Arneth, A., Bonan, G., Bopp, L., Canadell, J. G., Chevallier, F., Ciais, P., Ellis, R., Gloor, M., Peylin, P., Piao, S. L., Le Quéré, C., Smith, B., Zhu, Z., & Myneni, R. (2015). Recent trends and drivers of regional sources and sinks of carbon dioxide. *Biogeosciences*, *12*(3), 653-679. https://doi.org/10.5194/bg-12-653-2015

Smith, B., Prentice, I. C., & Sykes, M. T. (2001). Representation of vegetation dynamics in the modelling of terrestrial ecosystems: comparing two contrasting approaches within European climate space. *Global Ecology and Biogeography*, *10*(6), 621-637. https://doi.org/10.1046/j.1466-822X.2001.t01-1-00256.x

Smith, B., Samuelsson, P., Wramneby, A., & Rummukainen, M. (2011). A model of the coupled dynamics of climate, vegetation and terrestrial ecosystem biogeochemistry for regional applications. *Tellus A: Dynamic Meteorology and Oceanography*, *63*(1), 87-106. https://doi.org/10.1111/j.1600-0870.2010.00477.x

Smith, B., Wårlind, D., Arneth, A., Hickler, T., Leadley, P., Siltberg, J., & Zaehle, S. (2014). Implications of incorporating N cycling and N limitations on primary production in an individual-based dynamic vegetation model. *Biogeosciences*, *11*(7), 2027-2054. https://doi.org/10.5194/bg-11-2027-2014

Stavert, A. R., Saunois, M., Canadell, J. G., Poulter, B., Jackson, R. B., Regnier, P., Lauerwald, R., Raymond, P. A., Allen, G. H., Patra, P. K., Bergamaschi, P., Bousquet, P., Chandra, N., Ciais, P., Gustafson, A., Ishizawa, M., Ito, A., Kleinen, T., Maksyutov, S., McNorton, J., Melton, J. R., Muller, J., Niwa, Y., Peng, S., Riley, W. J., Segers, A., Tian, H., Tsuruta, A., Yin, Y., Zhang, Z., Zheng, B., & Zhuang, Q. (2022). Regional trends and drivers of the global methane budget. *Glob Chang Biol*, *28*(1), 182-200. https://doi.org/10.1111/gcb.15901

Stuart Chapin Iii, F., McFarland, J., David McGuire, A., Euskirchen, E. S., Ruess, R. W., & Kielland, K. (2009). The changing global carbon cycle: linking plant-soil carbon dynamics to global consequences. *Journal of Ecology*, *97*(5), 840-850. https://doi.org/10.1111/j.1365-2745.2009.01529.x

Sturm, M. (2005). Changing snow and shrub conditions affect albedo with global implications. *Journal of Geophysical Research*, *110*(G1). https://doi.org/10.1029/2005jg000013

Sturm, M., Holmgren, J., McFadden, J. P., Liston, G. E., Chapin, F. S., & Racine, C. H. (2001). Snow–Shrub Interactions in Arctic Tundra: A Hypothesis with Climatic Implications. *Journal of Climate*, *14*(3), 336-344. https://doi.org/10.1175/1520-0442(2001)014<0336:Ssiiat>2.0.Co;2

Sundqvist, M. K., Björk, R. G., & Molau, U. (2008). Establishment of boreal forest species in alpine dwarf-shrub heath in subarctic Sweden. *Plant Ecology & Diversity*, *1*(1), 67-75. https://doi.org/10.1080/17550870802273395

Taylor, K. E., Stouffer, R. J., & Meehl, G. A. (2012). An Overview of CMIP5 and the Experiment Design. *Bulletin of the American Meteorological Society*, *93*(4), 485-498. https://doi.org/10.1175/bams-d-11-00094.1

Tokarska, K. B., Stolpe, M. B., Sippel, S., Fischer, E. M., Smith, C. J., Lehner, F., & Knutti, R. (2020). Past warming trend constrains future warming in CMIP6 models. *Sci Adv*, *6*(12), eaaz9549. https://doi.org/10.1126/sciadv.aaz9549

UNFCCC. (2015). Adoption of the Paris Agreement. In.

Van Bogaert, R., Haneca, K., Hoogesteger, J., Jonasson, C., De Dapper, M., & Callaghan, T. V. (2011). A century of tree line changes in sub-Arctic Sweden shows local and regional variability and only a minor influence of 20th century climate warming. *Journal of Biogeography*, *38*(5), 907-921. https://doi.org/10.1111/j.1365-2699.2010.02453.x

Viovy, N. (2018). *CRUNCEP Version 7 - Atmospheric Forcing Data for the Community Land Model* Research Data Archive at the National Center for Atmospheric Research, Computational and Information Systems Laboratory. https://doi.org/10.5065/PZ8F-F017

Virkkala, A. M., Aalto, J., Rogers, B. M., Tagesson, T., Treat, C. C., Natali, S. M., Watts, J. D., Potter, S., Lehtonen, A., Mauritz, M., Schuur, E. A. G., Kochendorfer, J., Zona, D., Oechel, W., Kobayashi, H., Humphreys, E., Goeckede, M., Iwata, H., Lafleur, P. M., Euskirchen, E. S., Bokhorst, S., Marushchak, M., Martikainen, P. J., Elberling, B., Voigt, C., Biasi, C., Sonnentag, O., Parmentier, F. W., Ueyama, M., Celis, G., St Loius, V. L., Emmerton, C. A., Peichl, M., Chi, J., Jarveoja, J., Nilsson, M. B., Oberbauer, S. F., Torn, M. S., Park, S. J., Dolman, H., Mammarella, I., Chae, N., Poyatos, R., Lopez-Blanco, E., Rojle Christensen, T., Jung Kwon, M., Sachs, T., Holl, D., & Luoto, M. (2021). Statistical upscaling of ecosystem CO2 fluxes across the terrestrial tundra and boreal domain: regional patterns and uncertainties. *Glob Chang Biol*. https://doi.org/10.1111/gcb.15659

Voigt, C., Marushchak, M. E., Abbott, B. W., Biasi, C., Elberling, B., Siciliano, S. D., Sonnentag, O., Stewart, K. J., Yang, Y., & Martikainen, P. J. (2020). Nitrous oxide emissions from permafrost-affected soils. *Nature Reviews Earth & Environment*, *1*(8), 420-434. https://doi.org/10.1038/s43017-020-0063-9

Vowles, T., & Björk, R. G. (2018). Implications of evergreen shrub expansion in the Arctic. *Journal of Ecology*, *107*(2), 650-655. https://doi.org/10.1111/1365-2745.13081

Vowles, T., Lovehav, C., Molau, U., & Björk, R. G. (2017). Contrasting impacts of reindeer grazing in two tundra grasslands. *Environmental Research Letters*, *12*(3). https://doi.org/10.1088/1748-9326/aa62af

Walker, A. P., De Kauwe, M. G., Bastos, A., Belmecheri, S., Georgiou, K., Keeling, R. F., McMahon, S. M., Medlyn, B. E., Moore, D. J. P., Norby, R. J., Zaehle, S., Anderson-Teixeira, K. J., Battipaglia, G., Brienen, R. J. W., Cabugao, K. G., Cailleret, M., Campbell, E., Canadell, J. G., Ciais, P., Craig, M. E., Ellsworth, D. S., Farquhar, G. D., Fatichi, S., Fisher, J. B., Frank, D. C., Graven, H., Gu, L., Haverd, V., Heilman, K., Heimann, M., Hungate, B. A., Iversen, C. M., Joos, F., Jiang, M., Keenan, T. F., Knauer, J., Korner, C., Leshyk, V. O., Leuzinger, S., Liu, Y., MacBean, N., Malhi, Y., McVicar, T. R., Penuelas, J., Pongratz, J., Powell, A. S., Riutta, T., Sabot, M. E. B., Schleucher, J., Sitch, S., Smith, W. K., Sulman, B., Taylor, B., Terrer, C., Torn, M. S., Treseder, K. K., Trugman, A. T., Trumbore, S. E., van Mantgem, P. J., Voelker, S. L., Whelan, M. E., & Zuidema, P. A. (2021). Integrating the evidence for a terrestrial carbon sink caused by increasing atmospheric CO2. *New Phytol*, *229*(5), 2413-2445. https://doi.org/10.1111/nph.16866

Wania, R., Ross, I., & Prentice, I. C. (2009a). Integrating peatlands and permafrost into a dynamic global vegetation model: 1. Evaluation and sensitivity of physical land surface processes. *Global Biogeochemical Cycles*, *23*(3), n/a-n/a. https://doi.org/10.1029/2008gb003412

Wania, R., Ross, I., & Prentice, I. C. (2009b). Integrating peatlands and permafrost into a dynamic global vegetation model: 2. Evaluation and sensitivity of vegetation and carbon cycle processes. *Global Biogeochemical Cycles*, *23*(3), n/a-n/a. https://doi.org/10.1029/2008gb003413

Wania, R., Ross, I., & Prentice, I. C. (2010). Implementation and evaluation of a new methane model within a dynamic global vegetation model: LPJ-WHyMe v1.3.1. *Geoscientific Model Development*, *3*(2), 565-584. https://doi.org/10.5194/gmd-3-565-2010

Weedon, G. P., Balsamo, G., Bellouin, N., Gomes, S., Best, M. J., & Viterbo, P. (2014). The WFDEI meteorological forcing data set: WATCH Forcing Data methodology applied to ERA-Interim reanalysis data. *Water Resources Research*, *50*(9), 7505-7514. https://doi.org/10.1002/2014wr015638

Xu, J., Morris, P. J., Liu, J., & Holden, J. (2018). PEATMAP: Refining estimates of global peatland distribution based on a meta-analysis. *Catena*, *160*, 134-140. https://doi.org/10.1016/j.catena.2017.09.010

Yang, Z., Hanna, E., & Callaghan, T. V. (2011). Modelling surface-air-temperature variation over complex terrain around abisko, swedish lapland: uncertainties of measurements and models at different scales. *Geografiska Annaler: Series A, Physical Geography*, *93*(2), 89-112. https://doi.org/10.1111/j.1468-0459.2011.00005.x

Yang, Z., Hanna, E., Callaghan, T. V., & Jonasson, C. (2012). How can meteorological observations and microclimate simulations improve understanding of 1913-2010 climate change around Abisko, Swedish Lapland? *Meteorological Applications*, *19*(4), 454-463. https://doi.org/10.1002/met.276

Yli-Juuti, T., Mielonen, T., Heikkinen, L., Arola, A., Ehn, M., Isokaanta, S., Keskinen, H. M., Kulmala, M., Laakso, A., Lipponen, A., Luoma, K., Mikkonen, S., Nieminen, T., Paasonen, P., Petaja, T., Romakkaniemi, S., Tonttila, J., Kokkola, H., & Virtanen, A. (2021). Significance of the organic aerosol driven climate feedback in the boreal area. *Nat Commun*, *12*(1), 5637. https://doi.org/10.1038/s41467-021-25850-7

Zelinka, M. D., Myers, T. A., McCoy, D. T., Po-Chedley, S., Caldwell, P. M., Ceppi, P., Klein, S. A., & Taylor, K. E. (2020). Causes of Higher Climate Sensitivity in CMIP6 Models. *Geophysical research letters*, *47*(1). https://doi.org/10.1029/2019gl085782

Zhang, W., Döscher, R., Koenigk, T., Miller, P. A., Jansson, C., Samuelsson, P., Wu, M., & Smith, B. (2020). The Interplay of Recent Vegetation and Sea Ice Dynamics—Results From a Regional Earth System Model Over the Arctic. *Geophysical research letters*, *47*(6). https://doi.org/10.1029/2019gl085982

Zhang, W., Jansson, C., Miller, P. A., Smith, B., & Samuelsson, P. (2014). Biogeophysical feedbacks enhance the Arctic terrestrial carbon sink in regional Earth system dynamics. *Biogeosciences*, *11*(19), 5503-5519. https://doi.org/10.5194/bg-11-5503-2014

Zhang, W., Miller, P. A., Jansson, C., Samuelsson, P., Mao, J., & Smith, B. (2018). Self-Amplifying Feedbacks Accelerate Greening and Warming of the Arctic. *Geophysical research letters*, *45*(14), 7102-7111. https://doi.org/10.1029/2018gl077830

Zhang, W., Miller, P. A., Smith, B., Wania, R., Koenigk, T., & Döscher, R. (2013). Tundra shrubification and tree-line advance amplify arctic climate warming: results from an individual-based dynamic vegetation model. *Environmental Research Letters*, *8*(3). https://doi.org/10.1088/1748-9326/8/3/034023

Acknowledgements

During my time as a PhD-student, I have met many new people. Some people I have met daily at the office, and some others only for a few days over conferences or courses. Many of whom have made a strong impression on me and have been an inspiration to my work. It is impossible to mention everyone, but I am truly grateful for having met so many positive, friendly and ambitious people. A few of these still need to be mentioned.

Firstly, I would like to thank my supervisors Paul Miller, Robert Björk and Ben Smith. Without our discussions and your guidance this thesis would not have been possible.

Secondly, I would like to mention the LPJ-GUESS group. Stefan, Tom, Johan, David, Lars, Wenxin, Jing, Anders. Your input and support have been invaluable for the model development and the experimental design of the studies.

Thirdly, I would like to thank the large PhD-community (some who are no longer PhD-students) around me, both at INES and at CEC. I have truly enjoyed my time with you, and had lots of fun, interesting conversations and memorable moments. A special thank goes to Klas Lucander, whom I have spent countless of hours with throughout my time as a PhD discussing science, our PhD-studies and deeply personal thoughts. Thank you!

I would also like to thank the PhD-students, and community at Gothenburg University and within the ClimBEco reseach school, especially the PhD-students participating in the mentor programme together with me. That was a great year, and I learned so much from our common experiences.

A big thanks for all the support from my family, I am truly lucky to have such a strong family to lean on and support me when times get rough.

Finally, I could not have made it through these years without the support, patience and love from Ingrid. You have endured my sleepless nights, absent-mindedness and anxiety. You and Signe are the love and joy of my life!

Paper I

Biogeosciences, 18, 6329–6347, 2021
https://doi.org/10.5194/bg-18-6329-2021

Biogeosciences Open Access EGU

Nitrogen restricts future sub-arctic treeline advance in an individual-based dynamic vegetation model

Adrian Gustafson[1,2], **Paul A. Miller**[1,2], **Robert G. Björk**[4,5], **Stefan Olin**[1], **and Benjamin Smith**[1,3]

[1]Department of Physical Geography and Ecosystem Science, Lund University, Sölvegatan 12, 223 62 Lund, Sweden
[2]Centre for Environmental and Climate Science, Lund University, Sölvegatan 37, 223 62 Lund, Sweden
[3]Hawkesbury Institute for the Environment, Western Sydney University, Penrith, NSW 2751, Australia
[4]Department of Earth Sciences, University of Gothenburg, P.O. Box 460, 405 30 Gothenburg, Sweden
[5]Gothenburg Global Biodiversity Centre, P.O. Box 461, 405 30 Gothenburg, Sweden

Correspondence: Adrian Gustafson (adrian.gustafson@nateko.lu.se)

Received: 24 June 2021 – Discussion started: 28 June 2021
Revised: 25 October 2021 – Accepted: 29 October 2021 – Published: 13 December 2021

Abstract. Arctic environmental change induces shifts in high-latitude plant community composition and stature with implications for Arctic carbon cycling and energy exchange. Two major components of change in high-latitude ecosystems are the advancement of trees into tundra and the increased abundance and size of shrubs. How future changes in key climatic and environmental drivers will affect distributions of major ecosystem types is an active area of research. Dynamic vegetation models (DVMs) offer a way to investigate multiple and interacting drivers of vegetation distribution and ecosystem function. We employed the LPJ-GUESS tree-individual-based DVM over the Torneträsk area, a sub-arctic landscape in northern Sweden. Using a highly resolved climate dataset to downscale CMIP5 climate data from three global climate models and two 21st-century future scenarios (RCP2.6 and RCP8.5), we investigated future impacts of climate change on these ecosystems. We also performed model experiments where we factorially varied drivers (climate, nitrogen deposition and [CO_2]) to disentangle the effects of each on ecosystem properties and functions. Our model predicted that treelines could advance by between 45 and 195 elevational metres by 2100, depending on the scenario. Temperature was a strong driver of vegetation change, with nitrogen availability identified as an important modulator of treeline advance. While increased CO_2 fertilisation drove productivity increases, it did not result in range shifts of trees. Treeline advance was realistically simulated without any temperature dependence on growth, but biomass was overestimated. Our finding that nitrogen cycling could modulate treeline advance underlines the importance of representing plant–soil interactions in models to project future Arctic vegetation change.

1 Introduction

In recent decades, the Arctic has been observed becoming greener (Epstein et al., 2012; Bhatt et al., 2010). Causes include an increased growth and abundance of shrubs (Myers-Smith et al., 2011; Elmendorf et al., 2012; Forbes et al., 2010), increased vegetation stature associated with a longer growing season, and poleward advance of the Arctic treeline (Bjorkman et al., 2018). Shrubs protruding through the snow and treeline advance alter surface albedo and energy exchange with potential feedback to the climate system (Chapin et al., 2005; Sturm, 2005; Serreze and Barry, 2011; Zhang et al., 2013, 2018). Warming and associated changes in high-latitude ecosystems have implications for carbon cycling through increased plant productivity, species shifts (Chapin et al., 2005; Zhang et al., 2014) and increased soil organic matter (SOM) decomposition with subsequent loss of carbon to the atmosphere. Studies of the Arctic carbon balance have shown that the region has been a weak sink in the past (Mcguire et al., 2009, 2012; Bruhwiler et al., 2021; Virkkala et al., 2021), although uncertainty is substantial, and it is difficult to determine accurately the strength of this sink. How climate and environmental changes will affect the relative balance between the carbon uptake, i.e. photosynthesis, and

release processes, i.e. autotrophic and heterotrophic respiration, will determine whether the Arctic will be a source or a sink of carbon in the future.

Forest–tundra ecotones constitute vast transition zones where abrupt changes in ecosystem functioning occur (Hofgaard et al., 2012). While a generally accepted theory of what drives treeline advance is currently lacking, several alternative explanations exist. Firstly, direct effects of rising temperatures have been thoroughly discussed (e.g. Rees et al., 2020; Hofgaard et al., 2019; Körner, 2015; Chapin, 1983). On the global scale, treelines have been found to correlate well with a 6–7 °C mean growing season ground temperature (Körner and Paulsen, 2004) and could thus be expected to follow isotherm movement as temperatures rise. A global study of alpine treeline advance in response to warming since 1900 showed that 52 % of treelines had advanced while the other half were stationary (47 %), with only occasional instances of retreat (1 %) (Harsch et al., 2009). Similar patterns have been observed on the circumarctic scale, although latitudinal treelines might be expected to shift more slowly than elevational treelines due to dispersal constraints (Rees et al., 2020). As trees close to the treeline often show ample storage of non-structural carbohydrates (Hoch and Körner, 2012), it has been suggested that a minimum temperature requirement for wood formation, rather than productivity, might constrain treeline position (Körner, 2003, 2015; Körner et al., 2016).

Secondly, it has been hypothesised that indirect effects of warming might be as important as or more important than direct effects (Sullivan et al., 2015; Chapin, 1983). For example, rising air and soil temperatures might induce increased mineralisation and plant availability of nitrogen in the litter layer and soil (Chapin, 1983). Increased nitrogen uptake could in turn enhance plant productivity and growth (Dusenge et al., 2019). Increased nitrogen uptake as a consequence of increased soil temperatures or nitrogen fertilisation has been shown to increase seedling winter survival among seedlings of mountain birch (*Betula pubescens* ssp. *tortuosa*) – the main treeline species in Scandinavia (Weih and Karlsson, 1999; Karlsson and Weih, 1996).

Thirdly, experiments exposing plants and ecosystems to elevated CO_2 often show increased plant productivity and biomass increase, especially in trees (Ainsworth and Long, 2005). Terrestrial biosphere models generally emulate the same response (Hickler et al., 2008; Smith et al., 2014; Piao et al., 2013). Although difficult to measure in field experiments, the treeline position seems unresponsive to increased [CO_2] alone (Holtmeier and Broll, 2007). Whether treelines are responsive to increased productivity through CO_2 fertilisation might yield insights into whether treelines are limited by their productivity, i.e. photosynthesis, versus their ability to utilise assimilated carbon, i.e. wood formation. However, the extent to which increased [CO_2] drives long-term tree and shrub encroachment and growth remains poorly studied.

For treeline migration to occur, it is not only the growth and increased stature of established trees but also the recruitment and survival of new individuals beyond the existing treeline that is important (Holtmeier and Broll, 2007). Seedlings of treeline species are sometimes observed above the treeline, especially in sheltered microhabitats (Hofgaard et al., 2009; Sundqvist et al., 2008). However, these individuals often display stunted growth and can be decades old, although age declines with elevation (Hofgaard et al., 2009). The suitability of the tundra environment for trees to establish and grow taller will thus be an important factor for the rate of treeline advance (Cairns and Moen, 2004). Interspecific competition and herbivory are known to be important modulators of range shifts of trees (Cairns and Moen, 2004; Van Bogaert et al., 2011; Grau et al., 2012). For instance, the presence of shrubs has been shown to limit tree seedling growth (Weih and Karlsson, 1999; Grau et al., 2012), likely as a consequence of competition with tree seedlings for nitrogen. Comparisons of a model incorporating only bioclimatic limits to species distributions and more ecologically complex models have also suggested interspecific plant competition to be important for range shifts of trees (Epstein et al., 2007; Scherrer et al., 2020). Thus, as a fourth factor, shrub–tree interactions could be important when predicting range shifts such as changing treeline positions under future climates. Rising temperatures have been suggested as the dominant driver of increased shrub growth, especially where soil moisture is not limiting (Myers-Smith et al., 2015, 2018). Furthermore, a changed precipitation regime, especially increased winter snowfall, might promote establishment of trees and shrubs through the insulating effects of snow cover with subsequent increases in seedling winter survival (Hallinger et al., 2010).

A narrow focus on a single variable, e.g. summer temperature, or a few driving variables may lead to overestimation of treeline advance in future projections (Hofgaard et al., 2019). Dynamic vegetation models (DVMs) offer a way to investigate the influence of multiple and interacting drivers on vegetation and ecosystem processes. Model predictions may be compared with observations of local treelines and ecotones to validate assumptions embedded in the models and to interpret causality in observed dynamics and patterns. DVMs also offer a way to extrapolate observable local phenomena to broader scales, such as that of circumarctic shifts in the forest–tundra ecotone and the responsible drivers. Here, we examine a sub-arctic forest–tundra ecotone that has undergone spatial shifts over recent decades (Callaghan et al., 2013), previously attributed to climate warming. Adopting an individual-based DVM incorporating a detailed description of vegetation composition and stature and nitrogen cycle dynamics, we apply the model at a high spatial resolution to compare observed and predicted recent treeline dynamics, and we project future vegetation change and its implications for carbon balance and biogeophysical vegetation–atmosphere feedbacks. In addition, we conduct three model experiments to separate and interpret the impact of driving

factors (climate, nitrogen deposition, [CO_2]) on vegetation in a forest–tundra ecotone in Sweden's sub-arctic north.

2 Materials and methods

2.1 Study site

Abisko Scientific Research Station (ANS; 68°21′ N, 18°49′ E), situated in the mountain-fringed Abisko Valley near Lake Torneträsk in northern Sweden, has a long record of ecological and climate research. The climate record dates back to 1913 and is still ongoing. The area is situated in a rain shadow and is thus relatively dry despite its proximity to the ocean (Callaghan et al., 2013). The forests in the lower parts of the valley consist mostly of mountain birch *Betula pubescens* ssp. *czerepanovii*, which is also dominant at the treeline. Treeline elevation in the Abisko Valley ranges between 600–800 m above sea level (a.s.l.) (Callaghan et al., 2013). Other tree types in lower parts of the valley are *Sorbus aucuparia* and *Populus tremula*, along with small populations of *Pinus sylvestris*, which are assumed to be refugia species from warmer periods during the Holocene (Berglund et al., 1996). Soils consist of glaciofluvial till and sediments. An extensive summary of previous studies and the environment around Lake Torneträsk can be found in Callaghan et al. (2013).

Our study domain covers an area of approximately 85 km^2 and extends from Mount Nuolja in the west to the mountain Nissončorru in the east (see Fig. 2). The northern part of our study domain is bounded by Lake Torneträsk. The mean annual temperature was -0.5 ± 0.9 °C for the 30-year period 1971–2000 (Fig. 1, Table 2), with January being the coldest month (-10.2 ± 3.5 °C) and July the warmest (11.3 ± 1.4 °C). Mean annual precipitation was 323 ± 66 mm for the same reference period. This reference period was chosen as it is the last one in the dataset by Yang et al. (2011).

2.2 Ecosystem model

We used the LPJ-GUESS DVM as the main tool for our study (Smith et al., 2001, 2014; Miller and Smith, 2012). LPJ-GUESS is one of the most ecologically detailed models of its class, suitable for regional- and global-scale studies of climate impacts on vegetation, employing an individual- and patch-based representation of vegetation composition and structure. It simulates the dynamics of plant populations and ecosystem carbon, nitrogen and water exchanges in response to external climate forcing. Biogeophysical processes (e.g. soil hydrology and evapotranspiration) and plant physiological processes (e.g. photosynthesis, respiration, carbon allocation) are interlinked and represented mechanistically. Canopy fluxes of carbon dioxide and water vapour are calculated by a coupled photosynthesis and stomatal conductance scheme based on the approach of BIOME3 (Haxeltine and Prentice, 1996). Photosynthesis is a function of air

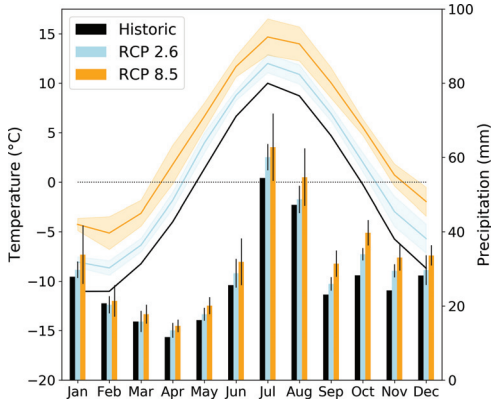

Figure 1. Historic (1971–2000) and projected (2071–2100) temperature (left) and precipitation (right) variability at the Abisko study area. The shaded areas (temperature) and narrow bars (precipitation) mark ±1 standard deviation uncertainty in the three CMIP5 multi-model means for RCP2.6 and RCP8.5.

temperature, incoming short-wave or photosynthetically active radiation, [CO_2], and water and nutrient availability. Autotrophic respiration has three components – maintenance, growth and leaf respiration. Tissue maintenance respiration is dependent on soil and air temperature for root and aboveground respiration, respectively, along with a dependency on tissue C : N stoichiometry. All assimilated carbon that is not consumed by autotrophic respiration, less a 10 % flux to reproductive organs, is allocated to leaves; fine roots; and, for woody plant functional types (PFTs), sapwood, following a set of prescribed allometric relationships for each PFT, resulting in biomass, height and diameter growth (Sitch et al., 2003). Consequently, an individual in the model is assumed to be carbon limited when autotrophic respiration equals or exceeds the amount of carbon assimilated by photosynthesis. A chronically negative carbon balance at the individual level eventually results in plant death.

The model assumes the presence of seeds in all grid cells, meaning that simulated PFTs can establish once the climate is favourable, as defined by each PFT's predefined bioclimatic limits. The competition between neighbouring plant individuals for light, water and nutrients, affecting establishment, growth and mortality, is modelled explicitly. Competition for light and nutrients is assumed to be asymmetric; i.e. individuals with taller canopies or larger root systems will be advantaged in the capture of resources under scarcity. Water uptake is divided equally among individuals according to the water availability and the fraction of each PFT's roots occupying each soil layer. Individuals of the same age co-occurring in a local neighbourhood or patch and belonging to the same PFT (see below) are assumed to be identical to each

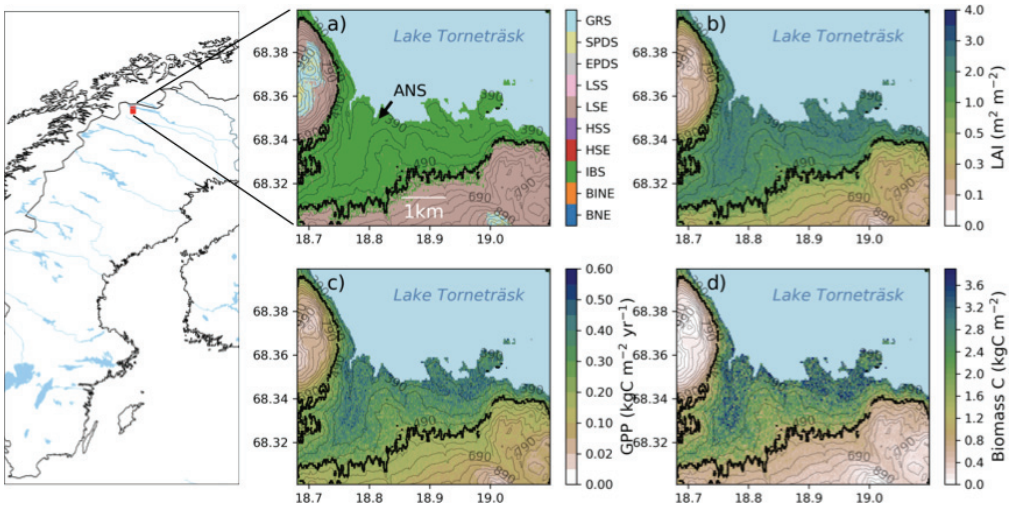

Figure 2. Map of Sweden and Scandinavia with a red square marking the study area. The location of the Abisko Scientific Research Station (ANS) is marked in panel **(a)**. Panels on the right show the study area in more detail and the modelled forest–tundra ecotone for the historic period (1990–2000). **(a)** Dominant PFT (BNE – boreal needle leaved evergreen tree; BINE – boreal shade-intolerant needle leaved tree; IBS – boreal shade-intolerant broadleaved tree; HSE – tall evergreen shrub; HSS – tall summergreen shrub; LSE – low evergreen shrub; LSS – low summergreen shrub; EPDS – evergreen prostrate dwarf shrub; SPDS – summergreen prostrate dwarf shrub; GRS – grasses) in the ecotone and total ecosystem, **(b)** LAI ($m^2\ m^{-2}$), **(c)** productivity (GPP; $kgC\ m^{-2}\ yr^{-1}$), and **(d)** plant biomass carbon density ($kgC\ m^{-2}$). The black line in panels **(a)**–**(d)** shows the modelled treeline position. Numbers on the contour lines mark the elevation in metres above sea level. Data source for map: Natural Earth.

other. Decomposition of plant litter and cycling of soil nutrients are represented by a CENTURY-based soil biogeochemistry module, applied at the patch scale (Smith et al., 2014). Biological N fixation is represented by an empirical relationship between annual evapotranspiration and nitrogen fixation (Cleveland et al., 1999). LPJ-GUESS does not currently incorporate PFT-specific nitrogen fixation, which for instance may be associated with species that form root nodules, such as *Alnus* spp. Additional inputs of nitrogen to the system occur through nitrogen deposition or fertilisation. Nitrogen is lost from the system through leaching, gaseous emissions from soils or wildfires (Smith et al., 2014).

For this study we employed LPJ-GUESS version 4.0 (Smith et al., 2014), enhanced with arctic-specific features (Miller and Smith, 2012; Wania et al., 2009). The combined model incorporates an updated set of arctic PFTs (described below), improved soil physics and a multi-layered dynamic snow scheme, allowing for simulation of permafrost and frozen ground. The soil scheme includes 15 equally distributed soil layers constituting a total soil depth of 1.5 m.

Vegetation in the model is represented by cohorts of individuals interacting in local communities or patches and belonging to a number of PFTs that are distinguished by growth form (tree, shrub, herbaceous), life history strategies (shade tolerant or intolerant) and phenology class (evergreen or summergreen). Herbaceous PFTs are represented as a dynamic, aggregate cover of ground layer vegetation in each patch. In this study 11 PFTs were implemented (see Table S2.1 in the Supplement for a description of included PFTs; see Table S2.2 in the Supplement for parameter values associated with each PFT). Out of these, three were tree PFTs: boreal needle-leaved evergreen tree (BNE), boreal shade-intolerant evergreen tree (BINE) and boreal shade-intolerant broad-leaved summergreen tree (IBS). Corresponding tree species present in the Torneträsk region include *Picea abies* (BNE), *Pinus sylvestris* (BINE), *Betula pubescens* ssp. *czerepanovii*, *Populus tremula* and *Sorbus aucuparia* (IBS). Following Wolf et al. (2008), shrub PFTs with different statures were implemented as follows: tall summergreen shrub (HSS) and tall evergreen shrub (HSE), corresponding to *Salix* spp. (HSS) and *Juniperus communis* (HSE), and low summergreen shrub (LSS) and low evergreen shrub (LSE) such as *Betula nana* (LSS) and *Empetrum nigrum* (LSE). We also included prostrate shrubs and two herbaceous PFTs.

Grid cell vegetation and biogeophysical properties are calculated by averaging over a number of replicate patches, each nominally 0.1 ha in area and subject to the same climate forcing. No assumptions are made about how the patches are distributed within a grid cell; they are a statistical sample of equally possible disturbance/demographic histories across the landscape of a grid cell. Within each patch, the establishment, growth and mortality of tree or shrub cohorts comprising individuals of equal age (and dynamic size/form) are modelled annually (Smith et al., 2001, 2014). Establishment and mortality have both an abiotic (bioclimatic) and a biotic (competition-mediated) component. Vegetation dynamics, i.e. changes in the distribution and abundance of different PFTs in grid cells over time, are an emergent outcome of the competition for resources between PFT cohorts at the patch level within an overall climate envelope determined by bioclimatic limits for establishment and survival. The bioclimatic envelope is a hard limit to vegetation distribution, intended to represent the physiological niche of a PFT. Furthermore, the climate envelope is a proxy not only for physiological processes such as meristem activity that may set species ranges but also for climatic stressors such as tissue freezing. The parameters are intended to capture broader climatic properties of each grid cell. A detailed description of each bioclimatic parameter and its respective values can be found in Table S2.2 in the Supplement. Disturbance is accounted for by the occasional removal of all vegetation within a patch with an annual probability of $300\,yr^{-1}$, representing random events such as storms, avalanches, insect outbreaks and windthrow. The study used three replicate patches within each 50×50 m grid cell. We judged this number sufficient to obtain a stable representation of vegetation dynamics given the relative area of each grid cell and replicate patches (0.1 ha). For summergreen PFTs we slightly modified the assumption of a fixed growing degree day (GDD) requirement for establishment, using thawing degree days (TDDs – degree days with a 0 °C basis; see Table S2.2) to capture the thermal sum requirement for the establishment of new individuals.

2.3 Forcing data

The input variables used as forcing in LPJ-GUESS simulations are monthly 2 m air temperature (°C), precipitation (mm) and incoming short-wave radiation ($W\,m^{-2}$) as well as annual atmospheric [CO_2] (ppm), soil texture (mineral fractions only) and nitrogen deposition (kgN per hectare per month). Monthly air temperature and short-wave radiation are interpolated to a daily time step, while precipitation is randomly distributed over the month using monthly wet days.

2.3.1 Historic period

A highly resolved (50×50 m) temperature and radiation dataset using field measurements and a digital elevation model (DEM) by Yang et al. (2011) provided climate input to the model simulations for the historic period (1913–2000). The field measurements were conducted in the form of transects that captured mesoscale climatic variations, i.e. lapse rates. In addition, the transects were placed to capture microclimatic effects of the nearby Lake Torneträsk and aspect effects on radiation influx. The temperature in the lower parts of the Abisko Valley in the resulting dataset was influenced by the lake, with milder winters and less yearly variability. At higher elevation, the temperature was more variable over the year and the local-scale variations were more dependent on the different solar angles between seasons and by aspect (Yang et al., 2011, 2012) (see Fig. S1.1 in the Supplement). For a full description of how this dataset was constructed we refer to Yang et al. (2011, 2012).

Monthly precipitation input was obtained from the Abisko Scientific Research Station weather records. Precipitation was randomly distributed over each month using the number of wet days from the CRUNCEP v.7 dataset (Wei et al., 2014). We assumed that local differences in precipitation can be neglected for our study domain, and thus the raw station data were used as input to LPJ-GUESS for the historic period. Nitrogen deposition data for the historic and future simulations were extracted from the grid cell including Abisko in the dataset of Lamarque et al. (2013). Nitrogen deposition was assumed to be distributed equally over the study domain.

Soil texture was extracted from the WISE soil dataset (Batjes, 2005) for the Abisko area and assumed to be uniform across the study domain. Callaghan et al. (2013) report that the soils around the Torneträsk areas are mainly glaciofluvial till and sediments. Clay and silt fractions vary between 20 %–50 % (Josefsson, 1990) with higher fractions of clay and silt in the birch forest and a larger sand content in the heaths. In the absence of spatial information on particle size distributions, the soil was prescribed as a sandy loam soil with 43 % sand and approximately equal fractions of silt and clay.

2.3.2 Future simulations

Future estimates of vegetation change were simulated for one low-emission (RCP2.6) and one high-emission (RCP8.5) scenario. For each scenario, climate change projections from three global climate models (GCMs) from the CMIP5 GCM ensemble (Taylor et al., 2012) were used to investigate climate effects on vegetation dynamics. The chosen GCMs (MIROC-ESM-CHEM, HadGEM2-AO, GFDL-ESM2M) were selected to represent the largest spread, i.e. the highest, the lowest and near average, in modelled mean annual temperature for the reference period 2071–2100. Only models with available simulations for both RCP2.6 and RCP8.5 were used in the selection. Monthly climate data for input to LPJ-GUESS (temperature, total precipitation and short-wave radiation) were extracted for the grid cell including Abisko for each GCM. The number of wet days per month was assumed not to change in the future scenario sim-

ulations, so we used the 1971–2000 climatology for this period.

The historic climate dataset by Yang et al. (2011) was extended into the projection period (2001–2100) using the delta change approach as follows. For each grid cell monthly differences were calculated between the projection climate and the dataset by Yang et al. (2011) for the last 30-year reference period in our historic dataset (1971–2000). For temperature, the arithmetic difference was extracted, while for precipitation and incoming short-wave radiation, relative (i.e. geometric) differences between the two datasets were extracted. The resulting monthly anomalies were then either added (temperature) to the GCM outputs or used to multiply (precipitation, radiation) the GCM outputs from 2001–2100, for each of the climate scenarios used. Forcing data of atmospheric [CO_2] for the two scenarios were obtained from the CMIP5 project.

2.4 Model experiments

To investigate the possible drivers of future vegetation change, we performed three model experiments. The model was forced with changes to one category of input (driver) variables (climate, [CO_2], nitrogen deposition) at a time for a projection period between the years 2001–2100. A full list of simulations can be found in Table S3 (Supplement).

A control scenario with no climate trend (and with [CO_2] and nitrogen deposition held at their respective year 2000 values) was also created. We estimated the effect of the transient climate change, [CO_2] or nitrogen deposition scenarios by subtracting model results for the last decade (2090–2100) in the no-trend scenario from those for the last decade (2090–2100) of the respective transient scenario. To estimate how sensitive the model was to different factors, we performed a Spearman rank correlation for each PFT in 50 m elevational bands over the forest–tundra ecotone. We chose Spearman rank over Pearson since not all correlations were linear.

2.4.1 Climate change

To estimate the sensitivity to climate change, the same scenarios as those used for the future simulations (Sect. 2.3.2) were used while [CO_2] and nitrogen deposition were held constant at their year 2000 value.

Climate anomalies without any trend were created by randomly sampling full years in the last decade (1990–2000) from the climate station data. The climate dataset was then extended using these data. The resulting climate scenario had the same interannual variability as the historic dataset and no trend for the years 2001–2100. This scenario was used to investigate any lag effects on vegetation change. This scenario also provided climate input for the nitrogen and [CO_2] sensitivity tests described below.

2.4.2 CO_2

For our projection simulations we used five different [CO_2] scenarios from the CMIP5 project. High-emission (RCP8.5), medium-emission (RCP6.0, RCP4.5) and low-emission (RCP2.6) scenarios as well as a "no change" emission scenario were used.

2.4.3 Nitrogen deposition

Scenarios of nitrogen deposition were obtained from the Lamarque et al. (2013) dataset. Since this dataset assumes a decrease in nitrogen deposition after the year 2000, we also added four scenarios where nitrogen deposition increased with 2, 5, 7.5 and 10 times the nitrogen deposition relative to the year 2000. These four scenarios were created to isolate the single-factor effect of nitrogen increase without any climate or [CO_2] change. The resulting additional loads of nitrogen after the year 2000 in these scenarios were 0.38, 0.97, 1.46 and 1.9 $gN\,m^{-2}\,yr^{-1}$, respectively.

2.5 Model evaluation

We evaluated the model against available observations in the Abisko area. Measurements of ecosystem productivity from an eddy covariance (EC) tower were obtained for 6 non-consecutive years (Olsson et al., 2017). Biomass and biomass change estimates were used to evaluate simulated biomass in the birch forest (Hedenås et al., 2011). Surveys of historic vegetation change above the treeline were obtained from Rundqvist et al. (2011). Leaf area index (LAI) and evapotranspiration estimates were obtained from Ovhed and Holmgren (1996).

The studies by Hedenås et al. (2011) and Rundqvist et al. (2011) were used to evaluate model outputs around the observation year 2010. To compare biomass and vegetation change with these studies, we extracted 5-year multi-model averages for 2008–2012 from our projection simulations (Sect. 2.3.2). These means were used to calculate modelled change in biomass and vegetation in our historic dataset and to compare the modelled output to the observational data.

To determine the local rates of treeline migration, several transects were defined within our study domain (Fig. S1.2 in the Supplement). These transects were chosen to represent a large spread in heterogeneity with regard to slope and aspect in the landscape. A subsample of the selected transects were placed close to the transects used by Van Bogaert et al. (2011) and used to evaluate model performance. Results from the model evaluation are summarised in Tables 1 and S1.1.

2.6 Determination of domains in the forest–tundra ecotone

In our analysis we distinguished between forest, treeline and shrub tundra, defined as follows. Any grid cell containing 30 % fractional projective cover or more of trees was clas-

Table 1. Model evaluation and benchmarking results.

Parameter	Unit	Domain	Time interval	Model value	Observed estimate	Reference
GPP (average)	$gC\,m^{-2}\,yr^{-1}$	Birch forest	2007–2014	410 ± 64	440 ± 54	Olsson et al. (2017)
Carbon density	$tC\,ha^{-1}$	Birch forest	2010	21.8 ± 10	4.39 ± 3.46	Hedenås et al. (2011)
Carbon density change	%	Birch forest	1997–2010	25	19	Hedenås et al. (2011)
LAI	$m^2\,m^{-2}$	Forest canopy Understorey	1988–1989	1.65 ± 0.66 0.17 ± 0.12	~ 2.0 ~ 0.5	Ovhed and Holmgren (1996)
Densification	%	Shrub tundra	1976–2010	$+87 \pm 15$	+50 to 80	Rundqvist et al. (2011)
Treeline elevation (min) Treeline elevation (mean) Treeline elevation (max)	m. a.s.l.	Treeline	2010	444 564 723	~ 600 – ~ 800	Callaghan et al. (2013)
Treeline elevation change (mean) Treeline elevation change (max)	Elevational metres	Treeline	1912–2009	80 123	24 145	Van Bogaert et al. (2011)
Treeline migration rate (mean) Treeline migration rate (max)	$m\,yr^{-1}$	Treeline	1912–2009	+0.85 +1.18	+0.6 +1.1	Van Bogaert et al. (2011)

sified as forest. This limit has been used by other studies in the area (e.g. Van Bogaert et al., 2011) to determine the birch forest boundary. The treeline was then determined by first selecting grid cells classified as forest. Any grid cell with four or more neighbours fulfilling the 30 % cover condition criterion was classified as belonging to the forest. The perimeter of the forest was then determined through sorting out grid cells with four or five neighbours classified as forest. Grid cells with fewer or more neighbours were regarded as tundra or forest, respectively. Grid cells below the treeline were classified as forest in the analysis, and grid cells above the treeline were classified as tundra.

2.7 Presentation of results

We present seasonal values for soil and air temperature. These are averages of the 3-month periods DJF, MAM, JJA and SON, referred to as winter, spring, summer and autumn below. For the RCPs average values are presented with the ranges of the different scenarios within each RCP given in parentheses. We report values of both gross primary production (GPP), which we benchmark the model against, and net primary productivity (NPP) as this is of relevance for the carbon limitation discussion.

3 Results

3.1 Historic vegetation shifts

The dominant PFT in the forest and at the treeline was IBS, which constituted 90 % of the total LAI (Figs. 2a–3a). The only other tree PFT present in the forest was BINE, which comprised a minor fraction of total LAI. However, in the lower (warmer) parts of the landscape, BINE comprised up to 20 % of the total LAI in a few grid cells. The forest understorey was mixed but consisted mostly of tall and low evergreen shrubs and grasses. Shrub tundra vegetation above the treeline was more mixed, but LSE dominated with 51 % of the total LAI. Grasses comprised an additional 25 % of the total LAI, and IBS was present close to the treeline, where it comprised up to 5 % of the LAI in some grid cells. NPP for IBS in the forest increased from 96 to 180 $gC\,m^{-2}\,yr^{-1}$ over our historic period (1913–2000). Corresponding values at the treeline did not increase but were saturated at around 60 $gC\,m^{-2}\,yr^{-1}$. Above the treeline, IBS showed very low NPP values (<15 $gC\,m^{-2}\,yr^{-1}$), while NPP for the dominant shrub (LSE) doubled from 20 $gC\,m^{-2}\,yr^{-1}$ at the treeline to 40 $gC\,m^{-2}\,yr^{-1}$ in the tundra.

Between the start and end of our historic (1913–2000) simulation the treeline shifted upwards by 67 elevational metres on average, corresponding to a rate of 0.83 $m\,yr^{-1}$. However, during the 20th century both a period (1913–1940) with more rapid warming (0.8 °C) and a faster tree migration rate (1.23 $m\,yr^{-1}$) and a period (1940–1980) with a cooling trend (−0.3 °C) and stationary treeline occurred (Fig. 5). Between 1913–2000, the lower boundary of the treeline shifted upwards by 2 m, while treeline upper boundaries shifted upwards by 123 m. These shifts corresponded to rates of 0.03 and 1.54 $m\,yr^{-1}$, respectively. Similar rates were also found in the transects established to test how the model simulates the heterogeneity of treeline migration (Fig. S1.2 and Table S1.1 in the Supplement), where the average migration rate was 0.87 (0.54–1.25) $m\,yr^{-1}$.

During the 1913–2000 period, annual average air temperature at the simulated treeline warmed from −2.0 to −0.8 °C. Warming occurred throughout the year but was strongest in winter and spring, when temperatures increased by 3.0 and 1.4 °C, respectively. In contrast, both summer and autumn

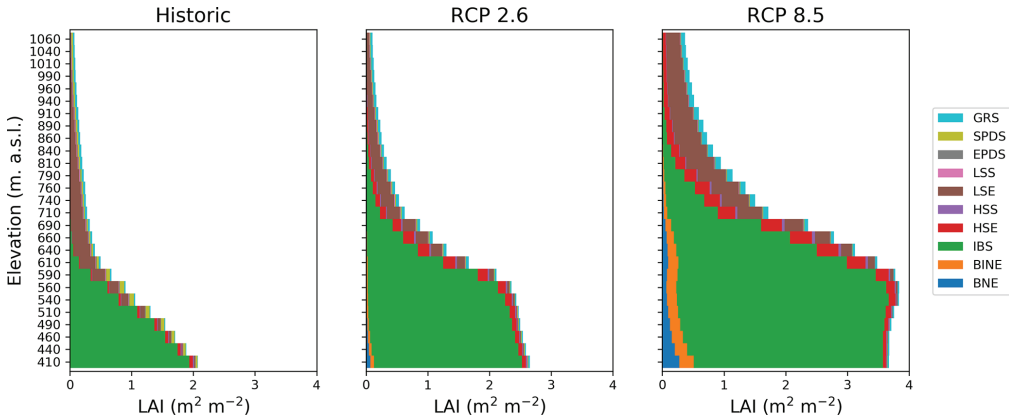

Figure 3. Leaf area index (LAI) in the forest–tundra ecotone for the historic period (1990–2000) **(a)** and at the end of the century (2090–2100) for **(b)** RCP2.6 and **(c)** RCP8.5, respectively. Each bar represents 50 elevational metres.

temperatures warmed by only 0.6 °C. The resulting winter, spring, summer and autumn air temperatures at the treeline in 1990–2000 were −8.7, 3.3, 8.8 and −0.1 °C, respectively. The warming was also reflected in annual average soil temperature increases of a similar magnitude, by 2.1 °C from −0.8 to 1.3 °C. Winter soil temperature increased by 3.7 °C from −5.6 °C in 1913 to −1.9 °C in 2000. The warmer soil temperatures resulted in a 4.8 % simulated increase in the annual net nitrogen mineralisation rate in the treeline soils over the same period. In absolute numbers, nitrogen mineralisation increased from 1.29 to 1.36 gN m^{-2}. Combined with an increased nitrogen deposition load from 0.06 gN m^{-2} in 1913 to 0.20 gN m^{-2} in 2000 and an increased nitrogen fixation from 0.13 to 0.18 gN m^{-2}, plant-available nitrogen was simulated to increase by 15.9 %. Simulated permafrost with an active layer thickness of <1.5 m was present at elevations down to 560 m a.s.l. in a few grid cells but was always well above the treeline. More shallow permafrost (active layer thickness <1 m) was only present in grid cells at elevations of 940 m a.s.l. and above.

3.2 Projected vegetation shifts

During the 100-year projection period (2001–2100) treelines advanced by between 45 (HadGEM2-AO-RCP2.6) and 195 (GFDL-ESM2M-RCP8.5) elevational metres in the different scenarios, corresponding to rates of 0.45 and 1.95 elevational metres per year. The total LAI increased in the entire ecotone in both RCP2.6 and RCP8.5 compared to the historic (1990–2000) values (Fig. 3b–c). The increase was more pronounced in RCP8.5, which also saw a large increase in low evergreen shrubs (LSE) at the end of the century (2090–2100). While the forest was still dominated by IBS, evergreen trees (BNE and BINE) increased and together comprised approximately 15 % of the total LAI. The fraction of evergreen trees in the forest correlated well with the degree of warming in each scenario. Forest GPP was mainly driven by tree PFTs and increased by 50 % (12 %–99 %) for RCP2.6 and 177 % (98 %–270 %) for RCP8.5. Above the treeline, low shrubs (LSS and LSE) contributed the most to annual GPP change, which increased by 33 % (−12 % to 67 %) and 239 % (105 %–370 %) in RCP2.6 and RCP8.5, respectively. Forest NPP, wherein IBS was always dominant, increased from 200 gC m^{-2} yr^{-1} in the year 2000 to 300 (220–375) gC m^{-2} yr^{-1} and 490 (380–610) gC m^{-2} yr^{-1} for RCP2.6 and RCP8.5, respectively, over the projection period. NPP for the same period for IBS at the treeline increased slightly from 60 gC m^{-2} yr^{-1} to 80 (74–90) gC m^{-2} yr^{-1} and 104 (80–116) gC m^{-2} yr^{-1} for RCP2.6 and RCP8.5. Above the treeline NPP remained low (<25 gC m^{-2} yr^{-1}) for IBS in all scenarios and always had a lower NPP than the most productive shrub PFT (LSE). NPP for this shrub was 49 (24–64) gC m^{-2} yr^{-1} and 130 (81–180) gC m^{-2} yr^{-1}. The productivity increase translated into a biomass C increase of the same magnitude both in the forest and above the treeline.

The average summer air temperature at the treeline between the last decade of the historic and projection periods increased by 0.3 and 6.7 °C for the coldest (GFDL-ESM2M-RCP2.6) and warmest (MIROC-ESM-CHEM-RCP8.5) GCM scenario, respectively. The advance of the 6 °C JJA soil temperature isotherm was more rapid than the treeline advance (Fig. 4). In the two warmest scenarios (MIROC-ESM-CHEM-RCP8.5 and HadGEM2-AO-RCP8.5) summer soil temperatures exceeded 6 °C in the whole study domain. Treeline elevations in these scenarios

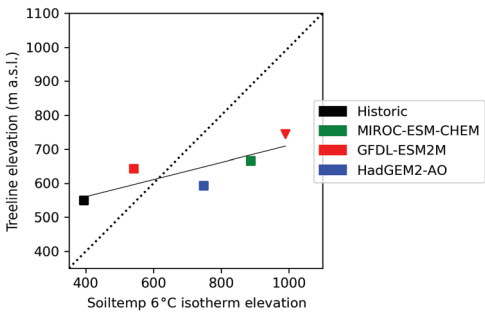

Figure 4. JJA 6 °C soil temperature isotherm elevation relative to average treeline elevation. Square markers represent RCP2.6, and triangles represent RCP8.5. In the two warmest scenarios (HadGEM2-AO-RCP8.5 and MIROC-ESM-CHEM-RCP8.5), the 6 °C soil temperatures exceed 6 °C in the whole landscape. The dotted line represents the 1 : 1 relationship between the treeline and isotherm placement, and the solid line displays the treeline–soil temperature regression.

only reached 745 and 660 m a.s.l., respectively. Treelines advanced almost twice as fast in RCP8.5 compared to RCP2.6, by 1.55 (1.10–1.96) m yr^{-1} and 0.84 (0.44–1.16) m yr^{-1}, respectively.

3.3 Model experiments

A slight treeline advance at the end of the projection period (2090–2100) of approximately 11 elevational metres was seen in the control simulation. As all drivers were held constant or trend-free in this simulation, this reveals a lag from the historical period, likely resulting from smaller trees that had established in the historic period that matured during the projection period.

3.3.1 Climate change

Treeline advance occurred in all climate change scenarios although the rate was not uniform throughout the projection period (Fig. 5). When driven by climate change alone, migration rates were faster compared to simulations where nitrogen deposition and [CO_2] were also changed (Sect. 3.2). Treeline advance in climate-change-only scenarios ranged between 60 elevational metres (HadGEM2-AO-RCP2.6) and 245 elevational metres (MIROC-ESM-CHEM-RCP8.5) over the 100-year projection period.

Tree productivity was strongly enhanced by air temperature increase over the whole study domain (Fig. 6a). Weaker correlations between productivity and other climate factors such as precipitation and net short-wave radiation were also seen (Figs. S1.5 and S1.6 in the Supplement). Annual precipitation increased in all climate change scenarios (Table 2). In the lower parts of the valley, the increased precipitation did not result in increased soil moisture during summer as losses through evapotranspiration driven by temperature exceeded the additional input. Spring and autumn soil moisture increased in the forest, mainly because of earlier snowmelt and thawing ground in spring and relatively weaker evapotranspiration in autumn. Above the treeline, soil moisture increased as the lower temperatures and LAI did not drive evapotranspiration as strongly as in the lower parts of the valley, and the increased moisture input thus outweighed the slightly increased evapotranspiration.

Increased tree productivity in the forest resulted in an increased LAI of 0.3–1.5 $m^2\ m^{-2}$ (18 %–90 %). BNE appeared in the forest and dominated in a few grid cells. In most places BNE constituted approximately 5 % of the total LAI. Tall shrub (HSE and HSS) productivity and the LAI increased in the forest. This increase was negatively correlated with temperature; i.e. the increase was highest in the coolest climate change scenarios. Above the treeline, tall shrubs showed the opposite pattern, increasing by 8 %–50 % to finally constitute 10 %–36 % of the total LAI.

Higher soil moisture content in spring and autumn favoured trees in the whole ecotone, while the forest understorey suffered from the earlier onset of the growing season with subsequent flushing of the leaf and light shading from taller competitors. Although soil moisture in summer decreased in the forest, the LAI and biomass carbon of summergreen shrubs were positively correlated with soil moisture. Higher soil moisture during summers in the wetter GCM scenarios promoted summergreen shrubs over evergreen shrubs in the whole ecotone. As an example, vegetation composition on the tundra above the treeline differed between GFDL-ESM2M and MIROC-ESM-CHEM under RCP8.5, where the warmer GCM showed a 52 % biomass C increase in the tall evergreen shrub, HSE. The intermediate warming scenario (GFDL-ESM2M-RCP8.5) showed a more mixed increase in biomass carbon in HSE (20 %) and HSS (24 %). While annual temperature differed by 3.9 °C between the two scenarios, average annual precipitation only differed by 6.2 mm, yielding much (26 %) lower JJA soil moisture in the warmest scenario (MIROC-ESM-CHEM-RCP8.5) compared to the coldest (GFDL-ESM2M-RCP8.5). Relatively higher soil moisture and subsequently lower water stress allow taller plants to establish.

Radiation correlated positively with the growth of tree PFTs, with spring and autumn radiation found to be especially important for height and biomass increase (Fig. S1.7 in the Supplement). Increased radiation provided a competitive advantage for taller trees and shrubs to shade out lower shrubs and grasses in the forest. Shrubs above the treeline were also favoured by increased light.

Net nitrogen mineralisation at the treeline showed great variation between different climate change scenarios, ranging from a 4 % decrease in GFDL-ESM2M-RCP8.5 to a 79 % increase in the strongest warming scenario (MIROC-ESM-

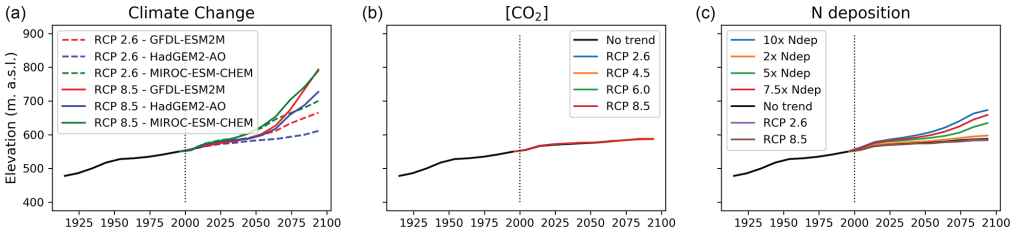

Figure 5. Shifts in average treeline elevation over the simulation period for the three experiments of **(a)** climate change, **(b)** CO_2 fertilisation and **(c)** nitrogen deposition. The start of projection simulations is marked with a vertical dotted line in all panels. The no-trend scenario in panels **(b)**–**(c)** represents a scenario where climate, CO_2 and nitrogen deposition are kept constant (without a trend) relative to the year 2000. The black line before the year 2000 represents the historic simulation.

Table 2. Seasonal temperature and precipitation for historic and scenario simulations.

		1971–2000			2071–2100			
		Yang et al. (2011)	GFDL-ESM2M		HadGEM2-AO		MIROC-ESM-CHEM	
	Season	Historic	RCP2.6	RCP8.5	RCP2.6	RCP8.5	RCP2.6	RCP8.5
Temperature (°C)	Winter (DJF)	−9.8	−8.2	−5.4	−8.1	−4.4	−7.4	−3.1
	Spring (MAM)	−2.1	−1.3	1.0	0.4	4.11	0.7	4.8
	Summer (JJA)	9.9	10.9	13.2	11.9	14.4	13.1	13.4
	Autumn (SON)	0.1	1.1	4.2	2.3	9.1	3.2	7.2
	Annual (mean)	−0.5	0.6	3.3	1.6	5.0	2.4	6.6
Precipitation (mm)	Winter (DJF)	75	80	85	75	80	70	95
	Spring (MAM)	45	40	45	40	45	50	55
	Summer (JJA)	125	130	130	130	150	135	145
	Autumn (SON)	75	90	95	85	95	95	110
	Annual (sum)	325	340	355	335	370	350	405

CHEM-RCP8.5). In absolute terms, the latter increase corresponds to an increase from 1.35 $gN\,m^{-2}\,yr^{-1}$ at the end of the historic period (1990–2000) to 2.43 $gN\,m^{-2}\,yr^{-1}$ at the end of the century (2090–2100). This is comparable to the nitrogen load in the 7.5× increased nitrogen deposition scenario. Interestingly, despite very different plant-available nitrogen and warming, the two scenarios displayed a similar resulting (2090–2100) treeline elevation (Fig. 5a).

Permafrost with an active layer thickness of <1.5 m disappeared completely from our study domain in all scenarios except the coldest (GFDL-ESM2M-RCP2.6), where it occurred in a few grid cells at elevations of approximately 600 m a.s.l. However, the shallow permafrost (<1 m) had also disappeared in this scenario.

3.3.2 CO_2

$[CO_2]$ increase enhanced productivity in most PFTs (Fig. 6b). The total GPP averaged over the forest increased by between 2 %–10 % depending on the $[CO_2]$ scenario, with the largest increase in RCP8.5 and smallest in RCP2.6. The CO_2 fertilisation effect was not uniform within the landscape but stronger towards the forest edge with increases from 2 % to 18 % from the weakest to the strongest $[CO_2]$ scenario. NPP for IBS increased uniformly over the forest with 2.5 %–8.4 % but decreased above the treeline. Thus, the productivity of the two dominant PFTs (IBS in the forest and LSE above the treeline) was reinforced in their respective domains. The increased productivity translated into a 1 %–5 % increase in the tree LAI in the forest, while the low shrub LAI increased by 24 %–77 %. Likewise, the increase in the leaf area of low shrubs was largest on the tundra under elevated $[CO_2]$, which saw a 15 %–40 % LAI increase in the low and high $[CO_2]$ scenario, respectively. Above the treeline, the productivity of grasses and low shrubs responded strongly to the CO_2 fertilisation with a 350 % increase in GPP for grasses and 150 % increase for low shrubs. The additional litter fall produced by the increased leaf mass did not lead to an increase in N mineralisation. However, immobilisation of nitrogen through increased uptake by microbes increased by 2 %–6 % between the lowest and highest $[CO_2]$ scenarios, yielding a net reduction in plant-available nitrogen. Despite productivity in-

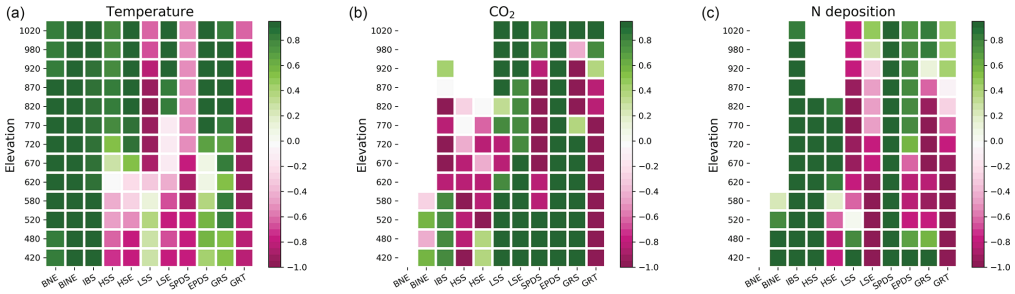

Figure 6. Correlation (Spearman rank) between annual GPP for each PFT and **(a)** average 2090–2100 temperature anomalies in the climate change experiment, **(b)** the CO_2 scenario and **(c)** the nitrogen deposition scenario. Each box represents a 50-elevational-metre band for a given PFT.

creases, the treeline remained stationary in all [CO_2] scenarios (Fig. 5b).

3.3.3 Nitrogen deposition

Productivity of woody PFTs was in general positively correlated with nitrogen in the different nitrogen deposition scenarios. In contrast, productivity of grasses was negatively correlated (Fig. 6c) as they suffered in competition for light with the trees. Annual GPP of trees (especially IBS) was positively correlated throughout the whole ecotone, but the increase in GPP was larger towards the forest boundaries than in the lower parts of the forest when nitrogen was added. Nitrogen-stressed plants in the model allocate more carbon to their roots at the expense of foliar cover when they suffer a productivity reduction (Smith et al., 2014). In the two scenarios with decreasing nitrogen deposition (RCP2.6, RCP8.5) there was an overall reduction in the LAI in both the tundra and the forest of 6 %–10 %. The largest reduction was seen in tree PFTs, which have the largest biomass and consequently will have the highest nitrogen demand, followed by tall shrubs. Low shrubs and grasses did however increase their LAI in the forest when nitrogen input decreased as a result of less light competition from trees. Above the treeline, the LAI of low shrubs and grass PFTs also decreased with less nitrogen input.

In all scenarios with increasing nitrogen deposition there was an advancement of the treeline on the order of 10–85 elevational metres with the smallest (2× nitrogen deposition) having the smallest change in treeline elevation and vice versa for the largest input (10× nitrogen deposition) (Fig. 5c). In the scenarios where nitrogen input was constant or decreasing, the treeline remained stationary.

4 Discussion

In our simulations, rates of treeline advance were faster under climate-change-only scenarios than when all drivers were changing. This revealed nitrogen as a modulating environmental variable, as nitrogen deposition was prescribed to decrease in both the RCP2.6 and the RCP8.5 scenarios. During our historic simulations, the treeline correlated well with a soil temperature isotherm close to the globally observed 6–7 °C isotherm. However, in our projection period the correlation between the treeline position and the isotherm weakened, revealing a fading or potential lag of the treeline–climate equilibrium that became stronger with increased warming. Future rates of treeline advance were thus constrained by factors other than temperature in our simulations. In contrast to previous modelling studies of treeline advance (e.g. Paulsen and Körner, 2014), we include not only temperature dependence on vegetation change but also the full nitrogen cycle and CO_2 fertilisation effects (Smith et al., 2014). Scenarios with increased nitrogen deposition induced treeline advance, further illustrating the modulating role played by nitrogen dynamics in our results. Rising [CO_2] induced higher productivity in our simulations, but these productivity enhancements alone did not lead to significant treeline advance. Furthermore, although NPP for IBS was lower at the treeline than in the forest, it was never close to zero. Such a pattern, which was seen above the treeline, indicates stagnant growth in which the carbon costs of maintaining a larger biomass cancel out any productivity increase. However, enhancement of productivity in combination with an allocation shift from roots to shoots, enabled by a greater nitrogen uptake, favoured taller plants over their shorter neighbours in the competition for light within the model. For treeline advance to occur, trees need to invade the space already occupied by other vegetation. As the model assumes asymmetric competition for nutrients, newly established seedlings have a disadvantage compared to incumbent vegetation, fur-

ther slowing down the modelled rate of treeline advance. Field experiments with nitrogen fertilisation have shown that mountain birches at the treeline display enhanced growth after nitrogen addition (Sveinbjörnsson et al., 1992). Furthermore, fertilisation with nitrogen improved birch seedling survival above the treeline (Grau et al., 2012) and is thus likely important for the establishment and growth of new individuals to form a new treeline. Historically, treeline positions show a strong correlation with the 6–7 °C isotherm (Körner and Paulsen, 2004). These records are, however, a snapshot in time and are not necessarily a strong predictor of the future treeline, with other factors (as with nitrogen in our results) potentially breaking the link to temperature. As pointed out by others (Hofgaard et al., 2019; Van Bogaert et al., 2011), considering climate change or temperature alone in projections of treeline advance could potentially result in overestimation of vegetation change. Our results clearly point to nitrogen cycling as a modulating factor when predicting future Arctic vegetation shifts.

In our simulations, the treeline advanced at similar rates to those experienced during the historic period, resulting in a displacement of 45–195 elevational metres over the 100-year projection period. Some estimates based on lake sediments in the Torneträsk region from the Holocene thermal maximum, when summer temperatures may have been about 2.5 °C warmer than present (Kullman and Kjällgren, 2006), indicate potential treeline elevations approximately 500 m above the present level in the warmer climate (Kullman, 2010). Macrofossil records from lakes in the area indicate that birch was present 300–400 m above the current treeline (Barnekow, 1999). Furthermore, pine might have occurred approximately 100–150 m above its present distribution (Berglund et al., 1996). IBS emerged as the dominant forest and treeline PFT in both our historic and our projection simulations but with larger fractions of evergreen trees (BNE and BINE) at the end of the century (2090–2100). Mountain birch, represented by IBS in our model, has historically dominated treelines in the study area, even during warmer periods of the Holocene (Berglund et al., 1996), but with larger populations of pine (BINE) and spruce (BNE) than seen at present. Both pine and spruce have been found in high-elevation lake pollen sediments and can thus be assumed to have grown in higher parts of the ecotone during warmer periods (Kullman, 2010). Treeline advance for the historic period in our simulations is broadly consistent with observational studies from the Abisko region (Van Bogaert et al., 2011).

Temperature was a strong driver of tree productivity and growth in the whole ecotone in our simulations. For the historic period, higher rates of treeline advance followed periods of stronger warming. However, other factors such as precipitation indirectly influenced treeline advance through changes in vegetation composition and nitrogen mineralisation. This is illustrated by the comparison of GFDL-ESM2M and MIROC-ESM-CHEM under RCP8.5, where the intermediate warming but wetter scenario had a very similar resulting treeline elevation to that of the warmer scenario. While the simulated treeline position was too low compared to the treeline elevation reported by Callaghan et al. (2013), the correlation with the globally observed 6–7 °C ground temperature isotherm (Körner and Paulsen, 2004) throughout the historic period gives confidence in the model results.

IBS at the treeline had a positive carbon balance (NPP) and was thus not directly limited by its productivity in our simulations. This is consistent with observations of ample carbon storage in treeline trees globally (Hoch and Körner, 2012). The modelled treeline is thus not set by productivity directly but rather by competition, as non-tree PFTs become more productive above the treeline. Whether the treeline is set by productivity constraints or by cold temperature limits on wood formation and meristematic activity has been a subject of debate in the literature (Körner, 2015, 2003; Körner et al., 2016; Fatichi et al., 2019; Pugh et al., 2016). DVMs assume NPP to be constraining for growth. On the other hand, trees close to the treeline have been shown to have ample stored carbon (Hoch and Körner, 2012). Furthermore, enhancement of photosynthesis through added CO_2 does not always result in increased tree growth close to the treeline (Dawes et al., 2013), and wood formation is slow below around 5 °C, leading to a hypothesis of reversed control of plant productivity and treeline position (Körner, 2015). As has also been highlighted in this study, ecological interactions as a component in the control of treeline position have been the subject of attention in some recent modelling studies (see for example Scherrer et al., 2020). Such studies add an extra dimension to the discussion as they not only consider plant physiology and hard limits to species distributions but also broadly accept ecological concepts such as realised versus fundamental niches.

The model overestimated biomass carbon in the forest but captured historic rates of biomass increase. The overestimation was more severe closer to the forest boundaries as the model showed a weaker negative correlation between biomass carbon and elevation than observed by Hedenås et al. (2011). The mean annual biomass increase in the same dataset is, although highly variable, on average 2.5 $gC\,m^{-2}\,yr^{-1}$ between 1997 and 2010. As the simulated GPP and LAI were within the range of observations in the area (Rundqvist et al., 2011; Ovhed and Holmgren, 1996; Olsson et al., 2017), this indicates a coupling between photosynthesis and growth in the model that is stronger than that observed. Terrestrial biosphere models often overestimate biomass in high latitudes (Pugh et al., 2016; Leuzinger et al., 2013) and potentially lack processes that likely limit growth close to low temperature boundaries. Examples of such processes are the carbon costs of nitrogen acquisition (Shi et al., 2016), including costs for mycorrhizal interactions (Vowles et al., 2018), and temperature limits on wood formation (Friend et al., 2019). However, data on carbon allocation and its temperature dependence are scarce (Fatichi

et al., 2019). Additionally, the overestimation in our study can be partly attributed to a lack of herbivory in the model. Outbreaks of the moth *Epirrita autumnata* are known to limit productivity and reduce biomass of mountain birch in the area in certain years (Olsson et al., 2017); however, this would not fully explain the overestimation of biomass at the treeline in our simulations. Since growth and biomass increments in the model do not include a direct temperature dependence or any decoupling of growth and productivity, we do not regard these mechanisms as necessary to accurately predict treeline dynamics. However, they might be important to accurately predict forest biomass at the treeline.

To examine variability in the simulated treeline dynamics across the study area, we established a number of transects close to observation points in the landscape. Average treeline advance in the transects showed a somewhat faster and more homogenous migration than reported (Van Bogaert et al., 2011). The model does not include historic anthropogenic disturbances, topographic barriers or insect herbivory, all of which have been invoked to explain the heterogeneity of treeline advance rates and placement in the landscape (Van Bogaert et al., 2011; Emanuelsson, 1987). Furthermore, our model does not include any wind-related processes such as wind-mediated snow transport or compaction. Thus, our simulations result in a homogenous snowpack during the winter months with no differentiation in sheltering or frost damage that may result from different snow and ice properties. Sheltered locations in the landscape are known to promote the survival of tree saplings (Sundqvist et al., 2008). For nitrogen cycling this may also mean that suggested snow–shrub feedbacks (Sturm et al., 2001; Sturm, 2005) are not possible to capture with the current version of our model. While overall rates of treeline migration were captured, local variations arising from physical barriers such as steep slopes, stony patches or anthropogenic disturbances were not possible to capture as these processes are not implemented in the model. High-resolution, local observations of vertically resolved soil texture and soil organic matter content (see, e.g., Hengl et al., 2017, for an example compiled using machine learning) have the potential to improve the spatial variability in modelled soil temperatures and nutrient cycling in our study domain.

A longer growing season favoured tree PFTs in the whole ecotone, which escaped early-season desiccation due to milder winters and earlier spring thaw. Permafrost was only present at the highest elevations during the historic simulation but had disappeared from the landscape by 2100 for all except the coolest scenario (GFDL-ESM2M-RCP2.6). The simulated permafrost was however always well above the treeline and did not have a significant impact on the treeline advancement. While some aspects of ground freezing are accounted for in the model, soil vertical and horizontal movement caused by frost, as well as the amelioration of such effects in the warmer future climate, is not. Such processes could affect survival and competition among the plant functional types, especially in the seedling stage when plants are most vulnerable to mechanical disturbance (Holtmeier and Broll, 2007). These effects could be relevant to treeline dynamics at the high grid resolution of our study but are not included in our model.

Higher summer soil moisture in the wetter climate scenarios shifted the ratio of summergreen to evergreen shrubs in favour of the summergreen shrubs, in line with observations (Elmendorf et al., 2012). Conversely, drier scenarios yielded an increased abundance of evergreen shrubs, similar to what has been observed in drier parts of the tundra heath in the Abisko region (Scharn et al., 2021). Within RCP8.5, the warmest (MIROC-ESM-CHEM-RCP8.5) and coldest (GFDL-ESM2M-RCP8.5) scenarios gave rise to very similar treeline positions at the end of the projection period (2090–2100). The cooler scenario led to both higher soil moisture and a greater abundance of summergreen shrubs. Higher soil moisture promoted carbon allocation to the canopy and thus favoured the taller IBS tree PFT over tall shrubs (HSS). Increased shrub abundance and nutrient cycling have been shown to have potentially non-linear effects on shrub growth and ecosystem carbon cycling (Buckeridge et al., 2009; Hicks et al., 2019), and some observations indicate that changes in the ratio of summergreen to evergreen shrubs or an increased abundance of trees might impact soil carbon loss (Parker et al., 2018; Clemmensen et al., 2021). Thus, our results indicate that any future change in soil moisture conditions could play an important role in the competitive balance between shrubs and trees and for carbon balance.

LPJ-GUESS assumes the presence of seeds in all grid cells, and PFTs may establish when the 20-year (running) average climate is within PFT-specific bioclimatic limits for establishment. This assumption may overlook potential constraints on plant migration rates such as seed dispersal and reproduction. On larger spatial scales, it is likely that lags in range shifts would arise from these additional constraints (Rees et al., 2020; Brown et al., 2018). Models that account for dispersal limitations generally predict slower latitudinal tree migration than models driven solely by climate (Epstein et al., 2007). However, on smaller spatial scales, the same models predict competitive interactions to be more dominant in determining species migration rates (Scherrer et al., 2020), and this is included in our model. In a seed transplant study from the Swiss Alps, seed viability could not be shown to decline towards the range limits of eight European broadleaved tree species (Kollas et al., 2012; Körner et al., 2016). Similarly, gene flow above the treeline could not be shown to be limited to near-treeline trees in the Abisko region (Truong et al., 2007). Furthermore, tree saplings have been reported to be common up to 100 m above the present treeline (Sundqvist et al., 2008; Hofgaard et al., 2009). As environmental conditions improve, these individuals may form the new treeline.

Above the treeline low evergreen shrubs (LSE) dominated the vegetation in both our historic and our projection simulations. The productivity of shrubs and grasses was greatly enhanced by CO_2 fertilisation in our [CO_2] model experiment,

and a large proportion of tundra productivity increases in our projection simulations could be attributed to rising [CO_2]. Physiological effects of elevated CO_2 on arctic and alpine tundra productivity and growth are understudied. Free-air CO_2 enrichment (FACE) experiments are generally considered the best method for quantifying long-term ecosystem effects of elevated CO_2 but are extremely costly, and very few have been deployed in near-treeline locations. A majority of FACE experiments have been implemented in temperate forests and grasslands, yielding limited evidence of relevance to boreal and tundra ecosystems (Hickler et al., 2008). One FACE experiment situated in a forest–tundra ecotone in the Swiss Alps showed differing responses to elevated CO_2 among shrub species where *Vaccinium myrtillys* showed 11 % increased shoot growth, while *Empetrum nigrum* was unresponsive and the response of *V. gaultherioides* depended on the forest type in which it was growing (Dawes et al., 2013). Our model results indicated that shrubs are carbon limited, and shrub productivity and growth are consequently responsive to CO_2 fertilisation.

5 Conclusions

In this study we examined treeline dynamics in the sub-arctic north of Sweden using an individual-based dynamic vegetation model at a high spatial resolution. The model identified nitrogen cycling and availability as important modulating factors for treeline advance in a warming future climate. Internal cycling of nitrogen in soils provides the main source of this usually limiting nutrient for Arctic plants (Chapin, 1983). The model performed well regarding rates of shrub increase and treeline advance but overestimated biomass carbon in the treeline forest. Treeline migration rates were realistically simulated even though the model did not represent temperature limitations on tree growth. While a decoupling between productivity and growth in the model could potentially have improved estimates of biomass carbon, it was not needed to correctly predict treeline elevation. Instead, our results point to the importance of indirect effects of rising temperatures on tree range shifts, especially with regard to nutrient cycling and competition between trees and shrubs. Furthermore, soil moisture strongly influenced vegetation composition within the model with implications for treeline advance. Improving how models represent nutrient uptake and cycling and incorporating empirical understanding of processes that determine tree and shrub growth will be key to making better predictions of Arctic vegetation change and carbon and nitrogen cycling. Models are a valuable aid in judging the relevance of these processes for sub-arctic treeline ecosystems.

Code availability. The LPJ-GUESS code is located at a non-public repository hosted by Lund University. The code can be accessed for scientific purposes upon inquiry to the authors. More information about the model can be found at https://web.nateko.lu.se/lpj-guess (LPJ-GUESS developers, 2021). All data analysis was carried out using Python pandas (https://doi.org/10.5281/zenodo.4309786, The pandas development team, 2020), NumPy (Harris et al., 2020) and SciPy (https://doi.org/10.5281/zenodo.595738, Gommers et al., 2021). Plots were created using Matplotlib (https://doi.org/10.5281/zenodo.592536, Caswell et al., 2021) and Cartopy (https://doi.org/10.5281/zenodo.1182735, Elson et al., 2021).

Data availability. The climate dataset by Yang et al. (2011) was generously shared with the authors but is not publicly accessible. The data can be accessed upon inquiry to the authors. CMIP5 climate data were downloaded from the ESGF data repository (https://esg-dn1.nsc.liu.se/projects/esgf-liu/, ESGF, 2021) and can be accessed through the ESGF service. The historic climate data for the Abisko Scientific Research Station were generously shared with the authors. Access to this data is provided by the Abisko Scientific Research Station. The soil data used in our study can be accessed through the ISRIC Data Hub (http://data.isric.org/geonetwork/srv/eng/catalog.search#/metadata/dc7b283a-8f19-45e1-aaed-e9bd515119bc, Batjes et al., 2005) The dataset with historic and projected nitrogen deposition is not publicly available but was generously shared with the authors.

Supplement. The supplement related to this article is available online at: https://doi.org/10.5194/bg-18-6329-2021-supplement.

Author contributions. AG designed the experiments with contributions from PAM and SO. AG also performed necessary model code developments and carried out model simulations and data analysis. RGB and BS contributed scientific advice and input throughout the study and contributed to the writing. AG prepared the manuscript with contributions from all co-authors.

Competing interests. The contact author has declared that neither they nor their co-authors have any competing interests.

Disclaimer. Publisher's note: Copernicus Publications remains neutral with regard to jurisdictional claims in published maps and institutional affiliations.

Acknowledgements. We would like to thank Christian Körner and Jed Kaplan for their thoughtful and constructive reviews, which greatly improved the manuscript and widened the scope of our analysis. We acknowledge the Lund University strategic research areas BECC and MERGE for their financial support. Abisko Scientific Research Station generously shared the data used in preparation of the future climate projections.

Financial support. This research was partly funded (Paul A. Miller, Robert G. Björk) by the project BioDiv-Support through the 2017–2018 Belmont Forum and BiodivERsA joint call for research proposals, under the BiodivScen ERA-Net COFUND programme, and with the funding organisations Academy of Finland (AKA) (contract no. 326328), Agence Nationale de la Recherche (ANR) (grant no. ANR-18-EBI4-0007), Bundesministerium für Bildung und Forschung (BMBF) (grant no. KFZ 01LC1810A), Svenska Forskningsrådet Formas (contract nos. 2018-02434, 2018-02436, 2018-02437, 2018-02438) and Ministerio de Ciencia e Innovación (MICINN) (through APCIN (grant no. PCI2018-093149)). Support was also provided by the Lund University strategic research areas BECC and MERGE.

Review statement. This paper was edited by Ben Bond-Lamberty and reviewed by Jed Kaplan and Christian Körner.

References

Ainsworth, E. A. and Long, S. P.: What have we learned from 15 years of free-air CO_2 enrichment (FACE)? A meta-analytic review of the responses of photosynthesis, canopy properties and plant production to rising CO_2, New Phytol., 165, 351–371, https://doi.org/10.1111/j.1469-8137.2004.01224.x, 2005.

Barnekow, L.: Holocene tree-line dynamics and inferred climatic changes in the Abisko area, nothern Sweden, based on macrofossil and pollen records, The Holocene, 9, 253–265, 1999.

Batjes, N. H.: ISRIC-WISE global data ser of derived soil properties on a 0.5 by 0.5° grid (version 3.0), ISRIC – World Soil Information, Wageningen, available at: http://data.isric.org/geonetwork/srv/eng/catalog.search#/metadata/dc7b283a-8f19-45e1-aaed-e9bd515119bc (last access: 10 December 2021) 2005.

Berglund, B. E., Barnekow, L., Hammarlund, D., Sandgren, P., and Snowball, I. F.: Holocene forest dynamics and climate changes in the Abisko area, northern Sweden – the Sonesson model of vegetation history reconsidered and confirmed, Ecol. Bull., 45, 15–30, 1996.

Bhatt, U. S., Walker, D. A., Raynolds, M. K., Comiso, J. C., Epstein, H. E., Jia, G., Gens, R., Pinzon, J. E., Tucker, C. J., Tweedie, C. E., and Webber, P. J.: Circumpolar Arctic Tundra Vegetation Change Is Linked to Sea Ice Decline, Earth Interact., 14, 1–20, https://doi.org/10.1175/2010ei315.1, 2010.

Bjorkman, A. D., Myers-Smith, I. H., Elmendorf, S. C., Normand, S., Ruger, N., Beck, P. S. A., Blach-Overgaard, A., Blok, D., Cornelissen, J. H. C., Forbes, B. C., Georges, D., Goetz, S. J., Guay, K. C., Henry, G. H. R., HilleRisLambers, J., Hollister, R. D., Karger, D. N., Kattge, J., Manning, P., Prevey, J. S., Rixen, C., Schaepman-Strub, G., Thomas, H. J. D., Vellend, M., Wilmking, M., Wipf, S., Carbognani, M., Hermanutz, L., Levesque, E., Molau, U., Petraglia, A., Soudzilovskaia, N. A., Spasojevic, M. J., Tomaselli, M., Vowles, T., Alatalo, J. M., Alexander, H. D., Anadon-Rosell, A., Angers-Blondin, S., Beest, M. T., Berner, L., Bjork, R. G., Buchwal, A., Buras, A., Christie, K., Cooper, E. J., Dullinger, S., Elberling, B., Eskelinen, A., Frei, E. R., Grau, O., Grogan, P., Hallinger, M., Harper, K. A., Heijmans, M., Hudson, J., Hulber, K., Iturrate-Garcia, M., Iversen, C. M., Jaroszynska, F., Johnstone, J. F., Jorgensen, R. H., Kaarlejarvi, E., Klady, R., Kuleza, S., Kulonen, A., Lamarque, L. J., Lantz, T., Little, C. J., Speed, J. D. M., Michelsen, A., Milbau, A., Nabe-Nielsen, J., Nielsen, S. S., Ninot, J. M., Oberbauer, S. F., Olofsson, J., Onipchenko, V. G., Rumpf, S. B., Semenchuk, P., Shetti, R., Collier, L. S., Street, L. E., Suding, K. N., Tape, K. D., Trant, A., Treier, U. A., Tremblay, J. P., Tremblay, M., Venn, S., Weijers, S., Zamin, T., Boulanger-Lapointe, N., Gould, W. A., Hik, D. S., Hofgaard, A., Jonsdottir, I. S., Jorgenson, J., Klein, J., Magnusson, B., Tweedie, C., Wookey, P. A., Bahn, M., Blonder, B., van Bodegom, P. M., Bond-Lamberty, B., Campetella, G., Cerabolini, B. E. L., Chapin, F. S., 3rd, Cornwell, W. K., Craine, J., Dainese, M., de Vries, F. T., Diaz, S., Enquist, B. J., Green, W., Milla, R., Niinemets, U., Onoda, Y., Ordonez, J. C., Ozinga, W. A., Penuelas, J., Poorter, H., Poschlod, P., Reich, P. B., Sandel, B., Schamp, B., Sheremetev, S., and Weiher, E.: Plant functional trait change across a warming tundra biome, Nature, 562, 57–62, https://doi.org/10.1038/s41586-018-0563-7, 2018.

Brown, C. D., Dufour-Tremblay, G., Jameson, R. G., Mamet, S. D., Trant, A. J., Walker, X. J., Boudreau, S., Harper, K. A., Henry, G. H. R., Hermanutz, L., Hofgaard, A., Isaeva, L., Kershaw, G. P., and Johnstone, J. F.: Reproduction as a bottleneck to treeline advance across the circumarctic forest tundra ecotone, Ecography, 42, 137–147, https://doi.org/10.1111/ecog.03733, 2018.

Bruhwiler, L., Parmentier, F.-J. W., Crill, P., Leonard, M., and Palmer, P. I.: The Arctic Carbon Cycle and Its Response to Changing Climate, Curr. Clim. Change Rep., 7, 14–34, https://doi.org/10.1007/s40641-020-00169-5, 2021.

Buckeridge, K. M., Zufelt, E., Chu, H., and Grogan, P.: Soil nitrogen cycling rates in low arctic shrub tundra are enhanced by litter feedbacks, Plant Soil, 330, 407–421, https://doi.org/10.1007/s11104-009-0214-8, 2009.

Cairns, D. and Moen, J.: Herbivory Influences Tree Lines, J. Ecol., 92, 1019–1024, 2004.

Callaghan, T. V., Jonasson, C., Thierfelder, T., Yang, Z., Hedenas, H., Johansson, M., Molau, U., Van Bogaert, R., Michelsen, A., Olofsson, J., Gwynn-Jones, D., Bokhorst, S., Phoenix, G., Bjerke, J. W., Tommervik, H., Christensen, T. R., Hanna, E., Koller, E. K., and Sloan, V. L.: Ecosystem change and stability over multiple decades in the Swedish subarctic: complex processes and multiple drivers, Philos. T. R. Soc. Lond. B, 368, 20120488, https://doi.org/10.1098/rstb.2012.0488, 2013.

Caswell, T. A., Droettboom, M., Lee, A., Sales de Andrade, E., Hoffmann, T., Hunter, J., Klymak, J., Firing, E., Stansby, D., Varoquaux, N., Nielsen, J. H., Root, B., May, R., Elson, P., Seppänen, J. K., Dale, D., Lee, J.-J., McDougall, D., Straw, A., Hobson, P., hannah, Gohlke, C., Vincent, A. F., Yu, T. S., Ma, E., Silvester, S., Moad, C., Kniazev, N., Ernest, E., and Ivanov, P.: matplotlib/matplotlib: REL: v3.5.0, Zenodo [code], https://doi.org/10.5281/zenodo.592536, 2021.

Chapin, F. S., 3rd, Sturm, M., Serreze, M. C., McFadden, J. P., Key, J. R., Lloyd, A. H., McGuire, A. D., Rupp, T. S., Lynch, A. H., Schimel, J. P., Beringer, J., Chapman, W. L., Epstein, H. E., Euskirchen, E. S., Hinzman, L. D., Jia, G., Ping, C. L., Tape, K. D., Thompson, C. D., Walker, D. A., and Welker, J. M.: Role of land-surface changes in arctic summer warming, Science, 310, 657–660, https://doi.org/10.1126/science.1117368, 2005.

Chapin, F. S. I.: Direct and Indirect Effects of Temperature on Arctic Plants, Polar Biol., 2, 47–52, 1983.

Clemmensen, K. E., Durling, M. B., Michelsen, A., Hallin, S., Finlay, R. D., and Lindahl, B. D.: A tipping point in carbon storage when forest expands into tundra is related to mycorrhizal recycling of nitrogen, Ecol. Lett., 24, 1193–1204, https://doi.org/10.1111/ele.13735, 2021.

Cleveland, C. C., Townsend, A. R., Schimel, D. S., Fisher, H., Howarth, R. W., Hedin, L. O., Perakis, S. S., Latty, E. F., Von Fischer, J. C., Elseroad, A., and Wasson, M. F.: Global patterns of terrestrial biological nitrogen (N_2) fixation in natural ecosystems, Global Biogeochem. Cy., 13, 623–645, https://doi.org/10.1029/1999gb900014, 1999.

Dawes, M. A., Hagedorn, F., Handa, I. T., Streit, K., Ekblad, A., Rixen, C., Körner, C., and Hättenschwiler, S.: An alpine treeline in a carbon dioxide-rich world: synthesis of a nine-year free-air carbon dioxide enrichment study, Oecologia, 171, 623–637, https://doi.org/10.1007/s00442-012-2576-5, 2013.

Dusenge, M. E., Duarte, A. G., and Way, D. A.: Plant carbon metabolism and climate change: elevated CO_2 and temperature impacts on photosynthesis, photorespiration and respiration, New Phytol., 221, 32–49, https://doi.org/10.1111/nph.15283, 2019.

Elmendorf, S. C., Henry, G. H. R., Hollister, R. D., Björk, R. G., Boulanger-Lapointe, N., Cooper, E. J., Cornelissen, J. H. C., Day, T. A., Dorrepaal, E., Elumeeva, T. G., Gill, M., Gould, W. A., Harte, J., Hik, D. S., Hofgaard, A., Johnson, D. R., Johnstone, J. F., Jónsdóttir, I. S., Jorgenson, J. C., Klanderud, K., Klein, J. A., Koh, S., Kudo, G., Lara, M., Lévesque, E., Magnússon, B., May, J. L., Mercado-Díaz, J. A., Michelsen, A., Molau, U., Myers-Smith, I. H., Oberbauer, S. F., Onipchenko, V. G., Rixen, C., Martin Schmidt, N., Shaver, G. R., Spasojevic, M. J., Þórhallsdóttir, Þ. E., Tolvanen, A., Troxler, T., Tweedie, C. E., Villareal, S., Wahren, C.-H., Walker, X., Webber, P. J., Welker, J. M., and Wipf, S.: Plot-scale evidence of tundra vegetation change and links to recent summer warming, Nat. Clim. Change, 2, 453–457, https://doi.org/10.1038/nclimate1465, 2012.

Elson, P., Sales de Andrade, E., Lucas, G., May, R., Hattersley, R., Campbell, E., Dawson, A., Raynaud, S., scmc72, Little, B., Snow, A. D., Donkers, K., Blay, B., Killick, P., Wilson, N., Peglar, P., lbdreyer, Andrew, Szymaniak, J., Berchet, A., Bosley, C., Davis, L., Filipe, Krasting, J., Bradbury, M., Kirkham, D., stephenworsley, Clément, Caria, G., and Hedley, M.: SciTools/cartopy: v0.20.1, Zenodo [code], https://doi.org/10.5281/zenodo.1182735, 2021.

Emanuelsson, U.: Human Influence on Vegetation in the Torneträsk Area during the Last Three Centuries, Ecol. Bullet., 38, 95–111, 1987.

Epstein, H. E., Kaplan, J. O., Lischke, H., and Yu, Q.: Simulating Future Changes in Arctic and Subarctic Vegetation, Comput. Sci. Eng., 9, 12–23, https://doi.org/10.1109/mcse.2007.84, 2007.

Epstein, H. E., Raynolds, M. K., Walker, D. A., Bhatt, U. S., Tucker, C. J., and Pinzon, J. E.: Dynamics of aboveground phytomass of the circumpolar Arctic tundra during the past three decades, Environ. Res. Lett., 7, 015506, https://doi.org/10.1088/1748-9326/7/1/015506, 2012.

Fatichi, S., Pappas, C., Zscheischler, J., and Leuzinger, S.: Modelling carbon sources and sinks in terrestrial vegetation, New Phytol., 221, 652–668, https://doi.org/10.1111/nph.15451, 2019.

Forbes, B. C., Fauria, M. M., and Zetterberg, P.: Russian Arctic warming and "greening" are closely tracked by tundra shrub willows, Glob. Change Biol., 16, 1542–1554, https://doi.org/10.1111/j.1365-2486.2009.02047.x, 2010.

Friend, A. D., Eckes-Shephard, A. H., Fonti, P., Rademacher, T. T., Rathgeber, C. B. K., Richardson, A. D., and Turton, R. H.: On the need to consider wood formation processes in global vegetation models and a suggested approach, Ann. Forest Sci., 76, 49, https://doi.org/10.1007/s13595-019-0819-x, 2019.

Gommers, R., Virtanen, P., Burovski, E., Oliphant, T. E., Weckesser, W., Cournapeau, D., alexbrc, Reddy, T., Peterson, P., Haberland, M., Wilson, J., Nelson, A., endolith, Mayorov, N., van der Walt, S., Polat, I., Laxalde, D., Brett, M., Larson, E., Millman, J., Lars, van Mulbregt, P., eric-jones, Carey, C. J., Moore, E., Kern, R., peterbell10, Leslie, T., Perktold, J., and Striega, K.: ScipPy python package, Zenodo [code], https://doi.org/10.5281/zenodo.595738, 2021.

Grau, O., Ninot, J. M., Blanco-Moreno, J. M., van Logtestijn, R. S. P., Cornelissen, J. H. C., and Callaghan, T. V.: Shrub-tree interactions and environmental changes drive treeline dynamics in the Subarctic, Oikos, 121, 1680–1690, https://doi.org/10.1111/j.1600-0706.2011.20032.x, 2012.

Hallinger, M., Manthey, M., and Wilmking, M.: Establishing a missing link: warm summers and winter snow cover promote shrub expansion into alpine tundra in Scandinavia, New Phytol., 186, 890–899, 2010.

Harris, C. R., Millman, K. J., van der Walt, S. J., Gommers, R., Virtanen, P., Cournapeau, D., Wieser, E., Taylor, J., Berg, S., Smith, N. J., Kern, R., Picus, M., Hoyer, S., van Kerkwijk, M. H., Brett, M., Haldane, A., Fernández del Río, J., Wiebe, M., Peterson, P., Gérard-Marchant, P., Sheppard, K., Reddy, T., Weckesser, W., Abbasi, H., Gohlke, C., and Oliphant, T. E.: Array programming with NumPy, Nature, 585, 357–362, https://doi.org/10.1038/s41586-020-2649-2, 2020.

Harsch, M. A., Hulme, P. E., McGlone, M. S., and Duncan, R. P.: Are treelines advancing? A global meta-analysis of treeline response to climate warming, Ecol. Lett., 12, 1040–1049, https://doi.org/10.1111/j.1461-0248.2009.01355.x, 2009.

Haxeltine, A. and Prentice, I. C.: A General Model for the Light-Use Efficiency of Primary Production, Funct. Ecol., 10, 551–561, https://doi.org/10.2307/2390165, 1996.

Hedenås, H., Olsson, H., Jonasson, C., Bergstedt, J., Dahlberg, U., and Callaghan, T. V.: Changes in Tree Growth, Biomass and Vegetation Over a 13-Year Period in the Swedish Sub-Arctic, Ambio, 40, 672–682, https://doi.org/10.1007/s13280-011-0173-1, 2011.

Hengl, T., Mendes de Jesus, J., Heuvelink, G. B., Ruiperez Gonzalez, M., Kilibarda, M., Blagotic, A., Shangguan, W., Wright, M. N., Geng, X., Bauer-Marschallinger, B., Guevara, M. A., Vargas, R., MacMillan, R. A., Batjes, N. H., Leenaars, J. G., Ribeiro, E., Wheeler, I., Mantel, S., and Kempen, B.: SoilGrids250m: Global gridded soil information based on machine learning, PLoS One, 12, e0169748, https://doi.org/10.1371/journal.pone.0169748, 2017.

Hickler, T., Smith, B., Prentice, I. C., MjÖFors, K., Miller, P., Arneth, A., and Sykes, M. T.: CO_2 fertilization in temperate FACE experiments not representative of boreal and tropical forests, Glob. Change Biol., 14, 1531–1542, https://doi.org/10.1111/j.1365-2486.2008.01598.x, 2008.

Hicks, L. C., Rousk, K., Rinnan, R., and Rousk, J.: Soil Microbial Responses to 28 Years of Nutrient Fertiliza-

tion in a Subarctic Heath, Ecosystems, 23, 1107–1119, https://doi.org/10.1007/s10021-019-00458-7, 2019.

Hoch, G. and Körner, C.: Global patterns of mobile carbon stores in trees at the high-elevation tree line, Glob. Ecol. Biogeogr., 21, 861–871, https://doi.org/10.1111/j.1466-8238.2011.00731.x, 2012.

Hofgaard, A., Dalen, L., and Hytteborn, H.: Tree reqruitment above the treeline and potential for climate-driven treeline change, J. Veg. Sci., 20, 1133–1144, 2009.

Hofgaard, A., Harper, K. A., and Golubeva, E.: The role of the circumarctic forest–tundra ecotone for Arctic biodiversity, Biodiversity, 13, 174–181, https://doi.org/10.1080/14888386.2012.700560, 2012.

Hofgaard, A., Ols, C., Drobyshev, I., Kirchhefer, A. J., Sandberg, S., and Söderström, L.: Non-stationary Response of Tree Growth to Climate Trends Along the Arctic Margin, Ecosystems, 22, 434–451, https://doi.org/10.1007/s10021-018-0279-4, 2019.

Holtmeier, F. K. and Broll, G. E.: Treeline advance – driving processes and adverse factors, Landscape Online, 1, 1–33, https://doi.org/10.3097/lo.200701, 2007.

Josefsson, M.: The Geoecology of Subalpine Heaths in the Abisko Valley, Northern Sweden, A study of periglacial conditions, Department of Physical Geography, Uppsala University, Sweden, 180 pp., 1990.

Karlsson, P. S. and Weih, M.: Relationships between Nitrogen Economy and Performance in the Mountain Birch *Betula pubescens* ssp. *tortuosa*, Ecol. Bull., 45, 71–78, 1996.

Kollas, C., Vitasse, Y., Randin, C. F., Hoch, G., and Korner, C.: Unrestricted quality of seeds in European broad-leaved tree species growing at the cold boundary of their distribution, Ann. Bot., 109, 473–480, https://doi.org/10.1093/aob/mcr299, 2012.

Kullman, L.: A richer, greener and smaller alpine world: review and projection of warming-induced plant cover change in the Swedish Scandes, Ambio, 39, 159–169, https://doi.org/10.1007/s13280-010-0021-8, 2010.

Kullman, L. and KjÄLlgren, L.: Holocene pine tree-line evolution in the Swedish Scandes: Recent tree-line rise and climate change in a long-term perspective, Boreas, 35, 159–168, https://doi.org/10.1111/j.1502-3885.2006.tb01119.x, 2006.

Körner, C.: Carbon limitation in trees, J. Ecol., 91, 4–17, 2003.

Körner, C.: Paradigm shift in plant growth control, Curr. Opin. Plant Biol., 25, 107–114, https://doi.org/10.1016/j.pbi.2015.05.003, 2015.

Körner, C. and Paulsen, J.: A World-Wide Study of High Altitude Treeline Temperatures, J. Biogeogr., 31, 713–732, 2004.

Körner, C., Basler, D., Hoch, G., Kollas, C., Lenz, A., Randin, C. F., Vitasse, Y., and Zimmermann, N. E.: Where, why and how? Explaining the low-temperature range limits of temperate tree species, J. Ecol., 104, 1079–1088, https://doi.org/10.1111/1365-2745.12574, 2016.

Lamarque, J. F., Dentener, F., McConnell, J., Ro, C. U., Shaw, M., Vet, R., Bergmann, D., Cameron-Smith, P., Dalsoren, S., Doherty, R., Faluvegi, G., Ghan, S. J., Josse, B., Lee, Y. H., MacKenzie, I. A., Plummer, D., Shindell, D. T., Skeie, R. B., Stevenson, D. S., Strode, S., Zeng, G., Curran, M., Dahl-Jensen, D., Das, S., Fritzsche, D., and Nolan, M.: Multi-model mean nitrogen and sulfur deposition from the Atmospheric Chemistry and Climate Model Intercomparison Project (ACCMIP): evaluation of historical and projected future changes, Atmos. Chem. Phys., 13, 7997–8018, https://doi.org/10.5194/acp-13-7997-2013, 2013.

Leuzinger, S., Manusch, C., Bugmann, H., and Wolf, A.: A sink-limited growth model improves biomass estimation along boreal and alpine tree lines, Glob. Ecol. Biogeogr., 22, 924–932, https://doi.org/10.1111/geb.12047, 2013.

LPJ-GUESS developers: LPJ-GUESS home page, available at: https://web.nateko.lu.se/lpj-guess/, last access: 10 December 2021.

McGuire, A. D., Anderson, L. G., Christensen, T. R., Dallimore, S., Guo, L., Hayes, D. J., Heimann, M., Lorenson, T. D., Macdonald, R. W., and Roulet, N.: Sensitivity of the carbon cycle in the Arctic to climate change, Ecol. Monogr., 79, 523–555, https://doi.org/10.1890/08-2025.1, 2009.

McGuire, A. D., Christensen, T. R., Hayes, D., Heroult, A., Euskirchen, E., Kimball, J. S., Koven, C., Lafleur, P., Miller, P. A., Oechel, W., Peylin, P., Williams, M., and Yi, Y.: An assessment of the carbon balance of Arctic tundra: comparisons among observations, process models, and atmospheric inversions, Biogeosciences, 9, 3185–3204, https://doi.org/10.5194/bg-9-3185-2012, 2012.

Miller, P. A. and Smith, B.: Modelling tundra vegetation response to recent arctic warming, Ambio, 41, 281–291, https://doi.org/10.1007/s13280-012-0306-1, 2012.

Myers-Smith, I. H., Forbes, B. C., Wilmking, M., Hallinger, M., Lantz, T., Blok, D., Tape, K. D., Macias-Fauria, M., Sass-Klaassen, U., Lévesque, E., Boudreau, S., Ropars, P., Hermanutz, L., Trant, A., Collier, L. S., Weijers, S., Rozema, J., Rayback, S. A., Schmidt, N. M., Schaepman-Strub, G., Wipf, S., Rixen, C., Ménard, C. B., Venn, S., Goetz, S., Andreu-Hayles, L., Elmendorf, S., Ravolainen, V., Welker, J., Grogan, P., Epstein, H. E., and Hik, D. S.: Shrub expansion in tundra ecosystems: dynamics, impacts and research priorities, Environ. Res. Lett., 6, 045509, https://doi.org/10.1088/1748-9326/6/4/045509, 2011.

Myers-Smith, I. H., Elmendorf, S. C., Beck, P. S. A., Wilmking, M., Hallinger, M., Blok, D., Tape, K. D., Rayback, S. A., Macias-Fauria, M., Forbes, B. C., Speed, J. D. M., Boulanger-Lapointe, N., Rixen, C., Lévesque, E., Schmidt, N. M., Baittinger, C., Trant, A. J., Hermanutz, L., Collier, L. S., Dawes, M. A., Lantz, T. C., Weijers, S., Jørgensen, R. H., Buchwal, A., Buras, A., Naito, A. T., Ravolainen, V., Schaepman-Strub, G., Wheeler, J. A., Wipf, S., Guay, K. C., Hik, D. S., and Vellend, M.: Climate sensitivity of shrub growth across the tundra biome, Nat. Clim. Change, 5, 887–891, https://doi.org/10.1038/nclimate2697, 2015.

Myers-Smith, I. H., Hik, D. S., and Aerts, R.: Climate warming as a driver of tundra shrubline advance, J. Ecol., 106, 547–560, https://doi.org/10.1111/1365-2745.12817, 2018.

Olsson, P.-O., Heliasz, M., Jin, H., and Eklundh, L.: Mapping the reduction in gross primary productivity in subarctic birch forests due to insect outbreaks, Biogeosciences, 14, 1703–1719, https://doi.org/10.5194/bg-14-1703-2017, 2017.

Ovhed, M. and Holmgren, B.: Modelling and measuring evapotranspiration in a mountain birch forest, Ecol. Bull., 45, 31–44, 1996.

Parker, T. C., Sanderman, J., Holden, R. D., Blume-Werry, G., Sjogersten, S., Large, D., Castro-Diaz, M., Street, L. E., Subke, J. A., and Wookey, P. A.: Exploring drivers of litter decomposition in a greening Arctic: results from a trans-

plant experiment across a treeline, Ecology, 99, 2284–2294, https://doi.org/10.1002/ecy.2442, 2018.

Paulsen, J. and Körner, C.: A climate-based model to predict potential treeline position around the globe, Alpine Bot., 124, 1–12, https://doi.org/10.1007/s00035-014-0124-0, 2014.

Piao, S., Sitch, S., Ciais, P., Friedlingstein, P., Peylin, P., Wang, X., Ahlstrom, A., Anav, A., Canadell, J. G., Cong, N., Huntingford, C., Jung, M., Levis, S., Levy, P. E., Li, J., Lin, X., Lomas, M. R., Lu, M., Luo, Y., Ma, Y., Myneni, R. B., Poulter, B., Sun, Z., Wang, T., Viovy, N., Zaehle, S., and Zeng, N.: Evaluation of terrestrial carbon cycle models for their response to climate variability and to CO_2 trends, Glob. Change Biol., 19, 2117–2132, https://doi.org/10.1111/gcb.12187, 2013.

Pugh, T. A. M., Muller, C., Arneth, A., Haverd, V., and Smith, B.: Key knowledge and data gaps in modelling the influence of CO_2 concentration on the terrestrial carbon sink, J. Plant Physiol., 203, 3–15, https://doi.org/10.1016/j.jplph.2016.05.001, 2016.

Rees, W. G., Hofgaard, A., Boudreau, S., Cairns, D. M., Harper, K., Mamet, S., Mathisen, I., Swirad, Z., and Tutubalina, O.: Is subarctic forest advance able to keep pace with climate change?, Glob. Change Biol., 26, 3965–3977, https://doi.org/10.1111/gcb.15113, 2020.

Rundqvist, S., Hedenås, H., Sandström, A., Emanuelsson, U., Eriksson, H., Jonasson, C., and Callaghan, T. V.: Tree and Shrub Expansion Over the Past 34 Years at the Tree-Line Near Abisko, Sweden, Ambio, 40, 683–692, https://doi.org/10.1007/s13280-011-0174-0, 2011.

Scharn, R., Brachmann, C. G., Patchett, A., Reese, H., Bjorkman, A., Alatalo, J., Björk, R. G., Jägerbrand, A. K., Molau, U., and Björkman, M. P.: Vegetation responses to 26 years of warming at Latnjajaure Field Station, northern Sweden, Arctic Science, 1–20, https://doi.org/10.1139/as-2020-0042, 2021.

Scherrer, D., Vitasse, Y., Guisan, A., Wohlgemuth, T., Lischke, H., and Gomez Aparicio, L.: Competition and demography rather than dispersal limitation slow down upward shifts of trees' upper elevation limits in the Alps, J. Ecol., 108, 2416–2430, https://doi.org/10.1111/1365-2745.13451, 2020.

Serreze, M. C. and Barry, R. G.: Processes and impacts of Arctic amplification: A research synthesis, Glob. Planet. Change, 77, 85–96, https://doi.org/10.1016/j.gloplacha.2011.03.004, 2011.

Shi, M., Fisher, J. B., Brzostek, E. R., and Phillips, R. P.: Carbon cost of plant nitrogen acquisition: global carbon cycle impact from an improved plant nitrogen cycle in the Community Land Model, Glob. Change Biol., 22, 1299–1314, https://doi.org/10.1111/gcb.13131, 2016.

Sitch, S., Smith, B., Prentice, I. C., Arneth, A., Bondeau, A., Cramer, W., Kaplan, J. O., Levis, S., Lucht, W., Sykes, M. T., Thonicke, K., and Venevsky, S.: Evaluation of ecosystem dynamics, plant geography and terrestrial carbon cycling in the LPJ dynamic global vegetation model, Glob. Change Biol., 9, 161–185, https://doi.org/10.1046/j.1365-2486.2003.00569.x, 2003.

Smith, B., Prentice, I. C., and Sykes, M. T.: Representation of vegetation dynamics in the modelling of terrestrial ecosystems: comparing two contrasting approaches within European climate space, Glob. Ecol. Biogeogr., 10, 621–637, https://doi.org/10.1046/j.1466-822X.2001.t01-1-00256.x, 2001.

Smith, B., Wårlind, D., Arneth, A., Hickler, T., Leadley, P., Siltberg, J., and Zaehle, S.: Implications of incorporating N cycling and N limitations on primary production in an individual-based dynamic vegetation model, Biogeosciences, 11, 2027–2054, https://doi.org/10.5194/bg-11-2027-2014, 2014.

Sturm, M.: Changing snow and shrub conditions affect albedo with global implications, J. Geophys. Res., 110, G01004, https://doi.org/10.1029/2005jg000013, 2005.

Sturm, M., Holmgren, J., McFadden, J. P., Liston, G. E., Chapin, F. S., and Racine, C. H.: Snow–Shrub Interactions in Arctic Tundra: A Hypothesis with Climatic Implications, J. Clim., 14, 336–344, https://doi.org/10.1175/1520-0442(2001)014<0336:Ssiiat>2.0.Co;2, 2001.

Sullivan, P., Ellison, S., McNown, R., Brownlee, A., and Sveinbjörnsson, B.: Evidence of soil nutrient availability as the proximate constraint on growth of treeline trees in northwest Alaska, Ecology, 96, 716–727, 2015.

Sundqvist, M. K., Björk, R. G., and Molau, U.: Establishment of boreal forest species in alpine dwarf-shrub heath in subarctic Sweden, Plant Ecol. Div., 1, 67–75, https://doi.org/10.1080/17550870802273395, 2008.

Sveinbjörnsson, B., Nordell, O., and Kauhanen, H.: Nutrient relations of mountain birch growth at and below the elevational treeline in Swedish Lapland, Funct. Ecol., 6, 213–220, 1992.

Taylor, K. E., Stouffer, R. J., and Meehl, G. A.: An Overview of CMIP5 and the Experiment Design, Bull. Am. Meteorol. Soc., 93, 485–498, https://doi.org/10.1175/bams-d-11-00094.1, 2012.

The pandas development team: pandas-dev/pandas, Zenodo [code], https://doi.org/10.5281/zenodo.4309786, 2020.

Truong, C., Palme, A. E., and Felber, F.: Recent invasion of the mountain birch *Betula pubescens* ssp. *tortuosa* above the treeline due to climate change: genetic and ecological study in northern Sweden, J. Evol. Biol., 20, 369–380, https://doi.org/10.1111/j.1420-9101.2006.01190.x, 2007.

Van Bogaert, R., Haneca, K., Hoogesteger, J., Jonasson, C., De Dapper, M., and Callaghan, T. V.: A century of tree line changes in sub-Arctic Sweden shows local and regional variability and only a minor influence of 20th century climate warming, J. Biogeogr., 38, 907–921, https://doi.org/10.1111/j.1365-2699.2010.02453.x, 2011.

Virkkala, A. M., Aalto, J., Rogers, B. M., Tagesson, T., Treat, C. C., Natali, S. M., Watts, J. D., Potter, S., Lehtonen, A., Mauritz, M., Schuur, E. A. G., Kochendorfer, J., Zona, D., Oechel, W., Kobayashi, H., Humphreys, E., Goeckede, M., Iwata, H., Lafleur, P. M., Euskirchen, E. S., Bokhorst, S., Marushchak, M., Martikainen, P. J., Elberling, B., Voigt, C., Biasi, C., Sonnentag, O., Parmentier, F. W., Ueyama, M., Celis, G., St Loius, V. L., Emmerton, C. A., Peichl, M., Chi, J., Jarveoja, J., Nilsson, M. B., Oberbauer, S. F., Torn, M. S., Park, S. J., Dolman, H., Mammarella, I., Chae, N., Poyatos, R., Lopez-Blanco, E., Rojle Christensen, T., Jung Kwon, M., Sachs, T., Holl, D., and Luoto, M.: Statistical upscaling of ecosystem CO_2 fluxes across the terrestrial tundra and boreal domain: regional patterns and uncertainties, Glob. Change Biol., 27, 4040–4059, https://doi.org/10.1111/gcb.15659, 2021.

Vowles, T., Lindwall, F., Ekblad, A., Bahram, M., Furneaux, B. R., Ryberg, M., and Bjork, R. G.: Complex effects of mammalian grazing on extramatrical mycelial biomass in the Scandes forest-tundra ecotone, Ecol. Evol., 8, 1019–1030, https://doi.org/10.1002/ece3.3657, 2018.

Wania, R., Ross, I., and Prentice, I. C.: Integrating peatlands and permafrost into a dynamic global vegetation

model: 1. Evaluation and sensitivity of physical land surface processes, Global Biogeochem. Cy., 23, GB3014, https://doi.org/10.1029/2008gb003412, 2009.

Wei, Y., Liu, S., Huntzinger, D. N., Michalak, A. M., Viovy, N., Post, W. M., Schwalm, C. R., Schaefer, K., Jacobson, A. R., Lu, C., Tian, H., Ricciuto, D. M., Cook, R. B., Mao, J., and Shi, X.: The North American Carbon Program Multi-scale Synthesis and Terrestrial Model Intercomparison Project – Part 2: Environmental driver data, Geosci. Model Dev., 7, 2875–2893, https://doi.org/10.5194/gmd-7-2875-2014, 2014.

Weih, M. and Karlsson, S.: The nitrogen economy of mountain birch seedlings: implications for winter survival, J. Ecol., 87, 211–219, 1999.

Wolf, A., Callaghan, T. V., and Larson, K.: Future changes in vegetation and ecosystem function of the Barents Region, Climatic Change, 87, 51–73, https://doi.org/10.1007/s10584-007-9342-4, 2008.

Yang, Z., Hanna, E., and Callaghan, T. V.: Modelling surface-air-temperature variation over complex terrain around abisko, swedish lapland: uncertainties of measurements and models at different scales, Geogr. Ann. A, 93, 89–112, https://doi.org/10.1111/j.1468-0459.2011.00005.x, 2011.

Yang, Z., Hanna, E., Callaghan, T. V., and Jonasson, C.: How can meteorological observations and microclimate simulations improve understanding of 1913–2010 climate change around Abisko, Swedish Lapland?, Meteorol. Appl., 19, 454–463, https://doi.org/10.1002/met.276, 2012.

Zhang, W., Miller, P. A., Smith, B., Wania, R., Koenigk, T., and Döscher, R.: Tundra shrubification and tree-line advance amplify arctic climate warming: results from an individual-based dynamic vegetation model, Environ. Res. Lett., 8, 034023, https://doi.org/10.1088/1748-9326/8/3/034023, 2013.

Zhang, W., Jansson, C., Miller, P. A., Smith, B., and Samuelsson, P.: Biogeophysical feedbacks enhance the Arctic terrestrial carbon sink in regional Earth system dynamics, Biogeosciences, 11, 5503–5519, https://doi.org/10.5194/bg-11-5503-2014, 2014.

Zhang, W., Miller, P. A., Jansson, C., Samuelsson, P., Mao, J., and Smith, B.: Self-Amplifying Feedbacks Accelerate Greening and Warming of the Arctic, Geophys. Res. Lett., 45, 7102–7111, https://doi.org/10.1029/2018gl077830, 2018.

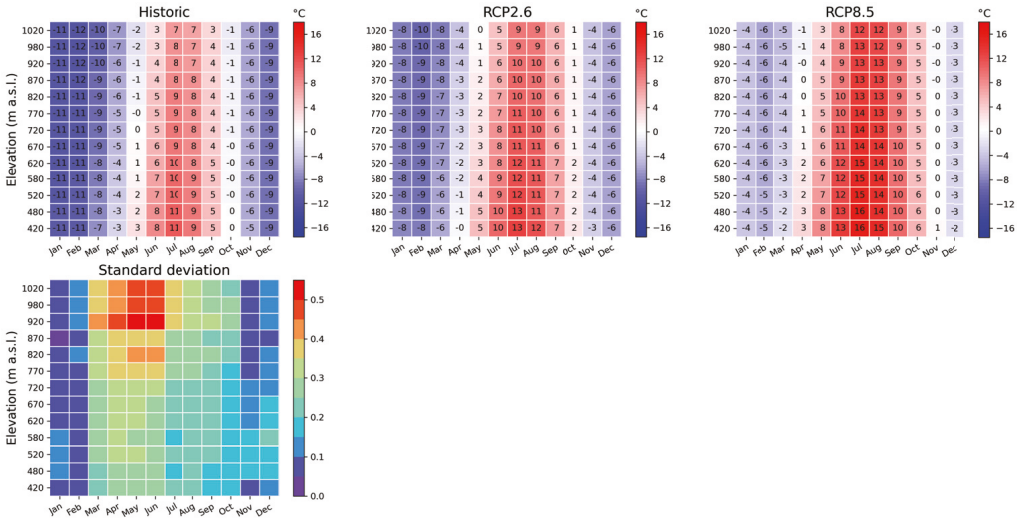

Figure S1.1. Upper row describes monthly averages in 2m air temperature in 50m bands along the elevational gradient for the historic (1971-2000) and projected (2071-2100) reference periods and climate scenarios. Values for RCP2.6 and RCP8.5 are an average of the three global climate models used in the study. Numbers in each square are the average temperature for the month and elevational band rounded to the closest integer. The panel on the lower row displays the standard deviation in the same 50m bands and for each month. This may be interpreted as the magnitude of the local effect, i.e., the effect of mountainside aspect and proximity to Lake Torneträsk.

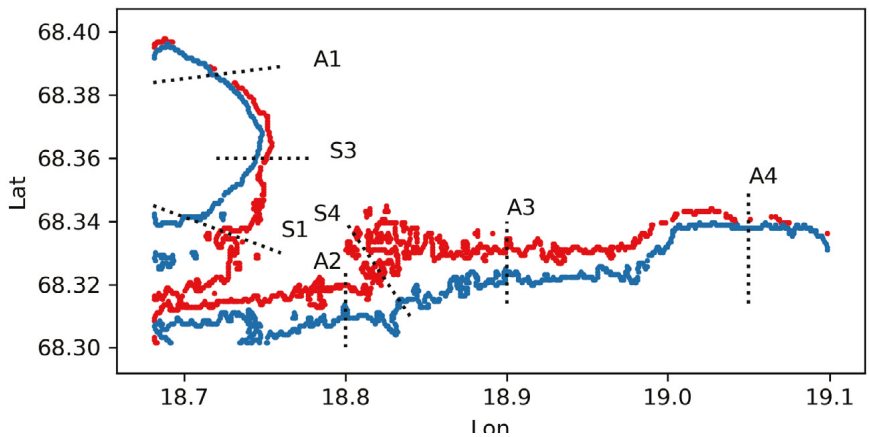

Figure S1.2. Treeline position in year 1915 (red) and 2010 (blue) along with placement of local transects (dashed lines). Transects were selected to represent a broad range of slopes and aspects in the landscape and were used to assess the heterogeneity of treeline advance within the landscape. Transects starting with S were also used by van Bogart et al. (2011).

Table S1.1 - Historical treeline migration rates in local transects with partial comparison to values reported by van Bogart et al. (2011). See Figure S1.2 above for a map of the transect locations

Transect	Elevation shift (m)	Modelled migration rate (m yr^{-1})	Reported elevational shifts (m) (van Bogart et al. 2011)
A1	57	0,6	
A2	90	0,95	
A3	112	1,18	
A4	75	0,79	
S1	119	1,25	40 +- 15
S3	78	0,82	60+-15
S4	94	0,99	145+-10

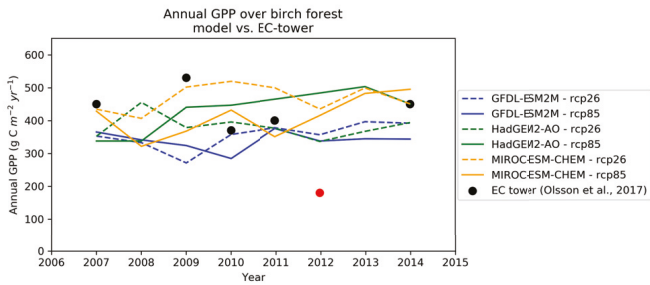

Figure S1.3. Annual GPP in the lower (warmer) section of the birch forest vs. Eddy covariance (EC) data obtained from Olsson et al (2017). Year 2012 (red marker) had a severe moth outbreak during the growing season and thus lower GPP.

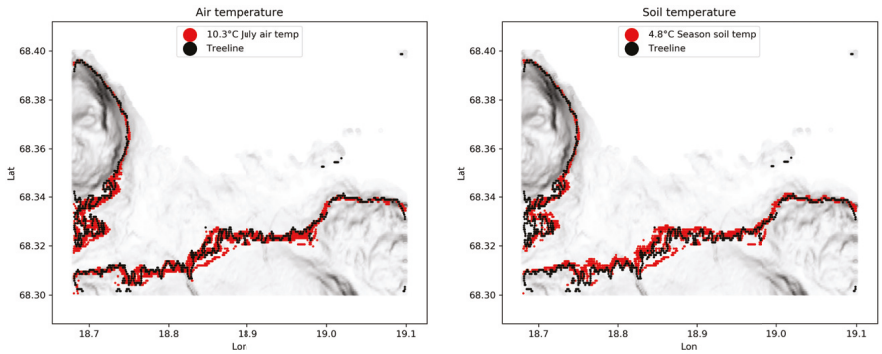

Figure S1.4. Correlation of historic (1990-2000) treeline with average growing season soil temperature and July air temperature. Grayscale indicates landscape relief. The white area marks lake Torneträsk.

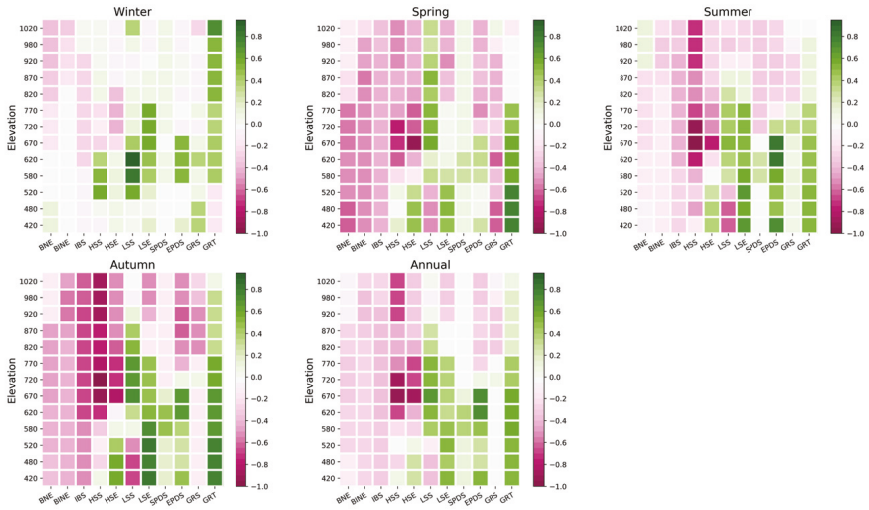

Figure S1.5. Spearman rank correlation between average annual GPP for the years 2090-2100 for each PFT and a-d) seasonal and e) annual precipitation in the forest tundra ecotone for the same time period. Precipitation is controlled by the bias adjusted precipitation output from each global climate model used in the study.

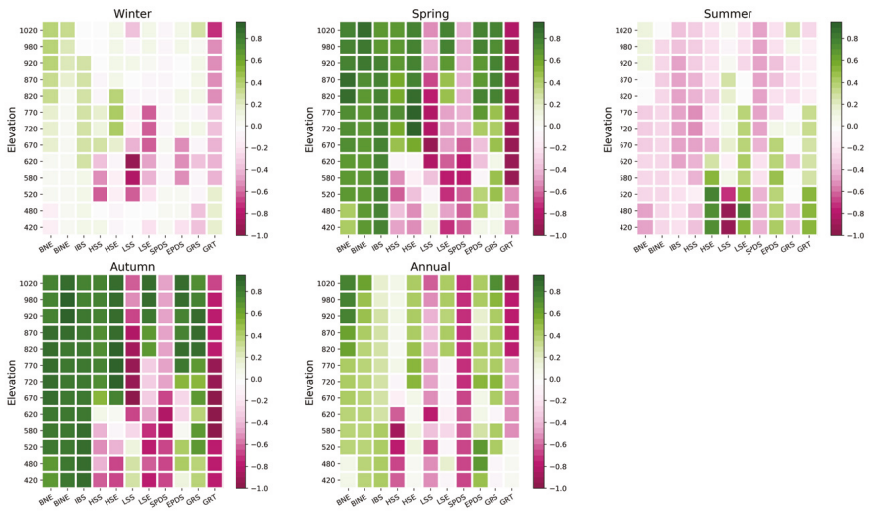

Figure S1.6 Spearman rank correlation between annual GPP for the years 2090-2100 for each PFT and a-d) seasonal and e) annual net shortwave radiation in the forest-tundra ecotone for the same time period. Shortwave radiation is controlled by the bias adjusted downwelling shortwave radiation output from each global climate model used in the study.

References

Olsson, P.-O., Heliasz, M., Jin, H., and Eklundh, L.: Mapping the reduction in gross primary productivity in subarctic birch forests due to insect outbreaks, Biogeosciences, 14, 1703-1719, 10.5194/bg-14-1703-2017, 2017.

Van Bogaert, R., Haneca, K., Hoogesteger, J., Jonasson, C., De Dapper, M., and Callaghan, T. V.: A century of tree line changes in sub-Arctic Sweden shows local and regional variability and only a minor influence of 20th century climate warming, Journal of Biogeography, 38, 907-921, 10.1111/j.1365-2699.2010.02453.x, 2011.

Table S2.1. Plant Functional Types (PFTs) simulated in the study.

PFT	Typical species
BNE Boreal needle-leaved evergreen tree	*Picea abies*
BINE Boreal needle-leaved shade-intolerant evergreen tree	*Pinus sylvestris*
IBS Boreal shade-intolerant broad-leaved summergreen tree	*Betula pubescens ssp. czerepanovii, Alnus glutinosa, Sorbus aucuparia, Populus tremula*
HSS Tall summergreen shrub	*Salix spp.*
HSE Tall evergreen shrub	*Juniperus communis*
LSS Low summergreen shrub	*Vaccinium myrtillus, Salix hastata*
LSE Low evergreen shrub	*Empetrum nigrum, Cassiope tetragona*
SPDS Prostrate summegreen dwarf shrub	*Saxifraga oppositifolia*
EPDS Prostrate evergreen dwarf shrub	*Arctostaphylos uva-ursi*
GRS Boreal C3 graminoids	Gramineae
CLM Cushion-forb-lichen-moss-tunda	Cushion-forming *Caryopyhyllaceae* and *Saxifragacea,* lichens, mosses

Table S2.2. Parameters for all simulated PFTs.
Empty cells indicate that this parameter is not applied to the PFT while "-" indicates a no-limit value

	Description	Unit	BNE	BINE	IBS	HSS	HSE	LSS	LSE	SPDS	EPDS	GRT	CLM
Allometry													
lifeform			Tree	Tree	Tree	Tree	Tree	Tree	Tree	Tree	Tree	Grass	Grass
leaf physiognomy			Needleleaf	Needleleaf	Broadleaf	Broadleaf	Needleleaf	Broadleaf	Needleleaf	Broadleaf	Broadleaf	Broadleaf	Broadleaf
$crownarea_{max}$	Maximum tree crown area	m^2	50	50	27,3	4	4	1	1	1	1		
$k_{allom,\ 1}$	Constant in allometry equation		150	150	200	30	28	10	10	10	10		
$k_{allom,\ 2}$	Constant in allometry equation		60	60	30	6	6	4	4	1	1		
$k_{allom,\ 3}$	Constant in allometry equation		0,67	0,67	0,67	0,67	0,67	0,67	0,67	0,67	0,67		
k_{rp}	Constant in allometry equation		1,6	1,6	1,6	1,6	1,6	1,6	1,6	1,6	1,6		
$k_{la:sa}$	Tree leaf to sapwood area ratio		5000	5000	4000	500	500	125	125	100	100		
$leaf{:}root_{max}$	Maximum leaf to root ratio		1	1	1	1	1	1	1	0,5	0,5	0,2	0,1
$beta_{root}$	Shape parameter for root distribution		0,982	0,982	0,982	0,978	0,978	0,978	0,978	0,9555	0,9555	0,9555	0,9555
intc	Interception coefficient		0,06	0,06	0,02	0,02	0,06	0,02	0,06	0.02	0,06	0,01	0,01
wooddens	Wood density	$kgC\ m^{-3}$	200	200	200	250	250	200	200	200	200		
Photosynthesis and canopy													
pathway	Phytosynthetic pathway		C3	C3	C3	C3	C3	C3	C3	C3	C3	C3	C3
$pstemp_{min}$	Approximate low temperature limit for photosynthesis	°C	–4	–4	–4	–4	–4	–4	–4	–4	–4	–5	–4
$pstemp_{low}$	Approximate lower temperature range for optimum photosynthesis	°C	5	5	5	5	5	5	5	5	5	10	5
$pstemp_{high}$	Approximate upper temperature range for optimum photosynthesis	°C	25	25	25	25	25	25	25	25	25	30	25
$pstemp_{max}$	Maximum temperature limit for photosynthesis	°C	38	38	38	38	38	38	38	38	38	45	38
respcoeff	Respiration coefficient		1	1	1	1	1	1	1	1	1	1	1
g_{min}	Canopy conductance not associated with photosynthesis	$mm\ s^{-1}$	0,3	0,3	0,5	0,5	0,3	0,5	0,3	0,5	0,3	0,5	0,5
g_a	aerodynamic conductance	$m\ s^{-1}$	0,140	0,140	0,040	0,40	0,140	0,040	0,140	0,03	0,030	0,030	0,03
e_{max}	Maximum evapotranspiration rate	$mm\ day^{-1}$	5	5	5	5	5	5	5	5	5	5	5
$lambda_{max}$	Non-water-stressed ratio of intercellular to ambient CO_2 partial pressure		0,8	0,8	0,8	0,8	0,8	0,8	0,8	0,8	0,8	0,8	0,8
Phenology													
phenology	Phonological type		Evergreen	Evergreen	Summergreen	Summergreen	Evergreen	Summergreen	Evergreen	Summergreen	Evergreen	Summergreen	Summergreen
$phengdd_{0,\ ramp}$	Thawing Degree Days (TDD) required to attain full leaf cover				550	200		200		50		100	5
$k_{chill,\ a}$	Constant in equation for bud burst chilling time requirement		0	0	0	-	-	-	-	-	-		
$k_{chill,\ b}$	Coefficient in equation for bud burst chilling time requirement		100	100	100	-	-	-	-	-	-		
$k_{chill,\ k}$	Exponent in equation for bud burst chilling time requirement		0,05	0,05	0,05	-	-	-	-	-	-		
Reproduction													

	Description	Unit	BNE	BINE	IBS	HSS	HSE	LSS	LSE	SPDS	EPDS	GRT	CLM
reprfrac	Fraction of NPP allocated to reproduction		0,1	0,1	0,1	0,1	0,1	0,1	0,1	0,1	0,1	0,1	0,1
est_{max}	Max sapling establishment rate	individuals m^{-2} yr^{-2}	0,05	0,2	0,05	0,2	0,05	0,4	0,2	0,4	0,4		
alphar	Shape parameter for recruitment-juvenile growth rate relationship		2	7	3	10	10	11	11	11	11		
$kest_{repr}$	Constant in equation for tree establishment rate		200	200	200	200	200	200	200	200	200		
$kest_{bg}$	Constant in equation for tree establishment rate		0,1	0,1	0,1	0,1	0,1	0,1	0,1	0,1	0,1		
$kest_{pres}$	Constant in equation for tree establishment rate		1	1	1	1	1	1	1	1	1		
Turnovers													
leaf longevity	Leaf life span	years	3	2	0,25	0,25	2	0,25	2	0,25	2	0,5	0,5
$turnover_{leaf}$	Turnover rate for leaves	years	0,33	0,5	1	1	0,5	0,5	0,5	1	0,5	1	0,6
$turnover_{sap}$	Turnover rate for tree sapwood	years	0,05	0,1	0,1	0,1	0,1	0,01	0,075	0,01	0,01		
$turnover_{root}$	Turnover rate for fine roots	years	0,7	0,7	0,6	0,6	0,6	0,6	0,6	0,7	0,7	0,7	0,5
longevity	Expected longevity under life-form non-stressed conditions	years	500	500	220	80	100	80	80	30	30		
Shade tolerance													
$parff_{min}$	Min forest floor PAR for grass growth/ tree establishment	J m^{-2} day^{-1}	350000	2500000	2000000	2500000	2500000	350000	2500000	1000000	1000000	1000000	1000000
$greff_{min}$	Threshold for growth suppression mortality	kgC m^{-2} $leaf^{-1}$ yr^{-1}	0,03	0,06	0,04	0,04	0,04	0,012	0,09	0,012	0,012		
Nutrient use													
$C:N_{root}$	Reference fine root C:N mass ratio		29	29	29	29	29	29	29	29	29	29	29
$C:N_{sap}$	Reference sapwood C:N mass ratio		330	330	330	330	330	330	330	300	300		
nuptoroot	Maximum N uptake per fine root	kgN kgC^{-1} day^{-1}	0,0028	0,0028	0,0028	0,0028	0,0028	0,0028	0,0028	0,0028	0,0028	0,00551	0,00551
fnstorage	Fraction of sapwood (root for herbaceous PFTs) that can be used as a nitrogen storage scalar		0,05	0,05	0,15	0,15	0,05	0,15	0,05	0,15	0,05	0,3	0,3
km_{volume}	Michaelis-Menten kinetic parameters for N uptake		0,000001477	0.000001477	0,000001477	0,000001477	0,000001477	0,000001477	0,000001477	0,000001477	0,000001477	0,000001876	0,000001876
Bioclimatic limits													
$tcmin_{surv}$	Minimum 20-year coldest month mean temperature for survival	°C	–31	–31	–30	-32.5	–32,5	-	-	-	-	-	-
$tcmin_{est}$	Minimum 20-year coldest month mean temperature for establishment	°C	–30	–30	–30	-32.5	–16	-	-	-	-	-	-
$tcmax_{est}$	Maximum 20-year coldest month mean temperature for establishment	°C	–1	–1	7	5	5	-	-	5	5	-	5
$twmin_{est}$			5	5	-	-	-	-	-	-	-	-	-
$gdd5min_{est}$	Minimum GDD on a 5°C basis for establishment		500	400	250	-	-	75	75	-	-	-	-
min_snow	Minimum snowdepth for survival	mm	-	-	-	-	-	-	-	20	20		50
gdd0_min	Minimum GDD on a 0°C basis for survival/establishment		950	800	450	400	400	250	250	150	150	250	50
gdd0_max	Maximum GDD on a 0°C basis for survival/establishment		-	-	-	-	-	-	-	-	-	-	500

Table S2.3 - Simulations performed in the study. Please refer to the main text for more information about global climate model (GCM) selection and model experiments

Climate source	Simulation period	Climate scenario*	CO2 scenario**	N-dep scenario**
Historic simulations				
Yang et al. (2011)	1913-2000	Historic	Historic	Historic
Projection Simulations				
Yang et al. (2011)	2000 - 2100	No trend	Constant	Constant
GFDL-ESM2M	2000 - 2100	RCP 2.6	RCP 2.6	RCP 2.6
		RCP 8.5	RCP 8.5	RCP 8.5
HadGEM2-AO	2000 - 2100	RCP 2.6	RCP 2.6	RCP 2.6
		RCP 8.5	RCP 8.5	RCP 8.5
MIROC-ESM-CHEM	2000 - 2100	RCP 2.6	RCP 2.6	RCP 2.6
		RCP 8.5	RCP 8.5	RCP 8.5
Climate change experiment				
GFDL-ESM2M	2000 - 2100	RCP 2.6 RCP 8.5	Constant	Constant
HadGEM2-AO	2000 - 2100	RCP 2.6 RCP 8.5	Constant	Constant
MIROC-ESM-CHEM	2000 - 2100	RCP 2.6 RCP 8.5	Constant	Constant
CO_2 experiment				
Yang et al. (2011)	2000 - 2100	No trend	RCP 2.6 RCP 4.5 RCP 6.0 RCP 8.5	Constant
Nitrogen deposition experiment				
Yang et al. (2011)	2000 - 2100	No trend	Constant	RCP 2.6 RCP 8.5 2x Ndep 5x Ndep 7.5x Ndep 10x Ndep

* No trend refers to extended climate dataset with climate sampled randomly from the period 1990-2000.
** Constant refers to values unchanged after year 2000 and throughout the projection period

Paper II

The contribution of shrubs to Arctic land surface feedbacks

Adrian Gustafson, Paul A. Miller, Wenxin Zhang, Jing Tang, Robert G. Björk, Benjamin Smith

Abstract

The northern high latitudes have experienced a pronounced increase in spectral greening over the past decades in response to strong warming. This greening has been attributed to an increased abundance of shrubs and woody vegetation, which is hypothesised to result in stronger warming of the high latitudes due to reduced albedo, earlier snowmelt, and enhanced nutrient cycling. Previous attempts to quantify this feedback have often built on simplified assumptions such as fixed amounts of vegetation increase. In this study, we provide an improved estimate of shrub-climate feedbacks in the Arctic by using a regional earth system model, capable of simulating dynamic vegetation and biogeochemical cycling, and recently improved with additional high-latitude processes. We found no strong effect of including shrubs on regional climate. However, strong warming over Siberia and the Northern Canadian Archipelago was experienced in spring. Furthermore, strong local effects of forest advance were found in parts of Siberia. A cold bias driven by albedo in the model may have reduced the shrub-climate effect in the model as mostly low shrubs were established over our domain. Our study advances previous studies of shrub-climate interactions and provides concrete advice for further model improvement of dynamically simulating high latitude vegetation-climate interactions.

1. Introduction

During the past decades, satellite observations over high-latitude regions have observed an increase in spectral vegetation greenness (Myers-Smith et al., 2020), which has been partially attributed to increased shrub growth (Epstein et al., 2012; Forbes et al., 2010). The increase in height and abundance of Arctic shrubs have also been shown in plot-scale measurements (Forbes et al., 2010; Elmendorf et al., 2012). These increases have been attributed to increasing air temperatures (Myers-Smith et al., 2015; Myers-Smith et al., 2018) and longer growing seasons as a consequence of decreasing sea ice cover (Bhatt et al., 2010). Shrub

advancement is however not uniform across the Arctic (Berner et al., 2020; Elmendorf et al., 2012), and though the causes of the spatial heterogeneity of shrub growth are not completely understood, growth has been shown to be more sensitive to warming in environments with higher soil moisture (Elmendorf et al., 2012; Bjorkman et al., 2018) and nitrogen availability (Martin et al., 2021; Mekonnen et al., 2020).

An increased shrub cover may have contrasting consequences for land surface feedbacks to both regional climate and biogeochemical cycling (Myers-Smith et al., 2011; Vowles and Björk, 2019). Feedbacks arise from interactions of processes that may either amplify or dampen the response to external forcing. Such effects may occur due to Arctic vegetation shifts (Chapin et al., 2005; Serreze and Barry, 2011). Relative to low-growing tundra, taller woody vegetation can both trap snow, thereby insulating the soil against cold air temperature in winter, and protrude through the snow in late winter and spring (Sturm et al., 2001), effectively lowering the surface albedo (Sturm, 2005). As a result, earlier snow-melt and higher soil temperatures have been hypothesised to occur, thus increasing soil nitrogen mineralisation (Sturm, 2005; Sturm et al., 2001). Furthermore, nutrient cycling may be enhanced by litter feedbacks arising from deciduous shrub advancement (Vowles and Björk, 2019; Buckeridge et al., 2009). In summer, by contrast, a taller and denser canopy may protect soils from direct sunlight, thus reducing permafrost decay (Blok et al., 2010) and cooling the land surface through increased evapotranspiration (Zhang et al., 2014). This negative land surface feedback would primarily occur during the growing season (Zhang et al., 2020). Furthermore, aerodynamically rougher surfaces resulting from increased shrub and forest cover may enhance air mixing between lower and higher atmospheric layers, facilitating the transport of warmer surface air to the atmosphere (Akperov et al., 2021).

The biogeophysical processes described above also have implications for the carbon balance of Arctic ecosystems. A longer and warmer growing season could lead to a larger uptake of atmospheric CO_2 through increased productivity and biomass production, thus providing an increased carbon sink (Bonan, 2008). Furthermore, some recent evidence points to the possibility of enhanced carbon storage and stabilisation of organic matter in soils through enhanced organo-mineral complexation (Cotrufo et al., 2019) as shrubs advance (Lynch et al., 2018). On the other hand, the advance of forest and tall shrubs into tundra has been associated

with loss of carbon through substrate priming and microbial nitrogen mining (Keuper et al., 2020; Clemmensen et al., 2021; Hartley et al., 2012). Carbon loss from Arctic soils has serious consequences for the global carbon cycle as Arctic permafrost soils are estimated to store between 1100-1500 PgC (Hugelius et al., 2014), far outweighing the global atmospheric (~829 PgC) and vegetation (450-650 PgC) carbon pools (Ciais et al., 2013).

Reductions in albedo have been confirmed to influence local climate (Te Beest et al., 2016), however, few studies that provide realistic quantification of the dynamic effects of recent vegetation shifts on a pan-Arctic scale are available. Previous studies have either used idealised scenarios to quantify climate feedback potentials (Bonfils et al., 2012), or used prescribed climate forcing with a dynamic vegetation model to calculate albedo reductions from vegetation shifts (Miller and Smith, 2012; Zhang et al., 2013). The significance of dynamically simulating land surface feedbacks for Arctic climate compared to using static vegetation has been demonstrated (Zhang et al., 2018), although these simulations did not include an explicit representation of shrubs. Despite, nitrogen being limiting for plants in high latitudes (Mekonnen et al., 2021), neither nitrogen cycling nor permafrost has been included in previous land surface feedback studies.

Current General Circulation Models (GCMs) typically lack dynamic feedbacks due to climate-induced changes in vegetation cover. Although GCMs capable of simulating dynamic land cover and carbon cycle (often referred to as Earth System Models, ESMs) have emerged, none of the ensembles of current models used in the latest set of global climate projections underpinning the IPCC climate assessments (Ipcc, 2021) includes explicit representations of Arctic shrubs or tundra vegetation and their dynamics in response to climate. Regional climate models (RCMs) offer an alternative to global models to either increase the spatial resolution, provide more representative parameterisations over certain domains or include more detailed process descriptions (See for instance Klaus et al., 2016). Similar to the GCMs, dynamic vegetation processes – such as a dynamically changing land cover – are seldom represented in RCMs.

Here we attempt to advance on previous studies by using a regional ESM to quantify the land-surface feedbacks associated with increasing shrub cover in the high latitudes, including

nitrogen cycling. As coupled vegetation-climate models are under-evaluated, we perform an evaluation against reanalysis data to highlight potential difficulties in modelling the coupling between terrestrial ecosystems and climate. Finally, we will investigate the relative importance of each feedback mechanism and discuss what factors might be important for future predictions of impacts of shrub advancement on regional climate.

2. Methods

2.1 Regional Earth System model - RCA-GUESS

RCA-GUESS (Smith et al., 2011) is a regional ESM that is capable of simulating the dynamic interactions between atmospheric processes and a dynamic land surface, including biogeochemical cycling. It couples biophysical climate fields from the RCA4 atmospheric model with outputs of vegetation cover and structure, leaf area index and dependent biophysical parameters that control albedo, surface roughness and evapotranspiration based on vegetation dynamics simulated by the dynamic ecosystem model LPJ-GUESS (Smith et al., 2001; Smith et al., 2014). The separate sub-models are described in more detail in Supplementary materials S1. New features in the current version of RCA-GUESS include (1) six updated Arctic shrub plant functional types (PFTs); (2) updated biogeochemical cycling from Smith et al. (2014) which considers interactions between carbon and nitrogen on vegetation growth and soil decomposition; (3) updated soil physics which enables simulations of soil freezing and permafrost formation.

At the daily time step, surface temperature, precipitation and downwelling shortwave radiation simulated by RCA4 were sent to the ecosystem model. LPJ-GUESS in turn simulated the daily ecosystem response and computed the variables required by the land surface scheme (LSS) of RCA4 to replace its standard ECOCLIMAP land surface representation. Variables returned to RCA4 were daily LAI of the open land and forest tiles, and the fractions of forest cover, broadleaved forest and coniferous forest. Low, and prostrate shrubs, as well as grasses, were counted towards the open land tile. The LSS of RCA4 assumes forests to have at least 2m in height and thus trees and tall (up to 2 m) shrubs with a total projective cover of 40%, the gridcell is counted towards open land. This limit has been used in previous versions of RCA-GUESS. The projective cover metric is derived from vegetation LAI, and thus the size of individuals. If total tree projective cover was lower than

40%, vegetation was thus considered stunted and more characteristic of tundra than forest ecosystems.

2.2 Simulation protocol

Our simulations were conducted for the Arctic domain from the Coordinated Regional Downscaling Experiment (CORDEX; https://cordex.org/domains/region-11-arctic/; last accessed 2022-01-11) at a spatial resolution of 0.44°x0.44° on a rotated pole grid with 40 vertical levels.

2.2.2 Historic simulations

We performed two historic simulations between the years 1979 to 2013. RCA was forced with ERA-Interim reanalysis fields at the domain boundaries as well as historical CO_2 and CH_4 concentrations. The first simulation (henceforth referred to as the 'NoShrub' run) used plant functional types (PFTs) commonly included in GCMs but did not include any shrub PFTs. In the second simulation (henceforth 'Shrub' run), six shrub PFTs (see Supplementary material S1) were added.

Other input data required by the dynamic vegetation model was obtained from the dataset by Lamarque et al. (2013) for nitrogen deposition. Information about soil texture was collected from Batjes (2005).

2.3 Evaluation

We conducted an evaluation of the simulations against available satellite-derived monthly LAI from the GIMMS-LAI3g climatology (Mao and Yan, 2019) and annual GLASS-GLC landcover data (Liu et al., 2020). Since the coupling between the models are largely dependent on LAI and landcover fractions, these variables will be of importance for the evaluation of our results. We classified the landcover into similar, but not identical, classes as the GLASS-GLC for comparison (Table 1).

Furthermore, we evaluate the climate simulated by RCA-GUESS against ERA-Interim (Dee et al., 2011) temperature, precipitation, and albedo to assess any biases that may arise from the atmospheric sub-model. Biogeophysically important parameters such as albedo and latent heat exchange were evaluated against the GlobAlbedo dataset by Muller et al. (2012) and upscaled FLUXNET data (Jung et al., 2011), respectively. Gross primary production (GPP),

Table 1 Landcover classification comparison between RCA-GUESS (our study) and the GLASS-GLC landcover product (Liu et al., 2020).

Landcover class	RCA-GUESS	GLASS-GLC
Coniferous forest	Forest cover > 40% Coniferous trees > 66%	Tree cover ≥ 10% Height > 5 m
Deciduous forest	Forest cover > 40 % Deciduous trees > 66%	
Grassland	-	Canopy cover ≥ 20%
Shrubland	Forest cover < 40% shrub LAI > grass LAI	Canopy cover ≥ 20% Height < 5m
Tundra	Forest cover < 40% shrub LAI < grass LAI	-

ecosystem respiration (R_{eco}) and net ecosystem exchange (NEE) were evaluated by the upscaled CO_2 flux dataset by Virkkala et al. (2021). Finally, we perform a landcover based

evaluation of monthly climate, latent heat, albedo, LAI and CO_2 flux data. Four sites were selected to be representative of a deciduous forest, coniferous forest, tundra, and shrubland. All datasets were interpolated to the rotated grid used by RCA-GUESS prior to analysis.

3. Results

3.1 Effects of including shrubs

The inclusion of shrubs had a non-significant (t-test; p>0.05) effect on the annual domain-averaged climate. The average annual temperature 'Shrub' was on average 0.10 ± 0.19°C colder than the 'NoShrub' run. Domain averaged seasonal averages were also small with mean temperature differences spanning 0.15 ± 0.63°C (DJF), 0.33 ± 1.10°C (MAM), -0.02 ± 0.37°C (JJA), 0.20 ± 0.53°C (SON) for the respective seasons. There were however large effects on warming over central Siberia and the Northern Canadian Archipelago during spring (Fig 1). In a few grid cells the additional warming in the 'Shrub' run reached up to 8°C.

Warming of this magnitude was however associated with large albedo reductions due to forest advance rather than increased LAI (Fig S2.1; Supplementary materials). Furthermore, the model did not display any drastic differences between tundra in the 'Shrub' and 'NoShrub' runs, despite drastically different vegetation physiognomy. Summer temperatures were characterized by slower warming over Northern Canada in the 'Shrub' run than in the 'NoShrub' run associated with a larger latent heat flux (Fig 1) and a smaller forest cover (Fig 2). The smaller forest extent over Northern Canada was a competitive effect of the inclusion of shrubs. While surface temperature over the forests were generally well captured compared to ERA-Interim, there was a severe cold-bias over the tundra during spring and summer months (Fig 5 and Fig. S2.5). This cold bias was reinforced in our dynamic vegetation simulations compared to the standalone RCA4 with prescribed vegetation, though the standalone version RCA4 also simulated a strong cold bias over tundra regions (Berg et al., 2013; Koenigk et al., 2015).

Precipitation showed no distinct patterns over land in any seasons. Annual sums of total precipitation were also not significantly (t-test; $p>0.05$) different between the 'Shrub' and the 'NoShrub' runs for the simulation domain.

3.2 Vegetation distribution

The model generally captured the forest extent over Northern Europe and Siberia well compared to the GLASS-GLC landcover product (Fig. 2) while the forest extent was underestimated in Eastern Canada. The spatial extent of the forest cover was slightly larger in the 'NoShrub' run compared to the 'Shrub' run. The main difference between the runs was in the *Larix* forests in mid-Siberia. The smaller forest extent was due to a competitive effect between shrubs and trees in the 'Shrub' run which both limited the forest extent and slowed down forest advance (Fig. 2). Similarly, there was a development of shrublands over Northern Canada in the 'Shrub' run, which was replaced with a forest advance in the 'NoShrub' simulation. Forests over Northern Europe were mainly comprised of needle-leaved evergreen trees while forests of Northern Canada were comprised of deciduous forest.

As expected, the two simulations had drastically different physiognomy index over the tundra (Fig 3), where the 'Shrub' simulation displayed higher values indicating more woody vegetation. Furthermore, the phenology index indicates that tundra in the 'Shrub' run had a larger dominance of evergreen vegetation compared to the 'NoShrub' run at the start of the simulation. The change in the two indexes over the simulation period indicates that there is a trend towards more woody and deciduous vegetation. This trend was robust between the two runs. While the increase in the normalized physiognomy index is correlated with forest advance in the 'NoShrub' run, there are additional tundra increases in the 'Shrub' run associated with increasing shrub cover.

The LAI climatology over the forests was well captured (Fig. 4) in comparison with the GIMMS-LAI3g. However, tundra LAI was largely underestimated, which was spatially linked to the cold bias over these regions (Fig S2.5; Supplementary materials). Subsequently, the shrub cover was underestimated compared to the GLASS-GLC product. Tundra shrub cover was dominated by deciduous prostrate shrubs while the shrub cover closer to the forests mainly comprised taller, deciduous shrubs.

3.3 Landcover-based evaluation

Simulated temperatures largely matched the seasonal dynamics of ERA-Interim for all landcover classes except the tundra class where spring temperatures were approximately 8°C too cold (Fig 5). The timing of the cold temperature bias matched an over-estimation of albedo in winter and spring compared to the GlobAlbedo product. ERA-Interim albedo showed less annual variability than both the GlobAlbedo product and the simulated data, although the three products agreed on summertime (JJA) albedo. Precipitation amounts were underestimated compared to ERA-Interim, although the seasonal dynamics were realistically captured.

Seasonal carbon fluxes generally indicated a lower amplitude of both GPP and R_{eco} when shrubs were included. Trends in NEE were in general stable while both GPP and R_{eco} increased slightly over the simulation period (Fig 5). Magnitudes of both GPP, R_{eco} and NEE were within the range of the upscaled carbon flux estimates, except for tundra where the

magnitudes were lower. As the tundra constituted a large part of the study domain, the domain averaged GPP and R_{eco} were slightly underestimated, although NEE was in good agreement with the upscaled flux data (Fig S2.6, supplementary materials). The Arctic region was estimated to have a net uptake of 13.7 $\pm$ 1.3 gC m^{-2} yr^{-1} by Virkkala et al. (2021), while corresponding simulated values were 12.4 $\pm$ 11.2 gC m^{-2} yr^{-1} and 32.5 $\pm$ 8.8 gC m^{-2} yr^{-1} for the 'Shrub' and 'NoShrub' run, respectively.

4. Discussion

We compared a simulation including PFTs commonly represented in GCMs with a simulation including six additional Arctic shrub PFTs. Both simulations were realistic in comparison to a broad set of independent data products. The model captures general trends in temperature, and precipitation and carbon exchange. Furthermore, seasonal dynamics of climate, LAI, fluxes of CO_2 and energy, as well as forest distributions were realistically simulated.

We found that the temperature increases due to inclusion of shrub PFTs were strongest during spring when regional warming occurred over parts of Siberia and Northern Canada. On the other hand, summer warming was only local and stronger in areas of advance or densification of the forest cover. Seasonal climatologies did not differ greatly between the two runs for any of the landcover classes. This was expected for forest cover, since it did not differ in extent or physiognomy between the two runs. However, the tundra displayed large differences in simulated vegetation physiognomy between the two runs, and therefore the minor difference in seasonal climatologies is unexpected. Tundra vegetation in the 'Shrub' run was mostly comprised of low shrubs, and eddy covariance flux measurements have found little effect of low shrub (<80cm) cover on energy fluxes (Lafleur and Humphreys, 2018). In addition, showed a 20% simulated increase in low shrub cover over the high latitudes a temperature increase of +0.66°C, whereas a similar increase in tall shrubs (> 2m) induced an annual regional change of +1.84°C (Bonfils et al. (2012). Thus, our dynamic simulations of shrub cover did not simulate regional warming or shrub increases on that scale, and our model suggests that an increased abundance of shrubs on the tundra will play a secondary role in forest advance for regional warming.

Forest extent largely matched the GLASS-GLC extent. The main differences were in the *Larix* forest of Siberia. The smaller extent of the Siberian *Larix* forest was due to competitive interactions with shrubs which limited the extent of the forest. However, future range shifts of *Larix spp. are* very likely (Mamet et al., 2019), but may be limited by seed dispersal (Rees et al., 2020; Brown et al., 2018), nutrients (Gustafson et al., 2021) or competitive effects (Pearson et al., 2013).

The stronger temperature increases occurring over the Siberian tundra in our model, suggest that the soil carbon in these carbon-rich soils could be mobilised by soil warming and permafrost thaw with subsequent feedbacks to the global carbon cycle (Hugelius et al., 2014; Schuur et al., 2015). However, the strong temperature bias restricted our analysis of this feedback. Future studies could be extended to further include estimates of carbon loss from these areas if the strong climate biases are overcome. Nevertheless, the carbon fluxes simulated by the model were compared with the dataset by Virkkala et al. (2021) for forests and shrublands. For the tundra, the net exchange of carbon and the Pan-Arctic fluxes was also captured, even though the GPP and R_{eco} were underestimated due to the cold bias. The simulated data had both a stronger trend and larger variability than the measured data (Virkkala et al., 2021). This may be attributed to the values reported, which are medians of five common methods to upscale fluxes (Virkkala et al., 2021). The aggregated trends from the median values may have lower variability than each individual method of upscaling.

Furthermore, we found that an overestimation of albedo was associated with the cold bias in the simulations over the tundra domain, especially in spring. RCA4 has previously been found to simulate a pressure gradient over the Arctic ocean, resulting in anomalously strong cold winds over the Siberian tundra (Koenigk et al., 2015). This cold bias was amplified in our simulations with dynamically changing vegetation compared to the standalone RCA4 with static vegetation. The cold bias was so strong that the simulated vegetation did not fully establish. What factor that drove the overestimation of albedo in our simulations was however somewhat unclear. Correlations between LAI and temperature were weak and could thus not drive large-scale reductions of albedo in the model. Therefore, it is not likely

that a larger LAI would have fully corrected the albedo bias, had the vegetation been more productive.

In LPJ-GUESS, lower temperatures generally lead to lower productivity as the temperature response of the assimilation would lead to reduced photosynthetic capacity. Our newly implemented features likely have further compounded the low productivity bias over tundra as the lower temperatures lead to lower soil nitrogen mineralisation and a shallower permafrost active layer. While increased realism in all models is a key research goal, it is important to be aware of similar patterns that may arise. The biases are furthermore difficult to overcome by model calibration, especially if simulated future projections are attempted. If model parameters (e.g. relating to vegetation) are tuned to compensate for biases in the atmospheric model, vegetation responses might be too strong in future scenarios.

Our study with dynamically changing vegetation and feedbacks is nonetheless a step forward from previous studies with prescribed shrub cover (Bonfils et al., 2012), purely local studies of albedo change (e.g., Te Beest et al., 2016), statistical relationships between vegetation and abiotic drivers (Pearson et al., 2013) or absence of important processes such as nitrogen cycling (Zhang et al., 2020; Zhang et al., 2014; Zhang et al., 2018). Furthermore, this study identifies potential areas for model improvements. The land surface scheme of RCA4 implicitly assumes vegetation above 2m belongs to the forest fraction. We thus counted the tall shrubs towards the forest tile rather than the tundra tile. However, this transition is likely more gradual than what is represented in the model. Model improvements should focus on a more detailed representation of shrub height and physiognomy. Such improvements could also consider snow dynamics to represent albedo change more accurately from protruding shrubs in winter and spring.

5. Summary

A new version of a regional ESM (RCA-GUESS) was developed and evaluated to determine the effect of including shrubs in simulations of Arctic climate. The shrub and no-shrub simulations were surprisingly similar, and the inclusion of shrubs was not found to significantly affect regional climate. The highest degrees of warming stemmed from the

advance and densification of forests, although these effects were only local. Shrub advance slightly warmed the climate and had significant effects on spring. Competitive effects held back forest advance in our 'Shrub' simulations, which slightly reduced warming.

The evaluation of the vegetation-climate coupling revealed a bias over large parts of the tundra domain, driven by albedo. This highlights the importance of evaluating the coupling between the sub-models, but also room for model improvement. The open-land tile in the LSS of RCA may need to be separated into more sub-classes, like bare ground, grassland and shrubland. Albedo calculations on the open land tile could include parameters than LAI for its albedo calculations. Such parameters would yield a more dynamic transition between open-land and forests, which could result in more realistic and robust projections of future impacts of shrubification on local and regional high latitude warming.

References

Akperov, M., Zhang, W., Miller, P. A., Mokhov, I. I., Semenov, V. A., Matthes, H., Smith, B., and Rinke, A.: Responses of Arctic cyclones to biogeophysical feedbacks under future warming scenarios in a regional Earth system model, Environmental Research Letters, 16, 10.1088/1748-9326/ac0566, 2021.

Batjes, N. H.: ISRIC-WISE global data set of derived soil properties on a 0.5 by 0.5 degree grid (version 3.0), ISRIC – World Soil Information, Wageningen, 2005.

Berg, P., Döscher, R., and Koenigk, T.: Impacts of using spectral nudging on regional climate model RCA4 simulations of the Arctic, Geoscientific Model Development, 6, 849-859, 10.5194/gmd-6-849-2013, 2013.

Berner, L. T., Massey, R., Jantz, P., Forbes, B. C., Macias-Fauria, M., Myers-Smith, I., Kumpula, T., Gauthier, G., Andreu-Hayles, L., Gaglioti, B. V., Burns, P., Zetterberg, P., D'Arrigo, R., and Goetz, S. J.: Summer warming explains widespread but not uniform greening in the Arctic tundra biome, Nat Commun, 11, 4621, 10.1038/s41467-020-18479-5, 2020.

Bhatt, U. S., Walker, D. A., Raynolds, M. K., Comiso, J. C., Epstein, H. E., Jia, G., Gens, R., Pinzon, J. E., Tucker, C. J., Tweedie, C. E., and Webber, P. J.: Circumpolar Arctic Tundra Vegetation Change Is Linked to Sea Ice Decline, Earth Interactions, 14, 1-20, 10.1175/2010ei315.1, 2010.

Bjorkman, A. D., Myers-Smith, I. H., Elmendorf, S. C., Normand, S., Ruger, N., Beck, P. S. A., Blach-Overgaard, A., Blok, D., Cornelissen, J. H. C., Forbes, B. C., Georges, D., Goetz, S. J., Guay, K. C., Henry, G. H. R., HilleRisLambers, J., Hollister, R. D., Karger, D. N., Kattge, J., Manning, P., Prevey, J. S., Rixen, C., Schaepman-Strub, G., Thomas, H. J. D., Vellend, M., Wilmking, M., Wipf, S., Carbognani, M., Hermanutz, L., Levesque, E., Molau, U., Petraglia, A., Soudzilovskaia, N. A., Spasojevic, M. J., Tomaselli, M., Vowles, T., Alatalo, J. M., Alexander, H. D., Anadon-Rosell, A., Angers-Blondin, S., Beest, M. T., Berner, L., Bjork, R. G., Buchwal, A., Buras, A., Christie, K., Cooper, E. J., Dullinger, S., Elberling, B., Eskelinen, A., Frei, E. R., Grau, O., Grogan, P., Hallinger, M., Harper, K. A., Heijmans, M., Hudson, J., Hulber, K., Iturrate-Garcia, M., Iversen, C. M., Jaroszynska, F., Johnstone, J. F., Jorgensen, R. H., Kaarlejarvi, E., Klady, R., Kuleza, S., Kulonen, A., Lamarque, L. J., Lantz, T., Little, C. J., Speed, J. D. M., Michelsen, A., Milbau, A., Nabe-Nielsen, J., Nielsen, S. S., Ninot, J. M., Oberbauer, S. F., Olofsson, J., Onipchenko, V. G., Rumpf, S. B., Semenchuk, P., Shetti, R., Collier, L. S., Street, L. E., Suding, K. N., Tape, K. D., Trant, A., Treier, U. A., Tremblay, J. P., Tremblay, M., Venn, S., Weijers, S., Zamin, T., Boulanger-Lapointe, N., Gould, W. A., Hik, D.

S., Hofgaard, A., Jonsdottir, I. S., Jorgenson, J., Klein, J., Magnusson, B., Tweedie, C., Wookey, P. A., Bahn, M., Blonder, B., van Bodegom, P. M., Bond-Lamberty, B., Campetella, G., Cerabolini, B. E. L., Chapin, F. S., 3rd, Cornwell, W. K., Craine, J., Dainese, M., de Vries, F. T., Diaz, S., Enquist, B. J., Green, W., Milla, R., Niinemets, U., Onoda, Y., Ordonez, J. C., Ozinga, W. A., Penuelas, J., Poorter, H., Poschlod, P., Reich, P. B., Sandel, B., Schamp, B., Sheremetev, S., and Weiher, E.: Plant functional trait change across a warming tundra biome, Nature, 562, 57-62, 10.1038/s41586-018-0563-7, 2018.

Blok, D., Heijmans, M. M. P. D., Schaepman-Strub, G., Kononov, A. V., Maximov, T. C., and Berendse, F.: Shrub expansion may reduce summer permafrost thaw in Siberian tundra, Global Change Biology, 16, 1296-1305, 10.1111/j.1365-2486.2009.02110.x, 2010.

Bonan, G. B.: Forests and Climate Change: Forcings, Feedbacks, and the Climate Benefits of Forests, Science, 320, 1444-1449, 10.1126/science.1155121, 2008.

Bonfils, C. J. W., Phillips, T. J., Lawrence, D. M., Cameron-Smith, P., Riley, W. J., and Subin, Z. M.: On the influence of shrub height and expansion on northern high latitude climate, Environmental Research Letters, 7, 10.1088/1748-9326/7/1/015503, 2012.

Brown, C. D., Dufour‐Tremblay, G., Jameson, R. G., Mamet, S. D., Trant, A. J., Walker, X. J., Boudreau, S., Harper, K. A., Henry, G. H. R., Hermanutz, L., Hofgaard, A., Isaeva, L., Kershaw, G. P., and Johnstone, J. F.: Reproduction as a bottleneck to treeline advance across the circumarctic forest tundra ecotone, Ecography, 42, 137-147, 10.1111/ecog.03733, 2018.

Buckeridge, K. M., Zufelt, E., Chu, H., and Grogan, P.: Soil nitrogen cycling rates in low arctic shrub tundra are enhanced by litter feedbacks, Plant and Soil, 330, 407-421, 10.1007/s11104-009-0214-8, 2009.

Chapin, F. S., 3rd, Sturm, M., Serreze, M. C., McFadden, J. P., Key, J. R., Lloyd, A. H., McGuire, A. D., Rupp, T. S., Lynch, A. H., Schimel, J. P., Beringer, J., Chapman, W. L., Epstein, H. E., Euskirchen, E. S., Hinzman, L. D., Jia, G., Ping, C. L., Tape, K. D., Thompson, C. D., Walker, D. A., and Welker, J. M.: Role of land-surface changes in arctic summer warming, Science, 310, 657-660, 10.1126/science.1117368, 2005.

Ciais, P., Sabine, C., Bala, G., Bopp, L., Brovking, V., Canadell, J., Chhabra, A., DeFries, R., Galloway, J., Heimann, M., Jones, C. D., Le Quéré, C., Myneni, R. B., Piao, S., and Thornton, P.: Carbon and Other Biogeochemical Cycles, in: The Physical Science Basis. Contribution of Working Group I to the Fifth Assessment Report of the Intergovernmental Panel on Climate Change, edited by: Stocker, T. F., Qin, D., Plattner, G.-K., Tignor, M., Allen, S. K., Boschung, J., Nauels, A., Xia, Y., Bex, V., and Midgley, P. M., Cambridge University Press, Cambridge, United Kingdom, 2013.

Clemmensen, K. E., Durling, M. B., Michelsen, A., Hallin, S., Finlay, R. D., and Lindahl, B. D.: A tipping point in carbon storage when forest expands into tundra is related to mycorrhizal recycling of nitrogen, Ecol Lett, 24, 1193-1204, 10.1111/ele.13735, 2021.

Cotrufo, M. F., Ranalli, M. G., Haddix, M. L., Six, J., and Lugato, E.: Soil carbon storage informed by particulate and mineral-associated organic matter, Nature Geoscience, 12, 989-994, 10.1038/s41561-019-0484-6, 2019.

Dee, D. P., Uppala, S. M., Simmons, A. J., Berrisford, P., Poli, P., Kobayashi, S., Andrae, U., Balmaseda, M. A., Balsamo, G., Bauer, P., Bechtold, P., Beljaars, A. C. M., van de Berg, L., Bidlot, J., Bormann, N., Delsol, C., Dragani, R., Fuentes, M., Geer, A. J., Haimberger, L., Healy, S. B., Hersbach, H., Hólm, E. V., Isaksen, L., Kållberg, P., Köhler, M., Matricardi, M., McNally, A. P., Monge-Sanz, B. M., Morcrette, J. J., Park, B. K., Peubey, C., de Rosnay, P., Tavolato, C., Thépaut, J. N., and Vitart, F.: The ERA-Interim reanalysis: configuration and performance of the data assimilation system, Quarterly Journal of the Royal Meteorological Society, 137, 553-597, 10.1002/qj.828, 2011.

Elmendorf, S. C., Henry, G. H. R., Hollister, R. D., Björk, R. G., Boulanger-Lapointe, N., Cooper, E. J., Cornelissen, J. H. C., Day, T. A., Dorrepaal, E., Elumeeva, T. G., Gill, M., Gould, W. A., Harte, J., Hik, D. S., Hofgaard, A., Johnson, D. R., Johnstone, J. F., Jónsdóttir, I. S., Jorgenson, J. C., Klanderud, K., Klein, J. A., Koh, S., Kudo, G., Lara, M., Lévesque, E., Magnússon, B., May, J. L., Mercado-Dı´az, J. A., Michelsen, A., Molau, U., Myers-Smith, I. H., Oberbauer, S. F., Onipchenko, V. G., Rixen, C., Martin Schmidt, N., Shaver, G. R., Spasojevic, M. J., Þórhallsdóttir, Þ. E., Tolvanen, A., Troxler, T., Tweedie, C. E., Villareal, S., Wahren, C.-H., Walker, X., Webber, P. J., Welker, J. M., and Wipf,

S.: Plot-scale evidence of tundra vegetation change and links to recent summer warming, Nature Climate Change, 2, 453-457, 10.1038/nclimate1465, 2012.

Epstein, H. E., Raynolds, M. K., Walker, D. A., Bhatt, U. S., Tucker, C. J., and Pinzon, J. E.: Dynamics of aboveground phytomass of the circumpolar Arctic tundra during the past three decades, Environmental Research Letters, 7, 10.1088/1748-9326/7/1/015506, 2012.

Forbes, B. C., Fauria, M. M., and Zetterberg, P.: Russian Arctic warming and 'greening' are closely tracked by tundra shrub willows, Global Change Biology, 16, 1542-1554, 10.1111/j.1365-2486.2009.02047.x, 2010.

Gustafson, A., Miller, P. A., Björk, R. G., Olin, S., and Smith, B.: Nitrogen restricts future sub-arctic treeline advance in an individual-based dynamic vegetation model, Biogeosciences, 18, 6329-6347, 10.5194/bg-18-6329-2021, 2021.

Hartley, I. P., Garnett, M. H., Sommerkorn, M., Hopkins, D. W., Fletcher, B. J., Sloan, V. L., Phoenix, G. K., and Wookey, P. A.: A potential loss of carbon associated with greater plant growth in the European Arctic, Nature Climate Change, 2, 875-879, 10.1038/nclimate1575, 2012.

Hugelius, G., Strauss, J., Zubrzycki, S., Harden, J. W., Schuur, E. A. G., Ping, C. L., Schirrmeister, L., Grosse, G., Michaelson, G. J., Koven, C. D., amp, apos, Donnell, J. A., Elberling, B., Mishra, U., Camill, P., Yu, Z., Palmtag, J., and Kuhry, P.: Estimated stocks of circumpolar permafrost carbon with quantified uncertainty ranges and identified data gaps, Biogeosciences, 11, 6573-6593, 10.5194/bg-11-6573-2014, 2014.

IPCC: Climate Change 2021: The Physical Science Basis. Contribution of Working Group I to the Sixth Assessment Report of the Intergovernmental Panel on Climate Change, Cambridge, United and New York, NY, USA, 10.1017/9781009157896, 2021.

Jung, M., Reichstein, M., Margolis, H. A., Cescatti, A., Richardson, A. D., Arain, M. A., Arneth, A., Bernhofer, C., Bonal, D., Chen, J., Gianelle, D., Gobron, N., Kiely, G., Kutsch, W., Lasslop, G., Law, B. E., Lindroth, A., Merbold, L., Montagnani, L., Moors, E. J., Papale, D., Sottocornola, M., Vaccari, F., and Williams, C.: Global patterns of land-atmosphere fluxes of carbon dioxide, latent heat, and sensible heat derived from eddy covariance, satellite, and meteorological observations, Journal of Geophysical Research, 116, 10.1029/2010jg001566, 2011.

Keuper, F., Wild, B., Kummu, M., Beer, C., Blume-Werry, G., Fontaine, S., Gavazov, K., Gentsch, N., Guggenberger, G., Hugelius, G., Jalava, M., Koven, C., Krab, E. J., Kuhry, P., Monteux, S., Richter, A., Shahzad, T., Weedon, J. T., and Dorrepaal, E.: Carbon loss from northern circumpolar permafrost soils amplified by rhizosphere priming, Nature Geoscience, 13, 560-565, 10.1038/s41561-020-0607-0, 2020.

Klaus, D., Dethlo, K., Dorn, W., Rinke, A., and Wu, D. L.: New insight of Arctic cloud parameterization from regional climate model simulations, satellite-based and drifting station data, Geophys Res Lett, 43, 5450-5459, 10.1002/2015GL067530, 2016.

Koenigk, T., Berg, P., and Döscher, R.: Arctic climate change in an ensemble of regional CORDEX simulations, Polar Research, 34, 10.3402/polar.v34.24603, 2015.

Lafleur, P. M. and Humphreys, E. R.: Tundra shrub effects on growing season energy and carbon dioxide exchange, Environmental Research Letters, 13, 10.1088/1748-9326/aab863, 2018.

Lamarque, J. F., Dentener, F., McConnell, J., Ro, C. U., Shaw, M., Vet, R., Bergmann, D., Cameron-Smith, P., Dalsoren, S., Doherty, R., Faluvegi, G., Ghan, S. J., Josse, B., Lee, Y. H., MacKenzie, I. A., Plummer, D., Shindell, D. T., Skeie, R. B., Stevenson, D. S., Strode, S., Zeng, G., Curran, M., Dahl-Jensen, D., Das, S., Fritzsche, D., and Nolan, M.: Multi-model mean nitrogen and sulfur deposition from the Atmospheric Chemistry and Climate Model Intercomparison Project (ACCMIP): evaluation of historical and projected future changes, Atmospheric Chemistry and Physics, 13, 7997-8018, 10.5194/acp-13-7997-2013, 2013.

Liu, H., Gong, P., Wang, J., Clinton, N., Bai, Y., and Liang, S.: Annual dynamics of global land cover and its long-term changes from 1982 to 2015, Earth System Science Data, 12, 1217-1243, 10.5194/essd-12-1217-2020, 2020.

Lynch, L. M., Machmuller, M. B., Cotrufo, M. F., Paul, E. A., and Wallenstein, M. D.: Tracking the fate of fresh carbon in the Arctic tundra: Will shrub expansion alter responses of soil organic matter to warming?, Soil Biology and Biochemistry, 120, 134-144, 10.1016/j.soilbio.2018.02.002, 2018.

Mamet, S. D., Brown, C. D., Trant, A. J., and Laroque, C. P.: Shifting global Larix distributions: Northern expansion and southern retraction as species respond to changing climate, Journal of Biogeography, 46, 30-44, 10.1111/jbi.13465, 2019.

Mao, J. and Yan, B.: Global Monthly Mean Leaf Area Index Climatology, 1981-2015, 10.3334/ORNLDAAC/1653, 2019.

Mekonnen, Z. A., Riley, W. J., Berner, L. T., Bouskill, N. J., Torn, M. S., Iwahana, G., Breen, A. L., Myers-Smith, I. H., Criado, M. G., Liu, Y., Euskirchen, E. S., Goetz, S. J., Mack, M. C., and Grant, R. F.: Arctic tundra shrubification: a review of mechanisms and impacts on ecosystem carbon balance, Environmental Research Letters, 16, 10.1088/1748-9326/abf28b, 2021.

Miller, P. A. and Smith, B.: Modelling tundra vegetation response to recent arctic warming, Ambio, 41 Suppl 3, 281-291, 10.1007/s13280-012-0306-1, 2012.

Muller, J.-P., Lopéz, G., Watson, G., Shane, N., Kennedy, T., Yuen, P., Lewis, P., Fischer, J., Guanter, L., Domench, C., Preusker, R., North, P., Heckel, A., Danne, O., Krämer, U., Zühlke, M., Brockmann, C., and Pinnok, S.: The ESA GlobAlbedo Project for mapping the Earth's land surface albedo for 15 years from European sensors, IEEE Geoscience and Remote Sensing Symposium (IGARSS) 2012, IEEE, Munich, Germany, 22-27.27.12,

Myers-Smith, I. H., Hik, D. S., and Aerts, R.: Climate warming as a driver of tundra shrubline advance, Journal of Ecology, 106, 547-560, 10.1111/1365-2745.12817, 2018.

Myers-Smith, I. H., Forbes, B. C., Wilmking, M., Hallinger, M., Lantz, T., Blok, D., Tape, K. D., Macias-Fauria, M., Sass-Klaassen, U., Lévesque, E., Boudreau, S., Ropars, P., Hermanutz, L., Trant, A., Collier, L. S., Weijers, S., Rozema, J., Rayback, S. A., Schmidt, N. M., Schaepman-Strub, G., Wipf, S., Rixen, C., Ménard, C. B., Venn, S., Goetz, S., Andreu-Hayles, L., Elmendorf, S., Ravolainen, V., Welker, J., Grogan, P., Epstein, H. E., and Hik, D. S.: Shrub expansion in tundra ecosystems: dynamics, impacts and research priorities, Environmental Research Letters, 6, 10.1088/1748-9326/6/4/045509, 2011.

Myers-Smith, I. H., Elmendorf, S. C., Beck, P. S. A., Wilmking, M., Hallinger, M., Blok, D., Tape, K. D., Rayback, S. A., Macias-Fauria, M., Forbes, B. C., Speed, J. D. M., Boulanger-Lapointe, N., Rixen, C., Lévesque, E., Schmidt, N. M., Baittinger, C., Trant, A. J., Hermanutz, L., Collier, L. S., Dawes, M. A., Lantz, T. C., Weijers, S., Jørgensen, R. H., Buchwal, A., Buras, A., Naito, A. T., Ravolainen, V., Schaepman-Strub, G., Wheeler, J. A., Wipf, S., Guay, K. C., Hik, D. S., and Vellend, M.: Climate sensitivity of shrub growth across the tundra biome, Nature Climate Change, 5, 887-891, 10.1038/nclimate2697, 2015.

Myers-Smith, I. H., Kerby, J. T., Phoenix, G. K., Bjerke, J. W., Epstein, H. E., Assmann, J. J., John, C., Andreu-Hayles, L., Angers-Blondin, S., Beck, P. S. A., Berner, L. T., Bhatt, U. S., Bjorkman, A. D., Blok, D., Bryn, A., Christiansen, C. T., Cornelissen, J. H. C., Cunliffe, A. M., Elmendorf, S. C., Forbes, B. C., Goetz, S. J., Hollister, R. D., de Jong, R., Loranty, M. M., Macias-Fauria, M., Maseyk, K., Normand, S., Olofsson, J., Parker, T. C., Parmentier, F.-J. W., Post, E., Schaepman-Strub, G., Stordal, F., Sullivan, P. F., Thomas, H. J. D., Tømmervik, H., Treharne, R., Tweedie, C. E., Walker, D. A., Wilmking, M., and Wipf, S.: Complexity revealed in the greening of the Arctic, Nature Climate Change, 10, 106-117, 10.1038/s41558-019-0688-1, 2020.

Pearson, R. G., Phillips, S. J., Loranty, M. M., Beck, P. S. A., Damoulas, T., Knight, S. J., and Goetz, S. J.: Shifts in Arctic vegetation and associated feedbacks under climate change, Nature Climate Change, 3, 673-677, 10.1038/nclimate1858, 2013.

Rees, W. G., Hofgaard, A., Boudreau, S., Cairns, D. M., Harper, K., Mamet, S., Mathisen, I., Swirad, Z., and Tutubalina, O.: Is subarctic forest advance able to keep pace with climate change?, Glob Chang Biol, 26, 3965-3977, 10.1111/gcb.15113, 2020.

Schuur, E. A., McGuire, A. D., Schadel, C., Grosse, G., Harden, J. W., Hayes, D. J., Hugelius, G., Koven, C. D., Kuhry, P., Lawrence, D. M., Natali, S. M., Olefeldt, D., Romanovsky, V. E., Schaefer, K., Turetsky, M. R., Treat, C. C., and Vonk, J. E.: Climate change and the permafrost carbon feedback, Nature, 520, 171-179, 10.1038/nature14338, 2015.

Serreze, M. C. and Barry, R. G.: Processes and impacts of Arctic amplification: A research synthesis, Global and Planetary Change, 77, 85-96, 10.1016/j.gloplacha.2011.03.004, 2011.

Smith, B., Prentice, I. C., and Sykes, M. T.: Representation of vegetation dynamics in the modelling of terrestrial ecosystems: comparing two contrasting approaches within European climate space, Global Ecology and Biogeography, 10, 621-637, 10.1046/j.1466-822X.2001.t01-1-00256.x, 2001.

Smith, B., Samuelsson, P., Wramneby, A., and Rummukainen, M.: A model of the coupled dynamics of climate, vegetation and terrestrial ecosystem biogeochemistry for regional applications, Tellus A: Dynamic Meteorology and Oceanography, 63, 87-106, 10.1111/j.1600-0870.2010.00477.x, 2011.

Smith, B., Wårlind, D., Arneth, A., Hickler, T., Leadley, P., Siltberg, J., and Zaehle, S.: Implications of incorporating N cycling and N limitations on primary production in an individual-based dynamic vegetation model, Biogeosciences, 11, 2027-2054, 10.5194/bg-11-2027-2014, 2014.

Sturm, M.: Changing snow and shrub conditions affect albedo with global implications, Journal of Geophysical Research, 110, 10.1029/2005jg000013, 2005.

Sturm, M., Holmgren, J., McFadden, J. P., Liston, G. E., Chapin, F. S., and Racine, C. H.: Snow–Shrub Interactions in Arctic Tundra: A Hypothesis with Climatic Implications, Journal of Climate, 14, 336-344, 10.1175/1520-0442(2001)014<0336:Ssiiat>2.0.Co;2, 2001.

te Beest, M., Sitters, J., Ménard, C. B., and Olofsson, J.: Reindeer grazing increases summer albedo by reducing shrub abundance in Arctic tundra, Environmental Research Letters, 11, 10.1088/1748-9326/aa5128, 2016.

Virkkala, A. M., Aalto, J., Rogers, B. M., Tagesson, T., Treat, C. C., Natali, S. M., Watts, J. D., Potter, S., Lehtonen, A., Mauritz, M., Schuur, E. A. G., Kochendorfer, J., Zona, D., Oechel, W., Kobayashi, H., Humphreys, E., Goeckede, M., Iwata, H., Lafleur, P. M., Euskirchen, E. S., Bokhorst, S., Marushchak, M., Martikainen, P. J., Elberling, B., Voigt, C., Biasi, C., Sonnentag, O., Parmentier, F. W., Ueyama, M., Celis, G., St Loius, V. L., Emmerton, C. A., Peichl, M., Chi, J., Jarveoja, J., Nilsson, M. B., Oberbauer, S. F., Torn, M. S., Park, S. J., Dolman, H., Mammarella, I., Chae, N., Poyatos, R., Lopez-Blanco, E., Rojle Christensen, T., Jung Kwon, M., Sachs, T., Holl, D., and Luoto, M.: Statistical upscaling of ecosystem CO2 fluxes across the terrestrial tundra and boreal domain: regional patterns and uncertainties, Glob Chang Biol, 10.1111/gcb.15659, 2021.

Vowles, T. and Björk, R. G.: Implications of evergreen shrub expansion in the Arctic, Journal of Ecology, 107, 650-655, 10.1111/1365-2745.13081, 2019.

Zhang, W., Jansson, C., Miller, P. A., Smith, B., and Samuelsson, P.: Biogeophysical feedbacks enhance the Arctic terrestrial carbon sink in regional Earth system dynamics, Biogeosciences, 11, 5503-5519, 10.5194/bg-11-5503-2014, 2014.

Zhang, W., Miller, P. A., Jansson, C., Samuelsson, P., Mao, J., and Smith, B.: Self-Amplifying Feedbacks Accelerate Greening and Warming of the Arctic, Geophysical Research Letters, 45, 7102-7111, 10.1029/2018gl077830, 2018.

Zhang, W., Miller, P. A., Smith, B., Wania, R., Koenigk, T., and Döscher, R.: Tundra shrubification and tree-line advance amplify arctic climate warming: results from an individual-based dynamic vegetation model, Environmental Research Letters, 8, 10.1088/1748-9326/8/3/034023, 2013.

Zhang, W., Döscher, R., Koenigk, T., Miller, P. A., Jansson, C., Samuelsson, P., Wu, M., and Smith, B.: The Interplay of Recent Vegetation and Sea Ice Dynamics—Results From a Regional Earth System Model Over the Arctic, Geophysical Research Letters, 47, 10.1029/2019gl085982, 2020.

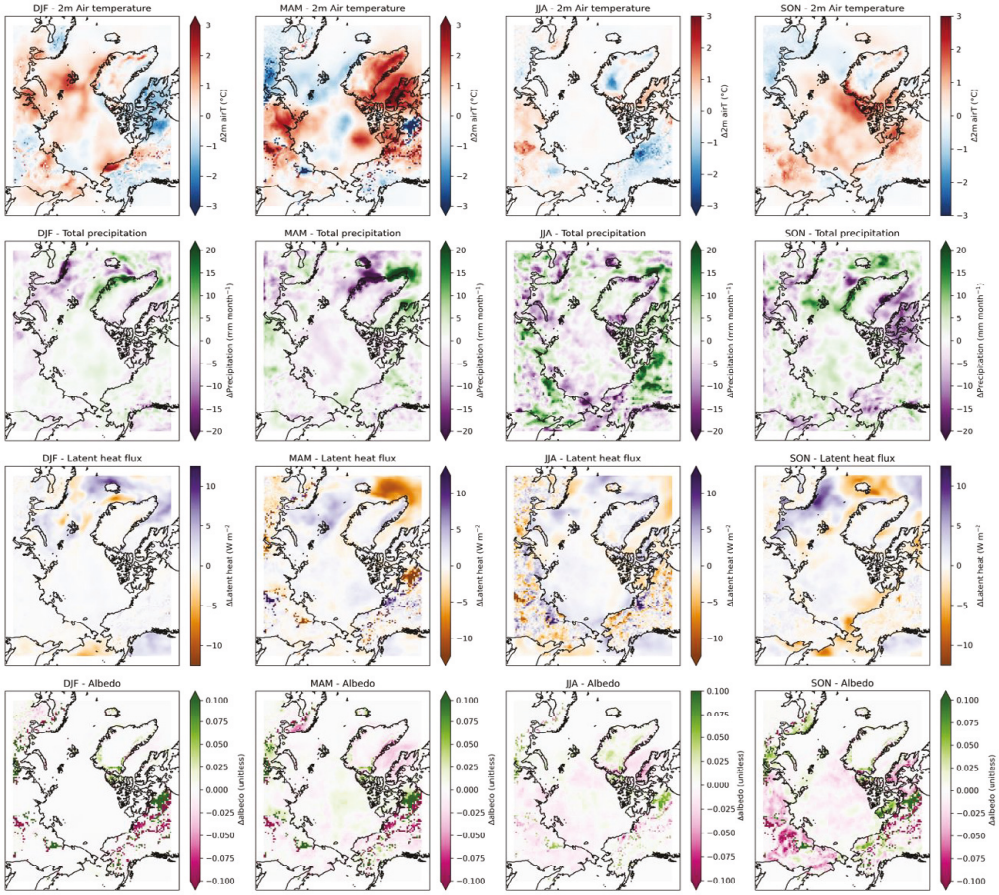

Figure 1 Difference in seasonal 2m air temperature (top row), latent heat flux (middle row) and albedo (lower row) change from inclusion of shrubs in the simulations. Values are the difference in each variable between the end (2008-2013) and start (1980-1985) and between simulations (Shrub – NoShrub).

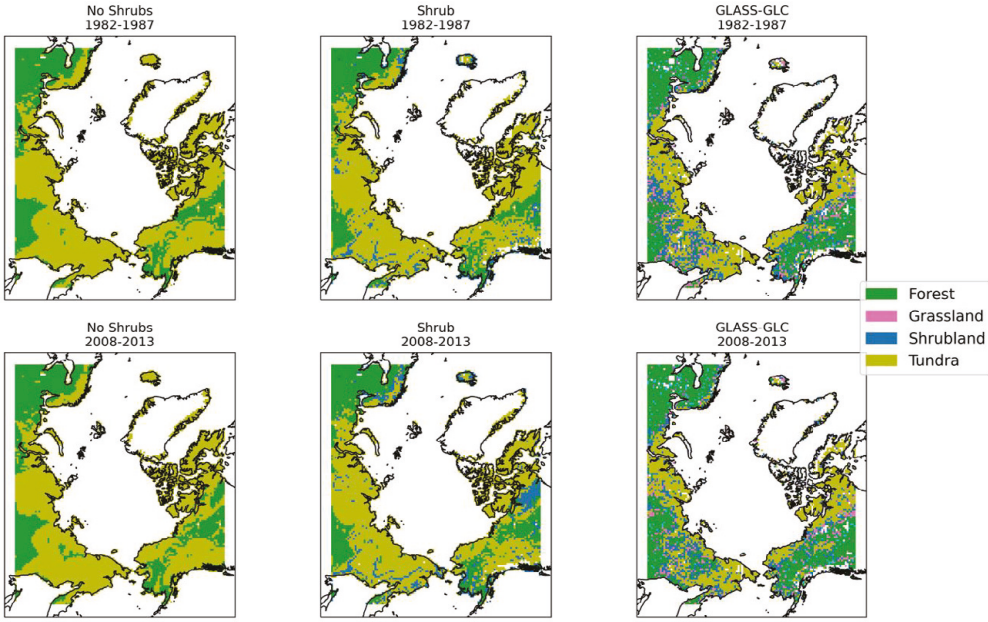

Fig. 2 Land cover classes and change between the beginning (1982-1987) and end (2008-2013) of the simulation period for the 'NoShrub' run (left column), the 'Shrub' run (middle column) and GLASS-GLC landcover product (Right column).

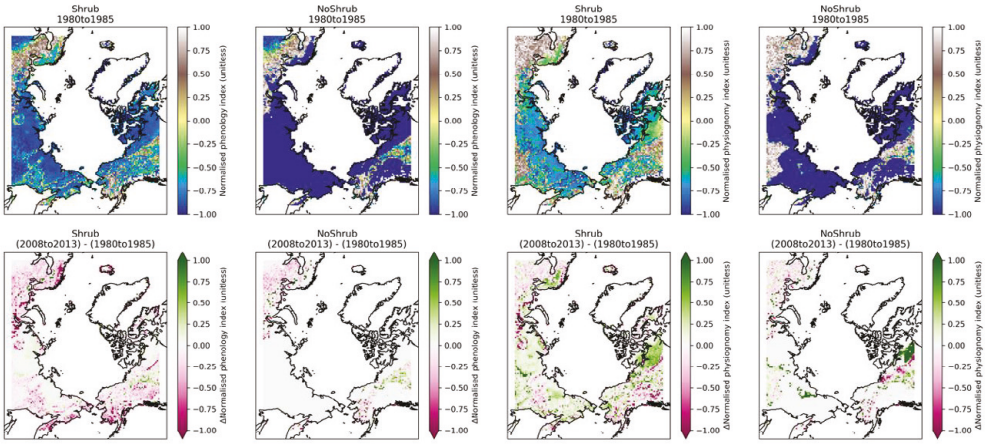

Fig. 3. Simulated normalised phenology index [(LAI_{eg} - LAI_{decid}) / (LAI_{eg} + LAI_{decid})] and normalised physiognomy index [(LAI_{woody}-LAI_{herb}) / (LAI_{woody} + LAI_{herb})] for the two simulations. The two indices indicate the relative abundance of evergreen vs. deciduous vegetation and woody vs. herbaceous vegetation, respectively. The normalised phenology index ranges between -1 (fully deciduous ecosystems) and +1 (fully evergreen ecosystems). Similarly, the normalised physiognomy index ranges between -1 (fully herbaceous ecosystems) to +1 (fully woody ecosystems). Top row shows average values between the year 1980-1985 while bottom row shows the change until 2008-2013.

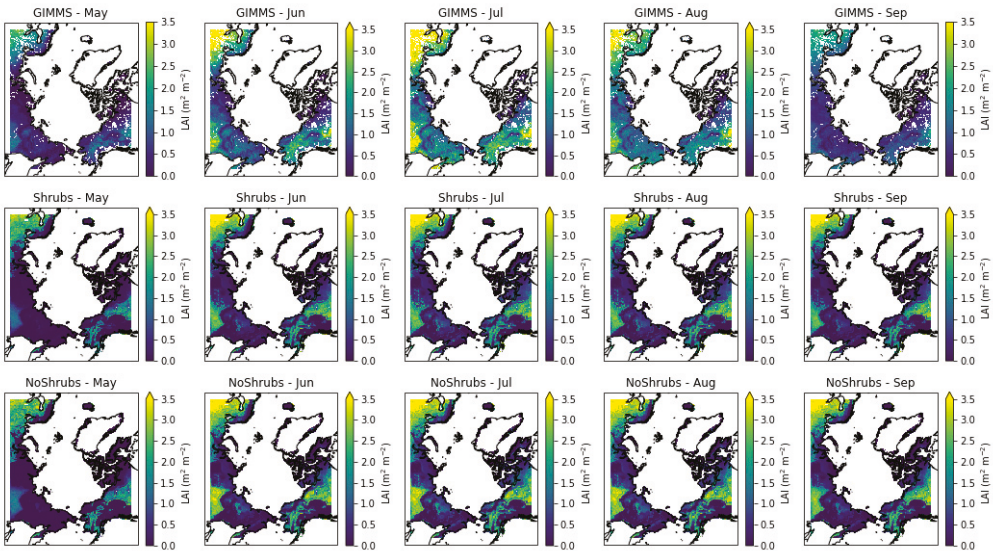

Fig. 4 Satellite inferred (top row) and RCA-GUESS simulated total summer LAI for the years 1980-2013. Middle row shows the RCA-GUESS simulation with dynamic vegetation but without shrubs. The lower row shows corresponding simulation but with shrubs included.

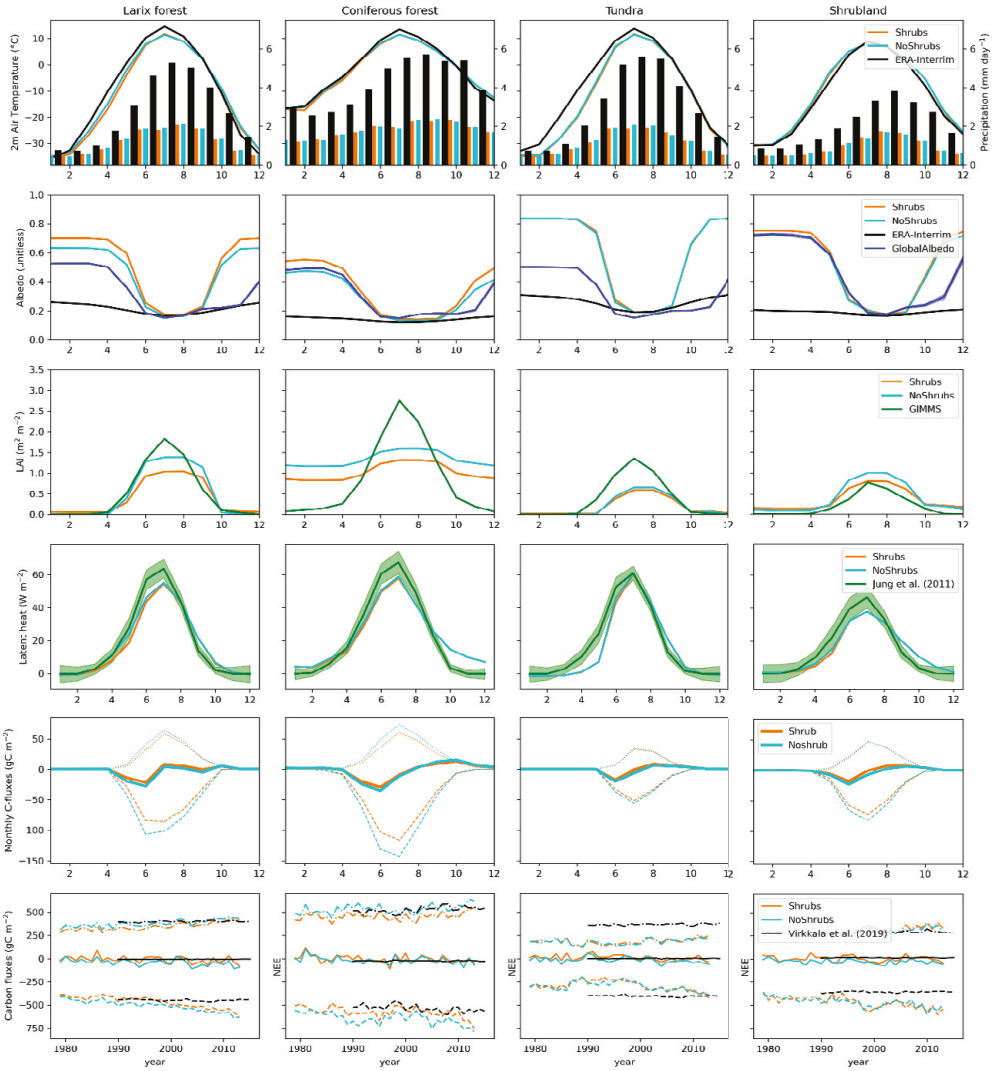

Fig. 5 Landcover based monthly averages over the years 1981-2010 and comparison to available datasets. Bottom row shows evaluation of annual CO_2 fluxes over our simulation period. Data are averages of grid cells representative of their respective land cover class. See text for references to comparison datasets.

Supplementary material S1 – Model description

Ecosystem model - LPJ-GUESS

LPJ-GUESS (Smith et al., 2001; Smith et al., 2014) is a dynamic vegetation model optimised for regional and global applications. It explicitly simulates primary production, growth, and competition between individuals belonging to a defined set of plant functional types (PFT). The simulated vegetation is the emergent outcome of the competition for light, water and nutrients between each PFT.

Vegetation dynamics, disturbance and landscape heterogeneity are represented by simulating dynamical processes co-occurring on a number of replicate patches. The likelihood of fire events is based on the amount of litter and soil water. In addition, patch destroying events occur within each patch with a 1 per 300-year likelihood.

Here we use an updated version of LPJ-GUESS with recently implemented features for high latitude applications, including soil freezing and updated soil thermal calculations. The new scheme applies 15 soil layers and up to 5 snow layers with dynamic thicknesses. Previous versions of the model used two soil layers and one snow layer. The soil thermal diffusion is solved using a Crank-Nicholson scheme, which greatly improves soil temperature calculations and enables simulations of permafrost. Furthermore, the model has been updated to include the full nitrogen cycle. The nitrogen cycle has previously been implemented and tested in LPJ-GUESS (Smith et al., 2014; Wårlind et al., 2014) but has not been applied in combination with RCA4 for the Arctic domain up until this point. Modelled processes include nitrogen limitations on primary productivity. Furthermore, turnover and dynamics of soil organic matter (SOM) is represented by a CENTURY-based soil model with 11 pools.

We extend the set of modelled PFTs in RCA-GUESS to include six shrub PFTs in our study (Gustafson et al., 2021). One evergreen and one deciduous shrub PFT is incorporated in each of the height classes tall (up to 2m), low (up to 0.5m) and prostrate dwarf (up to 0.2m) shrubs. For a full list of PFTs included in this study, see Table S.1 below.

Regional atmospheric model – RCA4

The Rossby Center Regional Atmospheric Model (Samuelsson et al., 2015), RCA4, is a generally applicable RCM capable of simulating atmospheric processes and land processes. It has been extensively used for regional climate downscaling over both the Arctic, Europe, and Tropical domains. RCA includes a tiled land surface scheme including one forest tile, one open-land tile and a snow-covered tile. The snow-covered tile is dynamically changing depending on snow conditions. The open land tile represents low-stature vegetation such as grasslands, pastures and tundra. The landcover is dynamically updated every simulation year during the simulation. The open land tile may never be smaller than 10% of the grid cell. The forested tile is further divided into broadleaved and needle-leaved fractions. LAI is used to calculate surface resistances for evapotranspiration, interception and aerodynamic processes. In its stand-alone version, RCA4 is supplied with these variables from ECOCLIMAP (Masson et al., 2003) with a monthly seasonality, but do not develop over time in a standard RCA4 simulation (Samuelsson et al., 2015).

Spin-up procedure

RCA-GUESS was spun up in two stages. In the first stage, the two models were spun up separately using their own forcing. LPJ-GUESS requires a longer spin-up than RCA and was forced with CRU-NCEP (Viovy, 2018). We repeatedly use the first 30 years of data to spinup the model for 500 years before the first common simulation year (1979). RCA was forced with ERA-Interim at the boundaries. After the separate spin-up legs, the two models were run together in the coupled mode for 30 years to be allowed to equilibrate. The climate output from this period was first detrended and then saved.

In the second spin-up stage, the detrended RCA climate was used to spin up LPJ-GUESS again, and the vegetation was then assumed to be in equilibrium with the RCA spin-up climate. After the second spin-up stage, RCA-GUESS was run in coupled mode with a transient climate from 1979-2013.

Table S.1 Plant functional types (PFTs) included in the study and their respective model species

PFT	Typical species
BNE	*Picea abies*
Boreal needle-leaved evergreen tree	
BINE	*Pinus sylvestris*
Boreal needle-leaved shade-intolerant evergreen tree	
IBS	*Betula pubescens ssp. czerepanovii, Alnus glutinosa, Sorbus aucuparia, Populus tremula*
Boreal shade-intolerant broad-leaved summergreen tree	
HSS	*Salix spp.*
Tall summergreen shrub	
HSE	*Juniperus communis*
Tall evergreen shrub	
LSS	*Vaccinium myrtillus, Salix hastata*
Low summergreen shrub	
LSE	*Empetrum nigrum, Cassiope tetragona*
Low evergreen shrub	
SPDS	*Salix Polaris*
Prostrate summergreen dwarf shrub	
EPDS	*Arctostaphylos uva-ursi*
Prostrate evergreen dwarf shrub	
GRS	Gramineae
Boreal C3 graminoids	
CLM	Cushion-forming *Caryopyhyllaceae* and *Saxifragacea*, lichens, mosses
Cushion-forb-lichen-moss-tunda	

References

Gustafson, A., Miller, P. A., Björk, R. G., Olin, S., and Smith, B.: Nitrogen restricts future sub-arctic treeline advance in an individual-based dynamic vegetation model, Biogeosciences, 18, 6329-6347, 10.5194/bg-18-6329-2021, 2021.
Masson, V., Champeaux, J.-L., Chauvin, F., Meriguet, C., and Lacaze, R.: A Global Database of Land Surface Parameters at 1-km Resolution in Meteorological and Climate Models, Journal of Climate, 16, 1261-1282, 10.1175/1520-0442(2003)16<1261:Agdols>2.0.Co;2, 2003.
Samuelsson, P., Gollvik, S., Kupiainen, M., Kourzeneva, E., and van de Berg, W. J.: The surface processes of the Rossby Centre regional atmospheric climate model (RCA4), SMHI0283-7730 ; 157, 2015.
Smith, B., Prentice, I. C., and Sykes, M. T.: Representation of vegetation dynamics in the modelling of terrestrial ecosystems: comparing two contrasting approaches within European climate space, Global Ecology and Biogeography, 10, 621-637, 10.1046/j.1466-822X.2001.t01-1-00256.x, 2001.
Smith, B., Wårlind, D., Arneth, A., Hickler, T., Leadley, P., Siltberg, J., and Zaehle, S.: Implications of incorporating N cycling and N limitations on primary production in an individual-based dynamic vegetation model, Biogeosciences, 11, 2027-2054, 10.5194/bg-11-2027-2014, 2014.
Viovy, N.: CRUNCEP Version 7 - Atmospheric Forcing Data for the Community Land Model, Research Data Archive at the National Center for Atmospheric Research, Computational and Information Systems Laboratory [dataset], 10.5065/PZ8F-F017, 2018.
Wårlind, D., Smith, B., Hickler, T., and Arneth, A.: Nitrogen feedbacks increase future terrestrial ecosystem carbon uptake in an individual-based dynamic vegetation model, Biogeosciences, 11, 6131-6146, 10.5194/bg-11-6131-2014, 2014.

Supplementary material S2

Additional figures for 'The contribution of shrubs to Arctic land surface feedbacks'

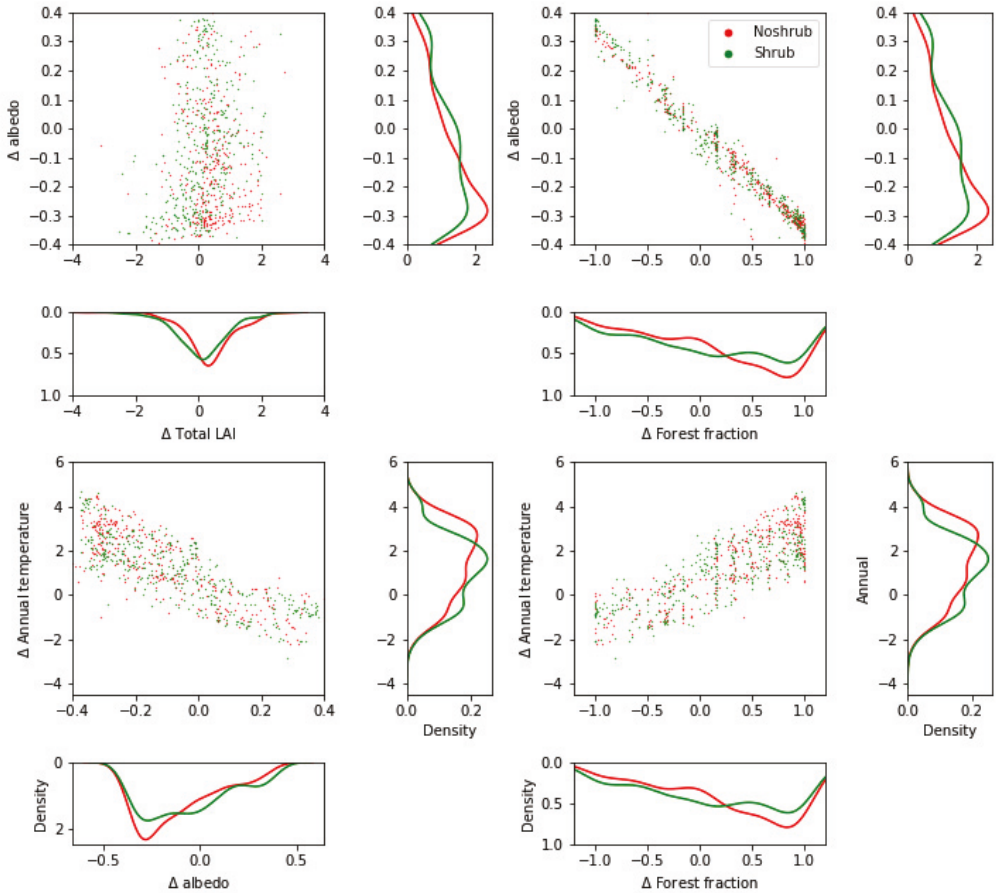

Fig S2.1. Change in albedo and annual 2m air temperature correlations with change in LAI and forest fraction. Distributions on the bottom and right side of each scatterplot are kernel density estimates of the data.

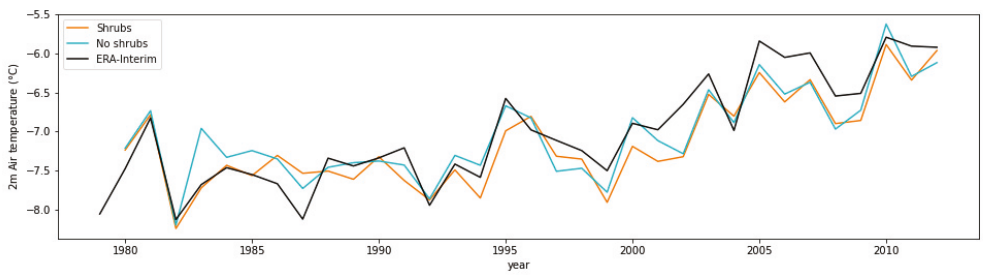

Fig S2.2. Temporal development of 2m air temperature as simulated by RCA-GUESS with and without shrubs included and comparison to ERA-Interim temperatures.

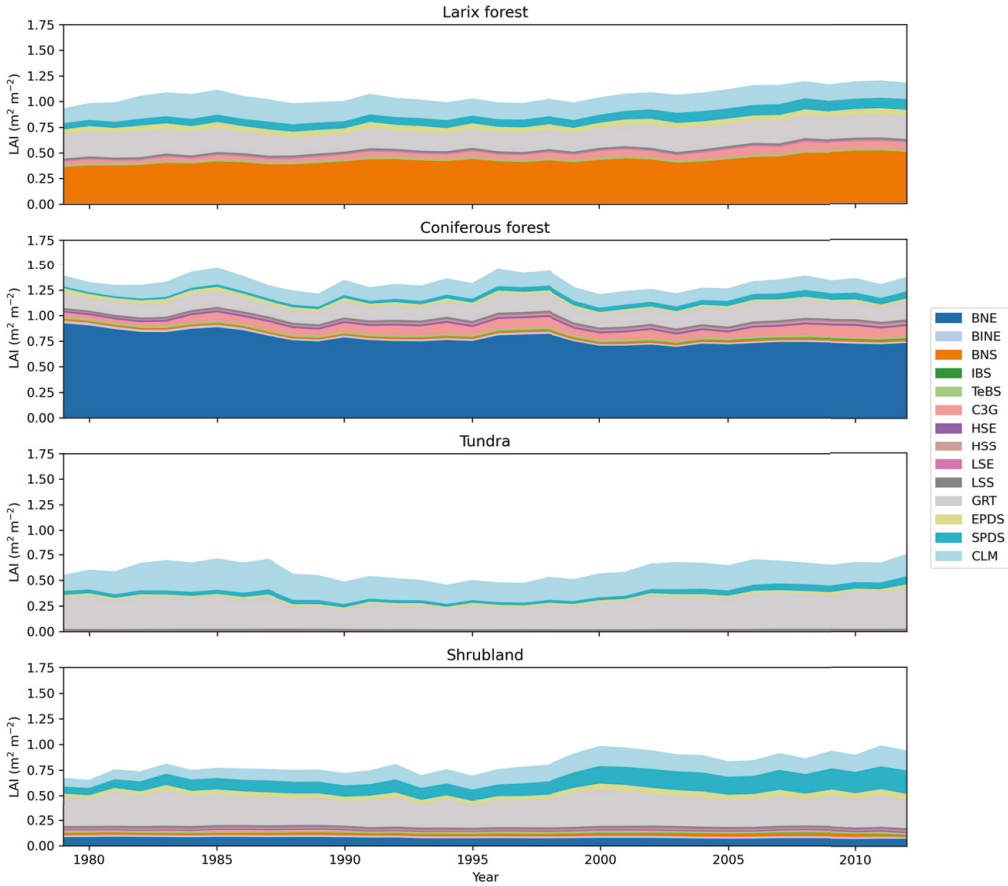

Fig. S2.3. Leaf area index (LAI) development for each landcover class. Full PFT names and model species can be found in Table S1.1 Values are averages of grid cells representative for each landcover class presented in Fig S2.4.

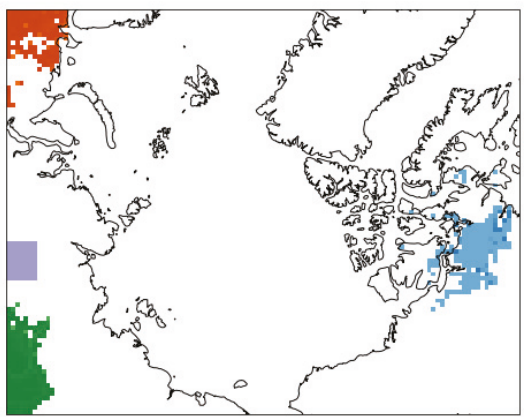

Fig S2.4. Areas representative of the presented landcover classes. Red color represent coniferous forest, green color *Larix* forest, blue color shrubland and purple color tundra.

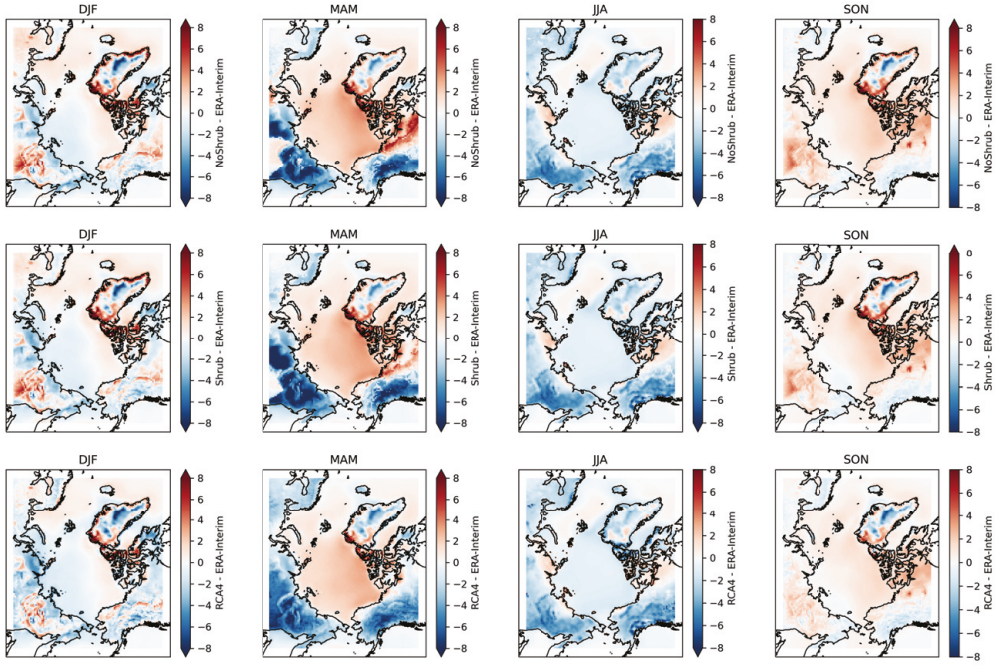

Fig S2.5. 2m air temperature bias from simulated climate compared to ERA-Interim for RCA-GUESS without (top row) and with (middle row) shrubs included as well as standalone RCA4 (bottom row). Standalone RCA4 has prescribed land surface parameters received from ECOCLIMAP.

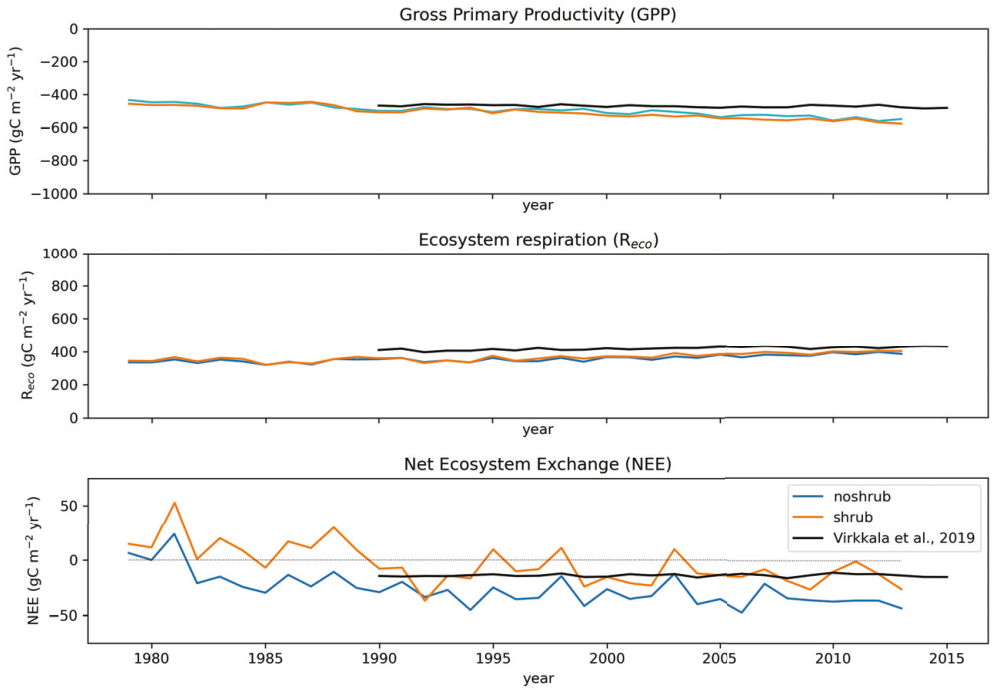

Fig S2.6. Regionally averaged CO2 fluxes for the two simulations, with and without shrubs as well as the upscaled flux data from Virkkala et al., 2019.

Paper III

High latitude terrestrial ecosystems' contribution to global warming – will the Arctic be a sink or source of greenhouse gases in the 21st century?

Adrian Gustafson[1,2], Stefan Olin[1], Anders Ahlström[1], Alexandra Pongrácz[1], Lars Niederazik[1], Jing Tang[1], Benjamin Smith[1,3], Paul A. Miller[1,2]

[1]Department of Physical Geography and Ecosystem Science, Lund University, Sölvegatan 12, 223 62 Lund, Sweden
[2]Center of Environmental and Climate Science, Lund University, Sölvegatan 37, 223 62 Lund, Sweden
[3]Hawkesbury Institute for the Environment, Western Sydney University, Penrith, NSW 2751, Australia

Correspondence to: Adrian Gustafson (adrian.gustafson@nateko.lu.se)

Abstract. The high latitudes are experiencing rapid climate warming with consequences for biogeochemical cycling and the greenhouse gas budget. We used the dynamic vegetation model LPJ-GUESS under a range of climate change scenarios and Genereal Circulation Models (GCMs) with different climate sensitivities to explore the impacts climate warming and the robustness of this signal. The model simulated fluxes of CO_2, CH_4 and N_2O as well as vegetation dynamics under these scenarios and we subsequently calculated the global warming potential over a 100-year window (GWP_{100}). Simulated fluxes were robust under future environmental change and more dependent on scenarios than in previous studies, where the choice of GCM has played a larger role. The region was consistently a sink of CO_2, which was also the strongest contributor to the GWP_{100}. Both the coldest and the warmest scenarios had the highest – but still negative – GWP_{100} at the end of the century compared to the more intermediately warmed scenarios. For the cold scenarios, this was driven by a weaker sink strength, while for the warmest scenarios the ecosystem respiration and non-CO_2 greenhouse gases became more important. Vegetation dynamics played a crucial role in the greenhouse gas fluxes with the boreal forests as drivers for both future carbon sequestration and N_2O emissions. Tundra productivity was underestimated and so its potential climate sink may also have been underestimated. Substantial uncertainties remain regarding losses of CO_2 to the atmosphere and the degree of permafrost carbon N_2O emissions. With better data and empirical knowledge regarding the environmental controls on these processes, model estimates of the contribution of high latitude ecosystems to global warming will be more reliable.

1 Introduction

Temperatures in the high latitudes are rising twice, or even three times, as fast as the global average (AMAP, 2021; IPCC, 2014), a phenomenon termed Arctic amplification. Warming will affect ecosystems and the physical environment in which plants and other living organisms grow. During recent decades satellites have recorded increases in vegetation greenness (Bhatt et al., 2017; Bhatt et al., 2010; Epstein et al., 2012; Forbes et al., 2010) which has been related to increasing temperatures, longer growing seasons, and decreasing sea ice cover. The greening has also been linked to an increasing abundance and stature of Arctic vegetation (Bjorkman et al., 2018), most notably among shrubs (Elmendorf et al., 2012; Myers-Smith et al., 2015). Furthermore, latitudinal treelines are expected to shift northwards. Studies of latitudinal treelines have shown advancing

behaviour in approximately half of the observations (Rees et al., 2020), which is similar to findings from studies of global altitudinal treelines (Harsch et al., 2009). Large-scale treeline advances have also been documented using satellite observations (Berner & Goetz, 2022; Rees et al., 2020) and are expected in the future (Mamet et al., 2019; Rees et al., 2020).

Vegetation shifts will impact ecosystem functioning with implications for biogeochemical cycling. Warmer temperatures, longer growing seasons, and increased atmospheric CO_2 are all expected to increase photosynthetic carbon assimilation by plants (Dusenge et al., 2019; Fernández-Martínez et al., 2018). Warming may also induce higher rates of nutrient cycling, which is of importance as Arctic woody vegetation is often nitrogen-limited (Gustafson et al., 2021; Martin et al., 2022; Mekonnen et al., 2021; Mekonnen et al., 2018). On the other hand, warming-induced mineralisation of soil organic matter will increase carbon losses from soils (Crowther et al., 2016). Permafrost soils are of particular importance as they contain vast amounts of carbon (Hugelius et al., 2014) and are likely to degrade and mobilise otherwise frozen carbon (Schuur et al., 2015) if warming continues. Furthermore, carbon may be released from the region's terrestrial ecosystems by increasing wildfire frequency and intensity (Bruhwiler et al., 2021) in response to warming. Loss of carbon has also been observed as tundra is converted to forest ecosystems (Hartley et al., 2012), although the magnitude and spatial extent of this loss are highly uncertain. Concerns that the Arctic will turn from a sink to a source of carbon have been raised and have sometimes been observed (Belshe et al., 2013). Current estimates of the Arctic CO_2 exchange indicate that the region is close to equilibrium, but there remains disagreement between process models, inversion models, and upscaling datasets (Bruhwiler et al., 2021; McGuire et al., 2012).

The region's soils may also become an important source of the potent greenhouse gas nitrous oxide, N_2O, as temperatures warm (Voigt et al., 2020). N_2O is formed through different microbial pathways in both upland and wetland soils (Pilegaard, 2013; Voigt et al., 2020). Warmer temperatures may induce higher rates of nitrogen mineralisation (Nadelhoffer et al., 1991), which is the primary source for denitrification and N_2O-forming microbial processes.

Approximately 8.6% of the terrestrial area north of 60°N is comprised of peatlands (Xu et al., 2018), which is a disproportionally large area compared to the globe as a whole. This also makes the high latitudes an important region for natural methane emissions (Saunois et al., 2020; Stavert et al., 2022). Northern high latitude peatlands are currently estimated to release 9 [2-18] TgCH4 yr^{-1} and 13 [7-16] TgCH4 yr^{-1} by process models and inversion models, respectively (Saunois et al., 2020). Methane is formed in anoxic environments, which arise in water-logged soils (Bridgham et al., 2013). The water-logged conditions furthermore prevent the decomposition of organic material, making it a carbon store. Future dry-up and increased temperature may however mobilise the stored carbon, although other estimates show an increased carbon accumulation. Simulations using process-based models have indicated that peatlands may remain a sink of CO_2 in a strong climate mitigation scenario while turning to a source in scenarios with high rates of greenhouse gas emissions (Qiu et al., 2022).

Future temperature trends are uncertain in the high latitudes, with multi-model estimates from the sixth phase of the Coupled Model Intercomparison Project, CMIP6 (Eyring et al., 2016), ranging from 0.34°C $decade^{-1}$ to

0.99°C decade^{-1} for SSP1-2.6 and SSP5-8.5 respectively during the 21st century (Cai et al., 2021). Different trajectories of climate adaptation and mitigation efforts may also play a role in both emission trends of CO_2 (Meinshausen et al., 2020) and nitrogen deposition, which further enhances the uncertainty of ecosystem responses in the northern high latitudes to these perturbations.

Global temperature change is proportional to the cumulative emissions of CO_2 in the atmosphere (IPCC, 2021; Matthews et al., 2009). Large effluxes of greenhouse gases from the Arctic may consequently have implications for the global carbon budget and climate change. Whether the Arctic is a sink or a source of greenhouse gases in the future is thus of vital importance for mitigation and adaptation efforts as the response of the region's natural ecosystems may either expand or shrink the budget space for reaching global climate goals such as the Paris agreement.

Dynamic vegetation models (DVMs) are designed to simulate ecosystem processes and estimate changes in biogeochemical cycling. They are thus excellent – and the only – tools for investigating the complex and interacting factors controlling greenhouse gas emissions in the changing Arctic.

In this study, we use a contemporary DVM with newly implemented Arctic features and drive it with a set of CMIP6 scenarios in order to determine the trajectories of ecosystem response in the region in the 21st century generally, and specifically to answer the following research questions:

i. Will the Arctic be a sink or a source of greenhouse gases in the future?
ii. Under what scenarios or conditions might the Arctic turn from a sink to a source of GHGs?
iii. How robust are these patterns between different scenarios of environmental change?
iv. How do vegetation dynamics and treeline migration influence these changes?

2 Methods

2.1 LPJ-GUESS

The Lund-Potsdam-Jena General Ecosystem Simulator (LPJ-GUESS) is a contemporary dynamic vegetation model (Smith et al., 2001; Smith et al., 2014) capable of simulating global and regional vegetation and biogeochemical dynamics (See Supplementary material S1 for a thorough description). The model simulates fluxes of carbon, nitrogen and water in response to a dynamic set of climatic and environmental conditions. Vegetation structure is the emergent outcome of the environmental drivers and competition among a set of plant functional types (PFTs) for light, water and nutrients.

In this study, we study the development of high-latitude vegetation and greenhouse gas fluxes over the 21st century using LPJ-GUESS v4.1 with newly implemented Arctic features as well as an updated nitrogen scheme and the SimFIRE-BLAZE fire model (Knorr et al., 2014; Pellegrini et al., 2018; Rabin et al., 2017). The Arctic updates include improved soil physics and a multi-layer snow scheme, enabling soil freezing and simulation of permafrost. Moreover, for peatland fractions of each gridcell, wetland features adapted from Wania et al. (2009a) and subsequent updates (Wania et al., 2009b, 2010) have been added, including wetland-specific moss and

graminoid PFTs, and climate-sensitive methane fluxes from diffusion, plant-mediated and ebullition pathways. The PFT set used for upland (non-peatland) gridcell fractions include boreal tree PFTs and high-latitude tundra PFTs following Wolf et al. (2007), and an updated set of shrub PFTs (Gustafson et al., 2021), which represents tall, low and prostrate shrub physiognomies with either evergreen or deciduous phenology (Table S2.1; Supplementary material). The updated nitrogen scheme is adapted from Xu and Prentice (2008) to simulate transformations of different N species and their release into the atmosphere. The updated fire model is capable of dynamically simulating fire probabilities from different weather conditions, and when a fire occurs, the biomass and litter combustion, fire-line intensity and vegetation mortality caused by fire is simulated.

2.2 Model evaluation

We evaluate the model against several available datasets. Carbon fluxes are evaluated against statistical- and machine-learning upscaled eddy covariance and flux data by Virkkala et al. (2021). This dataset contains annual fluxes of gross primary productivity (GPP), ecosystem respiration (R_{eco}), and net ecosystem exchange (NEE) between the years 1990-2015. We also compare simulated GPP to the GOSIF product (Li & Xiao, 2019), which provides global annual GPP values inferred from satellite-derived solar-induced chlorophyll fluorescence. Aboveground biomass estimated from satellite observed vegetation optical depth (VOD) between the years 1982-2015 (Liu et al., 2015) was used to evaluate simulated vegetation biomass carbon for our domain. Fluxes of CH_4 were evaluated against a monthly gridded data product based on upscaled eddy-covariance fluxes between the years 2013 and 2014 and regionally estimated numbers from the global methane budget (Saunois et al., 2020). The latter contains both estimates from process models and inversion models. Estimates of N_2O emissions from the high latitudes are currently lacking, however, we compare our regionally summed values to the estimates provided by Voigt et al. (2020) who provide estimates for permafrost soils.

2.3 Simulation protocol

Three Global Climate Models (GCMs) from the Coupled Model Intercomparison Project phase 6 (CMIP6, Eyring et al., 2016) were selected to provide forcing data for LPJ-GUESS. The GCMs were selected to represent a large spread within the 1.5-4.5 K likely range of Equilibrium Climate Sensitivity (ECS) (Nijsse et al., 2020; Tokarska et al., 2020). These include one high (EC-Earth3-Veg), one average (MRI-ESM2-0), and one low (NorESM2-LM) sensitivity GCM. Furthermore, we selected model outputs from GCM simulations following four Shared Socioeconomic Pathways (SSPs) from CMIP6 ScenarioMIP (O'Neill et al., 2016). These included SSP1-2.6, SSP2-4.5, SSP3-7.0, and SSP5-8.5. For the historical period (1901-2015), we also forced the model with CRU-NCEP (Viovy, 2018) for evaluation purposes

Daily GCM output was downloaded from the Earth System Grid Federation (ESGF) database and re-gridded to the 0.5° spatial resolution standard for LPJ-GUESS using the Climate Data Operators tool (Schulzweida, 2021). Variables downloaded for each GCM included minimum, mean and maximum surface air temperature, total precipitation, net incoming shortwave radiation, surface wind speed, and relative humidity. In case relative humidity was unavailable, specific humidity, surface pressure, and orography data were downloaded and used to calculate relative humidity according to Monteith and Unsworth (2013). All climate variables were subsequently bias-adjusted for the period 1901-2100 against the Watch Forcing Data applied to ERA-Interim (WFDEI,

Weedon et al., 2014) using the Inter-Sectoral Impact Model Intercomparison Project (ISIMIP) approach (Lange, 2019) and provided Python scripts (Lange, 2021). Additional input variables to LPJ-GUESS included soil texture (Batjes, 2005), and annual [CO_2], and monthly nitrogen deposition from the CMIP6 input4MIPs datasets for each scenario. Lastly, the peatland fraction of each grid cell was extracted from the PEATMAP product (Xu et al., 2018).

2.4 Global warming potential

To compare the climate effect of the total GHG emissions we calculated global warming potential over a 100-year window (GWP_{100}). The yearly net emissions of CO_2, CH_4, and N_2O were summed over a high-latitude domain consisting of all land points north of 60N (see Fig 1). The climate effect of each gas was then converted to CO_2eq by multiplying CH_4 by 27 and N_2O by 273 following the updated values in the IPCC Sixth Assessment Report (Forster et al., 2021). CO_2, by definition, has a multiplier of 1 for conversion to CO_2eq. The GWP_{100} values are reported as Gt CO_2eq.

2.5 Vegetation indices and classification

We distinguish between tundra and forests in our analysis. Gridcells with a tree fractional projective cover (FPC) of at least 30% were classified as forests. The FPC is based on LAI, and so gridcells with less than 30% Tree FPC were considered to have either no trees or trees with stunted growth and vegetation more resembling tundra vegetation.

To compare the vegetation structure between simulations spanning GCMs (i.e. ECS) and scenarios, we calculate the relative abundance of evergreens vs. deciduous PFTs and woody vs. herbaceous PFTs using the Normalised Phenology Index (NPI) and Normalised Physiognomy index. These indexes are calculated as:

$$NPI = \frac{CM_{eg} - CM_{decid}}{CM_{eg} + CM_{decid}}$$

where CM_{eq} and CM_{decid} is the summed biomass carbon of evergreen and deciduous PFTs, respectively. NPI ranges between -1 (for fully deciduous ecosystems) and +1 (for fully evergreen ecosystems). Similarly, the NPMI is calculated using the relative abundance of woody vegetation biomass carbon (CM_{woody}) to herbaceous (CM_{herb}):

$$NPMI = \frac{CM_{woody} - CM_{herb}}{CM_{woody} + CM_{herb}}$$

NPMI ranges between -1 (for fully herbaceous ecosystems) and +1 (for fully woody ecosystems).

3. Results

3.1 Vegetation change

Our simulations reveal that climate change will result in substantial changes to vegetation distribution and biomass, depending on the scenario and GCM.

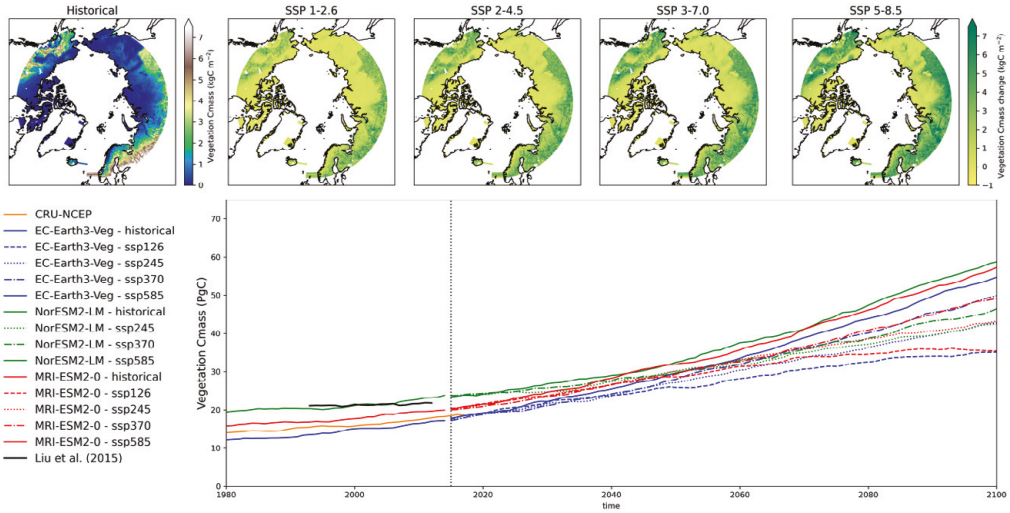

Fig 1 Simulated vegetation biomass carbon. The top row represents the spatial distribution of the multi-model averaged biomass carbon density for the historical (2001-2010) period and the end of the century (2091-2100) for the respective scenarios. The historical map displays absolute values of vegetation carbon density while the respective scenario displays the change from this value. The bottom row displays the temporal evolution of total biomass carbon for the simulated domain for each GCM and scenario as well as VOD-based aboveground biomass carbon estimates (Liu et al., 2015)

Vegetation biomass carbon was somewhat variable between GCMs with the highest amount of biomass carbon in the GCM with the lowest climate sensitivity (NorESM2-LM; Fig 1). This GCM was well within the range of remotely sensed vegetation optical depth (VOD) based biomass estimates. There was thus a low-bias of simulated biomass in our results. Outputs from runs forced with the other two GCMs, as well as CRU-NCEP, showed underestimations of biomass carbon for recent decades, with the GCM with the highest climate sensitivity (EC-Earth3-Veg) showing the lowest amount of biomass carbon. During the projection period, the biomass carbon developed towards being more robust between SSPs rather than GCMs. The biomass carbon change was thus scenario dependent with SSP1-2.6 showing the lowest amount of biomass carbon increase and SSP5-8.5 the highest. Biomass carbon increases were mainly driven by changes seen in the boreal forests, which became denser rather than showing considerable treeline advance (Fig S2.1; Supplementary materials).

The three GCMs showed surprising similarities in vegetation structure and distribution, despite their differences in climate sensitivities and the changes were largest between SSPs rather than GCMs at the end of the century (Fig. S2.2; Supplementary materials). The model simulated tundra vegetation with a relative abundance of herbaceous and deciduous vegetation over the tundra (Fig 2) during the historic period 2001-2010. The forests over Scandinavia and western Russia as well as eastern Canada were comprised of evergreen forests. The southern latitudes in Siberia showed a needleaved deciduous forest, mostly comprised of the PFT BNS, representing *Larix* species. During the projection period, woody vegetation increased over most of the tundra with the strongest changes over western Siberia and Canada. The strongest shifts from herbaceous to woody vegetation were also

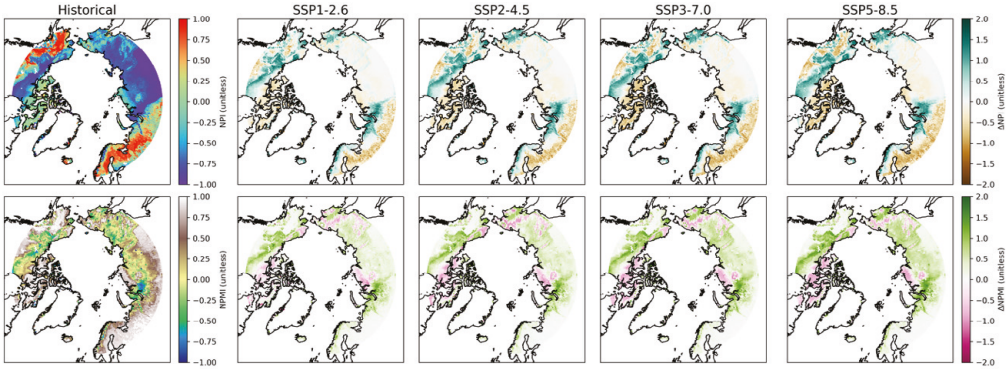

Fig 2 Multi-model means for the normalised phenology index (NPI; top row) and the normalised physiognomy index (NPMI; bottom row) for the historical period (2001-2010) and projected (2091-2100) for each scenario. Historical maps display absolute values while scenario maps display the projected difference to this value for each respective scenario. The NPI indicated the relative abundance of deciduous to evergreen vegetation. The index ranges from -1 for fully deciduous ecosystems to +1 for fully evergreen systems. Similarly, the NPMI indicates the relative abundance of herbaceous to woody vegetation with -1 indicating fully herbaceous vegetation and +1 indicating fully woody vegetation.

spatially linked to a shift from deciduous to evergreen PFTs, mainly driven by an increased abundance of boreal needleaved evergreen PFTs (BNE and BINE). The shift from evergreen to deciduous forests in the more southern latitudes was mainly driven by an increased abundance of boreal broadleaved deciduous species such as the IBS PFT, representing, e.g. *Betula* species, at the expense of boreal needleaved evergreen PFTs (Fig 2).

3.2 CO_2 fluxes

The simulations indicated that the tundra had a close to neutral carbon balance from 1850 to approximately 1980 when it turned into a sink of CO_2 (Fig 3). The boreal forests on the other hand acted as a sink during the same period, but like the tundra, became a stronger sink after 1980. During the projected period, the forests continued to act as a sink of CO_2 but stabilised towards the end of the century in all scenarios except for MRI-ESM2-0 under SSP5-8.5 and SSP3-7.0. Tundra on the other hand stabilised during the beginning of the century, and after the mid-century, the trend turned towards neutral carbon balance, and without fully becoming a source of CO_2 to the atmosphere. This made the forest ecosystems drivers of the carbon sink during the projected period in all scenarios.

Seasonal fluxes displayed a greater amplitude in the projection simulations compared to the historical simulations. Despite warming, the carbon balance did not turn to net uptake earlier in spring, likely as a result of limiting light. During autumn, the month when the ecosystems turned to a net release of carbon was on the other hand highly variable between scenarios, with almost a month differing between the earliest and the latest scenario on the tundra. The seasonal patterns are however surprisingly robust between GCMs and scenarios except for MRI-ESM2-0 which dominates the seasonal uptake in all scenarios except SSP1-2.6.

The domain-averaged fluxes of gross primary productivity were underestimated compared to both upscaled fluxes and satellite inferred productivity (Fig S2.3; Supplementary materials). R_{eco} was similarly underestimated,

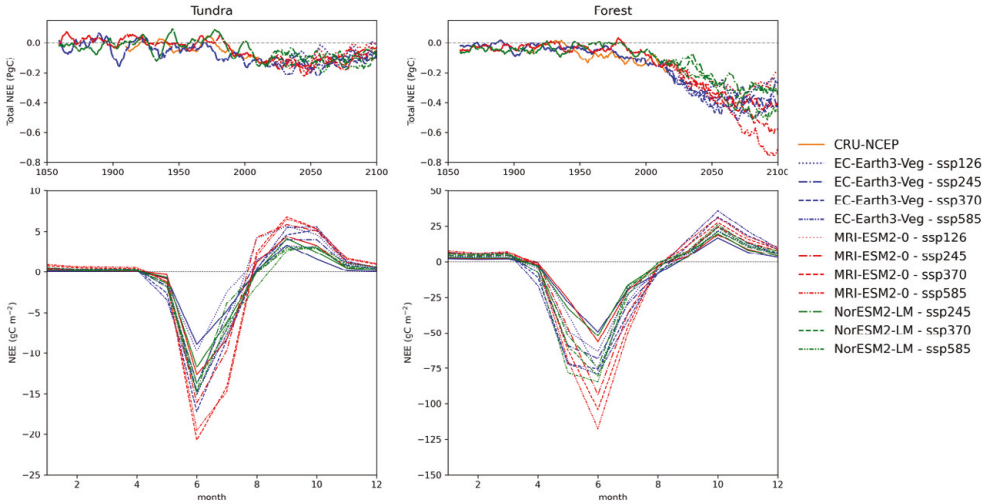

Fig 3 Simulated annual (top row) and seasonal (bottom row) net ecosystem exchange (NEE) for the tundra (left column) and forest (right column) respectively. Top row displays total summed NEE for our domain separated by tundra and forest ecosystems. Bottom row displays the seasonal NEE for each simulated scenario at the end of the century (2091-2100). Note the difference in scale in panels on the bottom row, displaying seasonal carbon fluxes of the forest and tundra.

resulting in a NEE that was well within the range of estimated values by Virkkala et al. (2021), both regarding magnitude and variation. The fluxes were robust between GCMs. The spatial comparison however revealed a low bias of GPP over the tundra, especially in the high-Arctic towards the Arctic Ocean, and a slight overestimation of boreal forest GPP over Western Russia and Canada.

3.3 CH_4 emissions

The model estimated present-day (2010-2014) CH_4 emissions of 11-14 Tg CH_4 yr^{-1} (Table 1), which is comparable to other estimates by inversion models of 13 [7-16] $TgCH_4$ yr^{-1} and process models of 9 [2-18] $TgCH_4$ yr-1 (Saunois et al., 2020). The model however simulated significantly lower annual CH_4 emissions compared to the upscaled estimates by Peltola et al. (2019). CH_4 emissions peak during the summertime and the lowest fluxes occured during the winter, although winter fluxes were much higher in the upscaled dataset compared to the modelled fluxes (Table 1; Fig S2.4). Modelled wintertime fluxes were close to zero, whereas Peltola et al. (2019) emissions are approximately 65% of the MAM emissions (4% in LPJ-GUESS). This indicated that LPJ-GUESS – like several other process-based models - underestimated cold-season methane fluxes.

As revealed by Fig. 4, the high ECS GCM (EC-Earth3-Veg) simulated the lowest historical but highest scenario emissions of CH_4. Under SSP1-2.6 and SSP2-4.5 there was a decrease in emissions from mid-century to 2100. Although all scenarios display increased CH_4 emissions compared to the present-day fluxes, the magnitude of the emissions were dependent on the SSP rather than GCM.

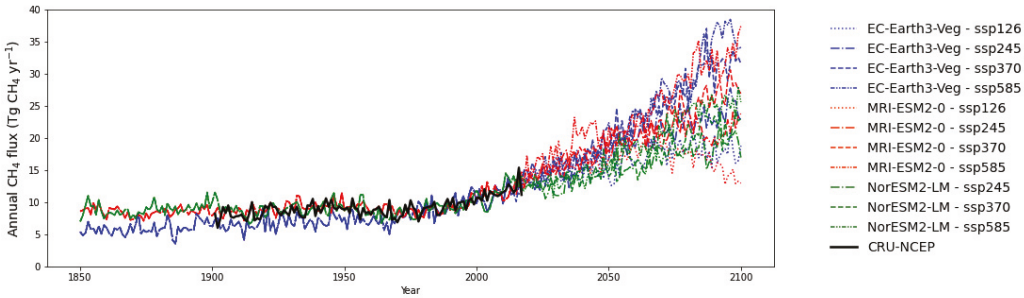

Fig 4 Simulated emissions of CH_4 from 1850-2100 for all GCMs and scenarios, including CRU-NCEP. Values are summed up for all fluxes over our simulation domain.

3.3.1 Vegetation effects on CH_4 fluxes

CH_4 fluxes were significantly affected not only by soil temperature but also by water table depth (WTD) and the dominant vegetation type as well (Fig S2.5; Supplementary materials). Lower soil temperature and drier conditions (WTD) yielded lower CH_4 emissions, whereas higher soil temperature and soil water saturation result in higher CH_4 emissions. Modelled CH_4 fluxes were more sensitive to surface temperature changes when the flood-tolerant graminoid PFT WetGRS were abundant. Graminoids were prevalent in areas with continuous or seasonal saturation of the peatlands. Furthermore, the gramonoid peatland PFTs support plant mediated CH_4 emissions through their aerenchyma, which together with the wetter and warmer conditions explained the significantly higher CH_4 emissions at sites with a large presence of graminoids.

Table 1. Model-data comparison of seasonal CH4 emissions. Seasonal and annual fluxes of LPJ-GUESS simulated CH_4-fluxes compared to eddy-covariance upscaling data (Peltola et al., 2019) and regional CH_4 budget estimations from inversion models (Saunois et al., 2020).

Historical CH4 emissions						
		Cumulative seasonal emissions $TgCH_4$ $season^{-1}$				Total annual emissions $TgCH_4$ yr^{-1}
		DJF	MAM	JJA	SON	
	Peltola et al., 2019 (mean 2013-2014)	1.72	2.52	12.37	5.55	22.15
	Saunois et al., 2020 Natural wetlands, 60°- 90°	-	-	-	-	9-13
LPJ-GUESS with GCM (mean 2010-2014)	EC-Earth3-Veg	0.04	0.98	7.78	2.88	11.68
	MRI-ESM2-0	0.06	0.71	7.37	3.09	11.23
	NorESM2-LM	0.04	1.12	9.45	2.91	13.52

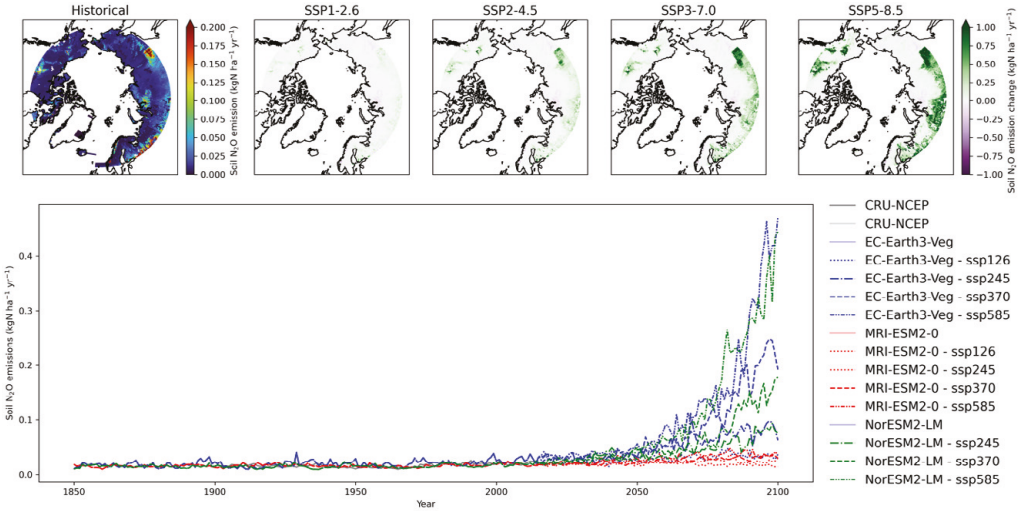

Fig 5 Simulated annual fluxes of N_2O by LPJ-GUESS. Top row displays the spatial extent of the simulations for the historical (2001-2010) and end of the century (2091-2100) for each scenario. The map over historical emissions displays absolute multi-model averages while scenario maps display the multi-model difference against the historical values. The lower panel displays a time series over emissions for each GCM and scenario.

3.4 N_2O emissions

The model simulated emissions of N_2O emissions between the years 2001 and 2010 with a magnitude of 0.038 ± 0.007, 0.029 ± 0.003 and 0.028 ± 0.005 Tg N_2O-N yr^{-1} for EC-Earth3-Veg, MRI-ESM2-0 and NorESM2-LM, respectively. The multi-model average was 0.03 ± 0.003 Tg N_2O-N yr^{-1}. N_2O emissions were in general robust between scenarios (Fig 5), however, the GCM MRI-ESM2-0 stood out with remarkably small changes in N_2O emissions in all projection scenarios. The lower latitude boreal forests and high latitude wetlands in our domain contributed most to the N_2O emissions during the recent decade (2001-2010) in the multi-model average. Changes in N_2O emissions were correlated with the degree of warming in the SSPs, except for MRI-ESM2-0. The largest contributor to the N_2O emissions increase were the boreal forests, both *Larix* forest and broadleaved deciduous forests (Fig. 2 and Fig 4). The increased N_2O emissions were driven by excess soil nitrogen as net mineralisation of SOM increased relatively faster than plant uptake of nitrogen (Fig S2.7; Supplementary material). Although a similar pattern of the nitrogen uptake to mineralisation ratio was observed at the tundra, this did not yield any significant increases in N_2O emissions as rates were still low. The high rates of mineralisation in the boreal forests in concert with the yielded excess nitrogen subsequently resulted in gaseous losses of soil N as N_2O.

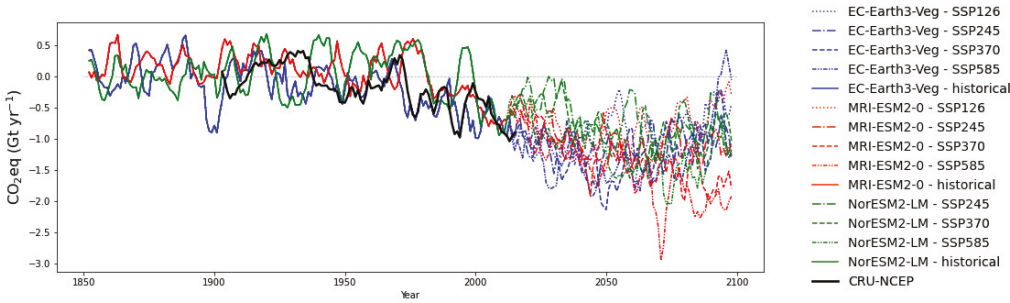

Fig 6 Simulated GWP_{100} between the years 1850-2100 for all GCMs and scenarios, including CRU-NCEP, summed over the simulation domain. Lines are 5-year rolling averages of the annual time series.

3.5 Global warming potential

The simulated GWP_{100} summed over the domain was neutral during the period 1850-1980 with some years having a net positive GWP_{100}, while other years had a net negative GWP_{100} (Fig 6). From the 1980s and onward the domain turned into a sink as temperatures showed stronger warming, this pattern was robust across all three GCMs and CRU-NCEP. Between the years 2001-2010 the Arctic was a clear sink of -0.97 ± 0.55, -0.99 ± 0.46, and -1.00 ± 0.56 Gt CO_2eq for EC-Earth3-Veg, MRI-ESM2-0, and NorESM2-LM, respectively (Fig. 7). Corresponding values for the CRU-NCEP forced run was -0.88 ± 0.39 Gt CO_2eq. The sink continued throughout the 21st century but stabilised by mid-century with the SSP1-2.6 scenarios breaking the trend and annual GWP_{100} increased, while not turning positive (Fig 6).

The largest contributors to the GWP_{100} trends in all scenarios were the CO_2 fluxes (Fig 7). The strength of the CO_2-CO_2eq generally determined whether our domain had a positive or negative GWP_{100} and thus contributed to global climate warming or not. The projected GWP_{100} were generally larger in the SSP1-2.6 scenarios than in the stronger warming scenarios, although the GWP_{100} were also high in the two scenarios with the strongest warming (EC-Earth3-Veg-SSP3-7.0 and EC-Earth3-Veg-SSP5-8.5). In particular, the intermediate sensitive GCM MRI-ESM2-0 had the lowest GWP_{100} values between GCMs in all scenarios. CH_4 emissions were the second largest contributor to the net GWP_{100}. The CH_4-CO_2eq contribution was generally robust in magnitude and variance between SSPs and showed a slightly positive correlation with climate sensitivity. Lastly, the N_2O-CO_2eq varied most between GCMs with almost no contribution in MRI-ESM2-0, but a significant contribution in SSP5-8.5 for NorESM2-LM and EC-Earth3-Veg.

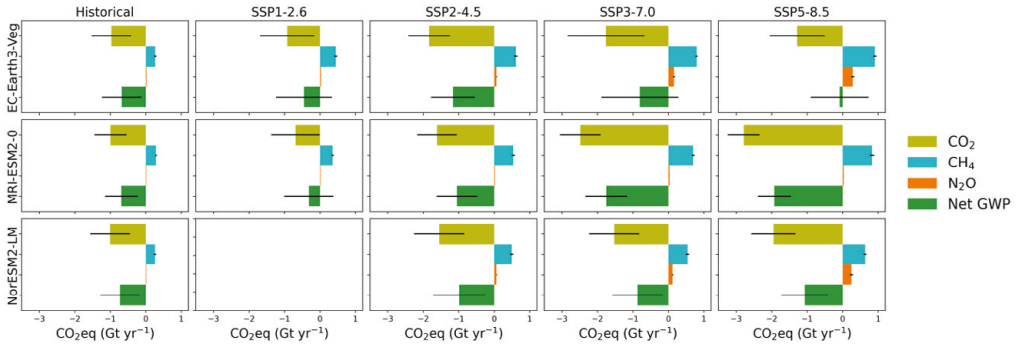

Fig 7 Contribution of each flux CO_2, CH_4 and N_2O to net GWP_{100} summed over the simulation domain at the end of the historical (2001-2010) and scenario (2091-2100) periods. Black bars represent ± 1 standard deviation of interannual variability.

4. Discussion

We simulated fluxes of greenhouse gases over the terrestrial land 60°N under three GCMs selected to represent one high, one middle and one low climate sensitivity GCM within the likely range of ECS under four SSPs. Our results show a robust climate-positive effect, despite emissions of both CH_4 and N_2O. The cooling effect of the Arctic greenhouse gas balance is robust between both climate sensitivity (GCMs) and projected environmental change (SSPs). The region will however be a source during some years, and with a higher frequency under either the SSP1-2.6 scenarios or strongest climate warming (EC-Earth3-Veg SSP3-7.0 and SSP5-8.5). The intermediately warmed scenarios yield the strongest cooling feedbacks to the global climate at the end of the century. As CO_2 is clearly the driver in our simulations, this is likely a result of a weaker uptake strength in the colder scenarios and a larger release in the warmer scenarios. GWP_{100} in the warmer scenarios is furthermore increased by the added non-CO_2 greenhouse gases, especially CH_4. This may contrast with expectations of Arctic ecosystems, and tundra becoming a source of carbon in the future (Belshe et al., 2013; Crowther et al., 2016). Our simulations, however, indicate that this might not be the case as uptake could still outweigh the release of greenhouse gases for the domain as a whole and under most years.

The vegetation stature did matter for the strength of the CO_2 sink, where the tundra and forest behaved differently. While both forest and tundra acted as CO_2 sinks, the forest was by far the strongest driver in the projected CO_2 sink. This sink also persisted longer in the projected estimates, where it stabilised only last half of the 21st century. Tundra on the other hand stabilised already after the year 2000 and had a slightly positive trend during the 21st century while remaining a net sink of CO_2 at the end of the century. The forest sink was driven both by treeline advancement, but a stronger sink was the densification of the forests below the treeline. This may make the future carbon sink more dependent on anthropogenic activities such as forestry in the boreal forests as these will likely become more important in the region when productivity increases. A full analysis of potential impacts of anthropogenic activities is however outside the scope of this study.

The impact of non-CO_2 forcings on GWP_{100} was also dependent on vegetation stature and composition. CH_4 fluxes were more temperature sensitive at sites with a higher abundance of flood-tolerant graminoids as these

plants mediated the CH_4 flux from deeper soil layers to the atmosphere. The emergence of the PFT representing these plants (WetGRS) is furthermore dependent on the WTP, which in turn is dependent on the hydroclimate. Although only briefly analysed in this study, the precipitation regime may be important for future CH_4 emissions as vegetation might shift from both temperature and precipitation change. The CH_4 emissions were scenario-dependent rather than dependent on the GCM. This is in line with results from a larger ensemble of process models simulating CH_4 and CO_2 emissions under one high and one low emission scenario (Qiu et al., 2022). Our analysis further shows that this is robust when the model is forced by a range of GCMs under CMIP6 and not just a range of scenarios.

Our N_2O emissions did not contribute largely to the total warming potential (GWP_{100}) from our region during the historic period. The model simulated emissions of N_2O emissions 0.03 ± 0.003 Tg N_2O-N between the years 2001-2010. This was lower than the first-order estimate reported by Voigt et al. (2020) of 0.07-0.63 Tg N_2O-N from permafrost-affected soils. Our newly implemented nitrogen cycling scheme is an initial attempt at modelling the transformation of nitrogen species globally and was not specifically designed for permafrost soils. It may as such lack processes important in cold areas, such as freeze-thaw cycles and wintertime emissions (Voigt et al., 2020). Furthermore, the partitioning between nitrogen species such as NO and N_2O is unknown (Pilegaard, 2013). High latitude regions are difficult to investigate due to the vast uninhabited areas and the long winter season. Data from ecosystem flux measurements of greenhouse gases are thus poorly constrained due to data scarcity. Our estimates however provide initial modelling estimates of emissions from high latitude soils and are, us knowingly, the first study to quantify both historic and future emissions of N_2O fluxes.

The N_2O emissions were more than ten times higher under SSP5-8.5 for NorESM2-LM and EC-Earth3-Veg compared to the historic emissions, pointing to the large potential for N_2O fluxes to become even more important in the future. This increase was dominated by additional release from the boreal forest soils. The large emissions were a result of larger net nitrogen mineralisation than was taken up by the vegetation, which subsequently led to substantial losses through N_2O emissions. The large emissions were however not apparent in the intermediate sensitivity GCM MRI-ESM2-0. Scenarios forced with this GCM also displayed the highest seasonal uptake of CO_2, but only intermediate losses during autumn, which could indicate that the demand for nitrogen within the model was higher. These results point to the importance of mobilised nitrogen for N_2O emissions. That N_2O emissions are dependent on the available nitrogen pool is known (Pilegaard, 2013; Voigt et al., 2020), however, that the excess nitrogen would occur in boreal forests – which traditionally are regarded as nitrogen limited – is more uncertain. Emerging evidence does however point to a large potential for boreal forests to release N_2O (Burnett et al., 2022), something which may make our projections more plausible.

Despite the large differences between SSPs, our simulations are surprisingly robust within each SSP. Biomass carbon density as well as CH_4 and N_2O emissions were more dependent on their SSP rather than the climate sensitivity of the GCM. This contrasts from similar studies (e.g., Ahlström et al., 2012) in which the GCM climate sensitivity was much larger. From Fig. 1 it is evident that the spread between GCMs was larger between GCMs during the historic period but converged around a narrower SSP mean at the end of the century. This may indicate that CMIP6 GCMs are more robust than previous iterations of the GCMs, or that other forcing, such as

nitrogen deposition and CO2 concentration, becomes more important during the projection simulations. Lastly, this study uses a more sophisticated bias-adjustment method (Lange, 2019), based on quantile mapping rather than delta change which was used by Ahlström et al. (2012). This may have yielded more similar climate forcing in our projections.

The simulated tundra region displayed a low bias in productivity which likely drove underestimations of the total GPP for the domain. The sink potential of the projections may thus have been underestimated. That DVMs underestimate productivity in high latitude ecosystems has been noted previously (Rogers et al., 2017), and attributed to a lower activation energy of the photosynthetic temperature response and higher investment in Rubisco in Arctic plants. Other causes may be the different microclimatic environment experienced by low-statured vegetation compared to trees. The lower GPP may also have contributed to the lower biomass carbon density than estimated by Liu et al. (2015), which in turn affects litter production and SOM build-up. Improving the underestimation of tundra productivity will be vital to more reliable predictions of greenhouse gas concentrations.

A recent improvement to the LPJ-GUESS snow-scheme highly improved winter soil temperatures, with implications for the winter SOM mineralisation and tundra carbon stocks (Pongracz et al., 2021). Such improvements could improve the robustness and reliability of carbon losses. Moreover, biotic interactions between plants and soil microbiota with apparently large implications for carbon losses have more recently taken place in the scientific discussion (Clemmensen et al., 2021; Keuper et al., 2020; Parker et al., 2018). Such processes are still not sufficiently well understood to be implemented in large-scale models. As knowledge matures, however, these processes will very likely be a part of projecting the effects of vegetation shifts on high latitude carbon stocks. Models could further aid in providing estimates where measurements are scarce and assessing the relevance of these and other processes for the global carbon cycle.

References

Ahlström, A., Schurgers, G., Arneth, A., & Smith, B. (2012). Robustness and uncertainty in terrestrial ecosystem carbon response to CMIP5 climate change projections. *Environmental Research Letters*, *7*(4). https://doi.org/10.1088/1748-9326/7/4/044008

AMAP. (2021). *Arctic Climate Change Update 2021: Key Trends and Impacts. Summary for Policy-makers*.

Batjes, N. H. (2005). *ISRIC-WISE global data set of derived soil properties on a 0.5 by 0.5 degree grid (version 3.0)*. I. W. S. Information.

Belshe, E. F., Schuur, E. A., & Bolker, B. M. (2013). Tundra ecosystems observed to be CO2 sources due to differential amplification of the carbon cycle. *Ecol Lett*, *16*(10), 1307-1315. https://doi.org/10.1111/ele.12164

Berner, L. T., & Goetz, S. J. (2022). Satellite observations document trends consistent with a boreal forest biome shift. *Glob Chang Biol*, *28*(10), 3275-3292. https://doi.org/10.1111/gcb.16121

Bhatt, U. S., Walker, D. A., Raynolds, M. K., Bieniek, P. A., Epstein, H. E., Comiso, J. C., Pinzon, J. E., Tucker, C. J., Steele, M., Ermold, W., & Zhang, J. (2017). Changing seasonality of panarctic tundra vegetation in relationship to climatic variables. *Environmental Research Letters*, *12*(5). https://doi.org/10.1088/1748-9326/aa6b0b

Bhatt, U. S., Walker, D. A., Raynolds, M. K., Comiso, J. C., Epstein, H. E., Jia, G., Gens, R., Pinzon, J. E., Tucker, C. J., Tweedie, C. E., & Webber, P. J. (2010). Circumpolar Arctic Tundra Vegetation Change Is Linked to Sea Ice Decline. *Earth Interactions*, *14*(8), 1-20. https://doi.org/10.1175/2010ei315.1

Bjorkman, A. D., Myers-Smith, I. H., Elmendorf, S. C., Normand, S., Ruger, N., Beck, P. S. A., Blach-Overgaard, A., Blok, D., Cornelissen, J. H. C., Forbes, B. C., Georges, D., Goetz, S. J., Guay, K. C., Henry, G. H. R., HilleRisLambers, J., Hollister, R. D., Karger, D. N., Kattge, J., Manning, P., Prevey, J. S., Rixen, C., Schaepman-Strub, G., Thomas, H. J. D., Vellend, M., Wilmking, M., Wipf, S., Carbognani, M., Hermanutz, L., Levesque, E., Molau, U., Petraglia, A., Soudzilovskaia, N. A., Spasojevic, M. J., Tomaselli, M., Vowles, T., Alatalo, J. M., Alexander, H. D., Anadon-Rosell, A., Angers-Blondin, S., Beest, M. T., Berner, L., Bjork, R. G., Buchwal, A., Buras, A., Christie, K., Cooper, E. J., Dullinger, S., Elberling, B., Eskelinen, A., Frei, E. R., Grau, O., Grogan, P., Hallinger, M., Harper, K. A., Heijmans, M., Hudson, J., Hulber, K., Iturrate-Garcia, M., Iversen, C. M., Jaroszynska, F., Johnstone, J. F., Jorgensen, R. H., Kaarlejarvi, E., Klady, R., Kuleza, S., Kulonen, A., Lamarque, L. J., Lantz, T., Little, C. J., Speed, J. D. M., Michelsen, A., Milbau, A., Nabe-Nielsen, J., Nielsen, S. S., Ninot, J. M., Oberbauer, S. F., Olofsson, J., Onipchenko, V. G., Rumpf, S. B., Semenchuk, P., Shetti, R., Collier, L. S., Street, L. E., Suding, K. N., Tape, K. D., Trant, A., Treier, U. A., Tremblay, J. P., Tremblay, M., Venn, S., Weijers, S., Zamin, T., Boulanger-Lapointe, N., Gould, W. A., Hik, D. S., Hofgaard, A., Jonsdottir, I. S., Jorgenson, J., Klein, J., Magnusson, B., Tweedie, C., Wookey, P. A., Bahn, M., Blonder, B., van Bodegom, P. M., Bond-Lamberty, B., Campetella, G., Cerabolini, B. E. L., Chapin, F. S., 3rd, Cornwell, W. K., Craine, J., Dainese, M., de Vries, F. T., Diaz, S., Enquist, B. J., Green, W., Milla, R., Niinemets, U., Onoda, Y., Ordonez, J. C., Ozinga, W. A., Penuelas, J., Poorter, H., Poschlod, P., Reich, P. B., Sandel, B., Schamp, B., Sheremetev, S., & Weiher, E. (2018). Plant functional trait change across a warming tundra biome. *Nature*, *562*(7725), 57-62. https://doi.org/10.1038/s41586-018-0563-7

Bridgham, S. D., Cadillo-Quiroz, H., Keller, J. K., & Zhuang, Q. (2013). Methane emissions from wetlands: biogeochemical, microbial, and modeling perspectives from local to global scales. *Glob Chang Biol*, *19*(5), 1325-1346. https://doi.org/10.1111/gcb.12131

Bruhwiler, L., Parmentier, F.-J. W., Crill, P., Leonard, M., & Palmer, P. I. (2021). The Arctic Carbon Cycle and Its Response to Changing Climate. *Current Climate Change Reports*, *7*(1), 14-34. https://doi.org/10.1007/s40641-020-00169-5

Burnett, M. S., Schütte, U. M. E., & Harms, T. K. (2022). Widespread capacity for denitrification across a boreal forest landscape. *Biogeochemistry*, *158*(2), 215-232. https://doi.org/10.1007/s10533-022-00895-y

Cai, Z., You, Q., Wu, F., Chen, H. W., Chen, D., & Cohen, J. (2021). Arctic warming revealed by multiple CMIP6 models: evaluation of historical simulations and quantification of future projection uncertainties. *Journal of Climate*, 1-52. https://doi.org/10.1175/jcli-d-20-0791.1

Clemmensen, K. E., Durling, M. B., Michelsen, A., Hallin, S., Finlay, R. D., & Lindahl, B. D. (2021). A tipping point in carbon storage when forest expands into tundra is related to mycorrhizal recycling of nitrogen. *Ecol Lett*, *24*(6), 1193-1204. https://doi.org/10.1111/ele.13735

Crowther, T. W., Todd-Brown, K. E., Rowe, C. W., Wieder, W. R., Carey, J. C., Machmuller, M. B., Snoek, B. L., Fang, S., Zhou, G., Allison, S. D., Blair, J. M., Bridgham, S. D., Burton, A. J., Carrillo, Y., Reich, P. B., Clark, J. S., Classen, A. T., Dijkstra, F. A., Elberling, B., Emmett, B. A., Estiarte, M., Frey, S. D., Guo, J., Harte, J., Jiang, L., Johnson, B. R., Kroel-Dulay, G., Larsen, K. S., Laudon, H., Lavallee, J. M., Luo, Y., Lupascu, M., Ma, L. N., Marhan, S., Michelsen, A., Mohan, J., Niu, S., Pendall, E., Penuelas,

J., Pfeifer-Meister, L., Poll, C., Reinsch, S., Reynolds, L. L., Schmidt, I. K., Sistla, S., Sokol, N. W., Templer, P. H., Treseder, K. K., Welker, J. M., & Bradford, M. A. (2016). Quantifying global soil carbon losses in response to warming. *Nature*, *540*(7631), 104-108. https://doi.org/10.1038/nature20150

Dusenge, M. E., Duarte, A. G., & Way, D. A. (2019). Plant carbon metabolism and climate change: elevated CO2 and temperature impacts on photosynthesis, photorespiration and respiration. *New Phytol*, *221*(1), 32-49. https://doi.org/10.1111/nph.15283

Elmendorf, S. C., Henry, G. H. R., Hollister, R. D., Björk, R. G., Boulanger-Lapointe, N., Cooper, E. J., Cornelissen, J. H. C., Day, T. A., Dorrepaal, E., Elumeeva, T. G., Gill, M., Gould, W. A., Harte, J., Hik, D. S., Hofgaard, A., Johnson, D. R., Johnstone, J. F., Jónsdóttir, I. S., Jorgenson, J. C., Klanderud, K., Klein, J. A., Koh, S., Kudo, G., Lara, M., Lévesque, E., Magnússon, B., May, J. L., Mercado-Dı´az, J. A., Michelsen, A., Molau, U., Myers-Smith, I. H., Oberbauer, S. F., Onipchenko, V. G., Rixen, C., Martin Schmidt, N., Shaver, G. R., Spasojevic, M. J., Þórhallsdóttir, Þ. E., Tolvanen, A., Troxler, T., Tweedie, C. E., Villareal, S., Wahren, C.-H., Walker, X., Webber, P. J., Welker, J. M., & Wipf, S. (2012). Plot-scale evidence of tundra vegetation change and links to recent summer warming. *Nature Climate Change*, *2*(6), 453-457. https://doi.org/10.1038/nclimate1465

Epstein, H. E., Raynolds, M. K., Walker, D. A., Bhatt, U. S., Tucker, C. J., & Pinzon, J. E. (2012). Dynamics of aboveground phytomass of the circumpolar Arctic tundra during the past three decades. *Environmental Research Letters*, *7*(1). https://doi.org/10.1088/1748-9326/7/1/015506

Eyring, V., Bony, S., Meehl, G. A., Senior, C. A., Stevens, B., Stouffer, R. J., & Taylor, K. E. (2016). Overview of the Coupled Model Intercomparison Project Phase 6 (CMIP6) experimental design and organization. *Geoscientific Model Development*, *9*(5), 1937-1958. https://doi.org/10.5194/gmd-9-1937-2016

Fernández-Martínez, M., Sardans, J., Chevallier, F., Ciais, P., Obersteiner, M., Vicca, S., Canadell, J. G., Bastos, A., Friedlingstein, P., Sitch, S., Piao, S. L., Janssens, I. A., & Peñuelas, J. (2018). Global trends in carbon sinks and their relationships with CO2 and temperature. *Nature Climate Change*, *9*(1), 73-79. https://doi.org/10.1038/s41558-018-0367-7

Forbes, B. C., Macias, F. M., & Pentti, Z. (2010). Russian Arctic warming and 'greening' are closely tracked by tundra shrub willows. *Global Change Biology*, *16*, 1542-1554. https://doi.org/10.1111/j.1365-2486.2009.02047.x

Forster, P., Storelvmo, T., Armour, K., Collins, W., Dufresne, J.-L., Frame, D., Lunt, D. J., Mauritsen, T., Palmer, M. D., Watanabe, M., Wild, M., & Zhang, H. (2021). The Earth's Energy Budget, Climate Feedbacks, and Climate Sensitivity. In V. Masson-Delmotte, P. Zhai, A. Pirani, S. L. Connors, C. Péan, S. Berger, N. Caud, Y. Chen, L. Goldfarb, M. I. Gomis, M. Huang, K. Leitzell, E. Lonnoy, J. B. R. Matthews, T. K. Maycock, T. Waterfield, O. Yelekçi, R. Yu, & B. Zhou (Eds.), *Climate Change 2021: The Physical Science Basis. Contribution of Working Group I to the Sixth Assessment Report of the Intergovernmental Panel on Climate Change* (pp. 923-1054). Cambridge University Press. https://doi.org/10.1017/9781009157896.009

Gustafson, A., Miller, P. A., Björk, R. G., Olin, S., & Smith, B. (2021). Nitrogen restricts future sub-arctic treeline advance in an individual-based dynamic vegetation model. *Biogeosciences*, *18*, 6329-6347. https://doi.org/10.5194/bg-18-6329-2021

Harsch, M. A., Hulme, P. E., McGlone, M. S., & P., D. R. (2009). Are treelines advancing? A global meta-analysis of treeline response to climate warming. *Ecology Letters*, *12*(10), 1040-1049. https://doi.org/10.1111/j.1461-0248.2009.01355.x

Hartley, I. P., Garnett, M. H., Sommerkorn, M., Hopkins, D. W., Fletcher, B. J., Sloan, V. L., Phoenix, G. K., & Wookey, P. A. (2012). A potential loss of carbon associated with greater plant growth in the European Arctic. *Nature Climate Change*, *2*(12), 875-879. https://doi.org/10.1038/nclimate1575

Hugelius, G., Strauss, J., Zubrzycki, S., Harden, J. W., Schuur, E. A. G., Ping, C. L., Schirrmeister, L., Grosse, G., Michaelson, G. J., Koven, C. D., amp, apos, Donnell, J. A., Elberling, B., Mishra, U., Camill, P., Yu, Z., Palmtag, J., & Kuhry, P. (2014). Estimated stocks of circumpolar permafrost carbon with quantified uncertainty ranges and identified data gaps. *Biogeosciences*, *11*(23), 6573-6593. https://doi.org/10.5194/bg-11-6573-2014

IPCC. (2014). *Climate Change 2014: Synthesis Report. Contribution of Working Groups I, II and III to the Fifth Assessment Report of the Intergovernmental Panel on Climate Change*.

IPCC. (2021). *Climate Change 2021: The Physical Science Basis. Contribution of Working Group I to the Sixth Assessment Report of the Intergovernmental Panel on Climate Change*. C. U. Press.

Keuper, F., Wild, B., Kummu, M., Beer, C., Blume-Werry, G., Fontaine, S., Gavazov, K., Gentsch, N., Guggenberger, G., Hugelius, G., Jalava, M., Koven, C., Krab, E. J., Kuhry, P., Monteux, S., Richter, A., Shahzad, T., Weedon, J. T., & Dorrepaal, E. (2020). Carbon loss from northern circumpolar permafrost soils amplified by rhizosphere priming. *Nature Geoscience*, *13*(8), 560-565. https://doi.org/10.1038/s41561-020-0607-0

Knorr, W., Kaminski, T., Arneth, A., & Weber, U. (2014). Impact of human population density on fire frequency at the global scale. *Biogeosciences*, *11*(4), 1085-1102. https://doi.org/10.5194/bg-11-1085-2014

Lange, S. (2019). Trend-preserving bias adjustment and statistical downscaling with ISIMIP3BASD (v1.0). *Geoscientific Model Development*, *12*(7), 3055-3070. https://doi.org/10.5194/gmd-12-3055-2019

Lange, S. (2021). *ISIMIP3BASD*. In Zenodo.

Li, & Xiao. (2019). Mapping Photosynthesis Solely from Solar-Induced Chlorophyll Fluorescence: A Global, Fine-Resolution Dataset of Gross Primary Production Derived from OCO-2. *Remote Sensing*, *11*(21). https://doi.org/10.3390/rs11212563

Liu, Y. Y., van Dijk, A. I. J. M., de Jeu, R. A. M., Canadell, J. G., McCabe, M. F., Evans, J. P., & Wang, G. (2015). Recent reversal in loss of global terrestrial biomass. *Nature Climate Change*, *5*(5), 470-474. https://doi.org/10.1038/nclimate2581

Mamet, S. D., Brown, C. D., Trant, A. J., & Laroque, C. P. (2019). Shifting global Larix distributions: Northern expansion and southern retraction as species respond to changing climate. *Journal of Biogeography*, *46*(1), 30-44. https://doi.org/10.1111/jbi.13465

Martin, A. C., Macias-Fauria, M., Bonsall, M. B., Forbes, B. C., Zetterberg, P., & Jeffers, E. S. (2022). Common mechanisms explain nitrogen-dependent growth of Arctic shrubs over three decades despite heterogeneous trends and declines in soil nitrogen availability. *New Phytol*, *233*(2), 670-686. https://doi.org/10.1111/nph.17529

Matthews, H. D., Gillett, N. P., Stott, P. A., & Zickfeld, K. (2009). The proportionality of global warming to cumulative carbon emissions. *Nature*, *459*(7248), 829-832. https://doi.org/10.1038/nature08047

McGuire, A. D., Christensen, T. R., Hayes, D., Heroult, A., Euskirchen, E., Kimball, J. S., Koven, C., Lafleur, P., Miller, P. A., Oechel, W., Peylin, P., Williams, M., & Yi, Y. (2012). An assessment of the carbon balance of Arctic tundra: comparisons among observations, process models, and atmospheric inversions. *Biogeosciences*, *9*(8), 3185-3204. https://doi.org/10.5194/bg-9-3185-2012

Meinshausen, M., Nicholls, Z. R. J., Lewis, J., Gidden, M. J., Vogel, E., Freund, M., Beyerle, U., Gessner, C., Nauels, A., Bauer, N., Canadell, J. G., Daniel, J. S., John, A., Krummel, P. B., Luderer, G., Meinshausen, N., Montzka, S. A., Rayner, P. J., Reimann, S., Smith, S. J., van den Berg, M., Velders, G. J. M., Vollmer, M. K., & Wang, R. H. J. (2020). The shared socio-economic pathway (SSP) greenhouse gas concentrations and their extensions to 2500. *Geoscientific Model Development*, *13*(8), 3571-3605. https://doi.org/10.5194/gmd-13-3571-2020

Mekonnen, Z. A., Riley, W. J., Berner, L. T., Bouskill, N. J., Torn, M. S., Iwahana, G., Breen, A. L., Myers-Smith, I. H., Criado, M. G., Liu, Y., Euskirchen, E. S., Goetz, S. J., Mack, M. C., & Grant, R. F. (2021). Arctic tundra shrubification: a review of mechanisms and impacts on ecosystem carbon balance. *Environmental Research Letters*, *16*(5). https://doi.org/10.1088/1748-9326/abf28b

Mekonnen, Z. A., Riley, W. J., & Grant, R. F. (2018). Accelerated Nutrient Cycling and Increased Light Competition Will Lead to 21st Century Shrub Expansion in North American Arctic Tundra. *Journal of Geophysical Research: Biogeosciences*, *123*(5), 1683-1701. https://doi.org/10.1029/2017jg004319

Monteith, J. L., & Unsworth, M. H. (2013). *Principles of Environmental Physics - Plants, Animals, and the Atmosphere* (4 ed.). Elsevier.

Myers-Smith, I. H., Elmendorf, S. C., Beck, P. S. A., Wilmking, M., Hallinger, M., Blok, D., Tape, K. D., Rayback, S. A., Macias-Fauria, M., Forbes, B. C., Speed, J. D. M., Boulanger-Lapointe, N., Rixen, C., Lévesque, E., Schmidt, N. M., Baittinger, C., Trant, A. J., Hermanutz, L., Collier, L. S., Dawes, M. A., Lantz, T. C., Weijers, S., Jørgensen, R. H., Buchwal, A., Buras, A., Naito, A. T., Ravolainen, V., Schaepman-Strub, G., Wheeler, J. A., Wipf, S., Guay, K. C., Hik, D. S., & Vellend, M. (2015). Climate sensitivity of shrub growth across the tundra biome. *Nature Climate Change*, *5*(9), 887-891. https://doi.org/10.1038/nclimate2697

Nadelhoffer, K. J., Giblin, A. E., Shaver, G. R., & Laundre, J. A. (1991). Effects of Temperature and Substrate Quality on Element Mineralization in Six Arctic Soils. *Ecology*, *72*(1), 242-253.

Nijsse, F. J. M. M., Cox, P. M., & Williamson, M. S. (2020). Emergent constraints on transient climate response (TCR) and equilibrium climate sensitivity (ECS) from historical warming in CMIP5 and CMIP6 models. *Earth System Dynamics*, *11*(3), 737-750. https://doi.org/10.5194/esd-11-737-2020

O'Neill, B. C., Tebaldi, C., van Vuuren, D. P., Eyring, V., Friedlingstein, P., Hurtt, G., Knutti, R., Kriegler, E., Lamarque, J.-F., Lowe, J., Meehl, G. A., Moss, R., Riahi, K., & Sanderson, B. M. (2016). The Scenario Model Intercomparison Project (ScenarioMIP) for CMIP6. *Geoscientific Model Development*, *9*(9), 3461-3482. https://doi.org/10.5194/gmd-9-3461-2016

Parker, T. C., Sanderman, J., Holden, R. D., Blume-Werry, G., Sjogersten, S., Large, D., Castro-Diaz, M., Street, L. E., Subke, J. A., & Wookey, P. A. (2018). Exploring drivers of litter decomposition in a greening Arctic: results from a transplant experiment across a treeline. *Ecology*, *99*(10), 2284-2294. https://doi.org/10.1002/ecy.2442

Pellegrini, A. F. A., Ahlstrom, A., Hobbie, S. E., Reich, P. B., Nieradzik, L. P., Staver, A. C., Scharenbroch, B. C., Jumpponen, A., Anderegg, W. R. L., Randerson, J. T., & Jackson, R. B. (2018). Fire frequency drives decadal changes in soil carbon and nitrogen and ecosystem productivity. *Nature*, *553*(7687), 194-198. https://doi.org/10.1038/nature24668

Peltola, O., Vesala, T., Gao, Y., Räty, O., Alekseychik, P., Aurela, M., Chojnicki, B., Desai, A. R., Dolman, A. J., Euskirchen, E. S., Friborg, T., Göckede, M., Helbig, M., Humphreys, E., Jackson, R. B., Jocher, G., Joos, F., Klatt, J., Knox, S. H., Kowalska, N., Kutzbach, L., Lienert, S., Lohila, A., Mammarella, I., Nadeau, D. F., Nilsson, M. B., Oechel, W. C., Peichl, M., Pypker, T., Quinton, W., Rinne, J., Sachs, T., Samson, M., Schmid, H. P., Sonnentag, O., Wille, C., Zona, D., & Aalto, T. (2019). Monthly gridded data product of northern wetland methane emissions based on upscaling eddy covariance observations. *Earth System Science Data*, *11*(3), 1263-1289. https://doi.org/10.5194/essd-11-1263-2019

Pilegaard, K. (2013). Processes regulating nitric oxide emissions from soils. *Philos Trans R Soc Lond B Biol Sci*, *368*(1621), 20130126. https://doi.org/10.1098/rstb.2013.0126

Pongracz, A., Wårlind, D., Miller, P. A., & Parmentier, F.-J. W. (2021). Model simulations of arctic biogeochemistry and permafrost extent are highly sensitive to the implemented snow scheme in LPJ-GUESS. *Biogeosciences*, *18*(20), 5767-5787. https://doi.org/10.5194/bg-18-5767-2021

Qiu, C., Ciais, P., Zhu, D., Guenet, B., Chang, J., Chaudhary, N., Kleinen, T., Li, X., Müller, J., Xi, Y., Zhang, W., Ballantyne, A., Brewer, S. C., Brovkin, V., Charman, D. J., Gustafson, A., Gallego-Sala, A. V., Gasser, T., Holden, J., Joos, F., Kwon, M. J., Lauerwald, R., Miller, P. A., Peng, S., Page, S., Smith, B., Stocker, B. D., Sannel, A. B. K., Salmon, E., Schurgers, G., Shurpali, N. J., Wårlind, D., & Westermann, S. (2022). A strong mitigation scenario maintains climate neutrality of northern peatlands. *One Earth*, *5*(1), 86-97. https://doi.org/10.1016/j.oneear.2021.12.008

Rabin, S. S., Melton, J. R., Lasslop, G., Bachelet, D., Forrest, M., Hantson, S., Kaplan, J. O., Li, F., Mangeon, S., Ward, D. S., Yue, C., Arora, V. K., Hickler, T., Kloster, S., Knorr, W., Nieradzik, L., Spessa, A., Folberth, G. A., Sheehan, T., Voulgarakis, A., Kelley, D. I., Prentice, I. C., Sitch, S., Harrison, S., & Arneth, A. (2017). The Fire Modeling Intercomparison Project (FireMIP), phase 1: experimental and analytical protocols with detailed model descriptions. *Geoscientific Model Development*, *10*(3), 1175-1197. https://doi.org/10.5194/gmd-10-1175-2017

Rees, W. G., Hofgaard, A., Boudreau, S., Cairns, D. M., Harper, K., Mamet, S., Mathisen, I., Swirad, Z., & Tutubalina, O. (2020). Is subarctic forest advance able to keep pace with climate change? *Glob Chang Biol*, *26*(7), 3965-3977. https://doi.org/10.1111/gcb.15113

Rogers, A., Serbin, S. P., Ely, K. S., Sloan, V. L., & Wullschleger, S. D. (2017). Terrestrial biosphere models underestimate photosynthetic capacity and CO2 assimilation in the Arctic. *New Phytol*, *216*(4), 1090-1103. https://doi.org/10.1111/nph.14740

Saunois, M., Stavert, A. R., Poulter, B., Bousquet, P., Canadell, J. G., Jackson, R. B., Raymond, P. A., Dlugokencky, E. J., Houweling, S., Patra, P. K., Ciais, P., Arora, V. K., Bastviken, D., Bergamaschi, P., Blake, D. R., Brailsford, G., Bruhwiler, L., Carlson, K. M., Carrol, M., Castaldi, S., Chandra, N., Crevoisier, C., Crill, P. M., Covey, K., Curry, C. L., Etiope, G., Frankenberg, C., Gedney, N., Hegglin, M. I., Höglund-Isaksson, L., Hugelius, G., Ishizawa, M., Ito, A., Janssens-Maenhout, G., Jensen, K. M., Joos, F., Kleinen, T., Krummel, P. B., Langenfelds, R. L., Laruelle, G. G., Liu, L., Machida, T., Maksyutov, S., McDonald, K. C., McNorton, J., Miller, P. A., Melton, J. R., Morino, I., Müller, J., Murguia-Flores, F., Naik, V., Niwa, Y., Noce, S., O'Doherty, S., Parker, R. J., Peng, C., Peng, S., Peters, G. P., Prigent, C., Prinn, R., Ramonet, M., Regnier, P., Riley, W. J., Rosentreter, J. A., Segers, A., Simpson, I. J., Shi, H., Smith, S. J., Steele, L. P., Thornton, B. F., Tian, H., Tohjima, Y., Tubiello, F. N., Tsuruta, A., Viovy, N., Voulgarakis, A., Weber, T. S., van Weele, M., van der Werf, G. R., Weiss, R. F., Worthy, D., Wunch, D., Yin, Y., Yoshida, Y., Zhang, W., Zhang, Z., Zhao, Y., Zheng, B., Zhu, Q., Zhu, Q., & Zhuang, Q. (2020). The Global Methane Budget 2000–2017. *Earth System Science Data*, *12*(3), 1561-1623. https://doi.org/10.5194/essd-12-1561-2020

Schulzweida, U. (2021). *CDO User Guide*. In (Version 2.0.0) Zenodo.

Schuur, E. A., McGuire, A. D., Schadel, C., Grosse, G., Harden, J. W., Hayes, D. J., Hugelius, G., Koven, C. D., Kuhry, P., Lawrence, D. M., Natali, S. M., Olefeldt, D., Romanovsky, V. E., Schaefer, K., Turetsky, M. R., Treat, C. C., & Vonk, J. E. (2015). Climate change and the permafrost carbon feedback. *Nature*, *520*(7546), 171-179. https://doi.org/10.1038/nature14338

Smith, B., Prentice, I. C., & Sykes, M. T. (2001). Representation of vegetation dynamics in the modelling of terrestrial ecosystems: comparing two contrasting approaches within European climate space. *Global Ecology and Biogeography*, *10*(6), 621-637. https://doi.org/10.1046/j.1466-822X.2001.t01-1-00256.x

Smith, B., Wårlind, D., Arneth, A., Hickler, T., Leadley, P., Siltberg, J., & Zaehle, S. (2014). Implications of incorporating N cycling and N limitations on primary production in an individual-based dynamic vegetation model. *Biogeosciences*, *11*(7), 2027-2054. https://doi.org/10.5194/bg-11-2027-2014

Stavert, A. R., Saunois, M., Canadell, J. G., Poulter, B., Jackson, R. B., Regnier, P., Lauerwald, R., Raymond, P. A., Allen, G. H., Patra, P. K., Bergamaschi, P., Bousquet, P., Chandra, N., Ciais, P., Gustafson, A., Ishizawa, M., Ito, A., Kleinen, T., Maksyutov, S., McNorton, J., Melton, J. R., Muller, J., Niwa, Y., Peng, S., Riley, W. J., Segers, A., Tian, H., Tsuruta, A., Yin, Y., Zhang, Z., Zheng, B., & Zhuang, Q. (2022). Regional trends and drivers of the global methane budget. *Glob Chang Biol*, *28*(1), 182-200. https://doi.org/10.1111/gcb.15901

Tokarska, K. B., Stolpe, M. B., Sippel, S., Fischer, E. M., Smith, C. J., Lehner, F., & Knutti, R. (2020). Past warming trend constrains future warming in CMIP6 models. *Sci Adv*, *6*(12), eaaz9549. https://doi.org/10.1126/sciadv.aaz9549

Viovy, N. (2018). *CRUNCEP Version 7 - Atmospheric Forcing Data for the Community Land Model* Research Data Archive at the National Center for Atmospheric Research, Computational and Information Systems Laboratory. https://doi.org/10.5065/PZ8F-F017

Virkkala, A. M., Aalto, J., Rogers, B. M., Tagesson, T., Treat, C. C., Natali, S. M., Watts, J. D., Potter, S., Lehtonen, A., Mauritz, M., Schuur, E. A. G., Kochendorfer, J., Zona, D., Oechel, W., Kobayashi, H., Humphreys, E., Goeckede, M., Iwata, H., Lafleur, P. M., Euskirchen, E. S., Bokhorst, S., Marushchak, M., Martikainen, P. J., Elberling, B., Voigt, C., Biasi, C., Sonnentag, O., Parmentier, F. W., Ueyama, M., Celis, G., St Loius, V. L., Emmerton, C. A., Peichl, M., Chi, J., Jarveoja, J., Nilsson, M. B., Oberbauer, S. F., Torn, M. S., Park, S. J., Dolman, H., Mammarella, I., Chae, N., Poyatos, R., Lopez-Blanco, E., Rojle Christensen, T., Jung Kwon, M., Sachs, T., Holl, D., & Luoto, M. (2021). Statistical upscaling of ecosystem CO2 fluxes across the terrestrial tundra and boreal domain: regional patterns and uncertainties. *Glob Chang Biol*. https://doi.org/10.1111/gcb.15659

Voigt, C., Marushchak, M. E., Abbott, B. W., Biasi, C., Elberling, B., Siciliano, S. D., Sonnentag, O., Stewart, K. J., Yang, Y., & Martikainen, P. J. (2020). Nitrous oxide emissions from permafrost-affected soils. *Nature Reviews Earth & Environment*, *1*(8), 420-434. https://doi.org/10.1038/s43017-020-0063-9

Wania, R., Ross, I., & Prentice, I. C. (2009a). Integrating peatlands and permafrost into a dynamic global vegetation model: 1. Evaluation and sensitivity of physical land surface processes. *Global Biogeochemical Cycles*, *23*(3), n/a-n/a. https://doi.org/10.1029/2008gb003412

Wania, R., Ross, I., & Prentice, I. C. (2009b). Integrating peatlands and permafrost into a dynamic global vegetation model: 2. Evaluation and sensitivity of vegetation and carbon cycle processes. *Global Biogeochemical Cycles*, *23*(3), n/a-n/a. https://doi.org/10.1029/2008gb003413

Wania, R., Ross, I., & Prentice, I. C. (2010). Implementation and evaluation of a new methane model within a dynamic global vegetation model: LPJ-WHyMe v1.3.1. *Geoscientific Model Development*, *3*(2), 565-584. https://doi.org/10.5194/gmd-3-565-2010

Weedon, G. P., Balsamo, G., Bellouin, N., Gomes, S., Best, M. J., & Viterbo, P. (2014). The WFDEI meteorological forcing data set: WATCH Forcing Data methodology applied to ERA-Interim reanalysis data. *Water Resources Research*, *50*(9), 7505-7514. https://doi.org/10.1002/2014wr015638

Xu, J., Morris, P. J., Liu, J., & Holden, J. (2018). PEATMAP: Refining estimates of global peatland distribution based on a meta-analysis. *Catena*, *160*, 134-140. https://doi.org/10.1016/j.catena.2017.09.010

Xu, R. I., & Prentice, I. C. (2008). Terrestrial nitrogen cycle simulation with a dynamic global vegetation model. *Global Change Biology*, *14*(8), 1745-1764. https://doi.org/10.1111/j.1365-2486.2008.01625.x

Appendix A. High-latitude and peatland updates in LPJ-GUESS version 4.1

Table of Contents

1. Updates to soil temperature and hydrology calculations

Introduction

Compared with the versions of the model (Smith et al. 2014) up to and including version 4, versions 4.1 and above include updated and differentiated representations of processes operating in upland (i.e. mineral soil) and peatland ecosystems of the tundra and taiga biomes, as well as PFTs characteristic of these ecosystems, including evergreen and deciduous shrubs, forbs, graminoids and bryophytes (Zhang et al., 2014; Tang et al. 2015). The model now includes improved soil temperature calculations, a description of soil freezing processes (affecting water available to plants), and, on the fraction of each gridcell deemed to be a peatland, a peatland hydrology, peatland-specific PFTs, and CH_4 emissions. These developments and process descriptions were adopted from updates to the LPJ DGVM made by Wania et al. (2009a, 2009b, 2010), and are described more briefly in McGuire et al. (2012).

Soil layers and their thermal properties

Calculations of soil temperature in versions of the model before version 4.1 are inaccurate for soils underlain by permafrost and in cold regions experiencing soil water phase change. Soil temperatures are now calculated and updated daily for each of fifteen, 10 cm layers in the 1.5 m-deep active soil column (i.e. those layers of greatest importance for vegetation and biological processes), overlain by up to 5 snow layers to a maximum depth corresponding to 10,000 mm water equivalent (see below), and underlain by 5 additional padding layers to a depth of 48m. See **Figure A.1** for an overview of the overall layer structure.

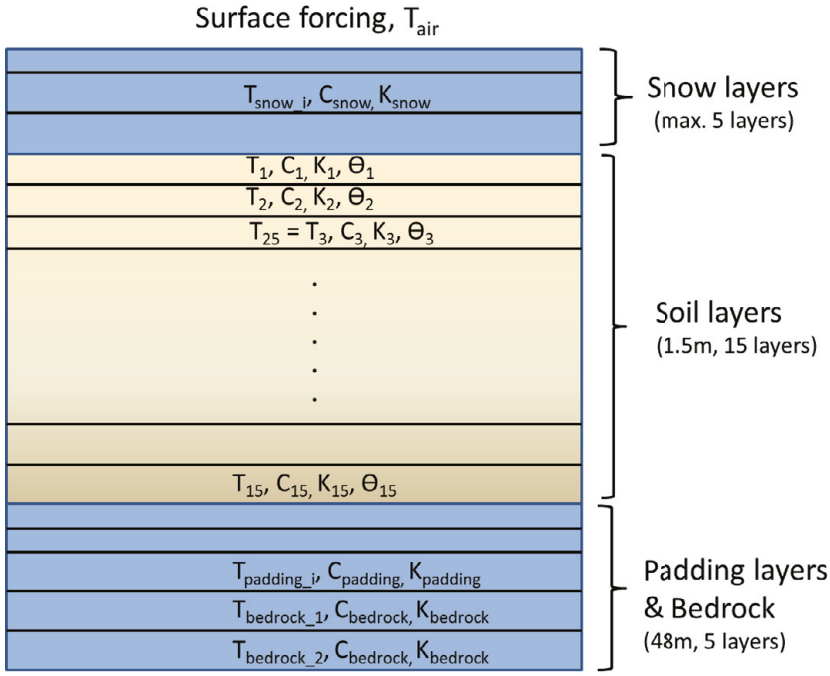

Figure A.1. Soil layer structure in upland/mineral soils (not to scale). Up to 5 snow layers overlie 15 active soil layers, underneath which 5 padding layers extend to a total depth of 49.5 m.

Each day, LPJ-GUESS numerically solves the heat diffusion equation

$$\frac{\partial T}{\partial t} = \frac{\partial}{\partial x}\left(D(z,t)\frac{\partial T}{\partial z}\right)$$

where $T(z,t)$ is the soil temperature at depth z (m) at time t, and $D(z,t)$ ($m^2\ s^{-1}$) is the thermal diffusivity at depth z, defined as

$$D(z,t) = \frac{K(z,t)}{C(z,t)}$$

where $K(z,t)$ is the thermal conductivity ($W\ m^{-1}\ K^{-1}$), and $C(z,t)$ ($J\ m^{-3}\ K^{-1}$) is the heat capacity of the soil layer, each at a depth z and time t.

Optionally, the model solves the more general equation:

$$C(z,t)\frac{\partial T}{\partial t} = \frac{\partial}{\partial x}\left(K(z,t)\frac{\partial T}{\partial z}\right)$$

which reduces to the equation above when $C(z,t)$ is constant.

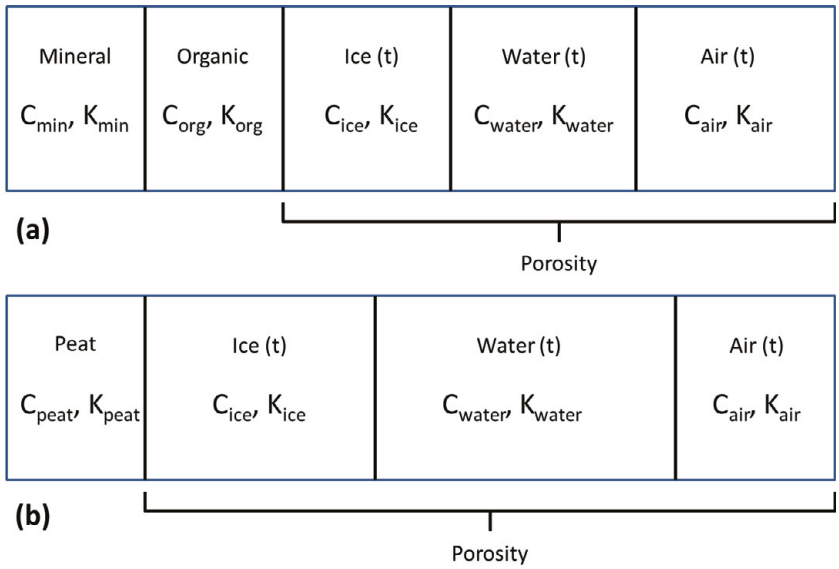

Figure A.2. Composition and thermal properties of upland (a) and peatland (b) soil layers.

As shown in **Figure A.2(a),** the mineral soil layers comprise fixed (in time) volumetric fractions of mineral (F_{min}) and organic (F_{org}) content, as well as dynamic volumetric fractions of water (F_{water}), ice (F_{ice}) and air (F_{air}). Both F_{min} and F_{org}, as well as the porosity, *por*, are calculated based on soil texture for each gridcell, specifying the percentage of sand, silt and clay, and organic content, such that

$$F_{min} + F_{org} + \text{por} = 1$$

Both the soil heat capacity and the thermal conductivity are updated daily for each snow, active soil and padding layer. For active soil layers in upland areas, *C(z,t)* is calculated as the weighted average of the heat capacities of the individual components of the soil layer (e.g. C_{water}, C_{ice} etc.), using the volumetric fractions as the weights:

$$F_{min}.C_{min} + F_{org}.C_{org} + F_{water}.C_{water} + F_{ice}.C_{ice} + F_{air}.C_{air} = C(z,t)$$

where we have dropped the subscripts for F_{water}, F_{ice}, and F_{air}, each of which vary with depth and time.

Table A.1 gives the heat capacities and thermal conductivities of the soil layer components.

Table A.1. Heat capacities and thermal conductivities of the soil layer components. Values taken from Bonan (2002), Wania et al. (2009a, 2009b), Granberg et al. (2008), and Chadburn et al. (2015).

Soil layer component	Heat capacity (10^6 J m^{-3} K^{-1})	Thermal conductivity (W m^{-1} K^{-1})
Mineral	2.38	2.0
Organic	2.5	0.25
Peat	0.58	0.06
Water	4.18	0.57
Ice	1.94	2.2
Air	0.0012	0.025
Bedrock	2.1	8.6

Calculation of *K(z,t)* follows Wania et al. (2012a) and Granberg et al. (2008), using geometric means, as follows:

Defining F_{total} as

$$F_{min} + F_{org} + F_{water} + F_{ice} = F_{total}$$

and

$$lK_* = \frac{F_*}{F_{total}} \ln (K_*)$$

for each (*) component (mineral, organic, water and ice), we define *K(z,t)* as:

$$K(z,t) = F_{air}.K_{air} + (1 - F_{air}).\, e^{(lK_{ice} + lK_{water} + lK_{org} + lK_{min})}$$

Soil column and temperature calculations

Besides the 15 active soil layers described above, the soil column is completed by overlying snow layers and underlying padding layers (**Figure A.1**).

Snow

Snow layers insulate the underlying active soil layers, and store both water and nitrogen (passively) for release each spring. LPJ-GUESS models the snow pack using up to 5 homogeneous layers of variable thickness. At the start of the period of snow accumulation, one snow layer is used until the snow thickness reaches 100mm. Thereafter, new layers of thickness 50mm are created each time the snow depth exceeds thresholds of 100mm, 150mm, 200mm and 250mm. The thinner 50mm layers are always placed at the top of the snow pack, nearest the overlying air. Above a depth of 250mm, the thickness of the bottom snow layer in contact with the uppermost active soil layer is allowed to grow.

The depth of the snow pack is determined by its density, ρ_{snow}. There are options to use a fixed density of 250 kg m^{-3} as in Ekici et al. (2015) or, following Wania et al. (2009a), a

variable density that remains at 275 kg m^{-3} until the final period (25%) of the snow season, during which the density increases linearly to a value more representative of older, more compact snow: $\rho_{snow\_compact}$ = 500 kg m^{-3}.

The heat capacity, C_{snow}, and thermal conductivity, K_{snow}, of snow are defined as (Wania et al., 2009a):

$$C_{snow} = 0.01.\rho_{ice}\,.(185 + 689.T_K)$$

where ρ_{ice} = 917 kg m^{-3}, and T_K is the air temperature in Kelvin.

Defining $\rho_{snow\_scaled} = \rho_{snow}/1000$, we define

$$K_{snow} = 0.138 - 1.01\,\rho_{snow\_scaled} + 3.233\,\rho^2_{snow\_scaled}$$

giving values that vary between 0.1 for fresh snow and 0.44 W m^{-1} K^{-1} for older snow with a higher density.

Snow melt (S_{melt}, mm day^{-1}) occurs when air temperature exceeds 0ºC:

$$S_{melt} = (1.5 + 0.007.P).T_C$$

Here, T_C is the air temperature in degrees Celsius, and P is the daily precipitation (mm day^{-1}). Snow melt enters the top of the soil in the hydrology scheme (see below).

Boundary conditions, padding layers & bedrock

Since LPJ-GUESS does not consider the full energy balance at the surface, the upper boundary condition driving the temporal evolution in the snow, soil and padding layer temperatures is the surface air temperature (**Figure A.1**). At the bottom of the soil column, we assume a zero-gradient condition, namely

$$\frac{\partial T}{\partial z} \to 0\ as\ z \to \infty.$$

Since a depth of 1.5m is insufficient to achieve this condition (Lawrence & Slater, 2008), the soil column has an additional 5 padding layers below the bottommost active soil layer with thicknesses 0.3, 1.0, 3.2, 10.4 and 33.1m, to give a total padding layer depth of 48m (default values). The padding layers are thermally active, but hydrologically inactive, i.e. there is no water infiltration from the upper soil layers and the maximum rooting depth is 1.5 m. The thermal properties of the three padding layers nearest the active soil layers are updated daily and assumed to be equal to the bottommost active soil layer. The two deepest padding layers have the thermal properties of bedrock (**Table A.1**, Chadburn et al. 2015).

The soil temperatures are calculated daily with a user-defined timestep (≤1 day) using the Crank-Nicolson finite difference scheme – see Wania et al. (2009a) for full details.

Soil water freezing and thawing processes

Since soil temperature varies with time and depth, $T(z,t)$, the fractional (volumetric) water and ice contents, F_{ice} and F_{water}, must also vary with the same spatial (10 cm) and temporal (1 day) resolution along the soil column. LPJ-GUESS adopts the simple approach to phase change described in more detail by Wania et al. (2009a), based on the following assumptions:

- Whenever water is freezing (ice is melting) in a layer, latent heat release (consumption) keeps the temperature at a constant value of 0ºC until the water is completely frozen (the ice has completely melted).
- Rainfall or snow melt both update F_{water} (see below), but they do not introduce additional heat from the atmosphere to the soil.
- Freezing is only permitted when temperature is falling. This is a numerical stability condition.
- Thawing is only permitted when temperature is rising. This is a numerical stability condition.

In contrast to Wania et al. (2009a, 2009b), LPJ-GUESS accounts for freezing and thawing of water below the wilting point. When water in a layer is freezing, it is assumed that water below the wilting point is frozen first and that liquid water above the wilting point can only freeze once all the water below the wilting point has frozen. Only then does this result in a potential reduction in plant water uptake. Similarly, water stored as ice above the wilting point can only melt after all the ice below the wilting point has melted.

The model calculates the daily thaw depth as the depth (z_{thaw}) of the first layer below the surface where $T(z_{thaw}) > 0$ºC.

Hydrology changes resulting from phase change

The introduction of phase change necessitated some minor adjustments to the standard hydrology for upland soils introduced and described by Gerten et al. (2004).

In the Gerten et al. scheme, phase change was not considered, and there were two active soil layers, consisting of a 0.5 m thick surface layer overlying a 1 m thick deep layer. However, though the fractional (volumetric) water and ice contents, F_{ice} and F_{water}, respectively, can now vary along the active soil column's 15, 10 cm layers, we use the same basic algorithm, updated to account for phase change, increased vertical resolution and water conservation.

We label the soil layers from 1 to 15 (**Figure A.1**), where layer 1 is the top soil layer in contact with air or snow, and layer 15 the bottommost layer in contact with the padding layers. In what follows, we refer to layers 1 to 5 (i.e. the top 50cm of soil) as the surface layers, and layers 6 to 15 as the deep layers, in keeping with Gerten et al. (2004).

The (volumetric) wilting point (wp_i), the (volumetric) field capacity (fc_i) and the (volumetric) water holding capacity ($whc_i = fc_i - wp_i$) have the same values for each soil layer, i (1 to 15), determined by the soil texture. All layers have the same thickness, $Dz_i = Dz = 100$mm.

We define the available water holding capacity for layer i (awc_i) as

$$awc_i = Dz_i \,.\, whc_i$$

which is the maximum amount of water (mm) layer i can hold (< 100mm).

We define the available (liquid) water in layer i (aw_i) as

$$aw_i = Dz_i \,.\, (F_{water,i} - wp_i)$$

which is the actual liquid water contained in layer i, such that $aw_i < awc_i$. Note that this definition does not include ice in layer i, $F_{ice,i}$.

The dimensionless ratio of these quantities, $wcont_i$:

$$wcont_i = \frac{aw_i}{awc_i}$$

is an indicator of the water available to plants in the layer, such that $0 \leq wcont_i \leq 1$. The *wcont* ratio is used by Gerten et al. (2004), but for the (top 50 cm) surface and (bottom 100 cm) deep layers only.

We now define the potential for water uptake, pot_i, for soil layer i as follows:

$$pot_i = Dz_i \,.\, (fc_i - F_{water,i} - F_{ice,i})$$

which is the upper limit to additional water (mm) that a soil layer can hold.

We can recover the Gerten et al. *wcont* definitions by first defining:

$$wcont_{a,b} = \frac{\sum_a^b aw_i}{\sum_a^b awc_i}$$

and defining $wcont_{surf} = wcont_{1,5}$, $wcont_{deep} = wcont_{6,15}$ and (for the evaporation layer); $wcont_{evap} = wcont_{1,2}$. Similary, the potential for uptake in the surface (pot_{surf}) and deep (pot_{deep}) layers is given by the sum of pot_i over layers 1 to 5, and 6 to 15, respectively, and the total available water the surface (aw_{surf}) and deep (aw_{deep}) layers is given by the sum of aw_i over layers 1 to 5, and 6 to 15, respectively.

Using the above definitions, we can now summarize the updates to the hydrology algorithm.

Evaporation

Evaporation (mm) occurs from the non-vegetated (i.e. 1-FPC_{total}) fraction, *fevap*, of the uppermost two 10 cm layers, i = 1, 2, following

$$evap = fevap * EET * PT * wcont_{evap} * wcont_{evap}$$

where *EET* is the daily equilibrium evapotranspiration (mm), and *PT* = 1.32 is the Priestley-Taylor constant. Water conservation is achieved by demanding that *evap* <= *(aw_1 + aw_2)*. Water evaporated is removed from layers 1 and 2 in proportion to their available water content as a fraction of the total available water in the evaporation layers, i.e. *aw_i/(aw_1 + aw_2)*, which acts to equalize the available water in these layers.

Input from rainfall and snowmelt - initial infiltration

An initial infiltration of rainfall and snowmelt, *rain_melt,* into the five surface layers is applied in the model's initial_infiltration() function. There are two conditions:

rain_melt <= pot_{surf}: distribute *rain_melt* over layers 1 to 5 in proportion to pot_i. This acts to equalize the available water in these layers. In this case no additional water enters the soil in the hydrology routine.

rain_melt > pot_{surf}: distribute pot_{surf} (mm) over layers 1 to 5 in proportion to pot_i. This equalizes the liquid water + ice fractions in these layers. The remaining water, *rain_melt* - pot_{surf} , enters the soil in the hydrology routine.

Input from rainfall and snowmelt – hydrology routine

In the hydrology routine, water input from rainfall and snowmelt (*rain_melt*, mm) that has not initially infiltrated now enters the five surface layers. There are two conditions:

rain_melt <= pot_{surf}: distribute *rain_melt* over layers 1 to 5 in proportion to pot_i. This acts to equalize the available water in these layers.

rain_melt > pot_{surf}: distribute pot_{surf} (mm) over layers 1 to 5 in proportion to pot_i. This equalizes the liquid water + ice fractions in these layers. The remaining water, *rain_melt* - pot_{surf} , enters surface runoff, $runoff_{surf}$.

Percolation

Percolation from the surface layers to the deep layers, and from the deep layers to base flow, is allowed each day if *rain_melt > 0.1 mm.*

Percolation of liquid water from the surface layers to the deep layers, P_{surf_deep} (mm) is calculated as

$$P_{surf\_deep} = \min(aw_{surf}, K_1 * e^{K_2 * wcont_{surf}})$$

where K_1 and K_2 are soil texture-dependent percolation coefficients (Eqn. 31, Haxeltine & Prentice, 1996). Percolated water is removed from each of the five surface layers in proportion to their available water content, aw_i/aw_{surf}, and fills the deeper soil layers as follows:

$P_{surf\_deep} <= pot_{deep}$: distribute over layers 6 to 15 in proportion to pot_i. This acts to equalize the available water in these layers.

$P_{surf\_deep} > pot_{deep}$: distribute pot_{deep} (mm) over layers 6 to 15 in proportion to pot_i. This equalizes the liquid water + ice fractions in these layers. The remaining water, $P_{surf\_deep} - pot_{deep}$, enters drainage runoff, $runoff_{drain}$.

Finally, percolation of liquid water from the deep layers - P_{deep_surf} (mm) - is lost to the soil column as base flow runoff and calculated as follows

$$P_{deep\_base} = \min(aw_{deep}, 0.5 * K_1 * e^{K_2 * wcont_{deep}})$$

Percolated water is removed from each of the ten deep layers in proportion to their available water content, aw_i/aw_{deep}.

Total daily runoff (mm), $runoff_{total}$, is then calculated as

$$runoff_{total} = runoff_{surf} + runoff_{drain} + P_{deep\_base}$$

Updates to SOM daily decay rates

As described in Smith et al. (2014), the daily decay rates for each pool (C fraction: C_j, kgC m^{-2}) in the CENTURY-based SOM scheme depend on soil temperature and moisture:

$$\frac{dC_j}{dt} = -k_{j,\max} f(T_{\text{soil}}) f(W) f(S) \cdot C_j$$

where $f(T_{\text{soil}})$ is a dimensionless scalar in the range 0-1 related to soil temperature (T_{soil}, °C) and $f(W)$ is a dimensionless scalar in the range 0-1 related to soil moisture.

The updates to soil temperature and moisture described above influence daily decay rates through $f(T_{\text{soil}})$ and $f(W)$. T_{soil} is updated daily as the temperature calculated for the third 10 cm soil layer, i.e. at 25 cm depth – see **Figure A.1** above. Similarly, $f(W)$ is determined by the amount of unfrozen (available) soil water in the surface layers.

Observations suggest that daily decay rates below 0ºC are small but non-negligible, and decrease rapidly as the temperature decreases (Schaefer & Jafarov, 2006). $f(T_{\text{soil}})$ is now adjusted to reflect this fact, such that:

$$f(T_{\text{soil}}) = 0.0326 + 0.00351 \cdot T_{\text{soil}}^{1.652} - (T_{\text{soil}} / 41.748)^{7.19}$$

for T_{soil} >= 0ºC (i.e. unchanged), and

$$f(T_{soil}) = 0.0326 \,.\, Q10_{subzero}{}^{T_{soil}/10}$$

for $T_{soil} < 0$ºC, where $Q10_{subzero} = 200.5$, a value calculated as the average of 164 and 237 based on incubation of frozen soil samples (Mikan et al., 2002). **Figure A.3** shows the resulting temperature profile.

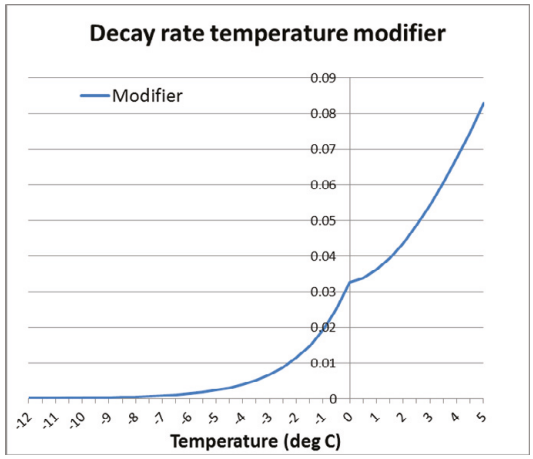

Figure A.3. Decay rate modifier based on temperature (ºC), $f(T_{soil})$, adjusted to account for decay below 0ºC.

Updated root distributions

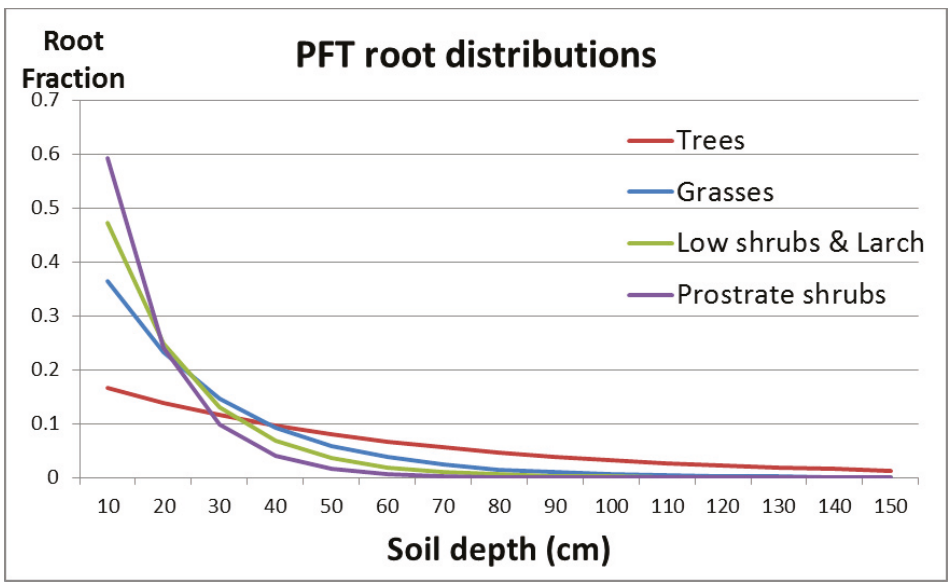

Figure A.4. PFT-specific root fractions for each 10 cm soil layer, parameterized following Jackson et al. (1996).

The model gives the option to specify how root distributions for each PFT are calculated. The root fractions in soil layer i, $root_i$, (1 to 15) can either be fixed and specified in the PFT descriptions as a one-dimensional array with 15 entries, or they can be calculated following

the parameterization described by Jackson et al. (1996) in their review of global root properties.

Jackson et al. (1996) parameterize the cumulative fraction Y (0-1) of roots to depth d (cm) using a single biome-specific parameter, β, as follows:

$$Y = 1 - \beta^d$$

Lower values of β result in a greater proportion of roots near the surface. Conversely, higher values of β result in a greater proportion of roots at depth.

Table A.2 shows the values used for each PFT or PFT class, and **Figure A.4** shows the resulting exponential root decrease with depth.

PFT or PFT class	B	**Fraction of roots in top 50cm**
Trees (except Larch (BNS))	0.9820	0.60
Larch (BNS)	0.9380	0.96
Grasses	0.9555	0.90
Low shrubs (< 50cm)	0.9380	0.96
Prostrate dwarf shrubs (< 20cm)	0.9140	0.99

Table A.2. Values of β used to parameterize the root fractions for each PFT or PFT class, and the resulting fractions in the surface layers.

2. High-latitude peatlands

Introduction

Here we describe the physical and biogeochemical process representations characterizing peatland ecosystems of the tundra and taiga biomes, as well as the PFTs characteristic of these ecosystems.

These developments and process descriptions were adopted from updates to the LPJ DGVM made by Wania et al. (2009a, 2009b, 2010), and are described more briefly in McGuire et al. (2012).

Peat stands and soil layers

A Stand object and associated Patch objects in the LPJ-GUESS C++ code represent the ecosystems on the fraction of each gridcell deemed to be a peatland. Differences to upland/mineral soils arise from the physical composition of the peat layers, from peatland-specific hydrological processes, peatland-specific PFTs, SOM decomposition and CH_4 emissions, described below.

Peatland soil temperature

For peatland patches we use the same process representations as described above to calculate soil temperature in each soil layer, each day. Layers (100 mm thick by default) are composed of fixed fractions of peat, and variable fractions of water, ice and air (**Figure A.2(b)**), with thermal properties given in **Table A.1**.

The peat layer profile is shown in **Figure A.5**. The uppermost three layers comprise the *acrotelm*, within which the water table can vary (see below), overlying 12 *catotelm* layers that are assumed to be permanently saturated (Wania et al. 2009a, 2009b). The porosity of acrotelm layers is 0.98 (*por_acro*), but the catotelm layers are assumed to be composed of older, more compact peat, with an assumed porosity (*por_caro*) of 0.92.

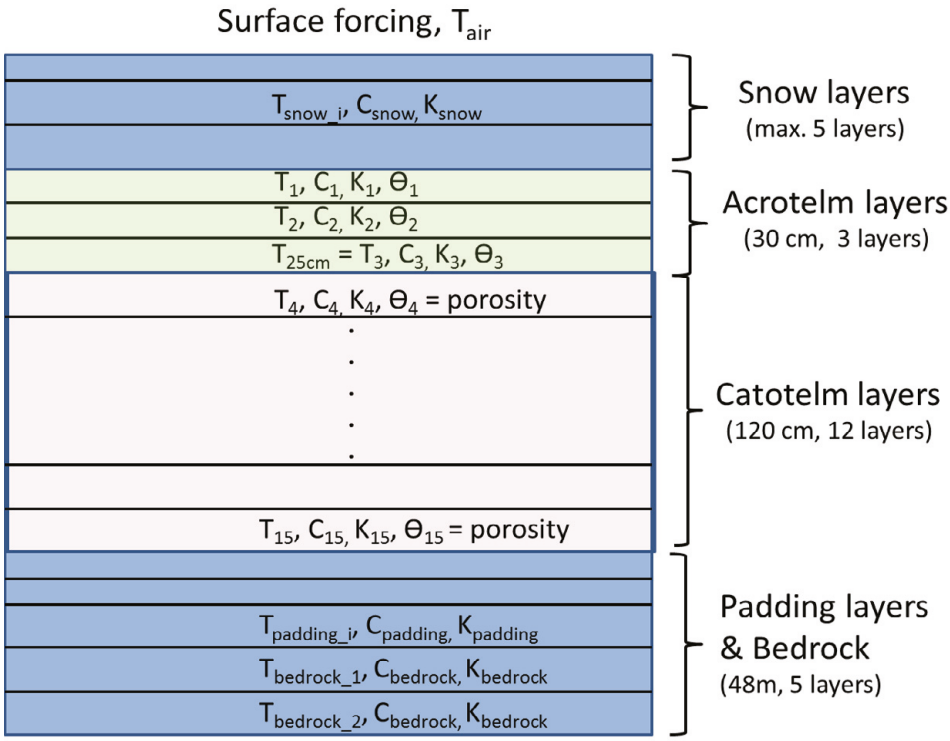

Figure A.5. Soil layer structure in peatland soils (not to scale). Up to 5 snow layers overlie 15 active soil layers, underneath which 5 padding layers extend to a total depth of 49.5 m. The uppermost three layers comprise the acrotelm, within which the water table can vary, overlying 12 catotelm layers that are assumed to be permanently saturated.

Peat hydrology

The hydrology of the acrotelm layers (upper 300 mm) of peat patches follows the description of Wania et al. (2019a, 2009b), first described in Granberg et al. (1999). The 12 catotelm layers are assumed to be permanently saturated, with no inflow or outflow, and water is added to these layers each day to enforce this if required, for example if water is taken up from these layers by PFTs with root access to the catotelm (only shrubs in the current configuration). Phase changes are described above, but are strongly influenced by the porosity and SOM content of peat layers (**Figure A.2 (b)**), with the result that summer soil temperatures are generally lower, and active layer depths shallower, in peat stands than they are in stands with mineral soils in the same gridcell.

The peat hydrology routine updates soil water content in the three acrotelm layers, and calculates the water table depth (wtd), where $0 <= wtd <= 300$ mm, i.e. wtd is positive below the surface, and no standing water is allowed.

The first step is to update the total volume of water (V) in the acrotelm each day, with the daily change calculated as follows:

$$\Delta V = run_{on/off} + rain\_melt - evap - aet_{acro} - runoff_{acro}$$

where *rain_melt* is the daily input to the patch as rainfall and/or snowmelt (mm), evap is the evaporation from the bare peat soil fraction, aet_{acro} is the transpiration (mm) from the acrotelm, calculated based on the peatland PFT root distributions in the acrotelm layers, and $runoff_{acro}$ (mm) is the runoff from the acrotelm. An optional, additional site-specific $run_{on/off}$ allows the user to add ($run_{on/off} > 0\ mm$) or to remove ($run_{on/off} < 0\ mm$) water from the acrotelm to mimic local site conditions, but is zero by default for global or regional applications.

In contrast to Wania et al., we do not combine transpiration and evaporation. Evaporation is allowed if *wtd* <= 200 mm and if the snow depth < 10 mm. If these conditions are satisfied, daily evaporation (mm) occurs from the non-vegetated (i.e. 1-FPC_{total}) fraction, *fevap*, of the acrotelm layers following:

$$evap = fevap * EET * PT * \frac{0.99}{1.02 + \exp(-1 * \frac{(-wtd + 98.7)}{22.6})}$$

where *EET* is the daily equilibrium evapotranspiration (mm), and *PT* = 1.32 is the Priestley-Taylor constant. (Assuming *fevap* = 1, *evap* then ranges from 0.96 * EET * PT when *wtd* = 0 mm (i.e. at the surface), to 0.011 * EET * PT when *wtd* falls to 200 mm.)

Daily runoff (mm) from the acrotelm follows Wania et al. (2009a, eqn.(24))

$$runoff_{acro} = \exp(-0.01 * wtd)$$

but is limited to days when the uppermost acrotelm layer (top 10 cm of peat) has $F_{ice} < 0.7$ (Granberg et al. 1999).

Updates to the water table depth (wtd)

The second step is to calculate the water table depth as a function of the total volume of water (*V*) in the acrotelm, following Wania et al (2009a), with a full motivation given by Granberg et al. (1999) who assume the soil water characteristics are linear in the top ("suction") interval 0-100 mm and constant below this depth to the lower limit of the acrotelm, i.e. 100-300 mm. We do not allow standing water in this version of the model, so wtd is first calculated as:

$$wtd = \sqrt{\frac{3(\mathrm{por_{acro}} * 300 - \mathrm{V})}{2 * \mathrm{a\_z}}}$$

which is used if for 100 >= wtd >= 0 (i.e. for a water table near the surface), but replaced by

$$wtd = 1.5 * (\mathrm{por_{acro}} * 300 - \mathrm{V})/(\mathrm{por_{acro}} - \mathrm{f\_surfmin})$$

if wtd > 100, where a_z = (por_{acro} - $f_{surfmin}$ / 100 (is the gradient in the top, 100 mm suction interval) and $f_{surfmin}$ = 0.25 is the minimum fractional water content at the surface in mm^3/mm^3.

To calculate the actual fractional water content (F_{water}) in each 100 mm sublayer in the acrotelm (needed for temperature calculations), wtd is first used to calculate the soil water profile, $\theta(z)$, in each 10 mm layer from the peat surface to the water table depth following the quadratic profile given by Granberg et al. (1999, eqn 1). First we define the surface water content, θ_{surf} as follows,

$$\theta_{surf} = \max\left(f_{surfmin}, por_{acro} - wtd * a\_z\right)$$

which ensures that $\theta_{surf} \geq f_{surfmin}$ with equality if wtd >= 100 mm.

For z <= wtd we use

$$\theta(z) = \min\left(por_{acro}, \theta_{surf} + \left(por_{acro} - \theta_{surf}\right) * \left(\frac{z}{wtd}\right)^2\right)$$

to calculate the the soil water profile, which results in a quadratic dependence from θ_{surf} at the surface to por_{acro} at wtd.

For 300 >= z > wtd $\theta(z) = por\_acro$, i.e. full saturation.

Once the soil water profile $\theta(z)$ in each 10 mm layer is known, F_{water} in each of the three 100 mm acrotelm sublayers is calculated by taking the average of the ten 10 mm layers it contains.

Table A.3 lists the new properties of the PFTs that can exist on peatland stands. Peatland PFTs inherit most properties from their parent groups, e.g. "grass" or "low shrub". We mostly follow the descriptions of Sphagnum mosses and C3 graminoids from Wania et al (2009b) appropriate for regional and global applications, building on work for mosses by Yurova et al. (2007). We also include low evergreen and deciduous shrubs (pLSE and pLSS, respectively) and a generic herbaceous cushion lichen moss PFT (pCLM), both of which are parameterized to prefer dry peatlands with low water table positions over an extended time (see below).

PFT	Maximum WTD for inundation (WTD_{inun}, mm)	Inundation duration (inund_days, days)	Has aerenchyma?	β	WTD Upper (WTD_U, mm)	WTD Lower (WTD_L, mm)	WTD photosynthesis stress scalar at WTD Lower
pLSE, pLSS	250	5	No	0.96	N/A	N/A	N/A
Sphagnum moss	50	15	No	0	0	280	0.3
C3 graminoids	N/A	N/A	Yes	0.9	10	100	0.0
pCLM	200	10	No	0.9	N/A	N/A	N/A

Table A.3. Peatland PFTs and important parameter values used in their definition. Columns are described in the text.

Peatland PFTs

Moss photosynthesis and leaf respiration

Following Wania et al. (2009b), mosses are assumed to have access to dissolved CO_2 from pore water in the acrotelm, so the CO_2 concentration used in the calculation of photosynthesis is calculated as a weighted mean of the atmospheric CO_2 concentration ($CO2_{atm}$) and CO_2 in the dissolved pore water with the previous year's average water table position (0 >= awtp >= –300) as the weighting factor. If the water table in a grid cell is high, mosses can access all of the acrotelm CO_2, but as the water table drops the CO_2 concentrations available to mosses decline to match the atmospheric CO_2 concentration when awtp = –300 mm.

Smolders et al (2001) give an average CO_2 concentration of 70 sites as 934 mimol L^{-1} so we calculate the moss CO_2 availability as follows

$$CO2_{moss} = \min\left(934, 934 + (934 - CO2_{atm}) * \frac{awtp}{300}\right)$$

Following Yurova et al. (2007), the scaling factor (BC) used to calculate the carboxylation capacity of rubisco (V_{max}) and the daily leaf respiration is set to BC = 0.03 for mosses, a value that can be compared to the leaf respiration fraction of maximum rubisco for C_3 plants and C_4 plants of BC = 0.015 and 0.02, respectively.

LAI limits

When the water table is near the surface, peatland PFTs are not shaded by trees or shrubs and are very productive as a result. An upper LAI limit of 2 m^2 m^{-2} is imposed on moss and graminoid PFTs by increasing shade mortality when the limit is exceeded. Their leaf and root carbon are then reduced consistent with that individual's allometric constraints and added to litter pools.

Assimilation stress due to water table fluctuations

Each day, after *wtd* has been updated, gross daily photosynthesis ($gC/m^2/day$) and leaf respiration ($gC/m^2/day$) are reduced in proportion to a stress factor [0, 1] if they become desiccated as the water table falls (applies only to mosses and graminoids), or subjected to inundation stress. Stress factors of 1 result in no stress, and values of 0 imply complete cessation of photosynthetic activity on that day. See Wania et al. (2009b – sections 2.1 and 2.2) for further details and motivation, but note that in contrast to Wania et al we apply these stresses daily.

Dessication stress

Though there is substantial specific variability, sphagnum moss productivity decreases when its water content decreases. As in Wania et al., we use water table position as a surrogate for moss water content. Similarly, graminoid productivity has been shown to drop when water table position decreases. We parameterize the fall in daily productivity for wtd values between the $\mathbf{WTD_U}$ and $\mathbf{WTD_L}$ limits set in **Table A.3** using a simple linear relationship between the dessication stress factor [0, 1] and wtd as follows:

$$Dessication_{stress} = 1 - (wtd - WTD_U) * (1 - stress_{scalar})/(WTD_L - WTD_U)$$

where $stress_{scalar}$ is the daily stress factor at wtd values below WTD_L. Above WTD_U, $Dessication_{stress} = 1$, i.e. no stress factor is applied. Thus, mosses are never fully dessicated since $stress_{scalar} = 0.3$ but experience stress as soon as the water table falls below the peat surface. In contrast, graminoid assimilation is fully restricted ($stress_{scalar} = 0.0$) when the water table drops below $WTD_L = 100$mm. We assume that $Dessication_{stress} = 1$ for pLSE, pLSS and pCLM.

Inundation stress

An inundation stress factor is applied to limit assimilation when there are anoxic conditions in the rooting zone. Unless specially adapted to these conditions (as is the case for C3 graminoids with aerenchyma allowing them to transport oxygen to the rooting zone and methane to the atmosphere – see below), plants can die in a matter of days (Wania et al. and references therein). To each peatland PFT we assign (**Table A.3**) both a maximum wtd threshold (WTD_{inun}) and the number of days (*inund_days*) the PFT can tolerate inundated conditions before assimilation is completely restricted.

Inundation stress is then calculated as follows:

$$Inundation_{stress} = 1 - \min(1, \frac{inund_{count}}{inund\_days})$$

Where $inund_{count}$ is the number of days for which wtd < WTD_{inun} i.e. when the water table is nearer the peat surface than the level tolerated by the PFT in question., Note that we restrict $inund_{count}$ to the range [0, *inund_days*+3] to allow plants to recover and again begin to assimilate carbon shortly after the water table drops below their WTD_{inun} limit. As the values in **Table A.3** indicate, even short periods with wet conditions affect short shrubs and the pCLM PFTs, which in practice restricts these PFTs to conditions typical of drier hummocks. In contrast, C3 graminoids are completely unaffected by inundation, and thrive in wetter or saturated conditions typical of peatland hollows. Mosses are an intermediate case, tolerating all but the wettest conditions.

SOM decomposition in peatland stands

SOM decomposition is treated slightly differently in peatland soils. As for mineral soils, daily decay rates for each CENTURY pool (C fraction: C_j, kg C m^{-2}) are determined by a prescribed maximum (base) decay rate ($k_{j,max}$; Parton et al. 2010; their Table 1) and dependencies on temperature, soil moisture and soil texture:

$$\frac{dC_j}{dt} = -k_{j,\max} f(T_{\text{soil}}) f(W) f(S) \cdot C_j$$

where $f(T_{\text{soil}})$ is a dimensionless scalar in the range [0, 1] related to soil temperature (T_{soil}, °C), with the modifications for sub-zero temperatures described above.

In contrast to mineral soils, peat soils are assumed to have negligible soil fractional silt plus clay content, (S), so $f(S)$ = 1 when $S = 0$, following Parton et al. (1993):

$$f(S) = 1 - 0.75 \cdot S$$

The biggest departure from mineral soil SOM decomposition relates to $f(W)$, the dimensionless scalar in the range [0, 1] related to soil moisture. Decomposition rates are slow in the wet and sometimes saturated conditions in the acrotelm, and especially so in the permanently saturated, anaerobic conditions in the catotelm (Frolking et al. 2001, 2010). Wania et al. (2009b) cite Segers (1998) to motivate $f(W)$ values in the range (0.37, 0.71), which is especially relevant for acrotelm conditions. We use $f(W) = R_{moist} = 0.4$ for carbon in the acrotelm here – see below.

To account for the extremely slow decomposition in the catotelm, we adopt an approach inspired by Wania et al. (2009b), who associated the intermediate carbon pool in LPJ-WHy DGVM with the acrotelm, and the slow carbon pool with the catotelm, and transferred carbon from the acrotelm to the catotelm once the soil carbon store had corresponded to that found in a fully developed acrotelm, i.e. a 30 cm deep peat layer with a carbon density of 25 kg C m^{-3}. This translates to a soil carbon amount across all pools of 7.5 kg C m^{-2}. However, we do not transfer carbon between the CENTURY pools in LPJ-GUESS (avoiding difficulties with N transfer). Instead we reduce $f(W)$ from values typical of the acrotelm ($f(W) = R_{moist} = 0.4$) once the total soil carbon pool (*soilC*) exceeds the same 7.5 kg C m^{-2} threshold, towards

decomposition moisture scalars for anaerobic conditions $f(W) = R_{moist\_anaerobic} = 0.025$ given by Frolking et al. (2001, 2010) and Ise et al. (2008), i.e. an order of magnitude smaller than acrotelm values. Thus, we assume:

$$f(W) = \begin{cases} R_{moist} & ; soilC \leq 7.5\ kgC\ m^{-2} \\ \dfrac{(7.5 * R_{moist} + (soilC - 7.5) * R_{moistanerobic})}{soilC} & ; soilC > 7.5\ kgC\ m^{-2} \end{cases}$$

A final assumption is that the passive SOM and slow SOM CENTURY pools (Smith et al. 2014) are always in the catotelm, and for those we always use $f(W) = R_{moist\_anaerobic} = 0.025$.

3. Methane dynamics

Introduction

Here we describe methane biogeochemistry, including production, oxidation, transport pathways and fluxes. Developments and process descriptions for methane dynamics in high-latitude peatland stands were adopted from LPJ-WHyMe (Wania et al. 2010), building on the development of LPJ-WHy (Wania et al. 2009a, 2009b) described above.

Low-latitude peatland stands – hydrology, PFTs and methane fluxes

The LPJ-WHy(Me) parameterizations are only valid for the carbon-rich peatlands found at high-latitudes. Peatland/wetland stands in gridcells with a latitude south of 40°N are treated more simply, and though they are not relevant for this paper, we describe them here for completeness.

Soil properties are assumed to be identical to the mineral soils in natural stands in the same gridcell. However, we keep their soil water content at field capacity by adding water each day as necessary, subtracting the input from runoff where possible. SOM decomposition is affected by assuming that the water-filled pore space is 100% and setting $\theta = \theta_{max}$ in the calculation of *f(W)*, the decomposition water scalar (0-1) (see above), where θ is the current soil water content and θ_{max} is soil water saturation capacity as a proportion of soil column depth. This gives *f(W) = 0.36*, approximately.

Only two PFTs are allowed to establish on peatland/wetland stands south of 40N, namely C_3 and C_4 grasses, which are parameterized identically to the C_3 and C_4 grass PFTs on natural stands apart from set bioclimatic limits (mimimum temperature of the coldest month for survival, *tcmin_surv* = 5 °C) to ensure that they do not establish on high-latitude peatland stands. Furthermore, since these PFTs are not shaded by trees they are very productive, so an upper LAI limit of 4 m^2 m^{-2} is imposed by increasing shade mortality when the limit is exceeded. Leaf and root carbon are reduced consistent with that individual's allometric constraints and added to litter pools.

Methane fluxes (F_{CH4}, gCH_4-C m^{-2} day^{-1}) are calculated using a simple parameterization introduced by Spahni et al. (2011). In non-peatland stands, decomposition results in heterotrophic respiration (R_h, release of CO_2) and transfer of C and N between pools, satisfying mass balance. In low-latitude peatland stands we assume that a set fraction of the carbon respired is instead released as carbon in methane, i.e.

$$F_{CH4} = r_{CH4toCO2inund} * R_h$$

Where $r_{CH4toCO2inund}$ = 0.027 is very close to the carbon conversion ratio value introduced by Spahni et al. (2011) to account for (low-latitude wetland) processes not yet treated in the model such as methane oxidation and transport. It can be used as a tuning parameter to match

global wetland emissions (approx. 180 $TgCH_4$ $year^{-1}$), but values of 0.03 +/- 0.02 are consistent with data from field studies compiled by Christensen et al. (1996). Once F_{CH4} has been calculated, R_h, the release of CO_2, is reduced by 2.7% to conserve carbon.

Methane fluxes in high-latitude peatland stands

The LPJ-WHyMe process descriptions for methane production, oxidation and transport described by Wania et al. (2010) are valid for the carbon-rich peatlands found at high-latitudes and are followed closely here. We do not reproduce all equations used, but rather refer to the equation numbers in Wania et al. (2010) where appropriate.

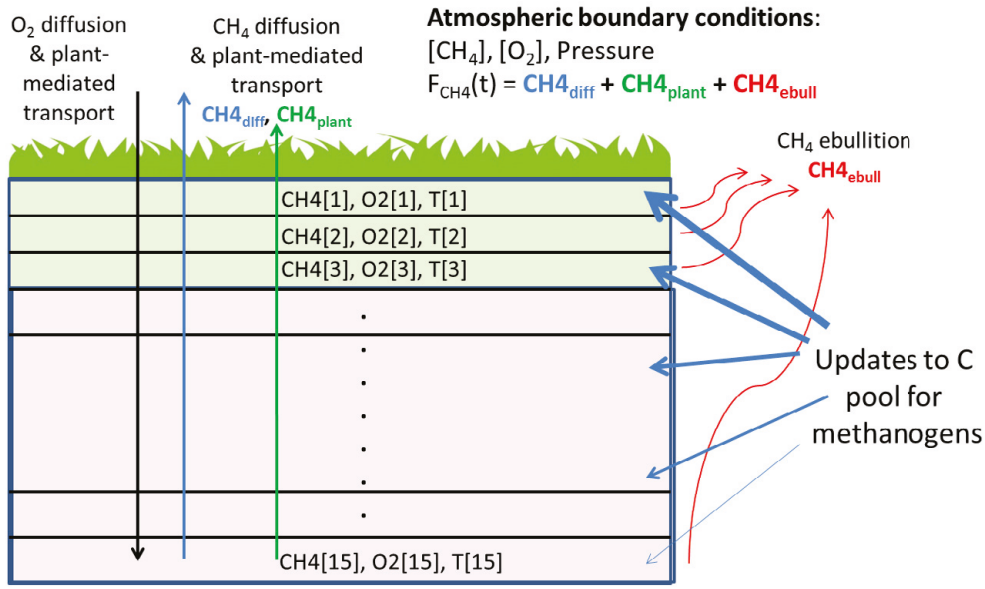

Figure A.6: Schematic representation of the methane model. The potential carbon pool for methanogens is allocated to each layer in proportion to root density, producing methane in each layer. Both oxygen and methane are diffused between the atmosphere and soil, with an additional transport pathway via aerenchyma when C3 graminoid PFTs are present. Methane in each layer is oxidised in the presence of oxygen. Bubble formation (ebullition) occurs once gaseous methane exceeds defined thresholds.

Methane production

In high-latitude peatland stands we assume that a set fraction of the carbon respired is made available as a potential carbon pool for methanogens (**Figure A.6**), but we assume that this pool is distributed vertically in the soil column in proportion to the degree of anoxia ($1 - F_{air(z)}$), and a vertical root distribution derived from fen and bog peat core data:

$$rootfrac\,(z) = C_{root} * e^{(z/\lambda_{root})}$$

Where C_{root} = 0.025 and λ_{root} = 25.17 cm are normalization constants. This distribution ensures that the majority of roots (60% approx.) are found in the acrotelm. The value of the root fraction in the bottom soil layer is chosen such that the root distribution sums to 1 across the 15 soil layers.

The daily production of methane in each layer is then given by

$$CH4_{prod} = \left(1 - F_{air}(z)\right) * rootfrac\,(z) * r_{CH4toCO2peat} * R_h \qquad \textbf{(Eq. A3.1)}$$

Where $r_{CH4toCO2peat}$ = 0.085 is a tuning parameter for the methane to carbon dioxide production ratio. Note that we set $CH4_{prod} = 0$ when $F_{water} < 0.1$, ensuring that there is no methane production in dry and/or frozen soils.

Gas diffusion

The diffusion of oxygen and methane between the soil and the atmosphere depends on the atmospheric concentrations of these gases, the air pressure, and the concentration of oxygen and methane in each layer. Numerical calculations of the diffusion process use the same Crank-Nicholson routine used for soil temperature calculations and daily updates to the molecular diffusivity of these gases (D_{CH4}, D_{O2}) in each layer. We follow Eqns. (8-12) to calculate D_{CH4} and D_{O2} in Wania et al. (2010) exactly, assuming polynomial dependence on layer temperature, *T(z)*, and strong dependence on both $F_{air}(z)$ and layer porosity.

The boundary conditions at interface between the top soil layer and the atmosphere are determined using the gas flux, J_{gas}, at the interface to update the concentration of dissolved gas in the top soil layer. Following Wania et al. (2010), Eqn. (4):

$$J_{gas} = -\varphi_{gas} * \left(C_{surf} - C_{equil}\right) \qquad \textbf{(Eqn. A3.2)}$$

where C_{surf} is the concentration of the gas in the top soil layer, and C_{equil} is the concentration of dissolved gas in equilibrium with the atmospheric concentration (partial pressure) of that gas. The so-called piston velocity, φ_{gas}, is updated daily for each gas (φ_{O2}, φ_{CH4}) using the polynomial dependence (of Schmidt numbers) on layer temperature, *T(z)*, following Wania et al. (2010), Eqns. (5-7).

C_{equil} (mol L^{-1}) is calculated using Henry's Law

$$C_{equil} = {}^{P_{partial}}\!/_{K_{Hinv}}$$

where $P_{partial}$ is the partial pressure of the gas in question (e.g. 1.7 * 10^{-6} atm for methane, 0.209 atm for oxygen), and K_{Hinv} is the Henry coefficient for that gas, given by Wania et al. Eqn. (8) and their Table 2.

Each day, J_{gas} above is used to update the dissolved gas content in the top soil layer before diffusion is calculated, resulting in fluxes of oxygen and methane into and out of the soil, respectively, though it is possible for methane to diffuse into the soil in small amounts if the concentrations at the surface are suitable (e.g. if the dissolved methane content in the top soil layer is very low). The resulting, daily flux of methane from diffusion, $CH4_{diff}$ (gCH_4-C m^{-2} day^{-1}), is one of three components of the total methane flux (**Figure A.6**).

Plant mediated gas transport

Both oxygen and methane can also be transported between the soil and the atmosphere through vascular plants that have adapted to survive in inundated conditions by developing aerenchyma, which are tissues that can transport oxygen to roots in anaerobic layers, but that can also transport methane to the atmosphere, potentially bypassing aerobic conditions near the soil-air interface. We assume that the flood-tolerant C_3 graminoid is the only PFT with aerenchyma, so plant-mediated transport of oxygen and methane can only occur when C_3 graminoids occur in a patch.

The gas flux calculated through vascular plants is assumed to be proportional to the cross-sectional area of tillers in each soil layer, where the term tiller refers to all the secondary shoots produced by grasses (Poaceae or Gramineae). Each tiller stem is segmented with its own two-part leaf. The total biomass of tillers, m_{tiller} (kgC m^{-2}) in a patch is determined by the carbon content of the flood-tolerant C3 graminoid leaves, taking into account phenological state (*phen*, 0-1), i.e. $m_{tiller} = phen * C_{leaf}^{graminoid}$. The density of tillers ($n_{tiller,}$ tillers m^{-2}) is then determined by dividing m_{tiller} by an observed average of tiller masses, 0.22 gC/tiller.

The cross-sectional area of an individual tiller is given by $\pi\ (r_{tiller})^2$, where r_{tiller} = 2.9 mm is an observed average of tiller radii. Finally, the tiller area in each soil layer at depth z is given by

$$A_{tiller}(z) = 0.5 * n_{tiller} * rootfrac\ (z) * \pi\ r_{tiller}^2$$

, where the factor of 0.5 is to account for the tiller porosity.

Plant-mediated transport from the atmosphere to each layer separately is calculated each day for oxygen and methane following Eqn. (14.2) above, assuming a rescaling of the gas diffusivity for that layer by $A_{tiller}(z)$.

The daily plant mediated flux of methane, $CH4_{plant}$ (gCH_4-C m^{-2} day^{-1}) (**Figure A.6**), is calculated by summing the plant-mediated methane fluxes from each layer.

Methane oxidation

A fraction, $f_{oxid,}$ of the oxygen transported to a soil layer by diffusion or mediated by plants (see above) is immediately used by roots themselves, or by other soil microorganisms. As in Wania et al. (2010), we assume that $f_{oxid} = 0.5$.

The remaining oxygen is used to oxidise available dissolved methane while maintaining stoichiometric balance:

$$CH_4 + 2\,O_2 \rightarrow CO_2 + 2\,H_2O$$

i.e. two moles of oxygen are needed to oxidise one mole of methane. The carbon in the oxidised methane is added to a CO_2 store to ensure carbon balance.

Methane ebullition

Citing Yamamoto et al. (1976), Wania et al. (2010, Eqn. 15) give the maximum solubility of methane at a given temperature ($T(z)$), S_B, as

$$S_B = 0.05708 - 0.001545 * T + 0.00002069 * T^2$$

with units of ml CH_4 ml^{-1} H_2O. The maximum number of moles of methane that can be dissolved ($CH4_{diss\_max}$) is calculated for each soil layer using the layer temperature and the total (atmospheric plus hydrostatic) pressure felt by gas in that layer in combination with the ideal gas law (Wania et al. 2010, Eqn. 16). After conversion to a maximum allowable dissolved mass of methane per layer, this limit is used to separate the methane in each layer into its dissolved and gaseous components, $CH4_{diss}$ and $CH4_{gas}$, respectively.

Ebullition, i.e. bubble formation, is assumed in a layer if volumetric gas content ($CH4_{gas\_vgc}$, m^3 m^{-3}) exceeds 0.15 * *bubble_CH4_frac*, where *bubble_CH4_frac* = 0.57 is a typical methane fraction of gas bubbles observed in the field. If bubble formation occurs, the total methane in a layer is reduced to 0.145 * *bubble_CH4_frac*, and the excess methane for that layer is emitted immediately to the atmosphere. Note that we set $CH4_{gas\_vgc} = 0$ when $F_{water} < 0.1$ or $T(z) < 0ºC$, ensuring that there is no methane ebullition in extremely cold and/or frozen soils.

The daily ebullition flux of methane, $CH4_{ebull}$ (gCH_4-C m^{-2} day^{-1}) (**Figure A.6**), is calculated by summing the ebullition fluxes from each layer.

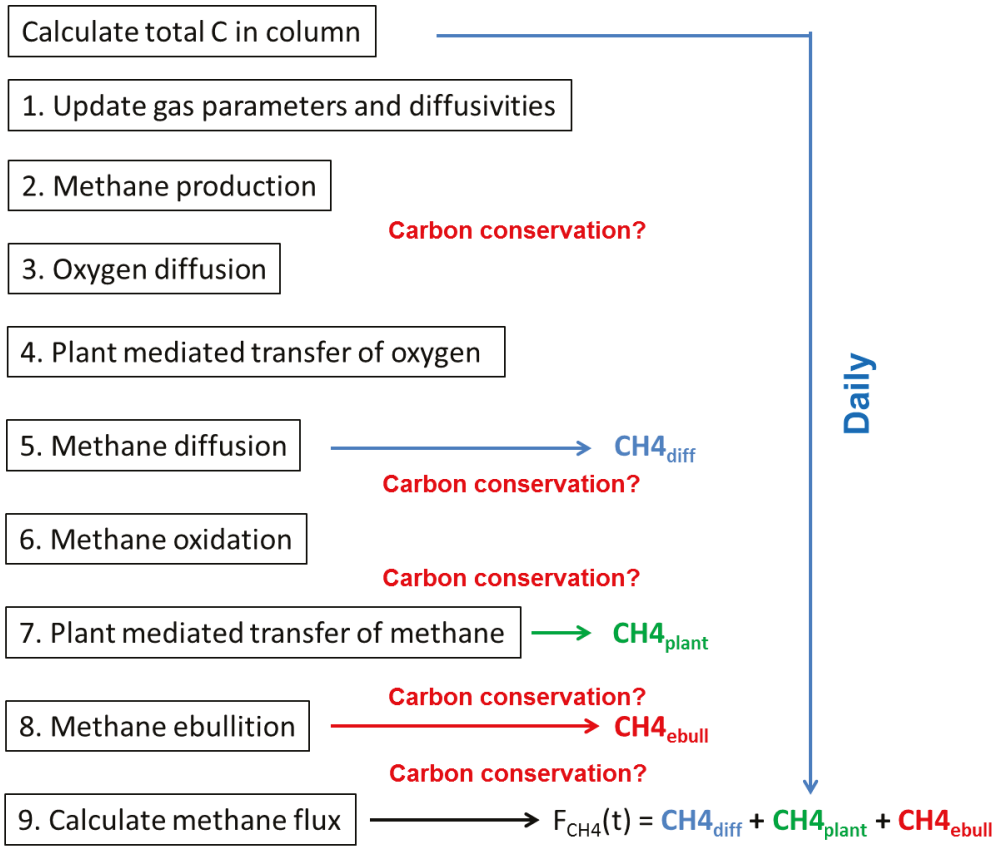

Figure A.7. Methane dynamics algorithm in LPJ-GUESS, showing the process descriptions considered and their order.

Total methane flux

Figure A.7 above shows the steps used to calculate the daily flux of methane (F_{CH4}, gCH_4-C m^{-2} day^{-1}) from high-latitude peatland patches:

$$F_{CH4} = CH4_{diff} + CH4_{plant} + CH4_{ebull}$$

Checks for carbon conservation are applied after each step that can potentially influence carbon content in soil layers in the form of carbon dioxide and methane. Since the daily production of methane in each layer, $CH4_{prod}$, is determined by daily heterotrophic respiration (R_h in Eqn. 14.1 above), we subtract F_{CH4} from R_h before saving the daily heterotrophic respiration. We assume that all carbon dioxide produced, e.g. through heterotrophic respiration or methane oxidation, is immediately released to the atmosphere.

References

Aerts, R., Verhoeven, J.T.A., & Whigham, D.F. (1999) Plant-mediated controls on nutrient cycling in temperate fenns and bogs, Ecology, 80 (7), 2170-2181.

Bonan, G.B. 2002 Ecological Climatology, Cambridge University Press

Chadburn, S., Burke, E., Essery, R., Boike, J., Langer, M., Heikenfeld, M., Cox, P., and Friedlingstein, P.: An improved representation of physical permafrost dynamics in the JULES land - surface model, Geosci.Model Dev., 8, 1493 - 1508, https ://doi.org/10.5194/gmd-8-1493-2015, 201

Christensen, T., Prentice, I., Kaplan, J., Haxeltine, A., and Sitch, S. (1996) Methane flux from northern wetlands and tundra - An ecosystem source modelling approach, Tellus B, 48, 652–661.

Clein, J. S., and J. P. Schimel, Microbial activity of tundra and taiga soils at sub-zero temperatures, Soil Biol. Biochem., 27(9), 1231-1234, 1995.

Ekici, A., Chadburn, S., Chaudhary, N., Hajdu, L. H., Marmy, A., Peng, S., Boike, J., Burke, E., Friend, A. D., Hauck, C., Krinner, G., Langer, M., Miller, P. A., and Beer, C.: Site-level model intercomparison of high latitude and high altitude soil thermal dynamics in tundra and barren landscapes, The Cryosphere, 9, 1343-1361, https://doi.org/10.5194/tc-9-1343-2015, 2015.

Frolking, S., Roulet, N. T., Moore, T. R., Richard, P. J. H., Lavoie, M., and Muller, S. D.: Modeling northern peatland decomposition and peat accumulation, Ecosystems, 4, 479-498, 2001.

Frolking, S., Roulet, N. T., Tuittila, E., Bubier, J. L., Quillet, A., Talbot, J., and Richard, P. J. H.: A new model of Holocene peatland net primary production, decomposition, water balance, and peat accumulation, Earth Syst. Dynam., 1, 1-21, https://doi.org/10.5194/esd-1-1-2010, 2010.

Fukusako, S. (1990) Thermophysical properties of ice, snow, and sea ice. Int. J. Thermophys., 11(2): 353-372. doi:10.1007/BF01133567

Gerten, D., Schaphoff, S., Haberlandt, W., Lucht, W. & Sitch, S. 2004. Terrestrial vegetation and water balance—hydrological evaluation of a dynamic global vegetation model. Journal of Hydrology 286: 249-270.

Granberg, et al. 1999 A simple model for simulation of water content, soil frost, and soil temperatures in boreal mixed mires. Water Resour. Res., 35(12), 3771-3782.

Ise, T., Dunn, A.L, Wofsy, S.C. & Moorcroft, P.R.: High sensitivity of peat decomposition to climate change through water-table feedback. Nature Geoscience volume 1, pages 763-766 (2008)

Jackson, R.B., Canadell, J., Ehleringer, J.R., Mooney, H.A., Sala O.E. & Schulze, E.D. 1996. A global analysis of root distributions for terrestrial biomes. Oecologia, Volume 108: 389–411

Jaehne, B., Heinz, G., and Dietrich, W.: Measurement of the diffusion coefficients of sparingly soluble gases in water, J. Geophys. Res., 92, 10767-10776, 1987.

Lawrence, D. M., and A. G. Slater, 2008: Incorporating organic soil into a global climate model. Climate Dynamics, 30, 145-160, doi:10.1007/s00382-007-0278-1.

McGuire, A. D., Christensen, T. R., Hayes, D., Heroult, A., Euskirchen, E., Kimball, J. S., Koven, C., Lafleur, P., Miller, P. A., Oechel, W., Peylin, P., Williams, M., and Yi, Y.: An assessment of the carbon balance of

Arctic tundra: comparisons among observations, process models, and atmospheric inversions, Biogeosciences, 9, 3185-3204, https://doi.org/10.5194/bg-9-3185-2012, 2012.

Mikan, C. J., Schimel, J. P., and Doyle, A. P. 2002. Temperature controls of microbial respiration in arctic tundra soils above and below freezing, Soil Biol.Biochem., 34, 1785–1795, 2002.

Schaefer, K. and Jafarov, E. 2016. A parameterization of respiration in frozen soils based on substrate availability Biogeosciences, 13, 1991 - 2001, https ://doi.org/10.5194/bg-13-1991-2016

Smolders, A. J. P., H. B. M. Tomassen, H. W. Pijnappel, L. P. M. Lamers, and J. G. M. Roelofs (2001), Substrate-derived CO2 is important in the development of Sphagnum spp., New Phytol., 152(2), 325- 332.

Spahni, R., Wania, R., Neef, L., van Weele, M., Pison, I., Bousquet, P., Frankenberg, C., Foster, P. N., Joos, F., Prentice, I. C., and van Velthoven, P.: Constraining global methane emissions and uptake by ecosystems, Biogeosciences, 8, 1643-1665, https://doi.org/10.5194/bg-8-1643-2011, 2011.

Tang, J., Miller, P. A., Persson, A., Olefeldt, D., Pilesjo, P., Heliasz, M., Jackowicz-Korczynski, M., Yang, Z., Smith, B., Callaghan, T. V., and Christensen, T. R.: Carbon budget estimation of a subarctic catchment using a dynamic ecosystem model at high spatial resolution, Biogeosciences, 12, 2791-2808, doi:10.5194/bg-12-2791-2015, 2015.

Wania, R., Ross, I., and Prentice, I. C.: Integrating peatlands and permafrost into a dynamic global vegetation model; 1, Evaluation and sensitivity of physical land surface processes, Global Biogeochemical Cycles, 23, doi:10.1029/2008gb003412, 2009a.

Wania, R., Ross, I., and Prentice, I. C.: Integrating peatlands and permafrost into a dynamic global vegetation model; 2, Evaluation and sensitivity of vegetation and carbon cycle processes, Global Biogeochemical Cycles, 23, doi:10.1029/2008gb003413, 2009b.

Wania, R., Ross, I., and Prentice, I. C.: Implementation and evaluation of a new methane model within a dynamic global vegetation model: LPJ-WHyMe v1.3.1, Geosci Model Dev, 3, 565-584, doi:DOI 10.5194/gmd-3-565-2010, 2010.

Wolf, A., Callaghan T.V., & Larson K. (2008) Future changes in vegetation and ecosystem function of the Barents Region. Climatic Change, 87:51-73 DOI 10.1007/s10584-007-9342-4

Yamamoto, S., Alcauskas, J. B., and Crozier, T. E.: Solubility of methane in distilled water and seawater, J. Chem. Eng. Data, 21, 78–80, 1976.

Yurova, A., Wolf, A., Sagerfors, J., & Nilsson, M. (2007) Variations in net ecosystem exchange of carbon dioxide in a boreal mire: Modeling mechanisms linked to water table position, Journal of Geophysical Research, 112, art. no. G02025, doi:10.1029/2006JG000342.

Zhang, W., Miller, P.A., Smith, B., Wania, R., Koenigk, T. & Doscher, R., 2013, Tundra shrubification and tree-line advance amplify arctic climate warming: results from an individual-based dynamic vegetation model. Environmental Research Letters 8: 034023.

Supplementary materials S2

'High latitude terrestrial ecosystems' contribution to global warming – will the Arctic be a sink or source of greenhouse gases in the 21st century?'

- Additional data, model evaluations and figures.

Table S2.1. Plant Functional Types (PFTs) simulated in the study.

PFT	Typical species
BNE Boreal needle-leaved evergreen tree	*Picea abies*
BINE Boreal needle-leaved shade-intolerant evergreen tree	*Pinus sylvestris*
IBS Boreal shade-intolerant broad-leaved summergreen tree	*Betula pubescens ssp. czerepanovii, Alnus glutinosa, Sorbus aucuparia, Populus tremula*
HSS Tall summergreen shrub	*Salix spp.*
HSE Tall evergreen shrub	*Juniperus communis*
LSS Low summergreen shrub	*Vaccinium myrtillus, Salix hastata*
LSE Low evergreen shrub	*Empetrum nigrum, Cassiope tetragona*
SPDS Prostrate summegreen dwarf shrub	*Salix Polaris*
EPDS Prostrate evergreen dwarf shrub	*Arctostaphylos uva-ursi*
GRS Boreal C3 graminoids	Gramineae
CLM Cushion-forb-lichen-moss-tunda	Cushion-forming *Caryopyhyllaceae* and *Saxifragacea,* lichens, mosses

Vegetation change

We calculated the treeline perimeter based on Gustafson et al. (2021) with the following routine. Any grid cell containing 30 % fractional projective cover or more of trees was classified as a forest. This limit has been used by other studies in the area (e.g. Van Bogaert et al., 2011) to determine the birch forest boundary. The treeline was then determined by first selecting grid cells classified as forest. Any grid cell with four or more neighbours fulfilling the 30 % cover condition criterion was classified as belonging to the forest. The perimeter of the forest was then determined by sorting out grid cells with four or five neighbours classified as forest. Grid cells with fewer or more neighbours were regarded as tundra or forest, respectively. Grid cells below the treeline were classified as forest in the analysis, and grid cells above the treeline were classified as tundra.

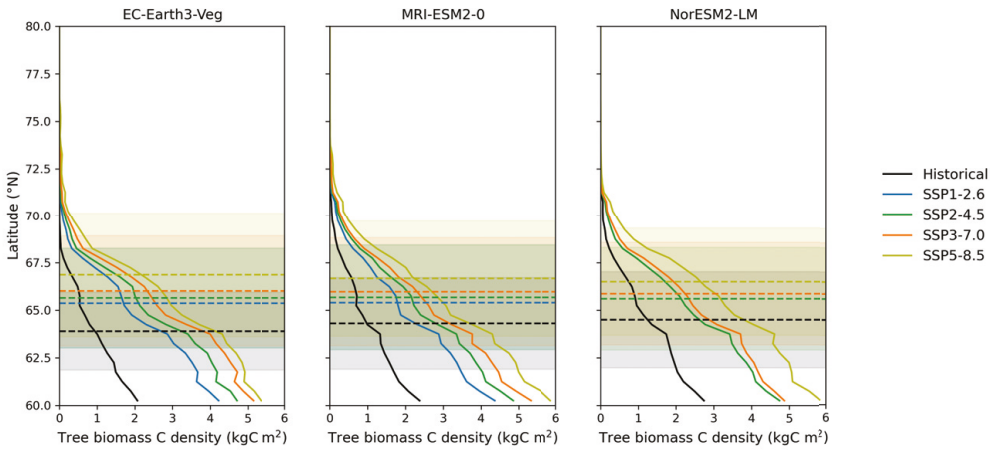

Fig S2.1 Latitudinally averaged tree biomass C density simulated by LPJ-GUESS under historical (2001-2010) and projected (2091-2100) time-slices for a) EC-Earth3-Veg, b) MRI-ESM2-0 and c) NorESM2-LM. Dashed horizontal lines denote the average treeline latitude in each simulation and the shaded area represents 1 standard deviation from the average. Treelines were estimated using the routine from Gustafson et al. (2021).

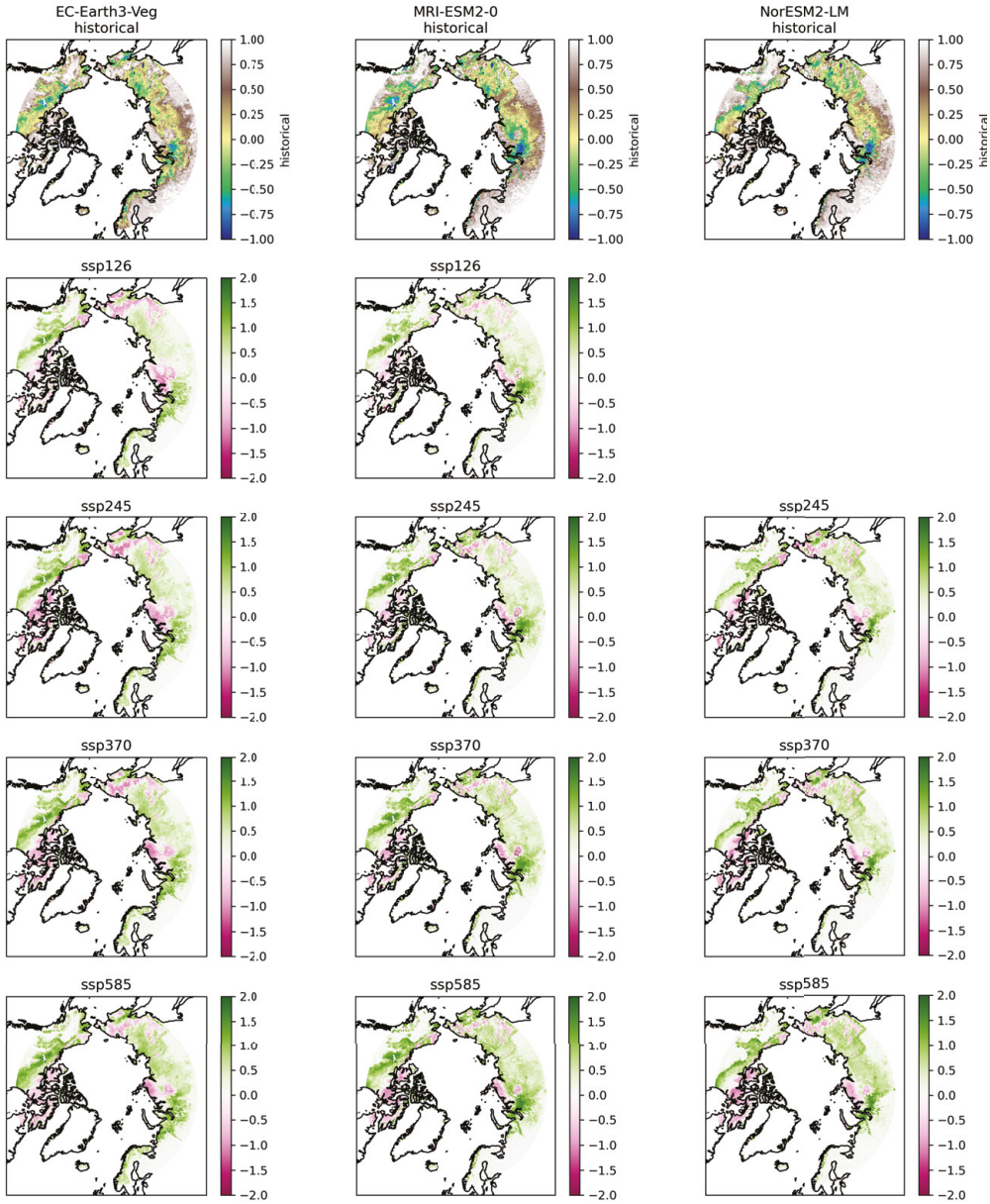

Fig S2.2 Difference in the normalised physiognomy index between models and scenarios. Top row displays absolute values from the historic (2001-2010) simulation, while scenarios show the difference to this value. The normalised physiognomy index denotes the relative abundance between herbaceous and woody vegetation. The index ranges between -1 (for fully herbaceous ecosystems) and 1 (for fully woody ecosystems). An increase in the index signals a shift towards a woodier – for instance increased abundance of shrubs – ecosystem.

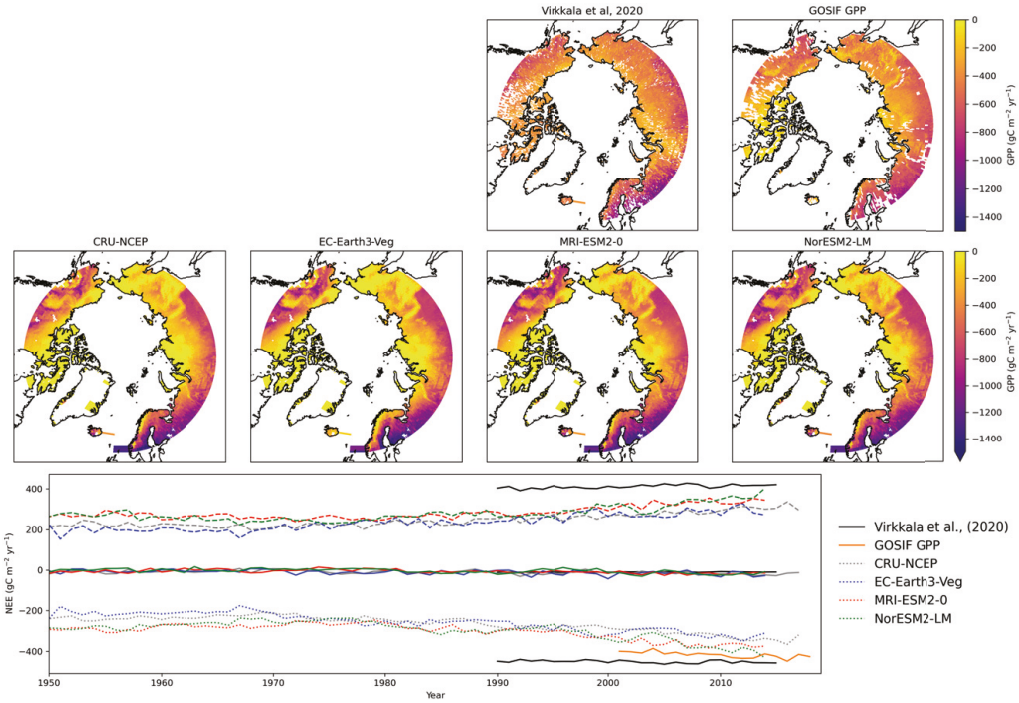

Fig S2.3. Evaluation of LPJ-GUESS simulated ecosystem carbon fluxes, gross primary productivity (GPP), ecosystem respiration (R_{eco}), and net ecosystem exchange (NEE). Data are compared against upscaled eddy covariance and chamber measurements by Virkkala et al. (2020) and sattelite inferred GPP from GOSIF (Li & Xiao, 2019).

CH_4 emissions

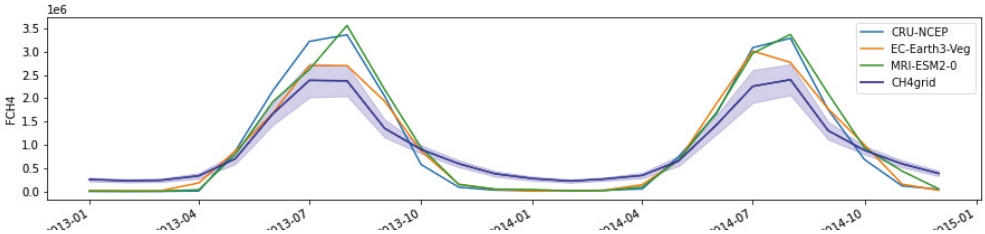

Fig S2.4. Seasonal time-series of LPJ-GUESS simulated CH_4 fluxes over the years 2013 and 2014 and upscaled eddy-covariance data from Peltola et al. (2019).

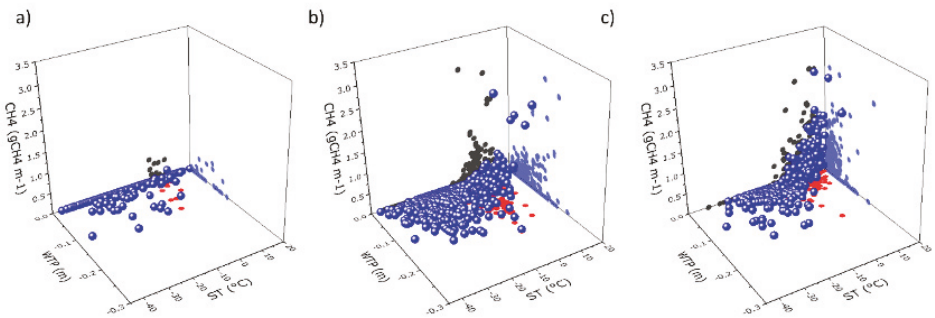

Fig S2.5 Relationship between water table depth (WTP), soil temperature at 25 cm depth (ST) and methane emissions (CH_4) at selected sites with low (a), average (b) and high (c) flood-tolerant graminoid PFT (WetGRS) presence. Each scatterpoint represent a monthly CH_4 for one gridcell.

N_2O emissions

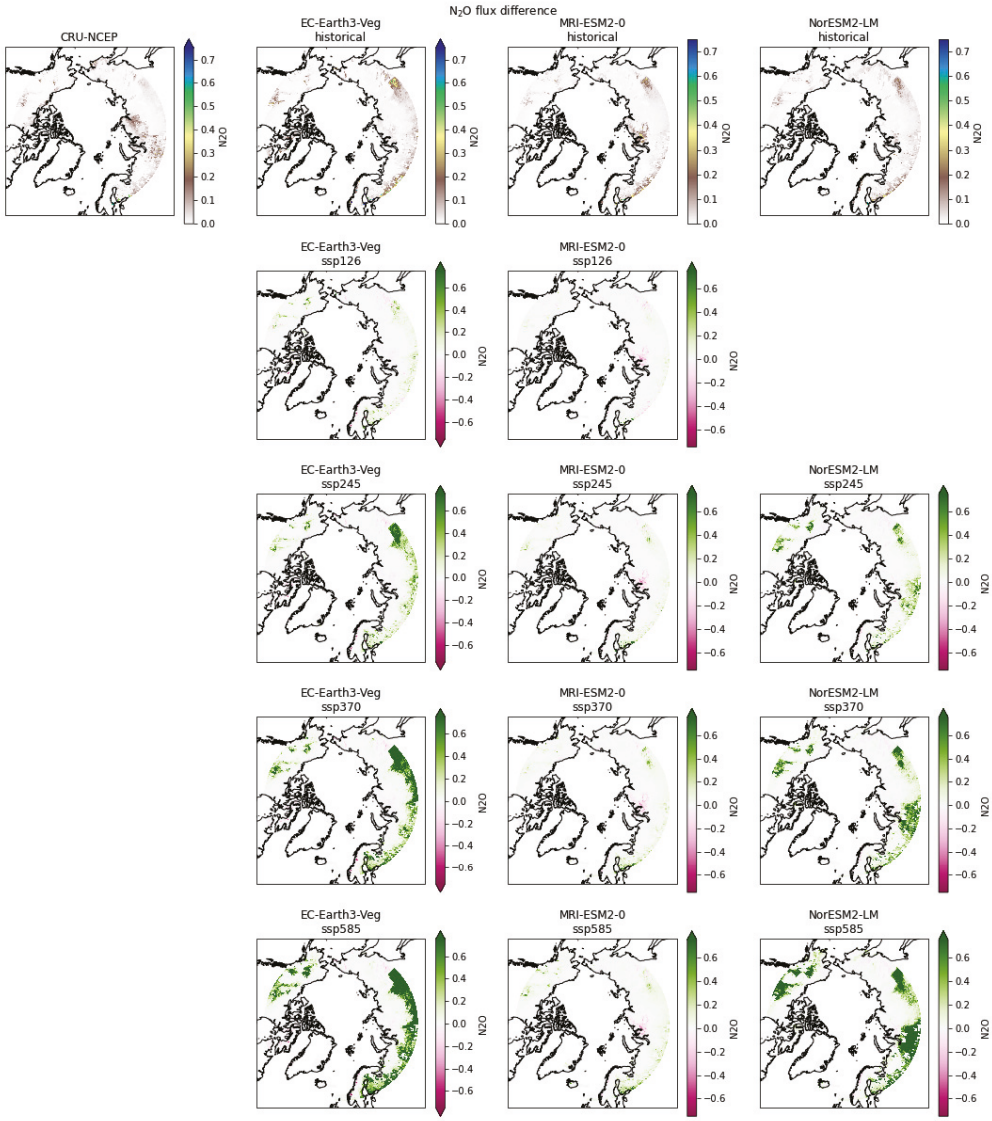

Fig S2.6 Spatial distribution of LPJ-GUESS simulated soil N_2O emissions. Top row displays absolute values from the historic (2001-2010) simulation, while scenarios show the difference to this value at the years 2091-2100.

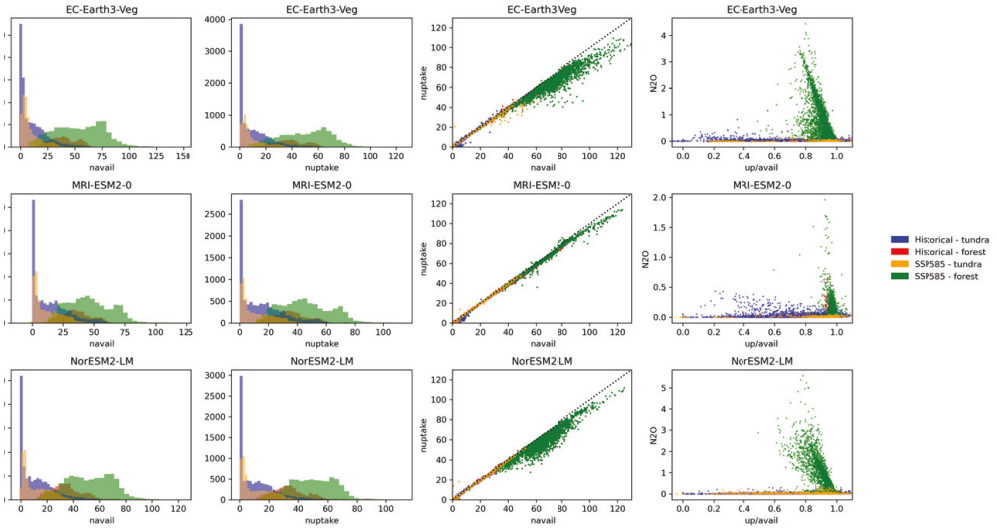

Fig S2.7. Simulated nitrogen availability and plant uptake and their ratios and relation to N_2O emissions between the historical period and SSP5-8.5 for the three included GCMs. Scatterpoints represent one gridcell in either the forest or on the tundra during the historical period 2001-2010 or the projected period 2091-2100 under SSP5-8.5. The nitrogen uptake is the total for the entire vegetation within the gridcell. The available nitrogen (navail) is the sum of average annual nitrogen sources (e.g., net mineralisation, biological fixation and deposition) and sinks (i.e., leaching).

Paper IV

High-latitude vegetation changes will determine future plant volatile impacts on atmospheric organic aerosols

Jing Tang[1,2,3*], Putian Zhou[4], Paul A. Miller[1], Guy Schurgers[3,5], Adrian Gustafson[1,6], Risto Makkonen[4,7], Yongshuo H. Fu[8], Riikka Rinnan[2,3]

[1.] Department of Physical Geography and Ecosystem Science, Lund University, Sölvegatan 12, SE-223 62, Lund, Sweden
[2.] Terrestrial Ecology Section, Department of Biology, University of Copenhagen, Universitetsparken 15, DK-2100, Copenhagen Ø, Denmark
[3.] Center for Permafrost (CENPERM), University of Copenhagen, Øster Voldgade 10, DK-1350, Copenhagen K, Denmark
[4.] Institute for Atmospheric and Earth Systems Research/Physics, University of Helsinki, 00014, Helsinki, Finland
[5.] Department of Geosciences and Natural Resource Management, University of Copenhagen, Copenhagen, Denmark
[6.] Center for Environmental and Climate Science, Lund University, Sölvegatan 37, 223 62, Lund, Sweden
[7.] Climate System Research, Finnish Meteorological Institute, Helsinki, Finland
[8.] College of Water Sciences, Beijing Normal University, Beijing, China

Corresponding author: Jing Tang (jing.tang@nateko.lu.se)

Abstract

Strong, ongoing high-latitude warming is causing changes to vegetation composition and plant productivity, modifying plant emissions of biogenic volatile organic compounds (BVOCs). In the sparsely populated high latitudes with clean background air, climate feedbacks resulting from BVOCs as precursors of atmospheric aerosols could be more important than elsewhere on the globe. Here, we quantitatively assess changes in vegetation composition, BVOC emissions, and secondary organic aerosol (SOA) formation under different climate scenarios. We show that warming-induced vegetation changes largely determine the spatial patterns of future BVOC impacts on SOA. The northward advances of boreal needle-leaved woody species result in increased SOA optical depth by up to 45%, causing a cooling feedback. However, areas dominated by temperate broad-leaved trees likely experience a large decline in monoterpene emissions and SOA formation, causing a warming feedback. We highlight the necessity of considering vegetation shifts when assessing radiative feedbacks on climate following the BVOC-SOA pathway.

Introduction

The northern high latitudes are experiencing stronger warming than the global average and this warming is reflected in observed changes to vegetation composition, plant traits, and plant productivity[1,2], which could profoundly alter the magnitude and composition of plant-emitted biogenic volatile organic compounds (BVOCs)[3]. Warming-induced permafrost thaw could release previously-locked nutrients, abating nutrient limitations, and thereby supporting enhanced plant productivity and growth in this region[4,5]. The predicted increase in atmospheric CO_2 concentrations might, however, inhibit BVOC production, so it remains unclear how BVOC emissions might respond to the fast and combined environmental changes in the high latitudes.

Constitutive BVOC emissions from plants are dominated by terpenoids[6] and the production of both isoprene and terpenes are expected to increase with temperature rise[3]. The production of terpenoids is coupled with plant photosynthesis, so factors such as the availability of water, nutrients, light, and atmospheric CO_2 concentrations that influence plant photosynthetic rates, can indirectly impact BVOC production. Plants growing under elevated CO_2 concentrations often show lower BVOC production (clear evidence for isoprene[7,8], but contrasting evidence for monoterpenes[9-11]). However, short-term laboratory studies have shown that the CO_2 inhibition of isoprene production decreases at higher leaf temperatures [12,13] and it is not well understood whether this pattern is sustainable in the long term. At landscape scales, BVOC emissions vary strongly in space, depending on the plant species composition as well as their emission profiles[14]. The projected increase in atmospheric CO_2 concentrations[15], together with rising temperatures, will likely stimulate plant productivity and thus, increase BVOC-emitting leaf biomass, while simultaneously imposing varying degrees of inhibition on BVOC production[16] and altering spatial distributions of high-latitude vegetation.

Plant-emitted BVOCs participate in a series of chemical reactions in the atmosphere. The atmospheric lifetimes of the dominant BVOCs range from minutes to hours[17] and the reactivity varies even within the same chemical group, depending on the structure of the molecule and the oxidant it reacts with. Once emitted to the air, these BVOCs, typically with the unsaturated functional groups, are susceptible to oxidation by hydroxyl radical (OH), ozone (O_3) and nitrate radical (NO_3) [18]. The major oxidation pathway of isoprene is via OH since they have similar diurnal variations. This pathway produces isoprene hydroxy peroxy radical (ISOPOO) which can either be further oxidized to form semi and extremely low volatility organic compounds (SVOCs and ELVOCs) to contribute to SOA formation [19], or undergo H-shift isomerization to recycle OH. The oxidation of isoprene by O_3 also produces SVOCs and ELVOCs, as well as other organic peroxy radicals and small molecules [18,19]. Similarly, the SOA precursors are also formed from the oxidation of monoterpenes by OH and O_3 but with about one order of magnitude larger yields than that of isoprene [19]. As NO_3 is photolyzed rapidly, the reactions of BVOCs with NO_3 mainly occur during nighttime, which produces organic nitrates, peroxy radicals and subsequent oxidized compounds [20]. When isoprene and monoterpenes coexist, isoprene can compete with monoterpenes to consume OH and produce relatively more volatile products than oxidation from monoterpenes. leading to suppressing SOA formation [21,22]. This suppression effect could be important to understand synergistic feedbacks of changing emissions of isoprene and monoterpenes in future high-latitude climate.

In the high-latitude atmosphere, anthropogenic sources of aerosols are generally lower than in more densely inhabited regions[23,24] and the Arctic is known to have low ambient concentrations of CCN[23,24]. Thus, the warming-induced changes in BVOC emissions may provide stronger feedbacks to the high-latitude climate system, through modulation of atmospheric SOA and CCN concentrations, than elsewhere on the globe. Regional and site-specific studies have revealed that concentrations of biogenic aerosols show a clear increase with temperature[25-27] and have further pointed to the significance of these biogenic aerosols for climate feedbacks. Nevertheless, the biochemical and biophysical BVOC-mediated feedbacks on climate have been

under-assessed in the high latitudes[23]. Furthermore, previous estimates of high-latitude BVOC emissions are highly uncertain[6,28], due to the scarcity of observation-based emissions data and/or underrepresented plant variations in large-scale modelling, particularly in the tundra biome[3]. Here, we quantitatively assess future BVOC dynamics in the Arctic and boreal regions, elucidate key processes driving the trends in BVOC emissions, and illustrate the contribution of BVOC emissions to our climate system through SOA-CCN-climate feedbacks.

Results

Future changes in isoprene and monoterpene emissions

We explore both historical and future emissions of the dominant BVOCs, isoprene and monoterpenes, using a dynamic vegetation model, LPJ-GUESS[29]. The model, driven by climate data, simulates plant competition and vegetation composition change, as well as plant and soil biochemical processes in response to changing environmental conditions (see Methods). Observation-based BVOC emission rates and temperature response curves, together with a detailed representation of tundra plant functional types (PFTs) in LPJ-GUESS have allowed us to simulate BVOC emissions for the Arctic area (defined here as north of 60 ^{o}N)[3,30]. Details of model evaluations over different historical periods can be found in the Supplementary Figs 1-3 and Supplementary Table 1.

For the future period (2015-2100), we select climate scenarios from three General Circulation Models (GCMs), following five different Shared Socioeconomic Pathways (SSPs) under the CMIP6 framework[15], and implement bias-correction of these climate predictions for temperature, precipitation, and radiation before using them to drive LPJ-GUESS (see Methods). Comparing with the emission scenarios of Representative Concentration Pathways (RCPs) used in CMIP5, the SSPs in CMIP6 comprise five narratives to describe socioeconomic trends, and both how and if climate change mitigation efforts can reach the radiative forcings in the RCPs. The resulting scenario names are combination of the SSP narratives with the targeted RCP's radiative forcing. The resulting 15 scenarios (see overview of the scenarios in the Supplementary Table 2 and future anomalies of temperature, precipitation, and radiation in the Supplementary Fig. 4) represent five levels of varying greenhouse gas projections and three GCMs with different climate sensitivities in the study region (tundra and boreal biomes based on RESOLVE Ecoregions 2017[31]). We select these 3 GCMs from the full set of CMIP6 GCMs to briefly represent high, median, and low projected temperature increases over the study region. The average temperature increases by year 2100 range from 1 °C to 12 °C across these 15 scenarios and the warmer it gets, the stronger the increase in annual precipitation, with a maximum projected increase of 50 % by the end of this century (Supplementary Fig. 4). These 15 scenarios also show both increases and decreases of incoming shortwave radiation. We use the LPJ-GUESS outputs driven by these 15 climate scenarios (hereafter "standard runs") to explore future BVOC emissions.

We simulate a clear increase in the annual, areal total emissions of isoprene (74-120% by the year 2100) and monoterpenes (11-36% by the year 2100) for the runs driven by the CanESM5 output (highest projected temperature increases) under different SSPs (Fig. 1d, 1h). For the simulations driven by scenarios with a more moderate temperature increase (such as MRI-ESM2_0 with an average temperature increase of 2.8 °C across 5 SSPs and GFDL-ESM4 with an average temperature increase of 2.4 ^{o}C across 5 SSPs, see temperature anomalies in Supplementary Fig. 4a), total isoprene emissions show moderate increases (Fig. 1d) and averaged total monoterpene emissions show clear decreases (see solid lines in Fig. 1h). We found that that spread in modelled total isoprene emissions across the three chosen GCMs is greater than the spread seen across the 5 SSPs. For the monoterpenes, the spread across SSPs is more comparable to that across GCMs.

Spatially, isoprene emissions significantly increase in many regions, with the largest increasing trends simulated in regions where the dominant PFTs shift strongly (Fig. 2). The projected shifts include the replacement of boreal needle-leaved evergreen trees with broad-leaved deciduous trees (shift from PFT BNE to PFT IBS in Fig. 2) in northern Canada and western Russia, and a northward movement of boreal needle-leaved evergreen trees replacing herbaceous vegetation and shrubs in eastern Russia, Alaska, and north-eastern Canada (see PFT BNE in these regions in Fig. 2b-e). In the High Arctic, shrub abundance increases strongly, especially under CanESM5 SSP585 (see PFT HSS in Fig. 2 and latitudinal fractions of each PFT in Supplementary Fig. 7b). These modelled PFT shifts are in agreement with predictions based on different approaches (such as the machine-learning based ecological niche model[27], and analysis of long-term satellite and air photos[32]) and consistent with paleo-records of warm periods[33].

Compared with the increasing trends seen under SSP119, the modelled isoprene emissions under SSP585 in Scandinavia show decreasing trends (Fig. 1), which might be linked to the unchanged dominant PFTs, in combination with strong CO_2 inhibition of isoprene production[34], because the atmospheric CO_2 concentrations reach up to 1100 ppm by the end of the 21st century. For monoterpenes, the largest increasing trends occur in

northern Canada and Russia (mainly for SSP585), where boreal needle-leaved evergreen (in Canada) and needle-leaved deciduous (in Russia) trees with relatively high emission capacities replace the isoprene-emitting grass PFTs (GRT and C3G) in the simulations. In the southernmost study regions, we observe a clear decrease in monoterpene emissions, especially under SSP585 (Fig. 1f), as broad-leaved, isoprene-emitting, deciduous trees replace monoterpene-emitting boreal needle-leaved trees. These unfavourable vegetation shifts for monoterpenes accompany high atmospheric CO_2 increases in this climate scenario. In general, the predicted changes in isoprene and monoterpene emissions vary among climate scenarios (Fig. 1), in agreement with global studies[35], and show regionally varying responses linked to shifts in the dominant vegetation.

Key processes regulating future BVOC trends

Changing temperature and atmospheric CO_2 concentrations can exert direct impacts on BVOC synthesis[8,36,37]. In addition, isoprene and monoterpene synthesis is linked to plant photosynthesis[34,38,39]. Atmospheric CO_2 concentrations, soil nitrogen, water availability, and climate conditions not only alter photosynthetic rates, but also vegetation dynamics (including plant growth and competition, migration, and mortality) indirectly influencing BVOC emission magnitudes and composition. To disentangle the key drivers of BVOC emission changes, we examine the individual effects of climate, vegetation changes, atmospheric CO_2 concentrations, and nitrogen (N) availability using a set of factorial simulations based on climate forcing data from CanESM5's outputs with the lowest and highest emission scenarios (i.e., SSP119 and SSP585, respectively). The modelled temperature changes from these two scenarios (2.6 and 6.4 °C temperature increases averaged over 2015-2100, respectively) are representative of the range of temperature changes across the 15 scenarios. We design four factorial experiments, in each of which we change one process at a time: (1) Ecosystem dynamics unaffected by CO_2, represented with a constant CO_2 concentration (using the value for 2014) for the future period (hereafter, termed "noCO2"); (2) BVOC dynamics unaffected by CO_2 inhibition, represented with constant CO_2 inhibition impacts on BVOC production (using the inhibition level for 2014) for the future period (noCO2Inhibition); (3) A removal of N limitation, achieved by adding 50 kg N/ha/yr to the annual nitrogen deposition input fields in the future period (noNlim). This N addition corresponds to what has been implemented in forest N fertilization trials in Davies-Barnard, et al. [40]; and (4) Ecosystem dynamics unaffected by climate change, achieved by using the monthly averages of climate drivers from the period 2005-2014 for driving ecosystem processes in the future period (noVegDym). In this simulation, the predicted temperature changes still affect BVOC production, but we remove future climate impacts on vegetation dynamics. Subsequently, we calculate the differences between the standard and factorial simulations (See Table 1) to tease apart the relative importance of CO_2 fertilization, CO_2 inhibition on BVOC production, N limitation, and vegetation changes as determinants of spatial and temporal patterns of future BVOC emissions (Fig. 3).

Under the low CO_2 emission scenario (CanESM5 SSP119), the overall positive trend in isoprene emissions is largely driven by vegetation changes (Fig. 3a, e). The small increasing emission trends by CO_2 inhibition in both isoprene and monoterpene emissions are driven by decreasing atmospheric CO_2 concentrations towards the end of the century in this scenario (see CO_2 inhibition in Fig. 3c, m). Overall, the impacts from CO_2 fertilization and N limitation are limited for both isoprene and monoterpenes under CanESM5 SSP119 (Fig. 3b, d, l, n).

Under the high CO_2 emission scenario (CanESM5 SSP585) with associated stronger warming and large increases in N deposition, the positive trends in isoprene emissions are associated with CO_2 fertilization of photosynthesis and vegetation changes, although high CO_2 concentration simultaneously inhibits BVOC production (Fig. 3g, h, j). Climate warming-induced vegetation changes promote the overall positive trend in isoprene (Fig. 3j), but not in monoterpene emissions, as seen in the simulation of positive and negative impacts under CanESM5 SSP585 (Fig. 3t). The impacts from N limitation are again, very small, and likely linked to the increased N deposition during this century in CanESM5 SSP585 and increased sources of mineral N from warming soil.

We also conduct the same factorial experiments under climate scenarios of GFDL-ESM4 SSP119 and GFDL-ESM4 SSP585, and we see similar patterns of important controlling processes (see Supplementary Figure 8) for future isoprene and monoterpene emissions.

BVOC impacts on the regional atmosphere

The modelled high-latitude BVOC emissions, together with vegetation status (including leaf area index, LAI, and vegetation cover fraction) from the years 2009 and 2100 from standard runs driven by CanESM5 SSP119 and CanESM5 SSP585 are fed into the global chemistry transport model, version 5 (TM5, Bergman, et al. [41]). To provide all of the input data needed at a global scale and to ensure that the changes to the atmospheric chemistry originate from high-latitude changes only, the emission data, LAI, and vegetation cover south of the study domain were all set to values from the same standard LPJ-GUESS global run from the year 2009. Furthermore, for the year 2100, we use LPJ-GUESS outputs from standard runs of CanESM5 SSP585 and CanESM5 SSP119,

as well as the outputs from different factorial experiments as inputs to TM5. In the result below, we present the TM5 outputs from two of the factorial experiments: i.e., noVegDym and noCO2Inhibition, where their associated processes contribute most to the simulated BVOC trends based on the averaged values and numbers of grid cells with significant trends (see the 3rd and 5th columns in Fig. 3, i.e., the trends from the processes of CO_2 inhibition and Vegetation changes) driven by CanESM5 SSP585 and CanESM5 SSP119 (see Methods for the detailed setup for TM5). TM5 is used to quantify the impacts of isoprene and monoterpene emissions on surface SOA concentrations (SOA_{surf}), SOA optical depths at 550 nm ($OD550_{SOA}$), and aerosol optical depths at 550 nm ($OD550_{aer}$). Aerosol optical depths describe how much the light penetration through the atmosphere is prevented by aerosols. 550 nm is at or near the energy peak of the solar radiation spectrum, which makes it a good representative of the incoming shortwave radiation spectrum, as applied in previous studies (e.g.,[42,43]). $OD550_{SOA}$ is the optical depth considering only the SOA component, while $OD550_{aer}$ is the optical depth considering all the aerosol components including SOA, sulfate, methane sulfonic acid, ammonium nitrate, black carbon, primary organic aerosols, sea salt, and mineral dust.

Our results demonstrate the important role of climate change-driven vegetation changes in regulating the spatial patterns of BVOC impacts on regional atmospheric aerosols. The increased BVOC emissions have largely contributed to the increase in SOA_{surf} for a major part of the study region, with a smaller area of increase for CanESM5 SSP119 than for CanESM5 SSP585 (Fig. 4g & Fig. 5g). Under both SSP scenarios, we see up to a 2.7-fold increase of SOA_{surf} in northern Canada and Russia in the standard run. The simulation without vegetation responses to climate change (noVegDym) results in a considerably lower increase in SOA_{surf} (Fig. 4h and Fig. 5h). The standard runs with vegetation changes show stronger increases over a larger area in aerosol optical depth ($OD550_{SOA}$ and $OD550_{aer}$, 41% and 4.9% increase under CanESM5 SSP119, Fig. 4 j & m, and 29 % and 4.1% increase under CanESM5 SSP585, Fig. 5 j & m, respectively). Without vegetation changes (noVegDym), only a limited increase of $OD550_{SOA}$ and $OD550_{aer}$ in a small region in the central and eastern Canada is simulated. As the changes in $OD550_{SOA}$ and $OD550_{aer}$ affect the reflection and absorption of visible light in the atmosphere, an increase in these values means that a reduced amount of radiation is received at the surface.

The strong spatial linkages that we show for vegetation shifts, BVOC dynamics, and SOA/aerosol changes are not captured when using static vegetation distributions for future conditions[6]. Under the warmest scenario (i.e., CanESM5 SSP585), the widespread replacement of boreal needle-leaved trees with broad-leaved deciduous trees (Fig. 2e) in Sweden and Finland clearly contributes to the local reductions of SOA_{surf} and optical depths (Fig. 5 g, j, m). When future CO_2 inhibition of BVOC production is excluded, TM5 estimates up to 10-fold increases in SOA_{surf} (mainly in the high latitudes), up to a 1.2-fold increase in $OD550_{SOA}$, and up to an 18% increase in $OD550_{aer}$ in the year 2100, as compared to 2009, under CanESM5 SSP585. Similar spatial patterns but with slightly smaller magnitudes are observed when CO_2 inhibition is excluded for monoterpenes (see Supplementary Figure 11). Under SSP119, the effects of atmospheric CO_2 on regional SOA and aerosols via BVOCs are limited. Our results emphasize the importance of monoterpenes in influencing SOA and aerosol yields[41,44], and show that we need to understand whether CO_2 inhibition affects monoterpene production in high-latitude plants similarly to those plants that were studied in the literature [8,36,45].

The simulated changes in BVOCs and SOA lead to increases in CCN concentrations at a supersaturation of 1.0 % near the surface, mainly for the Arctic region (See Fig. 4 p-r, Fig. 5 p-r), which indicates the potential for enhanced formation of low-level clouds. CCN (1.0 %) represents the number concentration of particles larger than 50 nm in diameter, so it is sensitive to new particle formation and growth, which are affected by the gas precursors, ELVOCs (extreme low volatile organic compounds) and SVOCs (semi-volatile organic compounds)[19]. There is a northward shift of increased CCN (1.0%), suggesting the potential for more clouds at high latitudes and fewer at mid latitudes. Without CO_2 inhibition under CanESM5 SSP585, CCN over Greenland and eastern Canada increased by 16 % (Fig. 5r), which highlights the strong expected impacts of CO_2 inhibition on BVOC emissions. Increased low-level cloud cover can have both warming (re-emitting received longwave radiation from the ground) and cooling (scattering and reflecting shortwave radiation) feedbacks on the climate.

Based on the modelled changes in SOA and aerosol optical depth (AOD) between the years 2100 and 2009, we further estimate the potential effects on aerosol radiative forcing among the standard, noVegDym, and noCO2Inhibition runs (see Supplementary Table 3). Based on parameters from three different references [26,43,46], we find that the radiative forcing estimates vary greatly depending on the method used. Yli-Juuti, et al. [26] derived the relationships between temperature, aerosol loading, and radiative forcing feedback based on summertime (July-August) field measurements in a boreal ecosystem, and based on this study, the differences in the estimated areal averaged radiative forcing between standard and noVegDym runs are smaller than the estimations from the other two studies [43,46], with parameterizations derived from annual data at the global scale. The overall cooling feedbacks are strongest for the noCO2Inhibition run following the CanESM5 SSP585 scenario. The strongest increase and decrease in radiative forcing in the standard run are -2.09 and 0.79 W m^{-2}, respectively, and these

two values are much weaker in the noVegDym run (which are -1.52 and 0.54 W m^{-2}, correspondingly), highlighting the importance of warming-induced vegetation changes on regulating local climatic impacts. Under CanESM5 SSP119, the changes in areal averaged radiative forcing over July and August are -0.44, -0.34, and -0.43 W m^{-2} for standard, noVegDym, and noCO2Inhibition simulations, respectively. The strongest cooling feedback can be seen with warming-induced vegetation changes included in the standard run under this climate scenario.

Discussion

Our results illustrate that vegetation changes in a warmer climate play a crucial role in shaping future BVOC feedbacks to atmospheric chemistry and climate. Most previous assessments of feedbacks between the land surface and atmosphere in the high latitudes, that involve vegetation changes, have focused on changes in surface albedo[27,47] and increases in atmospheric water vapour[48], but our study clearly demonstrates the strong and regionally diverse feedbacks of vegetation changes on our climate through the BVOC-SOA pathway.

The warming-induced widespread increase of broadleaved deciduous trees at the expense of boreal evergreen needle-leaved trees in the boreal region suppressed the emissions of monoterpenes and thereby, SOA formation, causing a regional warming feedback (up to 0.79 W m^{-2} for summer months driven by CanESM5 SSP585 standard run). In the High Arctic, the increased abundance of shrubs and the northward advance of boreal needle-leaved trees in northern Canada and Siberia contributed to an increase of surface SOA, resulting in an increase of up to 45% in SOA optical depth and likely leading to a cooling feedback (with the strongest cooling of -2.25 and -2.09 W m^{-2} for standard runs driven by CanESM5 SSP119 and SSP585, respectively). Currently, the Arctic features a lack of aerosol particles for cloud formation[24] and the northward shifts of vegetation bring in a new, important aerosol source: plant-emitted BVOCs. This 'new' source of aerosols might enhance cloud formation in this region, as we can see an overall increase of CCN under different runs, and can particularly increase the low-level cloud formation in the Arctic[23]. During the growing season, the enhanced cloud cover lead to cooling feedbacks through scattering shortwave radiation that counteract warming feedbacks associated with re-emission of longwave radiation received from the land surface[23,24]. Our estimations showed the overall cooling feedback from warming-induced changes in BVOC and SOA (negative aerosol radiative forcing, -0.44 and -0.45 W m^{-2} for CanESM5 SSP119 and CanESM5 SSP585, respectively, when comparing the year 2100 and the year 2009) during summer months, and these values are comparable to the effective radiative forcing (ERF) caused by aerosol-radiation interactions over the industrial era globally (-0.3 W m^{-2} for 1750-2014)[49]. At an annual scale, the estimated aerosol radiative forcing (-0.04 and -0.05 W m^{-2} for CanESM5 SSP585 and CanESM5 SSP119, respectively) are of a similar magnitude to the impacts from the stratospheric water vapour (0.05±0.05 W m^{-2}, [49]). We note that our simplistic methods of estimating aerosol impacts on radiative forcing are strongly linked to the assumptions originated from the references used[26,43,46]. The overall net feedbacks from the vegetation-BVOC-SOA pathway thus need to be comprehensively evaluated using a more comprehensive Earth System Model to fully consider the negative feedbacks from scattering and cloud formation from SOA, and also the positive feedbacks from increased longwave radiation emitted from low-level clouds[23,50].

Under high CO_2 emission scenarios, the climate warming-induced increase of natural aerosols from plant BVOC emissions is largely constrained by CO_2 inhibition of BVOC (mainly monoterpene) production, which means that future anthropogenic CO_2 increase might provide an indirect positive feedback to the climate through this inhibition. In an example of an indirectly negative climate feedback, Young et al. [51] showed that the inhibition of isoprene production by future CO_2 increases can, via atmospheric oxidation, increase hydroxyl radical (OH) concentrations, which can then decrease the lifetime of methane by 7 months. The potential for strong atmospheric feedbacks associated with plant BVOC responses to the increasing atmospheric CO_2 concentrations makes urgent the need for more leaf- and ecosystem-level observations to unveil the mechanisms for the decoupling between photosynthesis and BVOC production under elevated CO_2. This is especially relevant in the context of climate change as the CO_2 inhibition of isoprene emission may be suppressed at higher temperature[12,13], adding uncertainty to the long-term impacts of rising CO_2 concentrations on isoprene emissions. Furthermore, it is still unclear whether elevated CO_2 inhibits monoterpene production to the same degree as isoprene production. The empirical function used in LPJ-GUESS to assess the CO_2 impact on terpenoid production[34] was derived from a limited number of observational studies on trees. Whether the BVOC emissions of low-statured Arctic plants respond similarly to CO_2 is unknown. We currently have no published data that enable a quantification of the low-statured plants' BVOC responses to the surrounding CO_2.

Because the current TM5 simulation settings neither consider the impacts from future changes in meteorology, nor other surface emissions except isoprene and monoterpenes, the current TM5 setup allows us to single out the 'isolated' impacts from plant-emitted isoprene and monoterpenes alone, regardless of interactions with future changes in other factors (see "Model uncertainties" in the Supplementary). Laboratory experiments have shown that higher temperatures can decrease SOA yield[52,53], as under warmer conditions, BVOC reaction products

remain volatile for a longer time. This process is not yet included in the large-scale model TM5, so we can only speculate that the scenarios with largest predicted temperature increases may overestimate the SOA yield. Globally, we expect reduction in anthropogenic emission, such as such as SO_2 and NOx as presented in the (See IPCC Technical Summary report, Figure TS.4 in [54]) under different SSPs. These changes mainly occur south of the study domain and can influence aerosol seeds and chemistry in the Arctic. It might be the case that the decrease of SO_2 dampens aerosol formation as well as potential cooling impacts in the high latitude regions, but we are not sure about the magnitude yet, as this is influenced by the background concentration (clean environment) in the high latitude regions as well as depending on the reduced amount of the transported SO_2. Climate warming will also likely change the baseline emissions from open oceans, and potentially increase marine biogenic trace gas, such as dimethyl sulfide (DMS), emissions, which can contribute to new particle formation[23]. With the predicted further reduction of the sea-ice extent, there will likely be more shipping and gas extraction in the Arctic, which could bring in new emissions of SO_2, NO_X and black carbon etc, which might counteract the emission reductions of these compounds further south[55]. Future studies should focus on quantification of the synergistic effects of future plant emissions from high latitudes with other anthropogenic and primary aerosol sources under dynamic changing climate conditions in a coupled Earth System Model (such as [56]).

In summary, our results show a potentially significant feedback mechanism linking climate change-induced vegetation changes, BVOC dynamics and aerosols in the high latitudes. The negative feedback mechanism between the biosphere, aerosols, and climate concluded from observational data[57] cannot be extrapolated into the future without considering climate change-induced vegetation changes and their impacts on emitted compounds. Our study confirms the importance of BVOCs for future atmospheric SOA concentration, optical depths and associated radiative forcing - in the high latitudes. Furthermore, the study also reveals that the overall impacts largely depend on how atmospheric CO_2 concentration influences monoterpene production. The net radiative feedbacks from BVOCs need a comprehensive evaluation in order to assess (1) vegetation change-induced shifts in emission profiles and (2) the balance between aerosol shortwave cooling and aerosol longwave warming feedbacks in the high latitude environment.

Methods

Dynamic vegetation model, LPJ-GUESS

We used the latest version of LPJ-GUESS v4.1 with the relevant developments of wetland biogeochemistry and soil physics following[58,59]. LPJ-GUESS is a dynamic ecosystem model, which simulates vegetation growth, mortality, and competition, as well as soil biogeochemistry[29]. The model has been widely used to assess water, nitrogen and carbon fluxes, as well as vegetation dynamics at regional and global scales. Plants are represented as plant functional types (PFTs) with a set of predefined bioclimatic, physiological, life history and phenological parameters that characterize specific plant growing requirements, structure and spatial distribution. For simulations in high latitudes, different levels of shrubs (high, low and prostrate), lichen, moss and wetland PFTs are specified[30]. Compared with the version of LPJ-GUESS described in Smith et al.,[29], the model version used here includes improved soil temperature calculations, allowing a better representation of soil thawing and freezing processes and influencing water availability to plants. The model also includes wetland biogeochemistry and wetland hydrology [60].

Daily leaf-level photosynthesis is based on the simplified version of the Farquhar biochemical model[61,62], which simulates a gradual transition between an electron-transport-limited and a rubisco-limited carbon assimilation. In the model, a fraction of the photosynthetic electron flux is used to produce isoprene[34] and monoterpenes[38], and the production rates of isoprene and monoterpenes are also influenced by PFT-specific emission factors, leaf temperature, seasonality and atmospheric CO_2 concentration. The PFT-specific emission factors (standardized emission rates at photosynthetically active radiation levels of 1000 $\mu mol/m^2/s$ and at a reference temperature of 20 °C for Arctic PFTs) in the tundra region are based on branch- or leaf-level measurement data (see details in[3,30]), and a stronger temperature sensitivity derived in Tang, et al. [30] has been applied for Arctic PFTs. For boreal and temperate PFTs, the global temperature response curve has been used and the emission factors are based on the reference temperature of 30 °C. The model dynamically compares plant water demand with liquid water supply from the model's 15, 10-cm thick soil layers to determine transpiration rate. If the water supply cannot meet the demand, plant photosynthetic rates are downregulated[29], which impacts the electron-flux used for isoprene and monoterpene production. In this way, the model considers substrate availability for BVOC production under drought and in the presence of frozen soil layers, but the model does not yet consider any potential effects of drought stress otherwise.

Standard runs

For simulation of the historical period in this study, we used temperature, precipitation and shortwave radiation fields from the monthly CRU-NCEP climate dataset[63] at 0.5° by 0.5° resolution as input to the model for the

period of 1901-2014. Detrended CRU-NCEP fields from the 1901-1930 period were repeated and looped through as input to the model for the period 1850-1900. For the future period (i.e., 2015-2100), we selected the climate outputs from three general circulation models (GCMs), each following five different Shared Socioeconomic Pathways (SSPs) from the latest CMIP6 project[15] to represent a range of predicted future climates (See LPJ-GUESS Standard runs in Figure 6). The three GCMs were selected based on our analysis of temperature changes in the high latitudes, and also on the completeness of the published outputs from these five SSPs (as of September 2020) to represent a wide range of future climate changes in the study region. The monthly climate data from each GCM and SSP for the future period were bias corrected. The biases were calculated as the difference between the monthly climate data (using delta change methods for temperature, and relative anomalies for precipitation and radiation) of the period 1985-2014 from CRU-NCEP and climate outputs from each GCM in the same period, and these biases were then only implemented to the future climate simulated by the GCM. A detailed description of the bias-correction approach can be found in Ahlström, et al. [64]. The predicted anomalies in future temperature, precipitation, and radiation for the 15 scenarios (3 GCMs x 5 SSPs) are presented in Supplementary Fig. 4. All 15 standard runs share a common climate development during the historical period and start to diverge from 2015 onwards following the different future scenarios.

Factorial simulations in LPJ-GUESS

Four factorial experiments were designed to separate the impacts on BVOC dynamics from all relevant processes in the model (see Figure 6). We have described how each factorial experiment were implemented in the main text (Section: Key processes regulating future BVOC trends). Briefly, we changed one process at a time and compared the differences between the standard and factorial simulations over the period 2015-2100. The factorial simulations were conducted under the climate scenarios of CanESM5 SSP119 & SSP585 (see the results in Figure 3), as well as GFDL-ESM4 SSP119&SSP585 (See the results in Supplementary Figure 8). We also conducted one additional factorial experiment where only monoterpene emissions are unaffected by CO_2 inhibition (namely noMT_CO2Inhibition) under CanESM5 SSP119 and SSP585 (See Supplementary Figures 10, 11).

Global chemistry transport model, TM5

To further assess the impacts of plant-emitted BVOCs on atmospheric aerosols and cloud condensation nuclei (CCN), the modelled leaf area index and vegetation coverage, together with isoprene and monoterpene emissions were fed into a global chemistry transport model, TM5-MP[65]. TM5-MP is a branch of TM5 with a massively parallel functionality and is now maintained by KNMI (Royal Netherlands Meteorological Institute). For simplicity, we refer to the model as TM5 throughout the text. The meteorological and surface fields driving the model were derived from ERA-Interim reanalysis datasets provided by ECMWF (European Centre for Medium-range Weather Forecasts)[66], which are the default forcing datasets for TM5. The chemistry scheme used in this study is a modified version of CB05 (carbon bond mechanism; Yarwood, et al. [67]) with more details described in Williams, et al. [65]. Aerosol processes are calculated with the modal two-moment model M7[68]. It includes seven log-normally distributed modes comprising four water-soluble modes (nucleation, Aitken, accumulation and coarse) and three insoluble modes (Aitken, accumulation and coarse). The dry diameter range of each mode is < 10 nm for nucleation mode, 10 nm to 100 nm for Aitken mode, 100 nm to 1000 nm for accumulation mode, and > 1000 nm for coarse mode.

Originally in TM5, inputs of monthly mean natural emissions of isoprene and monoterpenes are derived from MEGANv2.1[6,28]. Then a diurnal cycle is applied to the monthly mean values. However, in this study, we substituted these monthly mean emission data by the monthly emission outputs from individual LPJ-GUESS simulation runs. The emissions of isoprene and monoterpenes from biomass burning were applied from the default inventory provided by van Marle, et al. [69] without diurnal variations. Furthermore, the oceanic dimethylsulfide (DMS) emissions, the mineral dust emissions and the sea salt emissions are calculated within TM5[70]. The other natural emissions such as CO, non-methane VOCs, NOx ($NO+NO_2$), NH_3 and SO_2 were prescribed as in van Noije, et al. [71]. The anthropogenic and biomass burning emissions of gases and particles were derived for present-day conditions from the CMIP6 input4MIPs inventory[69,72].

Once emitted, isoprene and monoterpenes can react with hydroxyl radical (OH) and ozone (O_3) to produce ELVOCs (extreme low volatile organic compounds) and SVOCs (semi-volatile organic compounds), which can condense on particles to increase SOA mass. In addition, ELVOCs can participate in new particle formation together with sulfuric acid. These processes were recently implemented in TM5, which led to improvements in comparisons with observed aerosol concentration and satellite estimates of AOD (see Bergman, et al. [41] for more details).

In this study, a horizontal resolution of 3 degrees in longitude and 2 degrees in latitude was applied in TM5. In the vertical direction, 34 hybrid-sigma levels were used. The time step was one hour. All the simulations were run for the year 2009 with a spin-up period of one year. The meteorological and surface fields in 2009 were

applied for all the simulation cases, which omitted the meteorological impacts in future scenarios when compared to the present case (see TM5 in Figure 6). Similarly, the non-BVOC emission datasets applied in all simulations were from the year 2009 except those derived from LPJ-GUESS output as mentioned above. TM5 was installed and configured in CSC (Finnish IT Center for Science) Puhti.

Estimation of radiative forcings caused by SOA changes

The radiative forcings due to SOA changes in six simulation cases (including standard, noVegDym, and noCO2Inhibition under two climate scenarios CanESM5 SSP585 and SSP119) were calculated according to the methods and results described in Zhu, et al. [46], Yli-Juuti, et al. [26] and Bellouin, et al. [43], respectively (Table 1). The model results in Zhu, et al. [46] showed that SOA burden can increase by 6.8 % in 2100 compared to 2000 under RCP8.5 scenario considering the combined effects of the future changes. From their results we can derive that the changing rate of radiative forcing due to SOA burden change is -0.441 W m^{-2} mg^{-1} m^2. The radiative forcing estimated from our simulation cases was then calculated by multiplying this value by the burden change north of 45 N. Yli-Juuti, et al. [26] analyzed multiple datasets at a boreal measurement station Hyytiälä in Finland. Using a multivariate mixed-effect model, they found that in July and August the organic aerosol (OA) mass loading changed with temperature at a rate of 0.24 (ranging from 0.22 to 0.25) μg m^{-3} K^{-1} while the all-sky total radiative forcing feedback based on sun photometer observations is -0.47 W m^{-2} K^{-1}. We derived the radiative forcing due to SOA surface concentration change by dividing the radiative forcing feedback by OA mass loading change, which is equal to -1.96 W m^{-2} μg^{-1} m^3. Based on this, we estimated the radiative forcing feedback for our simulation cases using the SOA surface concentration in July and August north of 45 N. Bellouin, et al. [43] calculated the present-day effective radiative forcing compared to pre-industrial with a theoretical formula which is a function of aerosol optical depth change. This formula with the suggested parameters was applied to calculate the radiative forcing of our simulation cases both at the global scale and for the region north of 45 N. All the parameters in Bellouin, et al. [43] were estimated with a confidence interval, and we only used their median values to show an estimation of radiative forcing due to SOA change.

Data availability

The modelling datasets used in the current study are available in the Dryad Digital repository.

Code availability

LPJ-GUESS is tested, refined, and developed by a global research community, but the model code is managed and maintained by the Department of Physical Geography and Ecosystem Science, Lund University, Sweden. The source code can be made available under a collaboration agreement upon the acceptance of certain conditions. Additional details and code about factorial experiments can be obtained by contacting the corresponding author.

Acknowledgement

J.T. is supported by Swedish FORMAS (Forskningsråd för hållbar utveckling) mobility Grant (2016-01580) and European Union's Horizon 2020 research and innovation programme under Marie Sklodowska-Curie Grant 707187. R.R. would like to acknowledge the support by the European Research Council under the European Union's Horizon 2020 research and innovation programme (TUVOLU, Grant No 771012) and the Independent Research Fund Denmark (DFF–4181-00141, 1026-00127B). J.T., G.S., and R.R acknowledge the Danish National Research Foundation (CENPERM DNRF100). P. Z. and R. M. would like to acknowledge the funding from EU H2020 project FORCeS (grant agreement No 821205), University of Helsinki Three Year Grant AGES, the ACCC Flagship funded by the Academy of Finland (337549) and CSC (IT Center for Science, Finland) for computational resources. P. Z. also acknowledges the Arctic Avenue (spearhead research project between the University of Helsinki and Stockholm University).

P.A.M. and A.G. acknowledge the Lund University Strategic Research Areas BECC and MERGE for their financial support, and P.A.M. was partly funded by the project BioDiv-Support through the 2017-2018 Belmont Forum and BiodivERsA joint call for research proposals, under the BiodivScen ERA-Net COFUND programme, and with the funding organisations AKA (Academy of Finland contract no 326328), ANR (ANR-18-EBI4-0007), BMBF (KFZ: 01LC1810A), FORMAS (contract no:s 2018-02434, 2018-02436, 2018-02437, 2018-02438) and MICINN (through APCIN: PCI2018-093149).

J.T. would like to thank Roger Seco for providing eddy covariance-based BVOC measurement data from Abisko and thank Cleo L. Davie-Martin for language proofing. All LPJ-GUESS simulations in this paper were performed using Danish e-infrastructure Cooperation (DeiC) National Life Science Supercomputer at Technical

University of Denmark. All TM5 simulations in this paper were performed using the Atos Bullsequana X400 supercomputing platform Puhti provided by CSC (IT Center for Science) in Finland.

Author Contributions

J.T. designed the study, ran all LPJ-GUESS simulations, led writing and analysis; P.Z. and R.M conducted TM5 runs and analysis. P.A.M, G.S. and A.G, contributed to LPJ-GUESS analysis and model setup. Y.H.F contributed to statistical analysis, and R.R. provided BVOC observational data and data analysis. All co-authors contributed to manuscript writing.

Competing Interests

The authors declare no competing interests.

Figures

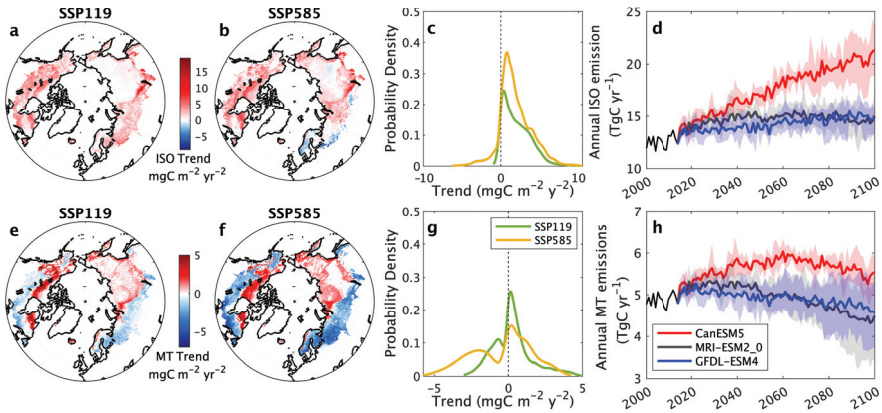

Figure 1. LPJ-GUESS modelled trends of isoprene and monoterpene emissions for the period of 2001-2100. (a-b): Modelled isoprene (ISO) trends for SSP119 and SSP585, respectively. The trends are analysed based on the averaged emissions over 3 General Circulation Models (GCMs) and only significant trends (Mann-Kendall trend test, $p<0.05$) are shown; (c) Probability density of significant trends (shown in panels a and b) in isoprene emissions with kernel smoothing distribution fit; (d) Time series of areal total (study region: tundra and boreal biomes) isoprene emissions for all standard runs driven by 3 GCMs following 5 SSPs; (e-f): Modelled monoterpene (MT) trends for SSP119 and SSP585, respectively. The trends are analysed based on the averaged emissions over 3 GCMs and only significant trends (Mann-Kendall trend test, $p<0.05$) are shown; (g) Probability density of significant trends (shown in panels e and f) in monoterpene emissions with kernel smoothing distribution fit.; (h) Time series of areal total monoterpene emissions for all standard runs driven by 3 different GCMs following 5 SSPs. SSP119: Shared Socioeconomic Pathway 1 reaching radiative forcing of 1.9 W/m^2 in 2100. SSP585: Shared Socioeconomic Pathway 5 reaching radiative forcing of 8.5 W/m^2 in 2100; (d, h) For each GCM, the solid line represents the average across 5 SSPs and the shaded area represents the predicted ranges from minimum to maximum. LPJ-GUESS runs at 0.5^o by 0.5^o resolution.

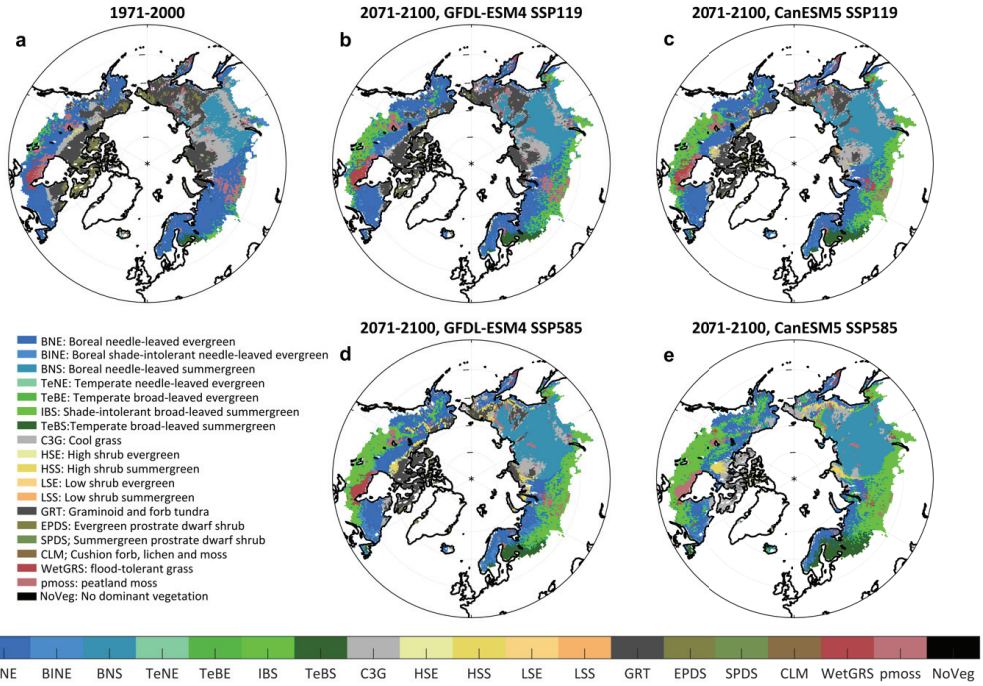

Figure 2. Distribution of the dominant plant functional types (PFTs) over the period 1971-2000 (a) and 2071-2100 (b-e) based on the modelled leaf area index. The outputs from the scenario SSP119 are shown in b, c, and the outputs from SSP585 are shown in d, e. The outputs from two GCMs are plotted separately: GFDL-ESM4 (b,d) and CanESM5 (c,e).

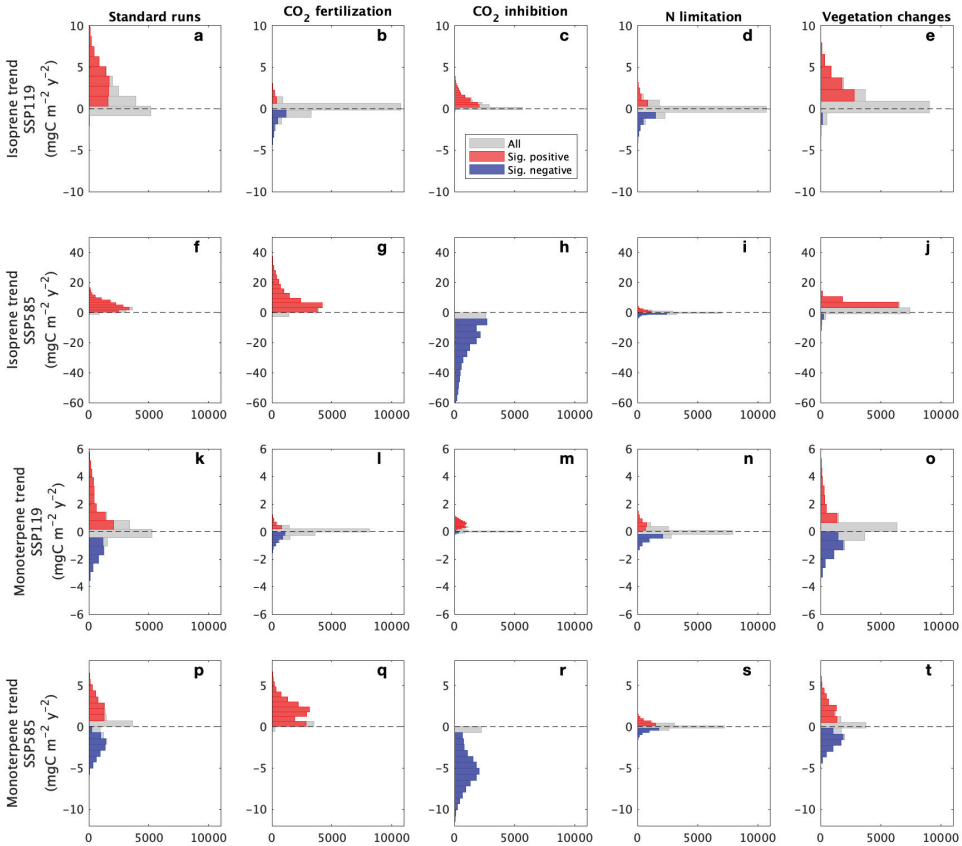

Figure 3 Histograms of trends in the modelled isoprene (first row for CanESM5 SSP119 and second row for CanESM5 SSP585) and monoterpene (third row for CanESM5 SSP119 and fourth row for CanESM5 SSP585) emissions from standard runs and from four investigated processes over the period 2015-2100. x-axis shows the number of gridcells and y-axis shows the values of estimated trends. The values used in the trend analysis of these four investigated processes are based on the differences of every two runs (see how the impacts from each process are extracted in Table 1). Trends are analysed using Mann-Kendall test, and the trends for all grid cells are marked as grey, while both significant positive and significant negative trends ($p < 0.05$) are indicated with red and blue bars, respectively. Sig.: Significant.

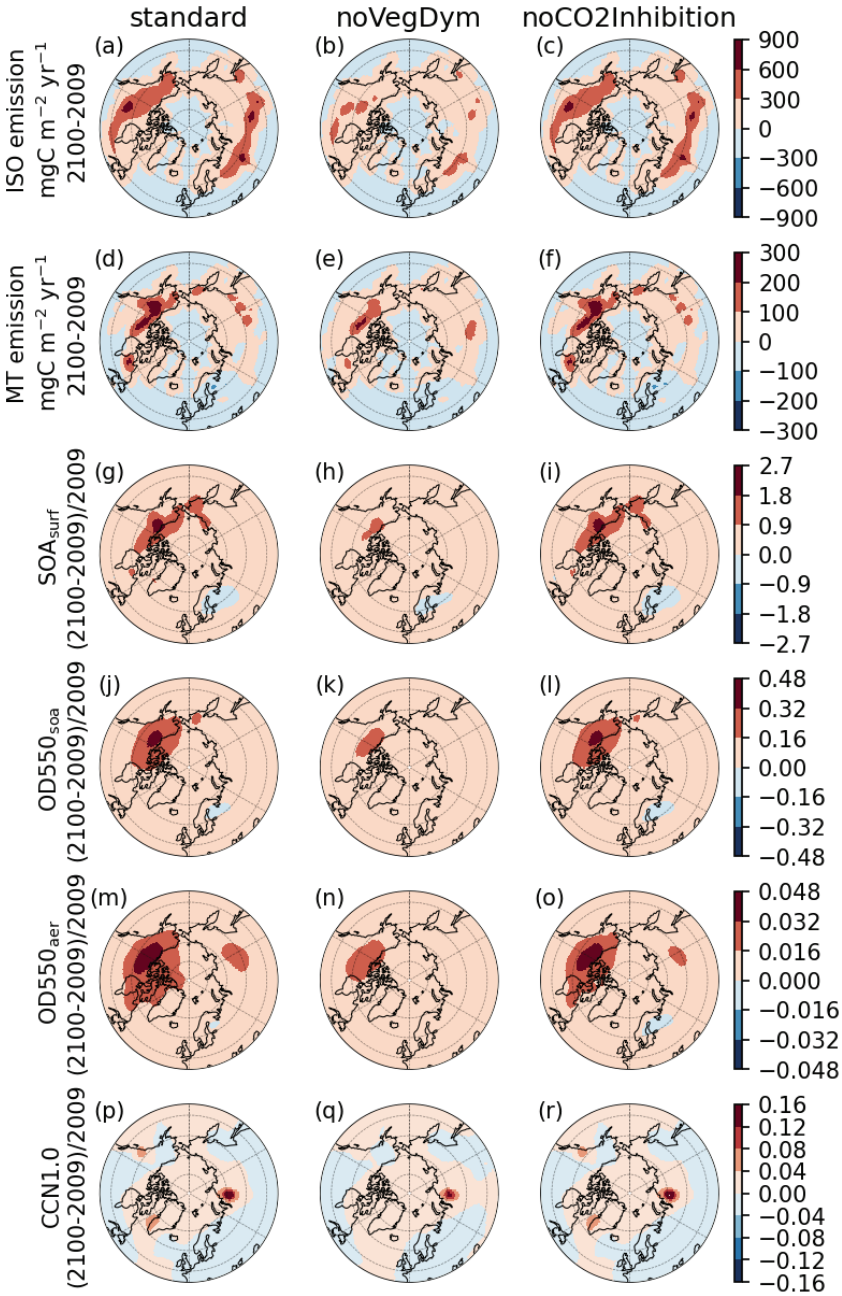

Figure 4 The inputs to and outputs from TM5 using CanESM5 SSP119. The first and second rows show LPJ-GUESS simulated isoprene (ISO) and monoterpene (MT) emission changes between 2100 and 2009. The emissions from the year 2100 are driven by CanESM5 SSP119. The third to the sixth rows show the TM5 simulated ratio in changes to surface SOA concentration (SOA_{surf}); optical depth of SOA at 550 nm ($OD550_{SOA}$); optical depth of aerosol at 550 nm ($OD550_{aer}$) and CCN concentrations at a supersaturation of 1.0 %. From left to right, we show the TM5 results fed with BVOC inputs from three LPJ-GUESS runs: the standard run (the 1st column), the noVegDym run (the 2nd column) and the noCO2Inhibition run (the 3rd column). The colour bars used for these three columns are kept the same for each corresponding output.

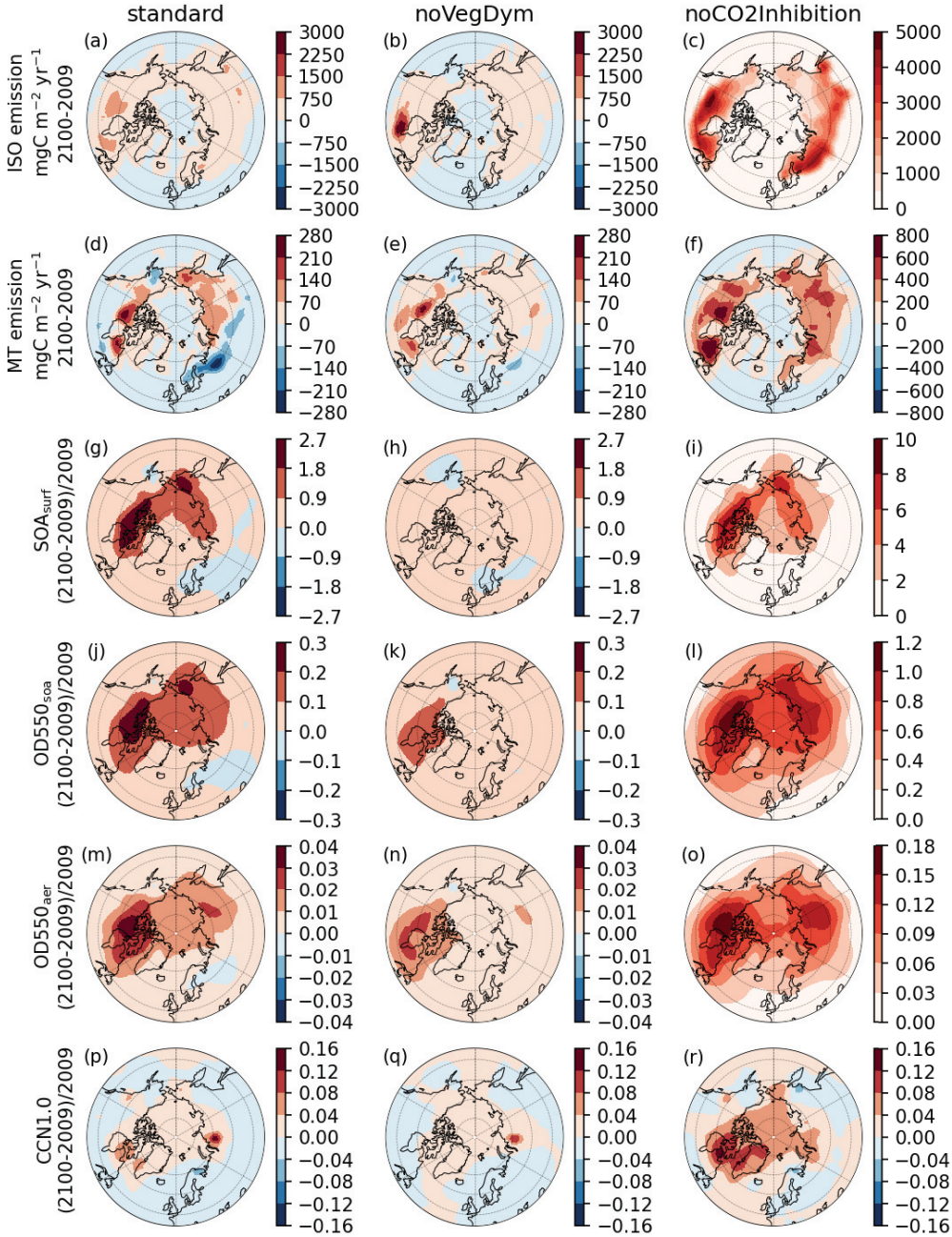

Figure 5 The inputs to and outputs from TM5 using CanESM5 SSP585. The first and second rows show LPJ-GUESS simulated isoprene (ISO) and monoterpene (MT) emission changes between 2100 and 2009. The emissions from the year 2100 are driven by CanESM5 SSP585. The third to the sixth rows show the TM5 simulated ratio in changes to surface SOA concentration (SOA_{surf}); optical depth of SOA at 550 nm ($OD550_{SOA}$); optical depth of aerosol at 550 nm ($OD550_{aer}$) and and CCN concentrations at a supersaturation of 1.0 %. From left to right, we show the TM5 results fed with BVOC inputs from three LPJ-GUESS runs, which are standard run (the 1st column), noVegDym run (the 2nd column) and noCO2Inhibition run (the 3rd column). The colour bars used for standard and noVegDym runs are kept the same for each corresponding output.

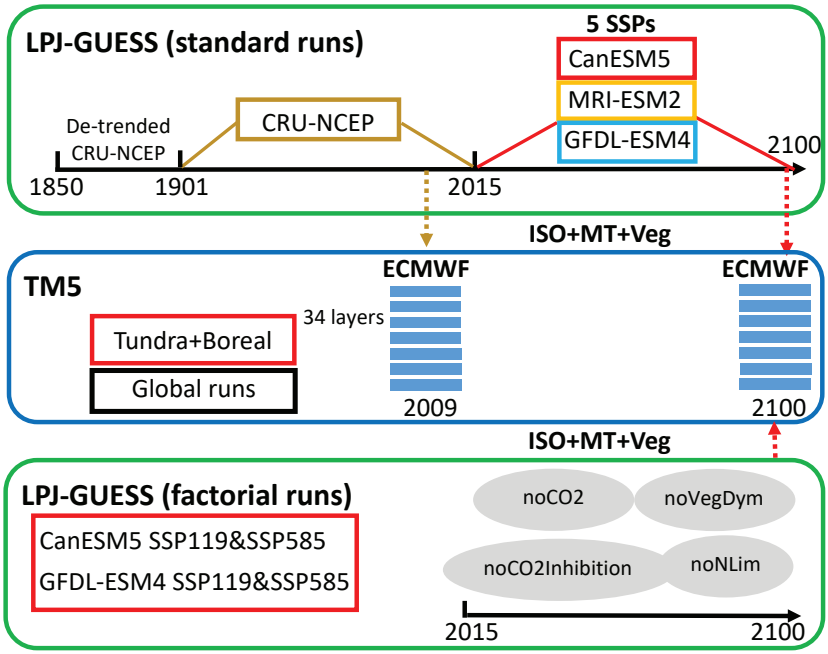

Figure 6 Model setup. The modelled monthly isoprene (ISO) and monoterpene (MT) emissions, as well as vegetation status (Veg) from LPJ-GUESS standard and factorial runs were used as inputs for TM5. The years 2009 and 2100 were selected to represent historical and future periods in the global model TM5. ECMWF: European Centre for Medium-Range Weather Forecasts. SSPs: Shared Socioeconomic Pathways (SSPs).

Tables

Table 1 Overview of factorial runs conducted with LPJ-GUESS following CanESM5 and GFDL-ESM4 SSP119 and SSP585.

	CO_2 inhibition of BVOC production	**CO_2 fertilization of photosynthesis**	**Climate change-induced Vegetation Changes**	**Nitrogen (N) limitation**	**Climate change impacts on BVOC production**	**Processes to analyse for 2015-2100**
Standard run	Yes	Yes	Yes	Yes	Yes	Full Set
noCO_2Inhibition	No	Yes	Yes	Yes	Yes	CO_2 inhibition = Standard run - noCO2Inhibition
noCO_2	No	No	Yes	Yes	Yes	CO_2 fertilization = noCO_2Inhibition – noCO_2
noNlim	Yes	Yes	Yes	No	Yes	N limitation = Standard runs – noNlim
noVegDym	Yes	Yes	No	Yes	Yes	Vegetation changes = Standard run - noVegDym

References

1 Bjorkman, A. D. *et al.* Plant functional trait change across a warming tundra biome. *Nature* **562**, 57-62, doi:10.1038/s41586-018-0563-7 (2018).

2 Myers-Smith, I. H. *et al.* Complexity revealed in the greening of the Arctic. *Nature Climate Change* **10**, 106-117, doi:10.1038/s41558-019-0688-1 (2020).

3 Rinnan, R. *et al.* Separating direct and indirect effects of rising temperatures on biogenic volatile emissions in the Arctic. *Proceedings of the National Academy of Sciences* **117**, 32476-32483, doi:10.1073/pnas.2008901117 (2020).

4 Finger, R. A. *et al.* Effects of permafrost thaw on nitrogen availability and plant–soil interactions in a boreal Alaskan lowland. *Journal of Ecology* **104**, 1542-1554, doi:https://doi.org/10.1111/1365-2745.12639 (2016).

5 Keuper, F. *et al.* A frozen feast: thawing permafrost increases plant-available nitrogen in subarctic peatlands. *Global Change Biology* **18**, 1998-2007, doi:https://doi.org/10.1111/j.1365-2486.2012.02663.x (2012).

6 Guenther, A. B. *et al.* The Model of Emissions of Gases and Aerosols from Nature version 2.1 (MEGAN2.1): an extended and updated framework for modeling biogenic emissions. *Geosci. Model Dev.* **5**, 1471-1492, doi:10.5194/gmd-5-1471-2012 (2012).

7 Arneth, A. *et al.* CO2 inhibition of global terrestrial isoprene emissions: Potential implications for atmospheric chemistry. *Geophysical Research Letters* **34**, doi:https://doi.org/10.1029/2007GL030615 (2007).

8 Rosenstiel, T. N., Potosnak, M. J., Griffin, K. L., Fall, R. & Monson, R. K. Increased CO2 uncouples growth from isoprene emission in an agriforest ecosystem. *Nature* **421**, 256-259, doi:10.1038/nature01312 (2003).

9 Tiiva, P., Tang, J., Michelsen, A. & Rinnan, R. Monoterpene emissions in response to long-term night-time warming, elevated CO2 and extended summer drought in a temperate heath ecosystem. *Science of The Total Environment* **580**, 1056-1067, doi:https://doi.org/10.1016/j.scitotenv.2016.12.060 (2017).

10 Loreto, F. *et al.* Monoterpene emission and monoterpene synthase activities in the Mediterranean evergreen oak Quercus ilex L. grown at elevated CO2 concentrations. *Global Change Biology* **7**, 709-717, doi:https://doi.org/10.1046/j.1354-1013.2001.00442.x (2001).

11 Staudt, M., Joffre, R., Rambal, S. & Kesselmeier, J. Effect of elevated CO2 on monoterpene emission of young Quercus ilex trees and its relation to structural and ecophysiological parameters. *Tree Physiol* **21**, 437-445, doi:10.1093/treephys/21.7.437 (2001).

12 Potosnak, M. J., Lestourgeon, L. & Nunez, O. Increasing leaf temperature reduces the suppression of isoprene emission by elevated CO_2 concentration. *Sci Total Environ* **481**, 352-359, doi:10.1016/j.scitotenv.2014.02.065 (2014).

13 Sharkey, T. D. & Monson, R. K. The future of isoprene emission from leaves, canopies and landscapes. *Plant Cell Environ* **37**, 1727-1740, doi:10.1111/pce.12289 (2014).

14 Schollert, M., Burchard, S., Faubert, P., Michelsen, A. & Rinnan, R. Biogenic volatile organic compound emissions in four vegetation types in high arctic Greenland. *Polar Biology* **37**, 237-249, doi:10.1007/s00300-013-1427-0 (2014).

15 Eyring, V. *et al.* Overview of the Coupled Model Intercomparison Project Phase 6 (CMIP6) experimental design and organization. *Geosci. Model Dev.* **9**, 1937-1958, doi:10.5194/gmd-9-1937-2016 (2016).

16 Hantson, S., Knorr, W., Schurgers, G., Pugh, T. A. M. & Arneth, A. Global isoprene and monoterpene emissions under changing climate, vegetation, CO2 and land use. *Atmospheric Environment* **155**, 35-45, doi:https://doi.org/10.1016/j.atmosenv.2017.02.010 (2017).

17 Atkinson, R. & Arey, J. Gas-phase tropospheric chemistry of biogenic volatile organic compounds: a review. *Atmospheric Environment* **37**, 197-219, doi:https://doi.org/10.1016/S1352-2310(03)00391-1 (2003).

18 Wennberg, P. O. *et al.* Gas-Phase Reactions of Isoprene and Its Major Oxidation Products. *Chemical Reviews* **118**, 3337-3390, doi:10.1021/acs.chemrev.7b00439 (2018).

19 Jokinen, T. *et al.* Production of extremely low volatile organic compounds from biogenic emissions: Measured yields and atmospheric implications. *Proceedings of the National Academy of Sciences* **112**, 7123-7128, doi:doi:10.1073/pnas.1423977112 (2015).

20 Ng, N. L. *et al.* Nitrate radicals and biogenic volatile organic compounds: oxidation, mechanisms, and organic aerosol. *Atmos. Chem. Phys.* **17**, 2103-2162, doi:10.5194/acp-17-2103-2017 (2017).

21 McFiggans, G. *et al.* Secondary organic aerosol reduced by mixture of atmospheric vapours. *Nature* **565**, 587-593, doi:10.1038/s41586-018-0871-y (2019).
22 Heinritzi, M. *et al.* Molecular understanding of the suppression of new-particle formation by isoprene. *Atmos. Chem. Phys.* **20**, 11809-11821, doi:10.5194/acp-20-11809-2020 (2020).
23 Schmale, J., Zieger, P. & Ekman, A. M. L. Aerosols in current and future Arctic climate. *Nature Climate Change* **11**, 95-105, doi:10.1038/s41558-020-00969-5 (2021).
24 Mauritsen, T. *et al.* An Arctic CCN-limited cloud-aerosol regime. *Atmos. Chem. Phys.* **11**, 165-173, doi:10.5194/acp-11-165-2011 (2011).
25 Scott, C. E. *et al.* Substantial large-scale feedbacks between natural aerosols and climate. *Nature Geoscience* **11**, 44-48, doi:10.1038/s41561-017-0020-5 (2018).
26 Yli-Juuti, T. *et al.* Significance of the organic aerosol driven climate feedback in the boreal area. *Nature Communications* **12**, 5637, doi:10.1038/s41467-021-25850-7 (2021).
27 Pearson, R. G. *et al.* Shifts in Arctic vegetation and associated feedbacks under climate change. *Nature Climate Change* **3**, 673-677, doi:10.1038/nclimate1858 (2013).
28 Sindelarova, K. *et al.* Global data set of biogenic VOC emissions calculated by the MEGAN model over the last 30 years. *Atmos. Chem. Phys.* **14**, 9317-9341, doi:10.5194/acp-14-9317-2014 (2014).
29 Smith, B. *et al.* Implications of incorporating N cycling and N limitations on primary production in an individual-based dynamic vegetation model. *Biogeosciences* **11**, 2027-2054, doi:10.5194/bg-11-2027-2014 (2014).
30 Tang, J. *et al.* Challenges in modelling isoprene and monoterpene emission dynamics of Arctic plants: a case study from a subarctic tundra heath. *Biogeosciences* **13**, 6651-6667, doi:10.5194/bg-13-6651-2016 (2016).
31 Dinerstein, E. *et al.* An Ecoregion-Based Approach to Protecting Half the Terrestrial Realm. *BioScience* **67**, 534-545, doi:10.1093/biosci/bix014 (2017).
32 Fraser, R. H., Lantz, T. C., Olthof, I., Kokelj, S. V. & Sims, R. A. Warming-Induced Shrub Expansion and Lichen Decline in the Western Canadian Arctic. *Ecosystems* **17**, 1151-1168, doi:10.1007/s10021-014-9783-3 (2014).
33 Edwards, M. E., Brubaker, L. B., Lozhkin, A. V. & Anderson, P. M. Structurally novel biomes: a response to past warming in Beringia. *Ecology* **86**, 1696-1703, doi:https://doi.org/10.1890/03-0787 (2005).
34 Arneth, A. *et al.* Process-based estimates of terrestrial ecosystem isoprene emissions: incorporating the effects of a direct CO₂-isoprene interaction. *Atmos. Chem. Phys.* **7**, 31-53, doi:10.5194/acp-7-31-2007 (2007).
35 Sporre, M. K., Blichner, S. M., Karset, I. H. H., Makkonen, R. & Berntsen, T. K. BVOC–aerosol–climate feedbacks investigated using NorESM. *Atmos. Chem. Phys.* **19**, 4763-4782, doi:10.5194/acp-19-4763-2019 (2019).
36 Possell, M., Nicholas Hewitt, C. & Beerling, D. J. The effects of glacial atmospheric CO2 concentrations and climate on isoprene emissions by vascular plants. *Global Change Biology* **11**, 60-69, doi:https://doi.org/10.1111/j.1365-2486.2004.00889.x (2005).
37 Peñuelas, J. & Staudt, M. BVOCs and global change. *Trends in Plant Science* **15**, 133-144, doi:https://doi.org/10.1016/j.tplants.2009.12.005 (2010).
38 Schurgers, G., Arneth, A., Holzinger, R. & Goldstein, A. H. Process-based modelling of biogenic monoterpene emissions combining production and release from storage. *Atmos. Chem. Phys.* **9**, 3409-3423, doi:10.5194/acp-9-3409-2009 (2009).
39 Niinemets, Ü., Tenhunen, J. D., Harley, P. C. & Steinbrecher, R. A model of isoprene emission based on energetic requirements for isoprene synthesis and leaf photosynthetic properties for Liquidambar and Quercus. *Plant Cell Environ* **22**, 1319-1335, doi:https://doi.org/10.1046/j.1365-3040.1999.00505.x (1999).
40 Davies-Barnard, T. *et al.* Nitrogen cycling in CMIP6 land surface models: progress and limitations. *Biogeosciences* **17**, 5129-5148, doi:10.5194/bg-17-5129-2020 (2020).
41 Bergman, T. *et al.* Description and evaluation of a secondary organic aerosol and new particle formation scheme within TM5-MP v1.2. *Geosci. Model Dev.* **15**, 683-713, doi:10.5194/gmd-15-683-2022 (2022).
42 Li, F., Vogelmann, A. M. & Ramanathan, V. Saharan Dust Aerosol Radiative Forcing Measured from Space. *Journal of Climate* **17**, 2558-2571, doi:10.1175/1520-0442(2004)017<2558:Sdarfm>2.0.Co;2 (2004).
43 Bellouin, N. *et al.* Bounding Global Aerosol Radiative Forcing of Climate Change. *Reviews of Geophysics* **58**, e2019RG000660, doi:https://doi.org/10.1029/2019RG000660 (2020).

44 Bergman, T. *et al.* Description and Evaluation of a Secondary Organic Aerosol and New Particle Formation Scheme within TM5-MP v1.1. *Geosci. Model Dev. Discuss.* **2021**, 1-43, doi:10.5194/gmd-2021-49 (2021).
45 Wilkinson, M. J. *et al.* Leaf isoprene emission rate as a function of atmospheric CO2 concentration. *Global Change Biology* **15**, 1189-1200, doi:https://doi.org/10.1111/j.1365-2486.2008.01803.x (2009).
46 Zhu, J. *et al.* Mechanism of SOA formation determines magnitude of radiative effects. *Proceedings of the National Academy of Sciences* **114**, 12685-12690, doi:doi:10.1073/pnas.1712273114 (2017).
47 Chapin, F. S., 3rd *et al.* Role of land-surface changes in arctic summer warming. *Science* **310**, 657-660, doi:10.1126/science.1117368 (2005).
48 Swann, A. L., Fung, I. Y., Levis, S., Bonan, G. B. & Doney, S. C. Changes in Arctic vegetation amplify high-latitude warming through the greenhouse effect. *Proceedings of the National Academy of Sciences* **107**, 1295-1300, doi:10.1073/pnas.0913846107 (2010).
49 Forster, P. *et al.* Climate Change 2021: The Physical Science Basis. Contribution of Working Group I to the Sixth Assessment Report of the Intergovernmental Panel on Climate Change. (Cambridge, United Kingdom and New York, NY, USA, 2021).
50 Dong, X. *et al.* A 10 year climatology of Arctic cloud fraction and radiative forcing at Barrow, Alaska. *Journal of Geophysical Research: Atmospheres* **115**, doi:https://doi.org/10.1029/2009JD013489 (2010).
51 Young, P. J., Arneth, A., Schurgers, G., Zeng, G. & Pyle, J. A. The CO₂ inhibition of terrestrial isoprene emission significantly affects future ozone projections. *Atmos. Chem. Phys.* **9**, 2793-2803, doi:10.5194/acp-9-2793-2009 (2009).
52 Clark, C. H. *et al.* Temperature Effects on Secondary Organic Aerosol (SOA) from the Dark Ozonolysis and Photo-Oxidation of Isoprene. *Environmental Science & Technology* **50**, 5564-5571, doi:10.1021/acs.est.5b05524 (2016).
53 Saathoff, H. *et al.* Temperature dependence of yields of secondary organic aerosols from the ozonolysis of α-pinene and limonene. *Atmos. Chem. Phys.* **9**, 1551-1577, doi:10.5194/acp-9-1551-2009 (2009).
54 IPCC. Climate Change 2021: The Physical Science Basis. Contribution of Working Group I to the Sixth Assessment Report of the Intergovernmental Panel on Climate Change. (Cambridge University Press, 2021).
55 Peters, G. P. *et al.* Future emissions from shipping and petroleum activities in the Arctic. *Atmos. Chem. Phys.* **11**, 5305-5320, doi:10.5194/acp-11-5305-2011 (2011).
56 Sporre, M. K. *et al.* Large difference in aerosol radiative effects from BVOC-SOA treatment in three Earth system models. *Atmos. Chem. Phys.* **20**, 8953-8973, doi:10.5194/acp-20-8953-2020 (2020).
57 Paasonen, P. *et al.* Warming-induced increase in aerosol number concentration likely to moderate climate change. *Nature Geoscience* **6**, 438-442, doi:10.1038/ngeo1800 (2013).
58 Wania, R., Ross, I. & Prentice, I. C. Integrating peatlands and permafrost into a dynamic global vegetation model: 1. Evaluation and sensitivity of physical land surface processes. *Global Biogeochemical Cycles* **23**, doi:https://doi.org/10.1029/2008GB003412 (2009).
59 Wania, R., Ross, I. & Prentice, I. C. Implementation and evaluation of a new methane model within a dynamic global vegetation model: LPJ-WHyMe v1.3.1. *Geosci. Model Dev.* **3**, 565-584, doi:10.5194/gmd-3-565-2010 (2010).
60 Tang, J. *et al.* Carbon budget estimation of a subarctic catchment using a dynamic ecosystem model at high spatial resolution. *Biogeosciences* **12**, 2791-2808, doi:10.5194/bg-12-2791-2015 (2015).
61 Collatz, G. J., Ball, J. T., Grivet, C. & Berry, J. A. Physiological and environmental regulation of stomatal conductance, photosynthesis and transpiration: a model that includes a laminar boundary layer. *Agricultural and Forest Meteorology* **54**, 107-136, doi:https://doi.org/10.1016/0168-1923(91)90002-8 (1991).
62 Farquhar, G. D., von Caemmerer, S. & Berry, J. A. A biochemical model of photosynthetic CO2 assimilation in leaves of C3 species. *Planta* **149**, 78-90, doi:10.1007/BF00386231 (1980).
63 Viovy, N. (Research Data Archive at the National Center for Atmospheric Research, Computational and Information Systems Laboratory, Boulder, CO, 2018).
64 Ahlström, A., Schurgers, G., Arneth, A. & Smith, B. Robustness and uncertainty in terrestrial ecosystem carbon response to CMIP5 climate change projections. *Environmental Research Letters* **7**, 044008, doi:10.1088/1748-9326/7/4/044008 (2012).

65 Williams, J. E., Boersma, K. F., Le Sager, P. & Verstraeten, W. W. The high-resolution version of TM5-MP for optimized satellite retrievals: description and validation. *Geosci. Model Dev.* **10**, 721-750, doi:10.5194/gmd-10-721-2017 (2017).
66 Dee, D. P. *et al.* The ERA-Interim reanalysis: configuration and performance of the data assimilation system. *Quarterly Journal of the Royal Meteorological Society* **137**, 553-597, doi:https://doi.org/10.1002/qj.828 (2011).
67 Yarwood, G. *et al.* in *9th Annual CMAS Conference* (Chapel Hill, 2010).
68 Vignati, E., Wilson, J. & Stier, P. M7: An efficient size-resolved aerosol microphysics module for large-scale aerosol transport models. *Journal of Geophysical Research: Atmospheres* **109**, doi:https://doi.org/10.1029/2003JD004485 (2004).
69 van Marle, M. J. E. *et al.* Historic global biomass burning emissions for CMIP6 (BB4CMIP) based on merging satellite observations with proxies and fire models (1750–2015). *Geosci. Model Dev.* **10**, 3329-3357, doi:10.5194/gmd-10-3329-2017 (2017).
70 van Noije, T. *et al.* EC-Earth3-AerChem: a global climate model with interactive aerosols and atmospheric chemistry participating in CMIP6. *Geosci. Model Dev.* **14**, 5637-5668, doi:10.5194/gmd-14-5637-2021 (2021).
71 van Noije, T. P. C. *et al.* Simulation of tropospheric chemistry and aerosols with the climate model EC-Earth. *Geosci. Model Dev.* **7**, 2435-2475, doi:10.5194/gmd-7-2435-2014 (2014).
72 Hoesly, R. M. *et al.* Historical (1750–2014) anthropogenic emissions of reactive gases and aerosols from the Community Emissions Data System (CEDS). *Geosci. Model Dev.* **11**, 369-408, doi:10.5194/gmd-11-369-2018 (2018).

High-latitude vegetation changes will determine future plant volatile impacts on atmospheric organic aerosols

Supplementary information

Jing Tang[1,2,3*], Putian Zhou[4], Paul A. Miller[1], Guy Schurgers[3,5], Adrian Gustafson[1,6], Risto Makkonen[4,7], Yongshuo H. Fu[8], Riikka Rinnan[2,3]

[1.] Department of Physical Geography and Ecosystem Science, Lund University, Sölvegatan 12, SE-223 62, Lund, Sweden

[2.] Terrestrial Ecology Section, Department of Biology, University of Copenhagen, Universitetsparken 15, DK-2100, Copenhagen Ø, Denmark

[3.] Center for Permafrost (CENPERM), University of Copenhagen, Øster Voldgade 10, DK-1350, Copenhagen K, Denmark

[4.] Institute for Atmospheric and Earth Systems Research/Physics, University of Helsinki, 00014, Helsinki, Finland

[5.] Department of Geosciences and Natural Resource Management, University of Copenhagen, Copenhagen, Denmark

[6.] Center for Environmental and Climate Science, Lund University, Sölvegatan 37, 223 62, Lund, Sweden

[7.] Climate System Research, Finnish Meteorological Institute, Helsinki, Finland

[8.] College of Water Sciences, Beijing Normal University, Beijing, China

Corresponding author: Jing Tang (jing.tang@nateko.lu.se)

Table of Content

Model evaluation for different historical periods

For the historical period (1901-2014) using observation-based climate data as forcing, we evaluate the modelled leaf area index (LAI), gross primary productivity (GPP) and aboveground carbon (ABC) against satellite-based datasets (Supplementary Figs.1-3). The modelled ecosystem-level BVOC emissions are evaluated with observations from the available literature (Supplementary Table 1).

The modelled gross primary productivity (GPP) is evaluated against the OCO-2-based SIF GPP product (GOSIF)[1], and the mapping of multiple-year averages shows general agreement in spatial patterns (Supplementary Fig. 1a, b). The modelled GPP is higher than estimates based on GOSIF in the southern boreal forest and also in terms of areal average. The modelled interannual variability of annual area-averaged GPP correlates well with the observations based on GOSIF (Supplementary Fig. 1c).

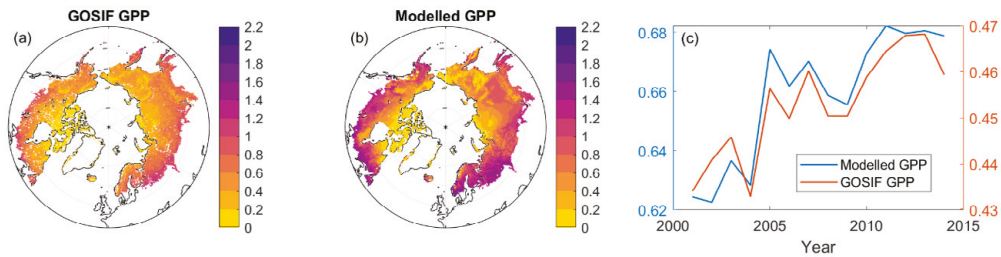

Supplementary Figure 1. Comparing the modelled annual gross primary productivity (GPP, kgC m^{-2}) with the GOSIF GPP product. (a) Annual GOSIF-based GPP averaged over the period 2001-2014; (b) LPJ-GUESS modelled annual GPP averaged over the period 2001-2014; (c) the timeseries of annual, area-averaged GPP over the study domain (including tundra and boreal regions).

The modelled LAI averaged over June, July and August is compared with estimates from the GIMMS LAI3g[2] product over the same period (Supplementary Fig. 2). We find that the modelled spatial patterns of LAI are similar to GIMMS LAI3g though the absolute differences (Supplementary Fig. 2c) show that the model tends to overestimate LAI in some of tundra regions, such as in north America, Norway, northern parts of Finland and small regions of Siberia. In contrast, slight underestimations are found in parts of the southern boreal region.

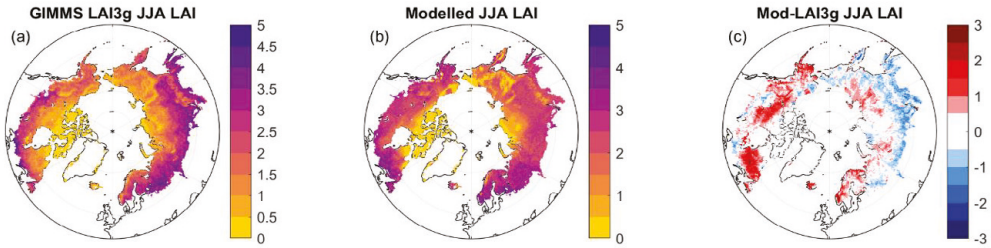

Supplementary Figure 2. Comparing the modelled leaf area index (LAI) over the growing season (June, July and August, JJA) with the GIMMS LAI3g product over the period 1982-2011. (a) GIMMS LAI3g-observed averaged LAI in JJA; (b) LPJ-GUESS modelled LAI in JJA; (c) the difference in the modelled JJA LAI between the modelled and the GIMMS LAI3g product.

The modelled aboveground carbon pool (i.e., leaf and stem carbon in vegetation) is compared with estimates from a vegetation optical depth (VOD)-based product[3]. The overall spatial patterns are captured by the model (Supplementary Fig. 3a, b), and though there is an overestimation of areal averages of aboveground carbon from our model, the increasing trends are well represented (Supplementary Fig. 3c).

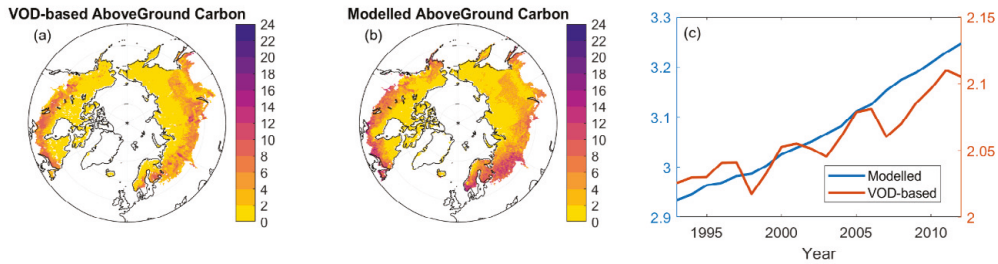

Supplementary Figure 3. Comparing the modelled annual aboveground biomass carbon (ABC, KgC m^{-2}) with vegetation optical depth (VOD)-based ABC product. (a) VOC-based ABC averaged over the period of 1993-2012; (b) LPJ-GUESS modelled aboveground carbon (including biomass from leaf and stem) averaged over the period 1993-2012; (c) the timeseries of areal averaged ABC over the study domain (including tundra and boreal regions).

The above comparison of modelled and regional estimates of GPP, LAI and ABC show that the model can generally capture the spatial and temporal changes of these variables, but with some overestimation of GPP and ABC for southern boreal regions and of LAI for the tundra region.

The modelled ecosystem-level isoprene and monoterpene fluxes are compared with published values from different ecosystems (Supplementary Table 1), showing that the model produces fluxes of similar magnitudes to the observed emissions. We note, however, that an exact comparison was not possible since the LPJ-GUESS model runs at a spatial resolution of 0.5 degrees, and although we used the output from the nearest gridcells with

a similar dominant vegetation type as observed at the sites, there could still be differences in overall vegetation composition and microclimatic conditions.

Supplementary Table 1 Ecosystem-level BVOC evaluation. The modelled values from the nearby gridcell were selected and the modelled units were converted to match those in the literature. Note: only ecosystem-level observations were extracted from the literature. Dom.: dominant; MT: monoterpenes; ISO: isoprene

Ecosystem types	Location	Dom. Species	Time period	Compounds	Units	Observed	Modelled	Refs
Boreal forest	Siberian larch tree	*Larix cajanderi*	Jun, 2009 Jul, 2009	MT MT	mgC/m^2/d	3.3±2.9 2.4±1.6	2.0 2.4	[4]
	Scots pine	*Pinus sylvestris*	Mar, 2010-2013 Apr, 2010-2013 May, 2010-2013 Jun, 2010-2013 Jul, 2010-2013 Aug, 2010-2013 Sep, 2010-2013 Oct, 2010-2013 Nov, 2010-2013 Dec, 2010-2013	MT	mgC/m2/m	10.87 27.44 85.08 114.35 163.07 103.98 57.18 30.72 6.63 7.56	6.82 23.40 54.99 75.96 111.15 77.53 42.97 24.18 15.73 9.33	[5]
Tundra upland	Greenland tundra	*Cassiope tetragona*	Aug, 2009	ISO MT	µgC/m2/h	1.38 21.54	0.014 0.014	[6]
	Alaska tundra	*Salix pulchra*	Jun-Jul 2005,2010&2011	ISO	µgC/m2/h	Up to 1200	63.2	[7]
	Alaska tundra	Tussock tundra	Summer, 2018&2019	ISO MT	µgC/m2/h	0.2-225 <1	0.2-118.8 0.34-4.81	[8]
Boreal wetland	Dry hummocks	Shrub and mosses	July, 2007	ISO	µgC/m2/h	24.5	85	[9]
	Boreal fen	*Sphagnum* mosses and sedges	July, 2007	ISO	µgC/m^2/h	186-220	198	[10]
	SubArctic fen	Graminoid	2006	ISO	µgC/m^2/h	Up to 1385	439	[11]
Tundra wetland	SubArctic fen	Graminoid	Jul, 2018 Jul, 2018	ISO MT	µgC/m^2/h	310 14	330 14	[12]

CMIP6 and predicted future climate change

We present details of the selected future emission scenarios and included general circulation models (GCM) in Supplementary Table 2. The design and description of the CMIP6 experimental protocol can be found in Eyring, et al. [13] and the outputs from these models necessary as input to LPJ-GUESS (variables temperature, precipitation and shortwave radiation) were downloaded through ESGF (https://esgf-node.llnl.gov/search/cmip6/) for the period 1901-2100 (Date of access: Sep-2020). The climatology of the CRU-NCEP and CMIP6 datasets over the period 1985-2014 was calculated for each variable, and the monthly biases between CRU-NCEP and each CMIP6 model data were then calculated. The biases were corrected in each climate field for the whole future period (2015-2100). The bias-corrected temperature, precipitation and radiation were then used to drive the LPJ-GUESS simulation over the future period. The anomalies (relative to period 1985-2014) shown in Supplementary Fig. 4 show that over the study region and relative to recent decades, the predicted temperature increase can be up to 12 °C, the annual precipitation increase can be up to 250 mm yr^{-1} and the annual radiation shows both increases and decreases. There is a general negative correlation between the

changes in temperature and annual radiation. All of these 15 scenarios show that this region is likely to become warmer and wetter, with a large range of responses between different CO_2 emission scenarios.

Supplementary Table 2 Overview of the selected future emission scenarios from CMIP6 and the general circulation models included in this study.

Scenario names	Shared Socioeconomic Pathways (SSPs)	Climate forcing levels	Included general circulation model (GCMs)
SSP585	SSP5	RCP8.5	CanESM5, MRI-ESM2-0, GFDL-ESM4
SSP370	SSP3	RCP7.0	CanESM5, MRI-ESM2-0, GFDL-ESM4
SSP245	SSP2	RCP4.5	CanESM5, MRI-ESM2-0, GFDL-ESM4
SSP126	SSP1	RCP2.6	CanESM5, MRI-ESM2-0, GFDL-ESM4
SSP119	SSP1	RCP1.9	CanESM5, MRI-ESM2-0, GFDL-ESM4

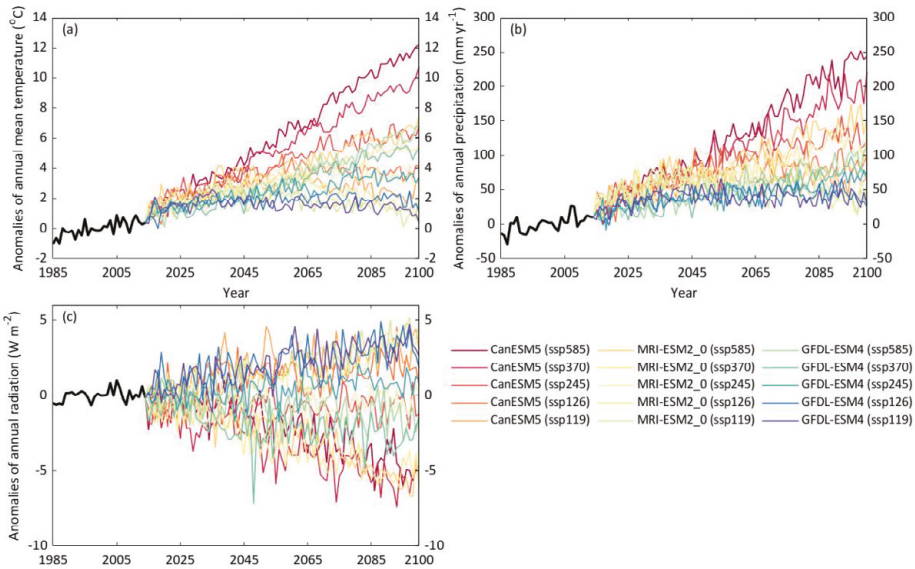

Supplementary Figure 4 Anomalies of annual mean temperature (a), precipitation (b) and surface shortwave radiation (c) over 1985-2100. The period 1985-2014 has been used as the base line to calculate anomalies.

Modelled isoprene and monoterpene emissions

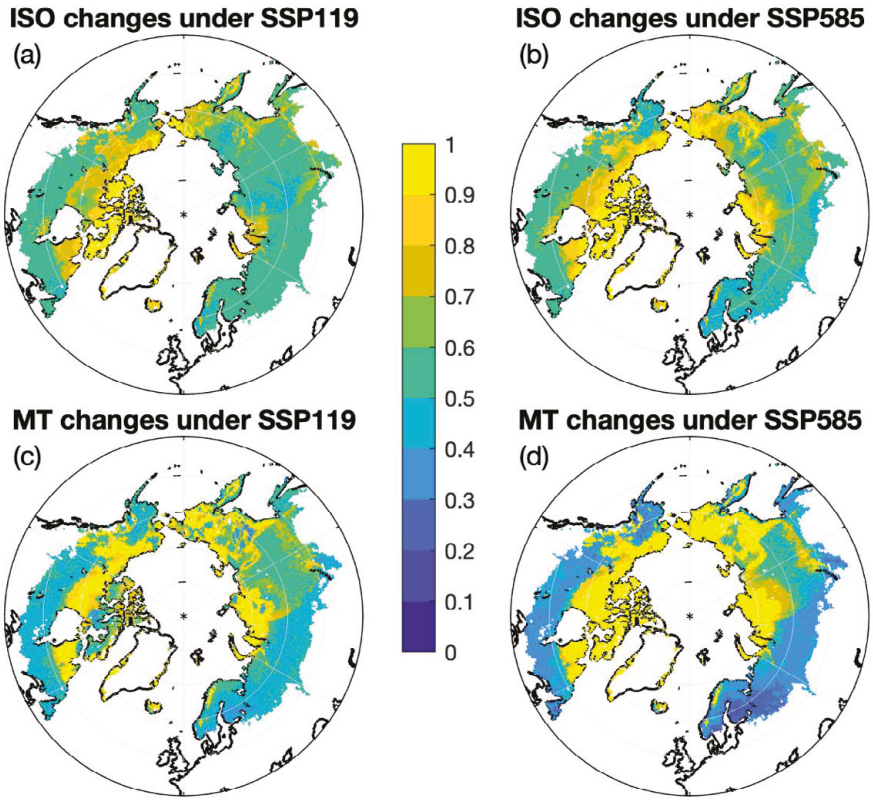

Supplementary Figure 5 Changing ratios of the annual isoprene (ISO) and monoterpene (MT) emissions under SSP119 and SSP585. The data were based on the averaged emissions across three GCMs. The ratios are calculated based on the average annual emissions from the period 2096-2100 divided by the sum of emissions for the periods of 2010-2014 and 2096-2100. The ratio values close to 0.5 represent no or small changes in emissions, the values close to 1 indicate large increase in emissions and the values close to 0 indicate large decrease in emissions.

The distribution of significant trends in isoprene emissions reveals that a larger area displays a positive trend in isoprene emission in predictions with greater levels of climate change, which is however not the same for monoterpene emissions (Supplementary Fig. 6). For monoterpenes, the higher CO_2 emission scenarios (such as SSP585) together with warmer climate conditions result in an increased area with significant negative trends, and a decrease in area with positive trends.

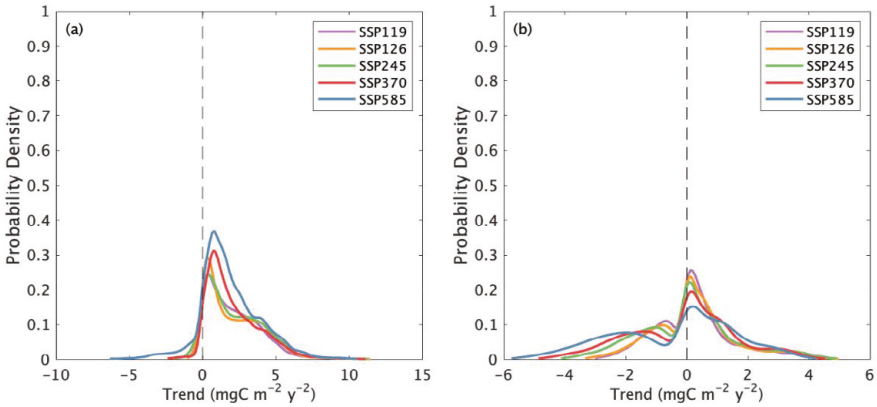

Supplementary Figure 6. Probability density of annual isoprene (left) and monoterpene (right) emission trends. The trends were calculated based on the averaged emissions over 3 GCMs under each SSP, and only significant trends (Mann-Kendall trend test, $p<0.05$) are shown and included in the plot.

The modelled latitudinal fractions of LAI, isoprene and monoterpene emissions for each PFT are shown in Supplementary Fig. 7. During the historical period 1971-2000, there is no significant presence of temperate evergreen species (represented by PFTs Temperate broad-leaved evergreen, TeBE, and Temperate needle-leaved evergreen,TeNE, in this region), but these two PFTs start to appear in the future (2071-2100) period in the CanESM5 SSP585 scenario. The modelled changes in LAI, annual isoprene and monoterpene emissions (Supplementary Fig. 7 b, d, f) show that: (1) in the high Arctic (north of 70 °N), there are large increases in the abundance of shrubs of different heights, cold grass (C3G) and boreal needle-leaved trees. Increases in the emissions of isoprene are mainly contributed by the emissions from graminoids (GRT), prostrate shrubs (SPDS), and different boreal tree PFTs. The increases of monoterpene emissions in this region result mainly from emissions from boreal needle-leaved tree PFTs. (2) in the low Arctic and boreal region, there are widespread increases of IBS and TeBS (mainly replacing BNE and BINE, see Supplementary Fig. 7b), which result in a large increase of isoprene emissions from these two new, dominant PFTs. The increased presence of these two PFTs also contributes to a slight increase of monoterpene emissions, but the PFTs they have replaced (i.e., BNE and BINE) show large decreases, leading to a net decrease in monoterpene emission for these southern latitudinal bands.

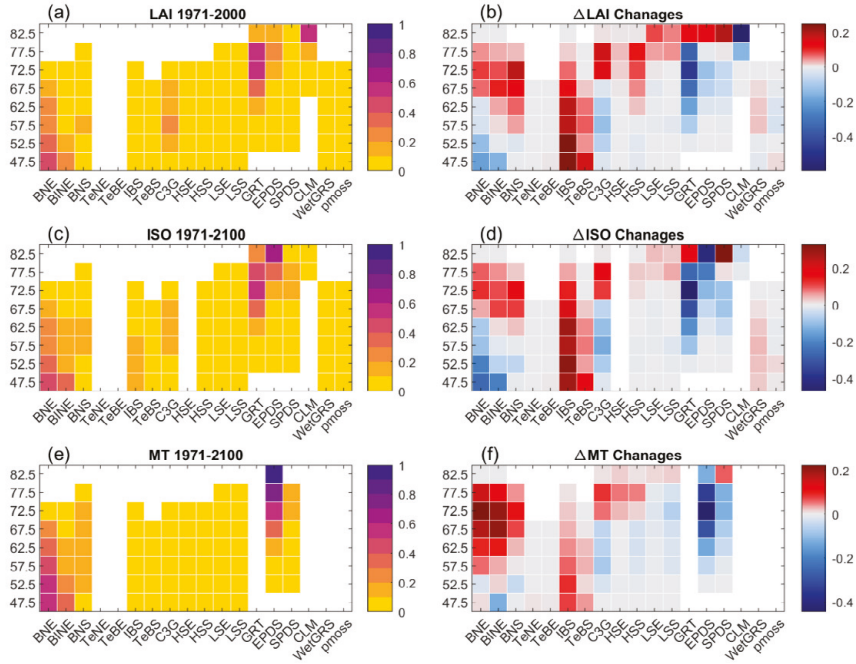

Supplementary Figure 7. Latitudinal fractions of leaf area index (LAI), annual isoprene (ISO) and annual monoterpene (MT) emissions for each modelled plant functions type (PFT, on the x-axis). The fractions of all PFTs within each latitudinal band add up till 1. The left column shows the modelled LAI, ISO and MT in latitudinal fractions for the period 1971-2000, and the right column shows the corresponding changes between 2071-2100 and 1971-2000 following the CanESM5 SSP585 scenario. BNE: Boreal needle-leaved evergreen; BINE: Boreal shade-intolerant needle-leaved evergreen; BNS: Boreal needle-leaved summergreen; TeNE: Temperate needle-leaved evergreen; TeBE: Temperate broad-leaved evergreen; C3G: Cool grass; HSE: High shrubs evergreen; HSS: High shrubs summergreen; LSE: Low shrub evergreen; LSS: Low shrub summergreen; GRT: Graminoid and forb tundra; EPDS: Evergreen prostrate dwarf shrub; SPDS; Summergreen prostrate dwarf shrub; CLM; Cushion forb, lichen and moss; WetGRS: flood-tolerant grass; pmoss: peatland moss.

Results of factorial experiments from GFDL-ESM4

Supplementary Figure 8 shows the same analysis as Figure 3 in the main text, but the model runs are driven by GFDL-ESM4 SSP119 and GFDL-ESM4 SSP585. We see similar patterns as to the ones shown in Figure 3 with some deviations in terms of magnitudes. Under SSP119, we still see the distribution of increasing and decreasing trends of standard runs is largely driven by vegetation changes (Supplementary Figure 8 e, o) and the impacts from CO_2 fertilization and N limitation are relatively small. Under SSP585, we see both increasing and decreasing trends in isoprene and monoterpene emissions. The positive trends are mainly associated with CO_2 fertilization and vegetation changes, while the negative trends are mainly linked to strong CO_2 inhibition and also vegetation changes.

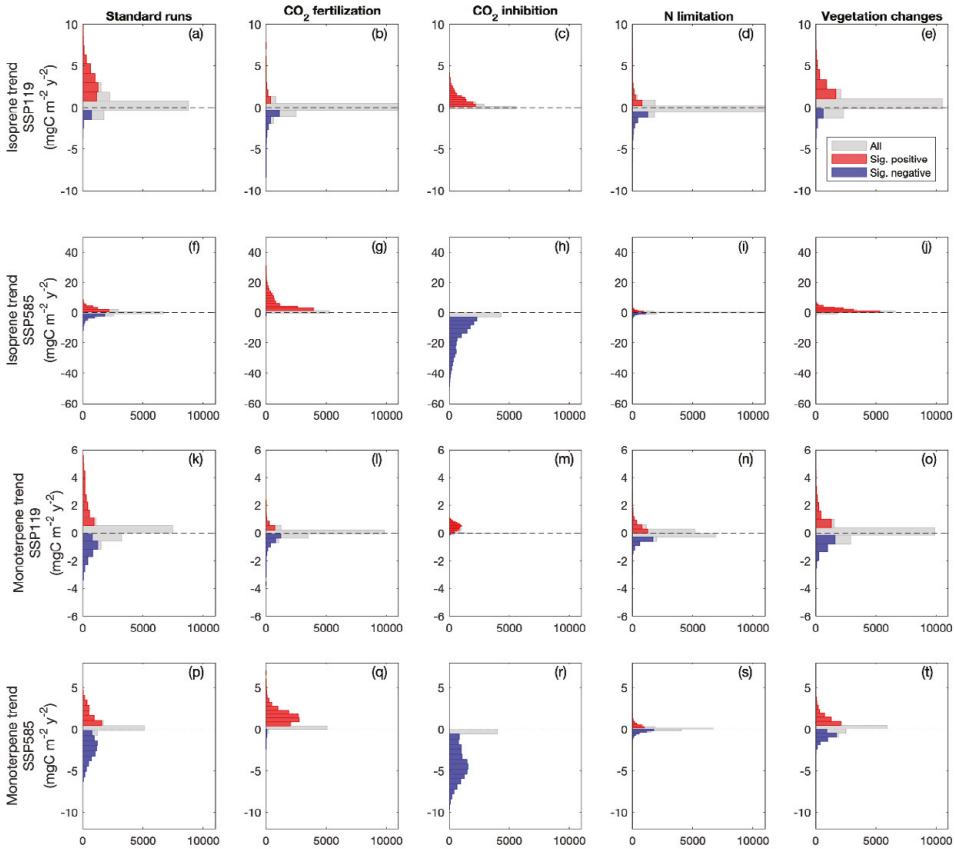

Supplementary Figure 8 Histograms of trends in the modelled isoprene (first row for GFDL-ESM4 SSP119 and second row for GFDL-ESM4 SSP585) and monoterpene (third row for GFDL-ESM4 SSP119 and fourth row for GFDL-ESM4 SSP585) emissions from standard runs and from four investigated processes over the period 2015-2100. x-axis shows the number of gridcells and y-axis shows the values of estimated trends. The values used in the trend analysis of these four investigated processes are based on the differences of every two runs (see how the impacts from each process are extracted in Table 1). Trends are analysed using Mann-Kendall test, and the trends for all grid cells are marked as grey, while both significant positive and significant negative trends ($p < 0.05$) are indicated with red and blue bars, respectively. Sig.: Significant.

Selected historical and future years for TM5 inputs

To illustrate the potential impacts of historical and future BVOC on atmospheric chemistry, one historical year and one future year were selected to drive TM5 runs. We checked the monthly differences in modelled isoprene and monoterpene emissions from the selected years of 2009 and 2100 in comparison with 10 years' range and found that the regional monthly emissions for these two selected years are representative of the values seen over the decade (Supplementary Figure 9).

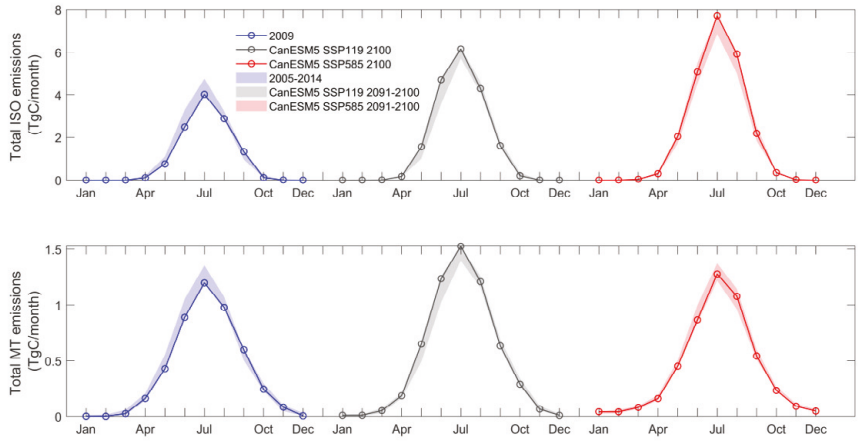

Supplementary Figure 9. LPJ-GUESS modelled total isoprene and monoterpene emissions for each month in the selected years 2009 and 2100 (solid lines) and the minimum and maximum values in their nearby period 2005-2014 and 2091-2100, respectively.

BVOC impacts on regional atmosphere

Here we show the outputs from another two factorial experiments: noMT_CO2Inhibition and noCO2 (see Supplementary Figures 10 and 11). In the noMT_CO2Inhibition run, future changes in CO_2 inhibition only affect isoprene production for the period 2015-2100. In the noCO2 run, we keep the CO_2 concentration constant at its year 2014 value (397.55 ppm) for the future period. The differences between the noCO2Inhibition and noMT_CO2Inhibition are caused by the CO_2 inhibition effects on isoprene only, and the differences between the noCO2Inhibition and noCO2 runs are caused by CO_2 fertilization effects on BVOC emissions mediated by changes in productivity and vegetation dynamics. As we can see from the first two columns in these two figures below, lifting CO_2 inhibition impacts on monoterpenes (noMT_CO2Inhibition) can give similar patterns as the outputs from noCO2Inhibition, indicating the importance of monoterpenes in forming SOA.

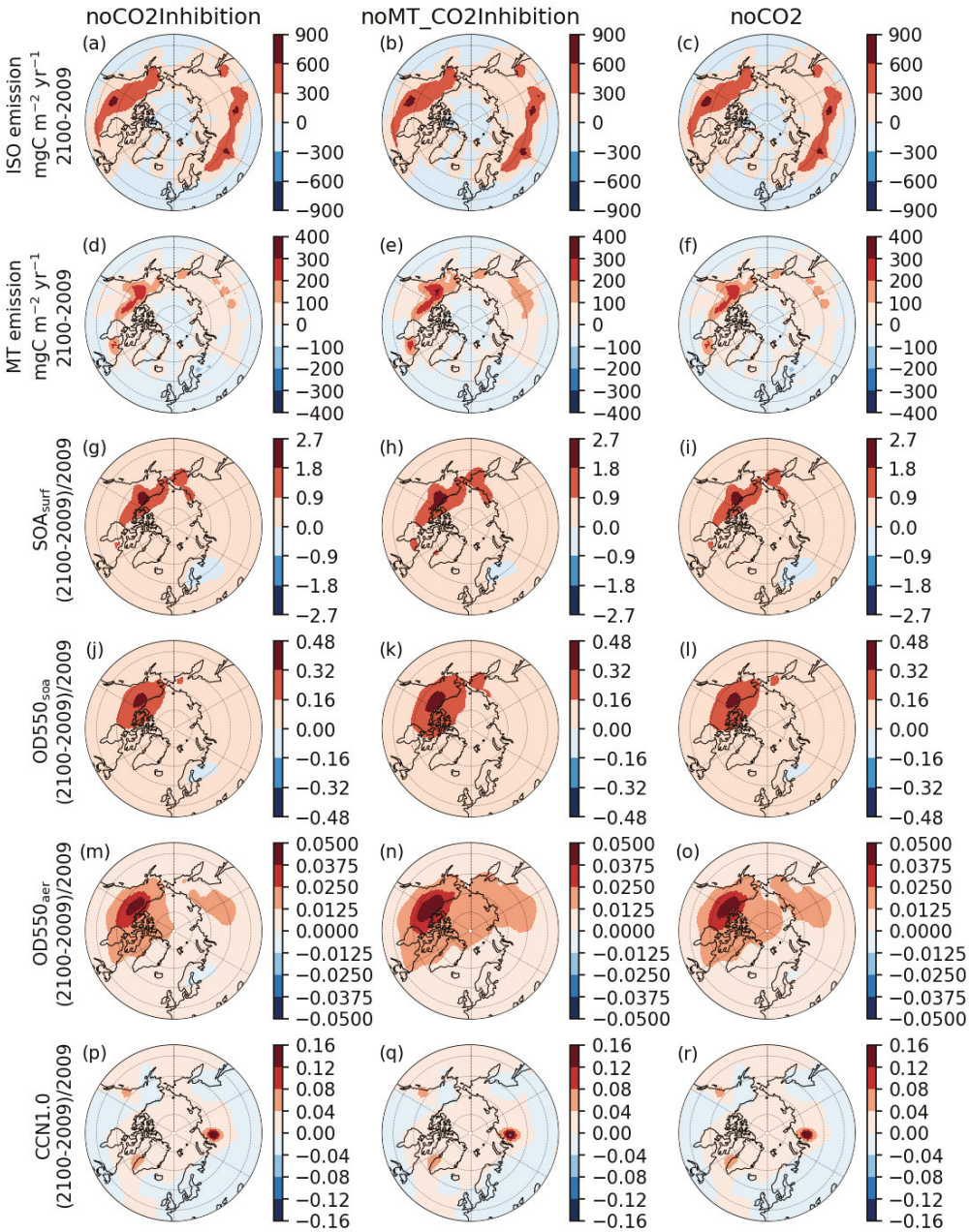

Supplementary Figure 10. The inputs to and outputs from TM5 using CanESM5 SSP119. The first and second rows show LPJ-GUESS simulated isoprene (ISO) and monoterpene (MT) emission changes between 2100 and 2009. The emissions from the year 2100 are driven by CanESM5 SSP119. The third to the sixth rows show the TM5 simulated ratio in changes to surface SOA concentration (SOA_{surf}); optical depth of SOA at 550 nm ($OD550_{soa}$); optical depth of aerosol at 550 nm ($OD550_{aer}$) and CCN concentrations at a supersaturation of 1.0 %. From left to right, we show the TM5 results fed with BVOC inputs from three LPJ-GUESS runs, which are noCO2Inhibition (the 1st column), noMT_CO2Inhibition run (the 2nd column) and noCO2 runs (the 3rd column).

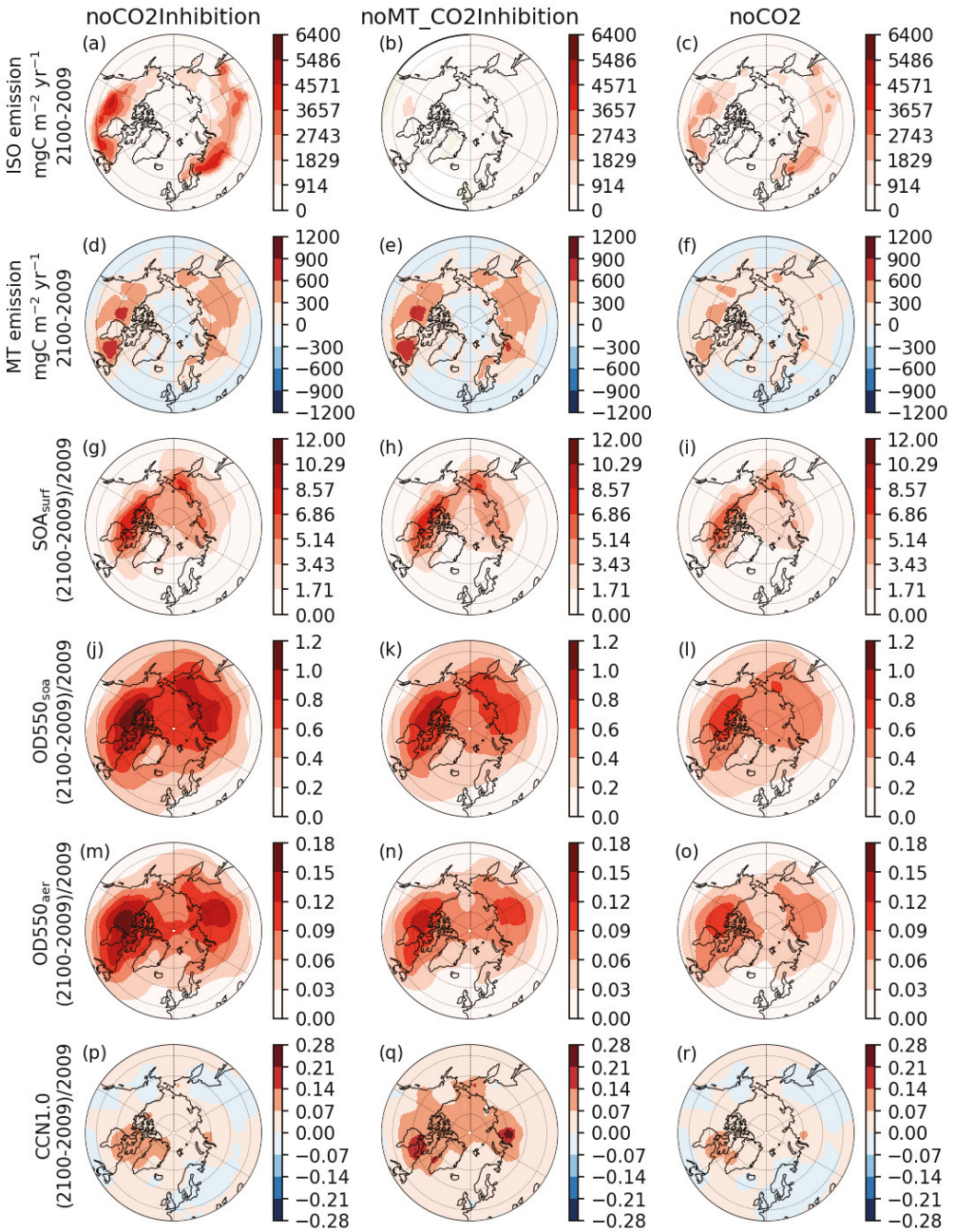

Supplementary Figure 11. The inputs to and outputs from TM5 using CanESM5 SSP585. The first and second rows show LPJ-GUESS simulated isoprene (ISO) and monoterpene (MT) emission changes between 2100 and 2009. The emissions from the year 2100 are driven by CanESM5 SSP585. The third to the sixth rows show the TM5 simulated ratio in changes to surface SOA concentration (SOA_{surf}); optical depth of SOA at 550 nm ($OD550_{soa}$); optical depth of aerosol at 550 nm ($OD550_{aer}$) and CCN concentrations at a supersaturation of 1.0 %. From left to right, we show the TM5 results fed with BVOC inputs from three LPJ-GUESS runs, which are noCO2Inhibition (the 1st column), noMT_CO2Inhibition run (the 2nd column) and noCO2 runs (the 3rd column).

Estimated radiative forcing

We have used the parameters and equations from three different studies to estimate potential radiative forcing impacts based on TM5 modelled changes in future SOA loading and concentration. As we can see from the Supplementary Table 3, there are large differences in the magnitudes between Yli-Juuti, et al. [14] and the other two studies for north of 45N. Zhu, et al. [15] and Bellouin, et al. [16] derived parameters (such as ratio of radiative forcing changes to SOA burden) based on the global datasets, while Yli-Juuti, et al. [14] is based on measurement data from one observation sites. Nevertheless, all three sets of estimations show that the warming-induced changes in SOA cause an overall reduction of radiative forcing, leading to cooling feedback north of 45 N. The cooling feedback from noVegDym run is weaker than the standard run and the relative differences between the standard and noVegDym runs are larger for the two estimations based on global dataset [15,16]. Under CanESM5 SSP585, the CO_2 inhibition effects become dominant and without CO2 inhibition on BVOCs, we see strong cooling feedback resulting from increased BVOC and SOA. Under CanESM5 SSP119, the strongest cooling feedback is from the standard run, and the noVegDym run shows a reduced cooling feedback (by approx. 25%).

Supplementary Table 3 Estimated radiative forcing (W m^{-2}) in 2100 in comparison to the year 2009.

Scenarios	***Extents***	***standard***	***noVegDym***	***noCO2Inhibition***	***Used References***
CanESM5 SSP585	*north of 45N*	*-0.224*	*-0.214*	*-1.746*	*(Yli-Juuti et al., 2021)*
	north of 45N	*-0.048*	*-0.037*	*-0.424*	*(Zhu et al., 2017)*
	north of 45N	*-0.039*	*-0.028*	*-0.318*	*(Bellouin et al., 2020)*
CanESM5 SSP119	*north of 45N*	*-0.223*	*-0.171*	*-0.216*	*(Yli-Juuti et al., 2021)*
	north of 45N	*-0.058*	*-0.044*	*-0.053*	*(Zhu et al., 2017)*
	north of 45N	*-0.045*	*-0.033*	*-0.037*	*(Bellouin et al., 2020)*

Model uncertainties

Uncertainties in modelled vegetation changes

The northward shifts of woody plants as well as changes to PFT compositions simulated by LPJ-GUESS consider PFT competition and PFT responses to changing climatic and environmental conditions, including soil conditions and nutrient (nitrogen) availability. Migration and establishment rates may be overestimated as constraints such as seed dispersal have not been accounted for in the model[17]. However, tree demography and competition rather than seed dispersal have been shown to be more important in limiting vegetation shifts in the Alps[18]. Gustafson, et al. [19] found that nitrogen could restrict treeline migration in a subarctic environment. Our

modelled vegetation responses to climate (e.g., replacement of evergreen trees with deciduous trees, shrubification and northward movements of evergreen trees) are consistent with experimental and paleo evidence[20-22] and other modelling studies[4,23].

Uncertainties in modelled aerosol changes

Uncertainties in the TM5 model itself also apply to this study. For example, the wet removal of aerosol particles may be overestimated, which results in lower aerosol optical depth (AOD) values[24,25]. However, the AOD comparisons of two different runs with the absolute differences can help to offset the overestimation, and the relative differences may be overestimated due to underestimated AOD values. The considered SOA formation process can also contribute to the uncertainties, partly due to the complicated mechanism and partly due to the relatively simplified implementation in the large-scale model, as in TM5[26].

References

1 Li, X. & Xiao, J. Mapping Photosynthesis Solely from Solar-Induced Chlorophyll Fluorescence: A Global, Fine-Resolution Dataset of Gross Primary Production Derived from OCO-2. *Remote Sensing* **11**, 2563 (2019).

2 Zhu, Z. *et al.* Global Data Sets of Vegetation Leaf Area Index (LAI)3g and Fraction of Photosynthetically Active Radiation (FPAR)3g Derived from Global Inventory Modeling and Mapping Studies (GIMMS) Normalized Difference Vegetation Index (NDVI3g) for the Period 1981 to 2011. *Remote Sensing* **5**, 927-948 (2013).

3 Liu, Y. Y. *et al.* Recent reversal in loss of global terrestrial biomass. *Nature Climate Change* **5**, 470-474, doi:10.1038/nclimate2581 (2015).

4 Arneth, A. *et al.* Future vegetation–climate interactions in Eastern Siberia: an assessment of the competing effects of CO2 and secondary organic aerosols. *Atmos. Chem. Phys.* **16**, 5243-5262, doi:10.5194/acp-16-5243-2016 (2016).

5 Rantala, P., Aalto, J., Taipale, R., Ruuskanen, T. M. & Rinne, J. Annual cycle of volatile organic compound exchange between a boreal pine forest and the atmosphere. *Biogeosciences* **12**, 5753-5770, doi:10.5194/bg-12-5753-2015 (2015).

6 Schollert, M., Burchard, S., Faubert, P., Michelsen, A. & Rinnan, R. Biogenic volatile organic compound emissions in four vegetation types in high arctic Greenland. *Polar Biology* **37**, 237-249, doi:10.1007/s00300-013-1427-0 (2014).

7 Potosnak, M. J. *et al.* Isoprene emissions from a tundra ecosystem. *Biogeosciences* **10**, 871-889, doi:10.5194/bg-10-871-2013 (2013).

8 Angot, H. *et al.* Biogenic volatile organic compound ambient mixing ratios and emission rates in the Alaskan Arctic tundra. *Biogeosciences* **17**, 6219-6236, doi:10.5194/bg-17-6219-2020 (2020).

9 Tiiva, P. *et al.* Contribution of vegetation and water table on isoprene emission from boreal peatland microcosms. *Atmospheric Environment* **43**, 5469-5475, doi:https://doi.org/10.1016/j.atmosenv.2009.07.026 (2009).

10 Haapanala, S. *et al.* Measurements of hydrocarbon emissions from a boreal fen using the REA technique. *Biogeosciences* **3**, 103-112, doi:10.5194/bg-3-103-2006 (2006).

11 Holst, T. *et al.* BVOC ecosystem flux measurements at a high latitude wetland site. *Atmos. Chem. Phys.* **10**, 1617-1634, doi:10.5194/acp-10-1617-2010 (2010).

12 Seco, R. *et al.* Volatile organic compound fluxes in a subarctic peatland and lake. *Atmos. Chem. Phys.* **20**, 13399-13416, doi:10.5194/acp-20-13399-2020 (2020).

13 Eyring, V. *et al.* Overview of the Coupled Model Intercomparison Project Phase 6 (CMIP6) experimental design and organization. *Geosci. Model Dev.* **9**, 1937-1958, doi:10.5194/gmd-9-1937-2016 (2016).

14 Yli-Juuti, T. *et al.* Significance of the organic aerosol driven climate feedback in the boreal area. *Nature Communications* **12**, 5637, doi:10.1038/s41467-021-25850-7 (2021).
15 Zhu, J. *et al.* Mechanism of SOA formation determines magnitude of radiative effects. *Proceedings of the National Academy of Sciences* **114**, 12685-12690, doi:doi:10.1073/pnas.1712273114 (2017).
16 Bellouin, N. *et al.* Bounding Global Aerosol Radiative Forcing of Climate Change. *Reviews of Geophysics* **58**, e2019RG000660, doi:https://doi.org/10.1029/2019RG000660 (2020).
17 Lehsten, V., Mischurow, M., Lindström, E., Lehsten, D. & Lischke, H. LPJ-GM 1.0: simulating migration efficiently in a dynamic vegetation model. *Geosci. Model Dev.* **12**, 893-908, doi:10.5194/gmd-12-893-2019 (2019).
18 Scherrer, D., Vitasse, Y., Guisan, A., Wohlgemuth, T. & Lischke, H. Competition and demography rather than dispersal limitation slow down upward shifts of trees' upper elevation limits in the Alps. *Journal of Ecology* **108**, 2416-2430, doi:https://doi.org/10.1111/1365-2745.13451 (2020).
19 Gustafson, A., Miller, P. A., Björk, R. G., Olin, S. & Smith, B. Nitrogen restricts future sub-arctic treeline advance in an individual-based dynamic vegetation model. *Biogeosciences* **18**, 6329-6347, doi:10.5194/bg-18-6329-2021 (2021).
20 Soja, A. J. *et al.* Climate-induced boreal forest change: Predictions versus current observations. *Global and Planetary Change* **56**, 274-296, doi:https://doi.org/10.1016/j.gloplacha.2006.07.028 (2007).
21 Fraser, R. H., Lantz, T. C., Olthof, I., Kokelj, S. V. & Sims, R. A. Warming-Induced Shrub Expansion and Lichen Decline in the Western Canadian Arctic. *Ecosystems* **17**, 1151-1168, doi:10.1007/s10021-014-9783-3 (2014).
22 Edwards, M. E., Brubaker, L. B., Lozhkin, A. V. & Anderson, P. M. Structurally novel biomes: a response to past warming in Beringia. *Ecology* **86**, 1696-1703, doi:https://doi.org/10.1890/03-0787 (2005).
23 Wolf, A., Callaghan, T. V. & Larson, K. Future changes in vegetation and ecosystem function of the Barents Region. *Climatic Change* **87**, 51-73, doi:10.1007/s10584-007-9342-4 (2008).
24 van Noije, T. P. C. *et al.* Simulation of tropospheric chemistry and aerosols with the climate model EC-Earth. *Geosci. Model Dev.* **7**, 2435-2475, doi:10.5194/gmd-7-2435-2014 (2014).
25 Aan de Brugh, J. M. J. *et al.* The European aerosol budget in 2006. *Atmos. Chem. Phys.* **11**, 1117-1139, doi:10.5194/acp-11-1117-2011 (2011).
26 Bergman, T. *et al.* Description and evaluation of a secondary organic aerosol and new particle formation scheme within TM5-MP v1.2. *Geosci. Model Dev.* **15**, 683-713, doi:10.5194/gmd-15-683-2022 (2022).

DOCTORAL THESES PUBLISHED IN ENVIRONMENTAL SCIENCE, LUND UNIVERSITY

1. Georg K.S. Andersson (2012) Effects of farming practice on pollination across space and time. Department of Biology/Centre for environmental and climate research

2. Anja M. Ödman (2012) Disturbance regimes in dry sandy grasslands – past, present and future. Department of Biology/ Centre for environmental and climate research

3. Johan Genberg (2013) Source apportionment of carbonaceous aerosol. Department of Physics/ Centre for environmental and climate research

4. Petra Bragée (2013) A palaeolimnological study of the anthropogenic impact on dissolved organic carbon in South Swedish lakes. Department of Geology/ Centre for environmental and climate research

5. Estelle Larsson (2013) Sorption and transformation of anti-inflammatory drugs during wastewater treatment. Department of Chemistry/ Centre for environmental and climate research

6. Magnus Ellström (2014) Effects of nitrogen deposition on the growth, metabolism and activity of ectomycorrhizal fungi. Department of Biology/ Centre for environmental and climate research

7. Therese Irminger Street (2015) Small biotopes in agricultural landscapes: importance for vascular plants and effects on management. Department of physical geography and ecosystem science/ Department of Biology/ Centre for environmental and climate research

8. Helena I. Hanson (2015) Natural enemies: Functional aspects of local management in agricultural landscapes. Department of Biology/ Centre for environmental and climate research

9. Lina Nikoleris (2016) The estrogen receptor in fish and effects of estrogenic substances in the environment: ecological and evolutionary perspectives and societal awareness Department of Biology/ Centre for environmental and climate research

10. Cecilia Hultin (2016) Estrogen receptor and multixenobiotic resistance genes in freshwater fish and snails: identification and expression analysis after pharmaceutical exposure. Centre for environmental and climate research

11. Annika M. E. Söderman (2016) Small biotopes: Landscape and management effects on pollinators. Department of Biology/ Centre for environmental and climate research

12. Wenxin Ning (2016) Tracking environmental changes of the Baltic Sea coastal zone since the mid-Holocene. Department of Geology/ Centre for environmental and climate research

13. Karin Mattsson (2016) Nanoparticles in the aquatic environment, Particle characterization and effects on organisms. Department of Chemistry/ Centre for environmental and climate research

14. Ola Svahn (2016) Tillämpad miljöanalytisk kemi för monitorering och åtgärder av antibiotika- och läkemedelsrester I Vattenriket. School of Education and Environment, Kristianstad University/ Centre for environmental and climate research

15. Pablo Urrutia Cordero (2016) Putting food web theory into action: Local adaptation of freshwaters to global environmental change. Department of Biology/ Centre for environmental and climate research

16. Lin Yu (2016) Dynamic modelling of the forest ecosystem: Incorporation of the phosphorous cycle. Centre for environmental and climate research

17. Behnaz Pirzamanbein (2016) Recontruction of past European land cover based on fossil pollen data: Gaussian Markov random field models for compositional data. Centre for Mathematical Sciences/ Centre for environmental and climate research

18. Arvid Bolin (2017) Ecological interactions in human modified landscapes – Landscape dependent remedies for the maintenance of biodiversity and ecosystem services. Department of Biology/ Centre for environmental and climate research

19. Johan Martinsson (2017) Development and Evaluation of Methods in Source Apportionment of the Carbonaceous Aerosol. Department of Physics/ Centre for environmental and climate research

20. Emilie Öström (2017) Modelling of new particle formation and growth in the atmospheric boundary layer. Department of Physics/ Centre for environmental and climate research

21. Lina Herbertsson (2017) Pollinators and Insect Pollination in Changing Agricultural Landscapes. Centre for environmental and climate research

22. Sofia Hydbom (2017) Tillage practices and their impact on soil organic carbon and the microbial community. Department of Biology/ Centre for environmental and climate research

23. Erik Ahlberg (2017) Speeding up the Atmosphere: Experimental oxidation studies of ambient and laboratory aerosols using a flow reactor. Department of Physics/ Centre for environmental and climate research

24. Laurie M. Charrieau (2017) DISCO: Drivers and Impacts of Coastal Ocean Acidification. Department of Geology/ Centre for environmental and climate research

25. Kristin Rath (2018) Soil salinity as a driver of microbial community structure and functioning. Department of Biology/ Centre for environmental and climate research

26. Lelde Krumina (2018) Adsorption, desorption, and redox reactions at iron oxide nanoparticle surfaces. Department of Biology/ Centre for environmental and climate research

27. Ana Soares (2018) Riverine sources of bioreactive macroelements and their impact on bacterioplankton metabolism in a recipient boreal estuary. Department of physical geography and ecosystem science/ Centre for environmental and climate research

28. Jasmine Livingston (2018) Climate Science for Policy? The knowledge politics of the IPCC after Copenhagen. Centre for environmental and climate research

29. Simon David Herzog (2019) Fate of riverine iron over estuarine salinity gradients. Department of Biology/ Centre for Environmental and Climate Research

30. Terese Thoni (2019) Making Blue Carbon: Coastal Ecosystems at the Science-Policy Interface. Centre for Environmental and Climate Research

31. Lovisa Nilsson (2019) Exploring synergies – management of multifunctional agricultural landscapes. Centre for Environmental and Climate Research

32. Zhaomo Tian (2019) Properties and fungal decomposition of iron oxide-associated organic matter. Centre for Environmental and Climate Research

33. Sha Ni (2020) Tracing marine hypoxic conditions during warm periods using a microanalytical approach. Department of Geology/Centre for Environmental and Climate Research

34. Julia Kelly (2021) Carbon exchange in boreal ecosystems: upscaling and the impacts of natural disturbances. Centre for Environmental and Climate Science

35. William Sidemo Holm (2021) Effective conservation of biodiversity and ecosystem services in agricultural landscapes. Centre for Environmental and Climate Science

36. John Falk (2021) Ice out of Fire: Ice and cloud condensation nucleation of aerosol particles emitted from controlled soot generation and combustion of renewable fuels. Department of Physics / Centre for Environmental and Climate Science

37. Maria Blasi i Romero (2021) Wild bees in agricultural landscapes: Modelling land use and climate effects across space and time. Centre for Environmental and Climate Science

38. Ivette Raices Cruz (2021) Robust analysis of uncertainty in scientific assessments. Department of Biology/ Centre for Environmental and Climate Science

39. Adrian Gustafson (2022) On the role of terrestrial ecosystems in a changing Arctic. Department of Physical Geography and Ecosystem Science/Centre for Environmental and Climate Science